Aalborg University

Voltage Control in Wind Power Plants with Doubly Fed Generators

Jorge Martínez García

Voltage Control in Wind Power Plants with Doubly Fed Generators

Jorge Martínez García

A Thesis Submitted to the Institute of Energy Technology
of Aalborg University
for the Degree of
Doctor of Philosophy

September 2010

Pontoppidanstraede 101
DK-9220 Aalborg East
Denmark

Printed in Denmark
ISBN: 978-87-89179-92-6

Don Quijote: La ventura va guiando nuestras cosas mejor de lo que acertáramos a desear; porque ves allí, amigo Sancho Panza, donde se descubren treinta o pocos más desaforados gigantes, con quien pienso hacer batalla y quitarles a todos las vidas, con cuyos despojos comenzaremos a enriquecer; que ésta es buena guerra, y es gran servicio de Dios quitar tan mala simiente de sobre la faz de la tierra.

Sancho Panza: ¿Qué gigantes?

Miguel de Cervantes

Abstract

In this work, the process of designing a wind power plant composed of doubly fed induction generators, a static compensator unit, mechanically switched capacitors, and on-load tap changer, for voltage control is shown. The selected control structure is based on a decentralized system, since it offers very fast system response to grid disturbances and lower sensitivity to the grid impedance, and moreover this control structure releases the central control of having grid impedance estimation techniques or adaptive control methods.

The difference between the required reactive power and the one supplied by the doubly fed induction generator wind turbines is overcome by installing a reactive power compensator, i.e. a static compensator unit, which is coordinated with the plant control by a specific dispatcher. This dispatcher is set according to the result of the wind power plant load flow.

To release the operation of the converters during steady-state voltage disturbances and to reduce electrical losses, mechanically switched capacitors are installed in the wind power plant, which due to their characteristics, they are appropriate for permanent disturbances compensation. The mechanically switched capacitors are controlled to allow the reactive power operation of the converters, in steady-state, within a maximum band of 10 %.

It is clear that an on-load tap changer system will help to keep the stator voltage close to its nominal value, but the action of the mechanically switched capacitors is badly influencing the on-load tap changer line drop calculation. It is proposed to coordinate the on-load tap changer system with the main substation control. By exchanging the information related to the mechanically switched capacitors switch status, the current injected from the mechanically switched capacitors can be removed from the total measured current at medium voltage, thus reducing the tap moving operations.

Finally, due to the wind power plant reactive power is sized for maximum active power level, it is expected that a big amount of reactive power remains unused most of the time due to the wind power generation characteristics. Hence, a VAr reserve concept system is proposed and applied, thereby the grid can be benefited from this extra available reactive power.

Acknowledgments

Thanks to my supervisors Dr. Remus Teodorescu and Dr. Pedro Rogriguez for their guidance and advice.

All this work has been carried out while I was employed by Vestas, in the Power Plant department. The Thesis is included under the Vestas Power Programme. Through visionary and coordinated research, the intention is to push the wind power technology to even higher levels of reliability and integration into the grid.

I gratefully appreciate all the synergies found during my work at Vestas (Power Plant department), meanwhile developing more advance control features for integrating Vestas wind power plants into the grid.

Thanks to everyone involved in the modeling department of Vestas and their support in solving all problems related to the models. Thanks to Florin Lungeanu, Power Plant department in Vestas, for his technical and formatting advices. Also, to all my department managers, which at some extend, allow me to dedicate more time to the Thesis.

Many thanks to Luis María Coronado, employed at REE (transmission system operator of Spain), for answering my questions and for his friendly help.

Specially thanks to Dr. Philip C. Kjær, chief specialist of Vestas, for his technical supervision and planning advices.

For helping me in keeping focus, thanks to the Unknown Man.

Finally and most important, for the support of my family and for giving me the opportunities to reach this point, I thank them. I would like to thank the most, my fellow and partner Ana M. Abadia for her constant understanding over the last years.

Table of contents

List of Figures

Nomenclature

AC	Alternate Current	
AQR	Automatic Reactive power Regulator	
AVR	Automatic Voltage Regulator	
Cap	Capacitor	
CC	Current control	
Ctrl	Control	
COMM	Communication	
CT	Current Transformer	
DC	Direct Current	
DFIG	Doubly Fed Induction Generator	
DB	Dead Band	
EMTP	Electromagnetic Transient Program	
FACTS	Flexible AC Transmission System	
G	Generator	
I	Current	[A]
j	Imaginary unit	
L	Inductance	[H]
LV	Low Voltage side	
LVRT	Low Voltage Ride Through	
LPF	Low Pass Filter	
M	Mutual Inductance	
MSC	Mechanically Switched Capacitor	
MV	Medium Voltage Side	
N	Stator to rotor turns ratio	
P	Active power	[W]
PCC	Point of Common Coupling	
PF	Power Factor	
PoM	Point of Measurement	
PI	Proportional and Integral control	

PWM	Pulse Width Modulation	
Q	Reactive power	[VA]
R	Resistance	[Ohm]
RTU	Remote Terminal Unit	
s	Laplace term	
SCR	Short Circuit Ratio	
SG	Synchronous Generator	
S/H	Sample and Hold	
SM	State Machine	
STATCOM	Static Compensator	
SVC	Static VAr Compensator	
SW	Switch	
T	Time Constant	[s]
T_{comm}	Communication Time	[s]
t_d	Delay Time	[s]
T_s	Sampling Time	[s]
t_s	Settling Time	[s]
t_p	Peak Time	[s]
t_r	Rise Time	[s]
TSO	Transmission System Operator	
V	Voltage	[V]
VT	Voltage Transformer	
OLTC	On-Load Tap Changer	
OS	Overshoot	[pu]
OVL	Overhead Line	
WPP	Wind Power Plant	
WTG	Wind Turbine Generator	
WPPC	Wind Power Plant Controller	
WPPT	Wind Power Plant Transformer	
X	Reactance	[Ohm]
Z	Impedance	[Ohm]
β	Pitch angle	[°]
ω	Angular frequency	[rad/s]

Subscripts

a, b, c	Three phase quantities
d, q	Direct and quadrature axes
r, s	Rotor and stator reference
ref	Reference
m	Measured
max, min	Maximum and minimum
σ	Leakage

Chapter 1

Introduction

This thesis describes the design and validation through simulations of a voltage control scheme for a wind power plant, composed of double fed induction generator (DFIG) wind turbines, mechanically switched capacitor banks (MSCs), static compensator (STATCOM) and an on-load tap changer (OLTC). This chapter provides the overview and an introduction to voltage control, and also presents and identifies some of the shortcomings. Finally, a problem definition is given and the objectives and outline of the thesis are presented.

1.1 Background

The following paragraph summarizes, in a very clear manner, some of the main topics related to reactive power and voltage control: "…the transmission of active power requires a difference in angular phase between voltages at the sending and receiving points (which is feasible within wide limits), whereas the transmission of reactive power requires a difference in magnitude of these same voltages (which is feasible only within very narrow limits). But why should we want to transmit reactive power anyway? Is it not just a troublesome concept, invented by the theoreticians, that is best disregarded? The answer is that reactive power is consumed not only by most of the network elements, but also by most of the consumer loads, so it must be supplied somewhere. If we can't transmit it very easily, then it ought to be generated where is needed." [1].

Hence, it can be extracted the following three main conclusions:

- The reactive power is needed in an AC system.
- The flowing of reactive power changes the node voltage amplitude.
- The reactive power should be generated as close as possible to where is needed, due to changes in the voltage and losses.

Due to this reactive power flow in the system, demanded by the network elements and the loads, it is necessary a control system which can ensure that this flow does not disturb the normal operation voltage limits, and transfer power capability of the grid.

It is possible to say, that the main goals of the reactive power and voltage control are the stabilization of the node voltage, and avoidance of violation of the maximum and minimum voltage levels. Therefore, the reactive power sources in the system should provide in every moment enough reactive power to keep the voltage close to its rated value; moreover the system should be able to cope with unexpected disturbances, which requires a provision of rapidly adjustable reactive power in case these disturbances happen.

The voltage stability of a power system can be understood as the ability to maintain steady acceptable voltages in the buses of the system under normal operating conditions and after being subjected to a disturbance [2].

One of the main factors causing voltage instability is the inability of the power system to meet the demand for reactive power [3]. Thus, the voltage stability margin of a node depends on the availability to support the system with reactive power [2], [4]. Even if this instability can be spread to a wide area in the power system, it is considered a local phenomenon [5], [6]. Therefore, by controlling the voltage of the nodes by adequate reactive power supply in every moment, transient (concerned with the ability of the system to control the voltage following large disturbances, such as short-circuits) and small voltage stability (concerned with the ability of the system to control the voltage after small perturbations) can be ensured [3].

The provision and planning of the reactive power needed is a challenging task of the grid operator, which also normally dictates the preferred method for voltage control to be applied by the equipments (i.e. synchronous generators) connected to the transmission and sub-transmission system.

In the literature, reactive power, as an ancillary service, has been mainly examined in the context of conventional generators. In many applications, the conventional generators are not used as a perfect terminal voltage regulator, but rather the terminal voltage is allowed to vary proportionally with the reactive current, this kind of control is often called slope voltage control [7].

There are several reasons for using this control type, e.g.: the linear operation range of the control can be extended if a voltage regulation with slope characteristics is used, allowing the voltage at point of common coupling (PCC) to be smaller for full capacitive compensation and, conversely to be higher for high inductive compensation levels; if no slope regulation is used and the system impedance is low, the voltage control loop could cause oscillatory behavior, and finally the slope regulation allows automatic reactive power load sharing between the voltage devices connected to the same area.

Voltage control, apart from traditional synchronous generators (SGs), is effectuated by dispersed devices throughout the network, since reactive power should not be transmitted over long distances.

SGs can generate or absorb reactive power according to the level of excitation, controlled by its automatic voltage regulator, which continuously controls this level to adjust the stator voltage; however this control is not perfect and have some limitations. SGs have differing VAr (VAr is the reactive or imaginary power) abilities depending on a number of factors such as: stator ampere rating, exciter system DC field current rating, AC terminal high voltage limit, actual MW output of the prime mover compared to generator rated power factor, control system variations, equipment changes due to age, etc.

Synchronous condensers are also used for voltage regulation; basically, they are synchronous machines without prime mover.

Apart from the SGs, some of the most common devices used for voltage control are listed below.

Shunt devices, i.e. reactors and capacitors are widely used to compensate for line capacitance and for reactive power losses due to active power transportation, respectively. Both devices are used in transmission and distribution levels. The combination of these devices controlled by static switches, it is also known as SVC. SVCs were first developed in the late 1960s for the compensation of large, fluctuating industrial loads, such as electric arc furnaces. By the late 1970s it became evident that dynamic compensation of electric power transmission systems was needed to achieve better utilization of existing generation and transmission facilities. SVCs were devised for this purpose [8]. Usually, the primary purpose of SVCs in power systems is rapid control of voltage at weak points in a network. Installation locations may be the midpoint of transmission interconnections or in load areas [9]. The main disadvan-

tage of the SVC is that the delivered maximum reactive power is dependant on the supplied voltage.

Additionally, series capacitors or thyristor controlled series capacitors, are used in transmission levels, to compensate for the inductive reactance of the line; in this case the reactive power supplied depends on the line current. The disadvantages of this device are possible resonances to happen with the SGs (sub-synchronous resonances) [10], and being series connected element has to be designed for maximum short-circuit current of the system (usually it is connected directly at extra high voltage or ultra high voltage levels).

Very commonly used, transformers with tap-changing facilities constitute an important means of controlling the voltage throughout the system at all voltage levels. And finally, static compensators (STATCOM) have to be included, which have been found of increasing utilization due to the decreasing price in electronic converters and their ability to provide continuous and rapid control of reactive power and voltage [11]. They are able to control individual phase voltages of the buses to which they are connected, and ideally their maximum current output is independent on the supplied voltage level, these static VAr systems are quite often used in sub-transmission and distribution system levels.

Since the voltage control can be considered a local issue, most of the utilities around the world are doing voltage control by manually controlling the reactive power sources [12], [13].

Depending on the countries, different strategies are used for controlling and coordinating voltage maps. Primary voltage controls fitted on the generating units are commonplace, and do provide local control, but broader-scale voltage control, capable of coordinating compensation systems, is not yet widespread [14].

In some countries, defining some superior voltage control hierarchical levels is normally used as a way to optimize the resources, and to enhance the overall system voltage profile. In this regulation scheme, the device controlling the voltage of its own monitored bus is called primary level, the following upwards level is monitoring a selected number of buses called pilot buses, and according to this measured voltage, references are dispatched to the devices around the area (secondary level) of this pilot bus.

The pilot bus is chosen so as to be representative for a whole voltage area. These, areas are assumed to be theoretically independent from each other [15]. That means that there is no significant permanent reactive power transit between adjacent areas [16]. Finally, the third level is altering the references of the secondary level voltage controllers, by considering an optimal load flow of the whole system [13]. Each control level is acting with a different time constant, i.e. primary level within a few seconds, secondary level below 1 minute, and the third level between 10-30 minutes.

Whereas secondary voltage control system has been broadly in operation since the early 1980s, tertiary control was introduced in the latest 1990s [14] - [17].

1.2 Voltage Control with Wind Power Plants

The traditional electrical grid, in which the power is produced at centralized power plants and delivered to the customers through transmission and distribution networks, is greatly challenged by the deregulation of the power system and the connection of wind power generation [19] - [21].

In the past, requirements for wind turbines generators (WTGs), if any, mainly were focused on protecting the system from the poor performance of the WTGs, and did not consider the effect on the power system operation, since the penetration level of wind power was quite low. However, this situation is changing drastically, and wind power is reaching high levels of penetration. The high penetration ratio (the wind power plants (WPPs) affect the power flows and hence the node voltages [5]) together with the fact, that at some moments WPPs replace

conventional generators which do voltage control, makes necessary that WPPs also contribute to voltage control.

Technical regulation requirements for wind power generation are growing at the same rate at its installation [20]. Hence, these requirements are not static, and they have upgrading versions almost yearly. A recent effort is taken in Europe (under the EWEA organization [18]) to create a uniform format for the wind power requirements, and also to create future requirements for the generators connected to the European transmission system (ENTSO-E [22]).

Grid codes in relation to wind power first became an issue from 1997 and ahead, being Denmark one of the pioneers. In the 1990s, wind turbines were passive elements solely connected in the distribution grids. The main topics were inrush current, power limitation (design on the electrical side), power quality (flicker, harmonics), power factor, and protection. The codes to be fulfilled were related to typical distribution aspects, and a typical example of such a code is the DEFU distribution code second edition in 1998.

It also can be found, that one of the first requirements for reactive power control was to set the power factor to one [23], in this case no consumption/absorption of reactive power was done. Lately, other complex power factor control schemes appeared, such as power factor scheduling according to the grid location area and time-table [24].

As wind power penetration was continuously increasing, harder requirements appeared in countries with considerable wind power generation, i.e. low voltage ride through performance (LVRT), firstly to stay connected to the grid during and after grid disturbances (time versus voltage profile), and secondly whenever it is possible the WTGs should supply reactive current to the system to support the voltage level (voltage level versus reactive current injected profile). Nowadays, the profile of non-disconnection during faults is required by most of the grid codes related to wind [25] - [28]. The main reason for that is that even if the faults and voltage disturbances can be considered as a local phenomenon, the sudden disconnection of production units will be translated to an angle and frequency problems, being these global quantities, thus affecting huge portions of the network.

Additionally, in the recent years, some voltage capability regulation has been introduced in some of the grid codes around the world. Typically, this voltage regulation is linked to the reactive power provision, which is also specified in the grid code, normally by means of a power factor requirement or a required active-reactive power chart.

Utilizing the reactive power capability regulation of the WTGs is a natural consequence to further enhance the interaction between the grid and WPPs.

However, there are some challenges related to the voltage control operation of a WPP composed of DFIG turbines. On the one hand, DFIGs can provide reactive power regulation to the grid, by means of their electronic converters, and on the other hand the DFIG converter size exhibits a clear limitation in the capability regarding reactive power injection, compared to what usually it is required. This situation, often forces the WPPs to have installed some extra reactive power compensators.

In addition, wind power plants comprise a large amount of small generation units, which need to be fully controlled and monitored; this large computational and communication effort could make the plant control to have a slow response nature according to current technologies (hundreds of milliseconds).

Usually, another inconvenient is that the PCC is located at the primary side of the main substation transformer, thus, having two serial transformer between the generator terminals and the PCC, being the amount of reactive power losses and the voltage changes at WTG stator terminals bigger than in conventional plants, which are connected to the grid by means of one transformer.

It is well known that the dynamic behavior of the voltage control is a function of the system impedance. This means that the time response, and thus the stability of the control are dependant on the system impedance. For this reason normally the control is optimized for the

maximum expected system impedance, thus avoiding instability in any case [29]. It is important to bear in mind that the SCR is changing constantly and unexpectedly.

Voltage step responses, with the same regulator but at different system strength, show that the control can not be applicable to all the systems; the weaker the system is, the greater the tendency to instability. It can be found that the weakest system has higher DC gain and wider bandwidth, consequently with faster response but less phase margin.

The communication control delay, between the wind turbine generators and the plant control, is a source of possible instability when adjusting the controllers with the wrong parameters. In most of the publications dealing with delays in controlled systems related to power plants, fuzzy-based and predictive controls were proposed [30] - [36].

Additionally, one option to achieve enhanced performance is to use a gain supervisor. The gain supervisor can promise faster response for normal system configuration without having to worry about instability for degraded conditions [37]. Such function, however, should be regarded as protection, which is milder on the power system than a trip, rather than control strategy. This protection cannot ensure a fast response during emergencies [38]. It is also noticeable that, usually, these methods use special hardware dedicated devices, and typically, involving large mathematical calculations [39] - [42].

Another peculiarity of the wind generation is its intermittent nature [43]. The power versus time profile of a WPP is quite different compared with traditional generators, most of the time it is below rated power (generally speaking, only 10% of the time above 90% of its active power). This intermittent behavior can be used to benefit the system voltage, i.e., making a reactive power provision for maximum active power injection level will offer more VAr than required most of the time. An appropriate control in the WPP should use this characteristic.

The aforementioned shortcomings and peculiarities could have an impact for grid code fulfillment, becoming a challenge when designing the voltage control of the wind power plant. All these aspects need a special consideration when trying to design the wind power plant voltage control.

1.3 Project Motivation and Objectives

The main purpose of this thesis is to investigate and design a plant voltage control for a generic DFIG wind power plant type, connected to the sub-transmission level, subjected to performance requirements extracted from different grid codes. Furthermore, this control should include features found in other AC voltage compensators.

As discussed, the design of a voltage control offers many choices, being the selection driver the lack of complexity and design fulfillment.

The main challenges are the following:

- Usually, the DFIG reactive power capability makes necessary to add reactive power compensators, which have to be integrated and coordinated with the WTGs for voltage regulation purposes.

- The plant control has to coordinate, besides the WTGs, with “slow” compensators, such as MSCs and OLTC, and also with a very fast one, such as a STATCOM.

- The control should be designed to accommodate all the possible short-circuit ratios that could be presented in the grid of consideration.

- The control should be designed to fulfill a collection of grid code requirements regarding voltage control. In particular, the control has to be designed by using simple and traditional control structures, which require low computational efforts.

- Moreover, the performance and control analysis during faults has to be included, since this can be considered as a voltage requirement during contingency conditions, thus, being important to understand the nature and capabilities of the DFIG during faults.

- Finally, a goal is to create a management system for using the remaining VAr capacity installed in the WPP. Owing to the low utilization rate of the wind turbines, and the fact that the reactive power of the WPP is sized for the worst case (rated active power), most of the time the available reactive power exceeds what is required by the transmission system operator (TSO).

1.4 Scope of the Work and Limitations

The WPP considered in the present work is connected to the sub-transmission system (this classification is country dependant, and comprises the voltage levels between the distribution and transmission system, which typically ranks between 69 kV to 138 kV). At this voltage level is where preferably small and medium generation plants are connected [1]. The size of the wind power plant to be studied is 46 MW. The layout is based on a existing project, deemed as representative for what is being installed and connected nowadays to the sub-transmission levels.

The PCC, which is the physical point in the grid where the power has to be delivered following the grid code, is considered to be in the primary side of the main substation transformer, since this is the most common location.

The slope or gain of the voltage controller is considered fixed, since it is given by the TSO and its change is a known action, in opposite to the grid impedance value, which is suffering unexpected changes. In some cases, the TSO could decide to change the predefined slope to another value, but since it is a known process, the controller can be adapted with new constants according to the new slope gain.

It should be noted once again, that the node voltage is a local quantity, as opposed to frequency, which is a system wide quantity. It is, therefore, not possible to control the voltage at a certain node from any point in the system, meaning that, the voltage of certain node should be controlled by the reactive power compensators located in the nearby area. Based on that, and for the sake of a generic approach, the network which the WPP is connected with is simplified, and represented as a Thevenin impedance [44], [45].

The interaction between the voltage controller and active power transient events is beyond the scope of this work. Hence, power system stabilizer and frequency excursions, which are related more to the nature of the control and flowing of active power into the system are not included.

Voltage collapse and islanding phenomenon are not considered either. The first issue is a phenomenon related to the lack of reactive power, linked to the active power flow, and it deals with the generator dispatching, switching and load shedding, and planning for the reactive power provision, this situation is related to steady-state load flow of the area of concerning [46] - [47]. Looking at the WPP from the point of view of thermal limits or steady-state voltage stability, WPP is like any other type of power generation, hence the same approach than traditional studies can be applied [5].

The islanding phenomenon is more related to the protection systems rather than control. It is of utmost importance to ensure fast, reliable and well coordinated fault current interruption in the connecting network, in the collector bus, as well as within the wind turbines.

Besides power system faults, characterized by a primary system fault current, the protection system also has to detect other types of abnormal conditions, such as high or low voltage, high or low frequency, out of synchronism, island operation, etc. Some of the protection systems have to be set according to what is specified in the grid codes, specially the protections related to over-/undervoltage and over-/underfrequency.

In general, and according to the relevant grid code, the WTGs and the WPP shall have such tolerance towards variations in voltage and frequency that they can handle the most common types of grid fault without being tripped or damaged. Thus, the protection schemes are out of the scope of this work.

Finally, the WTG control is based on giving priority to P over Q during normal voltage grid conditions (voltage variations of ±0.1 pu). Hence, the limits of the injected Q follow the programmed P-Q chart, and only during faults Q has been given priority over P.

1.4.1 Simulation Tools and Models

The selected simulation software for investigating the electrical performance is PSCAD (also known as PSCAD/EMTDC [48]). Used for transient studies, PSCAD is a powerful time domain electromagnetic transient simulation environment and study tool. It solves the power system differential equations with trapezoidal integration techniques with fixed time step. The software was developed by the Manitoba HVDC Research Centre. PSCAD allows programming modules in Fortran code, which permits to interface with discrete models created for control purpose.

The crucial models are the WTG, STATCOM, MSCs, OLTC and plant control. The DFIG WTG model is already known in the literature and will not be explained here, except what is related to voltage/reactive control. The WTG model includes all mechanical and electrical components that have been considered representative in the literature to study this kind of phenomenon, such as: drive train, aerodynamic curves, pitch control, power and speed control, generator, converters, DC-link, and their controls. The cables, over-head line (OVL), generator, and transformer models are taken from the PSCAD library. The STATCOM model is quite similar to the grid-connected converter part of the WTG.

No aggregation for representing the WTGs has been used, except when it is mentioned.

For frequency domain response, and more advanced mathematical analysis, MATLAB has been used.

The WTG model has been validated with some field tests, where the reactive control implemented in the simulation was modeled according to the existing WTG. It is expected that the performance validation can be extrapolated to the proposed reactive power control.

1.5 Outline of the thesis

The organization of the thesis and some of the original contributions are presented in the following points. The list of the author's publications is given in the publication section (last chapter).

The introduction chapter is followed by the main body thesis.

- Chapter 2: A brief overview about voltage control and grid code requirements is presented, which will be used as design requirements. Additionally, the control type for the plant is discussed.

- Chapter 3: Some generic characteristics of the main wind power plant components and their characteristics, regarding voltage control and reactive power are presented. The control candidates are presented in this chapter.

- Chapter 4: The stability and control analysis of the WPP is studied, also two different structures for voltage control are analyzed, i.e. distributed and centralized [A.1.]. To do this study, the WTG is linearized and represented as transfer functions; this work has been published in [A.6.]. Finally, a selection of the distributed control is done, based on lower SCR dependency and lower time response than the centralized control.

- Chapter 5: The interactions between different voltage controls using slope control are discussed, to conclude with the proposal of a new design for the WTG and plant voltage controls, which are designed according to the previous discussion. Fully fulfillment of the design requirements within the whole possible SCR range, which includes the contingency level, has been achieved [A.8.], [A.9.].

- Chapter 6: The integration in the system of the STATCOM, MSCs and OLTC are presented. In order these equipments get integrated with the plant control, a new dispatcher strategy for the STATCOM and a new control philosophy for the MSCs, are proposed. Moreover, the OLTC which is running independently of the plant control is improved by a new control method [A.7.].

- Chapter 7: Some validation tests for the WTG and grid models are shown. All proposed control designs are validated through extensive simulations, which are followed by an overview of the simulation results for small grid transients.

- Chapter 8: Describes the basic of the DFIG performance during faults and its similarities with conventional SGs, this work has been published in [A.5.]. Additionally, short-circuit current comparison between different generators is shown in [A.3.]. To achieve high reactive current injection at PCC during severe faults, a new control is proposed, which is based on off-line data of the WPP. This new control has been published in [A.4.]. Finally, the plant control and operation during faults are analyzed.

- Chapter 9: WPPs are perfect candidates to implement a VAr reserve due to their low ratio of produced energy per installed power. The concept of VAr reserve for a WPP and two different ways of implementing it are proposed. This work has been sent for publication [A.2.].

- Chapter 10: The extracted relevant conclusions and proposals for future research are summarized.

Chapter 2

Voltage Control, an Overview

The purpose of this chapter is to introduce and discuss the basics of the voltage control, including the selection of the plant voltage control type. Additionally, the control design requirements, which are a collection of the most demanding grid code requirements found in the literature, related to voltage performance, are introduced.

2.1 Introduction

In an AC electrical system, the voltage is controlled by actuating in the reactive power flow, whereas the frequency is actuated by the active power balance between the generators and loads in the system. Being a mayor difference between them, that voltage control is a local phenomenon, and frequency is a system global wise variable.

Replacing conventional generators with their respective automatic voltage regulator (AVR) makes necessary to increase the demands for WPP regarding voltage control. With increasing penetration of wind power generation, the requirements for the connection of wind power plants to the electrical grid are defined by the new and emerging grid connection codes.

The grid connection requirements vary in different parts of the world, but they share common aims, such as permitting the development, maintenance and operation of a coordinated, reliable and economical transmission or distribution system.

Generally, the new requirements demand that wind power plants provide ancillary services to support the network in which they are connected [26] - [34].

The performance during faults has been considered critical, and is quite related with the transient stability of the system. A local phenomenon such a grid fault can be translated to a global problem (frequency stability). For this reason, fault performance was considered earlier by the TSOs. The performance during faults can be classified as a kind of voltage regulation that has to be applied during severe transients.

The selection of the plant voltage control law is imposed by the TSO in most of the cases, being the proportional control one of the most demanded. One of the main reasons for being the proportional control the most preferred is given in the following sections, i.e., it allows paralleling generators, with individual voltage controllers, without hunting phenomena or instability.

2.2 Sign Convention

The sign convention applied during the whole work for the flowing power is as follows: reactive power injected by the WPP (capacitive) is considered positive, and injected active power (generation) is also considered positive.

When using d-q quantities, the q axis is in quadrature with the voltage vector and the d axis is aligned with the voltage vector. Thus, the q axis is linked with reactive power and d axis with the active power.

2.3 Plant Voltage Control

Figure 2.1 represents a simplified WPP connected to the grid. For the sake of simplification the WTGs are represented as an aggregated single unit (WTG). Z_{WTGT} is the wind turbine transformer impedance; Z_{WPPT} and Z_{GRID} are the wind power plant transformer and the grid impedance, respectively. The grid impedance indicates the strength of the system, and is the inverse in [pu] of the SCR, which is the ratio between the installed power and the grid short-circuit capacity.

The WTGs are controlled by their own "WTG control", which is commanded by the "Plant control", which allocates the outer control loops, including the voltage control. As it can be seen in Figure 2.1, the plant control feedbacks are the measurements of the CTs and VTs located at the PCC.

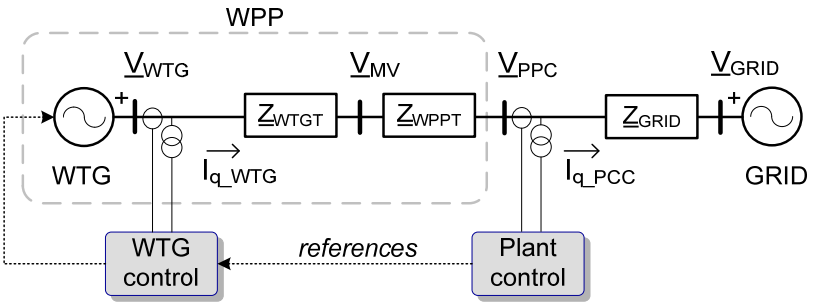

Figure 2.1. Simplified system single line diagram overview.

Basically, two main control concepts can be used for the plant AVR, i.e. a proportional (slope control) and a control with proportional and integral components (PI control). When choosing the voltage control for the plant, attention should be drawn to the use of the controller with integral action, since the SCR, and the impedance values between the generator terminals and the PCC, will dictate the validity of this control, i.e. high SCRs could drive to a constant saturation of the controllers, and low SCRs could induce high over-/under-voltages at generator terminals.

To represent the operational area of a generic PI voltage control, it is considered that the voltage at the PCC can be moved at least 5% of its rated value, by the reactive power injection of the WPP, and the voltage at the generator terminals can not be higher/lower than 10% of its rated value. Hence, by neglecting the impedance resistances and considering a constant grid voltage, the following equations can be obtained.

$$V_{PPC} \approx I_q X_{GRID} + V_{GRID} \Rightarrow \Delta V_{PPC} \approx \Delta I_q X_{GRID} \geq \overbrace{\Delta V_{PCC\_\min}}^{5\%} \tag{2.1}$$

$$V_{WTG} \approx I_q (X_{WTGT} + X_{WPPT} + X_{GRID}) + V_{GRID} \Rightarrow \Delta V_{WTG} \approx \Delta I_q (X_{WTGT} + X_{WPPT} + X_{GRID}) \leq \overbrace{\Delta V_{WTG\_\max}}^{10\%} \quad (2.2)$$

Therefore, the following inequality is obtained, which can be used to represent the operational are of a generic PI voltage control.

$$(X_{WTGT} + X_{WPPT}) \leq X_{GRID} \left(\frac{\Delta V_{WTG\_\max}}{\Delta V_{PCC\_\min}} - 1 \right) \quad (2.3)$$

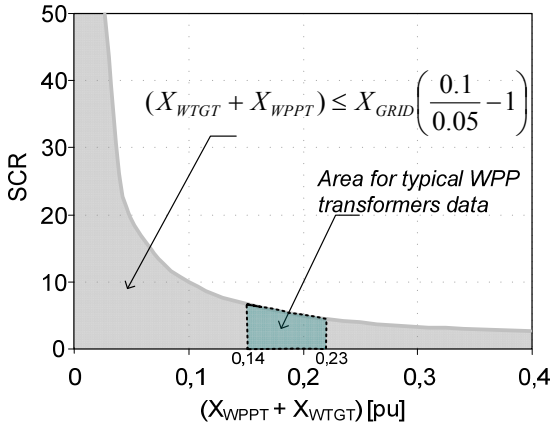

Figure 2.2. Operational area of a pure PI control for voltage control.

Figure 2.2 shows the PI control operational area (grey area) where the conditions, previously listed, are fulfilled. Moreover, considering typical transformer impedance values for WTGs (from 0.06 to 0.09 pu) and WPPs (from 0.08 to 0.14 pu), the possible operational area is reduced to the green area of the figure. It can be seen how a voltage controller with a pure integral controller is only recommended for wind power plants with low SCRs.

Finally, PI for voltage control is not very commonly used in power system due to its flat characteristic, see Figure 2.3, which at some extend could present hunting phenomenon if other plants are controlling voltage nearby.

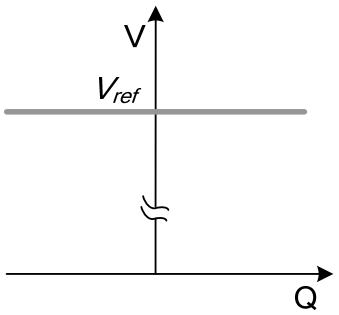

Figure 2.3. Characteristics of the PI voltage control.

2.3.1 Plant Voltage Control: Slope and PI with Line Drop Compensation

Taking into consideration the aforementioned limitations, a pure PI will unlikely be used as a voltage control scheme for WPP connected to strong grids*; however, the PI can be used in combination with a feedback of its output (PI with line drop compensation, see Figure 2.4-(b)), which offers a similar response in the frequency of interest than a proportional control (Figure 2.4-(a)). See the appendix A.

These two schemes (Figure 2.4-(a)-(b)) are the predominant in power system for voltage control, as it can be observed in the IEEE std. [35].

Therefore, in the following sections of this work, PI with line drop compensation control could be used instead of slope or proportional control indistinctly. See the equivalence between these two controls in the appendix A.

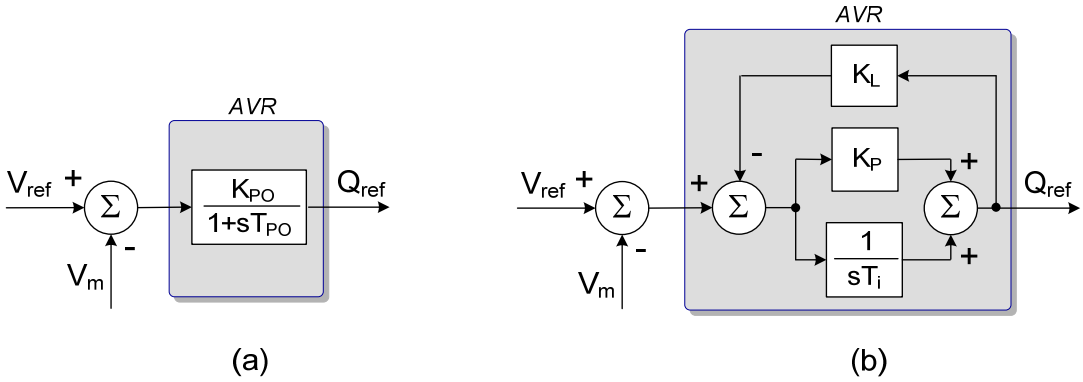

Figure 2.4. Case (a): Slope or proportional control. Case (b): PI with line drop compensation.

In Figure 2.4-(a) K_{PO} is the gain of the voltage controller, and defines the ratio between the measured voltage and the injected Q (see Figure 2.5), and T_{PO} should be used to respect the bandwidth of the inner loop controllers.

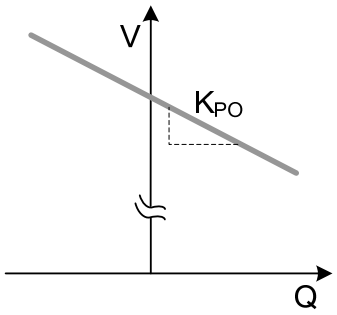

Figure 2.5. Characteristics of the slope control.

2.3.2 Slope Control Response

Figure 2.6 can be used as an illustrative example of the slope control performance. The grid voltage is stepped from 1 pu to 0.9 pu, and back to 1pu.

* The connection of a plant to the grid can be considered weak, when the power of the plant is at least 15% of the short circuit power of the grid [5].

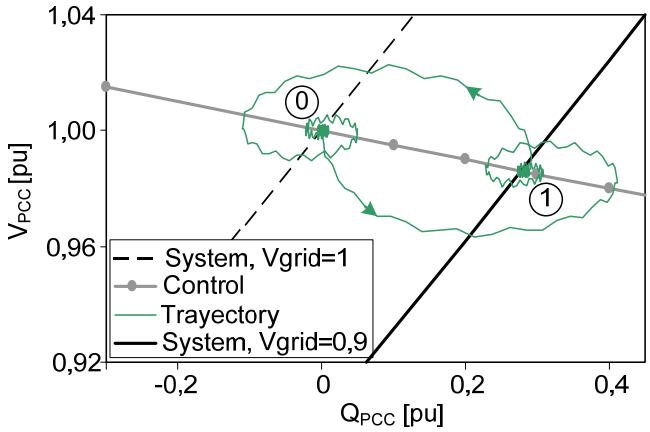

Figure 2.6. Characteristics of the slope control. X_{WPPT} +X_{WTGT}=0.31pu and K_{PO}=20 pu.

Figure 2.6 shows the equilibrium point (point 1) after stepping down the grid voltage, and the equilibrium point (point 0) when setting the voltage of the grid to 1 pu again. The horizontal axis shows the magnitude of the reactive power and the vertical axis displays the voltage. The equilibrium points are located at the intersection of the system and slope control characteristics. The reactive power trajectory during the transient event from point 0 to 1 and from 1 to 0, is depicted with a green line.

Figure 2.7, exemplified the aforementioned problems about the influence of the SCR when doing voltage control. The following figures show the performance of the slope control depicted in Figure 2.4 (tuned for a SCR of 25) for two different SCRs. The voltage of the grid is stepped down from 1 pu to 0.9 pu, at time equal to 10 s.

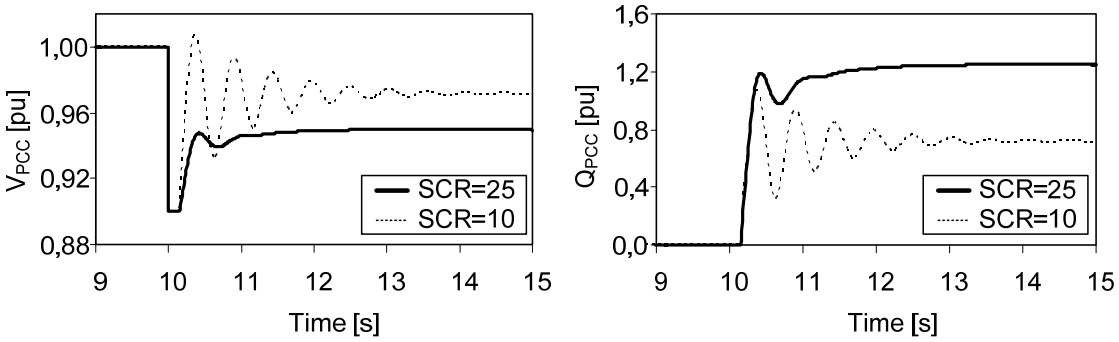

Figure 2.7. Slope control performance under different SCRs.

It can be observed how the performance of the system is degraded when the SCR is different to what it was planned.

2.4 Basics of Voltage Control

Figure 2.8 can be used to understand the nature and peculiarities of the voltage control and reactive power flow. In this figure, two generators (G_1, G_2) and one load are connected through lines.

The injected reactive power from the node *i* to the node *j*, can be expressed as (2.4). Often this term can be simplified, by neglecting the resistances connecting the nodes, i.e. the X/R ratio is very high for transformers and lines in the transmission and sub-transmission levels [49].

$$Q_{i\to j}=\frac{V_iV_j\left(X_{ij}\cos(\delta_j-\delta_i)-R_{ij}\sin(\delta_j-\delta_i)\right)-X_{ij}V_i^2}{X_{ij}}\underset{R\to 0}{\approx}\frac{V_iV_j\left(\cos(\delta_j-\delta_i)\right)-V_i^2}{X_{ij}} \tag{2.4}$$

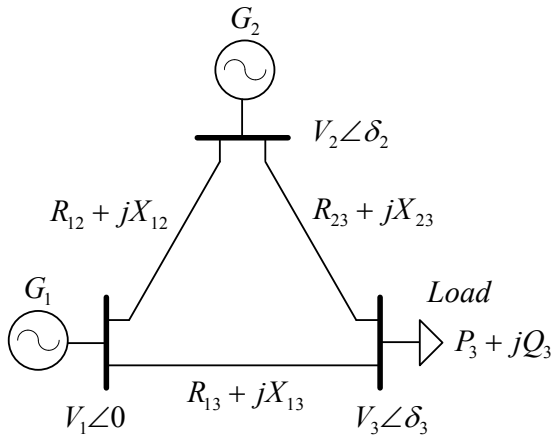

Figure 2.8. Simple grid for reactive power exchange study.

Since the angle change across the lines are usually small, cos(*Δδ*) can be approximated by 1, thus, being obvious that the reactive power flow of the system is controlled by the difference in the voltage magnitudes, or vice versa, the voltage magnitudes are controlled by the reactive power flow.

It should be noted, that there is a coupling between the active flow in the system and the voltage magnitude change. This can be appreciated by looking at (2.5), which represents the voltage drop across the impedance Z_{ij}. For the same reasons given previously, the voltage drop can be simplified and represented only in terms of reactive power transfer.

$$\underline{\Delta V}_{ij}=\frac{R_{ij}P_{ij}+X_{ij}Q_{ij}}{|V_i|}+\underline{j}\frac{X_{ij}P_{ij}-R_{ij}Q_{ij}}{|V_i|}\underset{\Delta\delta\to 0}{\approx}\frac{R_{ij}P_{ij}+X_{ij}Q_{ij}}{|V_i|}\underset{R\to 0}{\approx}\frac{X_{ij}Q_{ij}}{|V_i|} \tag{2.5}$$

The reactive power flow absorbed by the load (Q_3) can be represented as follows:

$$Q_3=-Q_{1\to 3}-Q_{2\to 3}+Q_{losses} \tag{2.6}$$

$$Q_3=-\frac{V_1V_3\cos(\delta_3)-V_1^2+(V_1-V_3)^2}{X_{13}}-\frac{V_2V_3\cos(\delta_3-\delta_2)-V_2^2+(V_2-V_3)^2}{X_{23}} \tag{2.7}$$

Easily, it can be noticed how the reactive power injected from the different generators to the load is inversely proportional to the magnitude of the impedance that is linking them to the load node. The closest generators to the event/load will supply most of the reactive power demanded.

For the sake of illustration, only small changes in the voltage generator terminals and small angles difference between nodes are considered. Based on that, and for a change of 5% in V_3 (load node), Figure 2.9 is depicted, which shows the reactive power injection from node *i* to *j,* as a function of the node impedance which connects them.

The different curves show the generator performance when using a proportional controller with different control gains (K_{PO}), see control in Figure 2.4. As it was expected, the higher the gain the bigger the Q injection is. Moreover, it can be appreciated how the longer the distance to the load node, the lower the impact in the generator is. It can be concluded, that voltage disturbances in the nodes can be considered as a local effect.

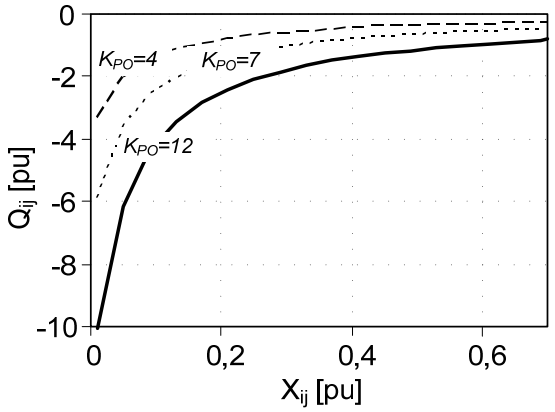

Figure 2.9. Q injection according to the controller gain and connection impedance.

This is especially clear in radial grids, whereas in meshed grids the addition of lines between nodes tend to decrease the node connecting impedance, making voltage events less local than in radial grids.

2.5 Grid Code Survey

WPP Voltage control requirements are specifically mentioned in several grid codes, but in most of them is considered as a "should" or a "possibility" and not as a "must", moreover, no details about this specification and/or the application description is given, e.g., Nordel, Ireland, France [50] - [52]. However, in some of them some specifics details about the expected performance are mentioned [24] - [28].

TABLE I
DESIGN REQUIREMENTS FOR VOLTAGE CONTROL

Parameter	Value	Unit
Overshoot	0.050	[pu]
Band for settling time	0.025	[pu]
t_d	0.200	[s]
t_r	1.000	[s]
t_p	Not defined*	[s]
t_s	2.000	[s]

The most demanding indices related to voltage control are extracted from different grid codes, and compiled in Table I.

The indices listed in Table I will be used in the following sections as the control design criteria. The referred indices are used to evaluate the measured output at the PCC. Step response indices are classified following IEEE standard [53]. See appendix A.

Small-signal performance measures provide a means of evaluating the response of the closed-loop excitation control systems to incremental changes in system conditions. In addition, small-signal performance characteristics provide a convenient means for determining or verifying excitation system model parameters for system studies. Small-signal performance may be expressed in terms of performance indices used in feedback control

* None of the examined grid codes make any mention to this parameter.

system theory. For a time response output, the associated indices of interest are the following: rise time (t_r), overshoot, settling time (t_s), and delay time response (t_d) [53].

When tuning the voltage regulator, an improvement to one index will most likely be to the detriment of other indices.

The reactive power provision for the WPP is to be considered as a voltage requirement, since, as it was mentioned, the voltage control will be actuated by the reactive power. The reactive power capability offered by the plant is often translated in a requirement in terms of power factor or P-Q charts. The most typical requirement for power factor is ± 0.95. But this requirement is quite dependent on the specifics of the grid, being cases where 0.90 capacitive is required, e.g., Canada-CanWEA, Germany-VDN [34].

Even though, the system has voltage controllers at several locations in the network, it is not possible to offer an uniform and constant voltage value in every node, as it was explained, voltage variation are of local nature. For this reason, usually the steady state node voltage is allowed to deviate from rated a maximum value; the most common band is ± 10%. It can be considered normal operation if the voltage level is inside this voltage range.

Regarding the wind power plant voltage control, the most demanded control scheme is the slope control, with a slope gain ranking from 2% to 25% [24]. A slope of 4% has been considered for the rest of the work, since this one is explicitly mentioned to be the preferred in NGCE [26].

Performance during faults was introduced much earlier than voltage control, since it is related to a possible massive loss of wind production at the same time, making possible the whole system to collapse. What it is most demanded is a voltage profile for non-disconnection; see Figure 2.10, being this profile quite country dependant.

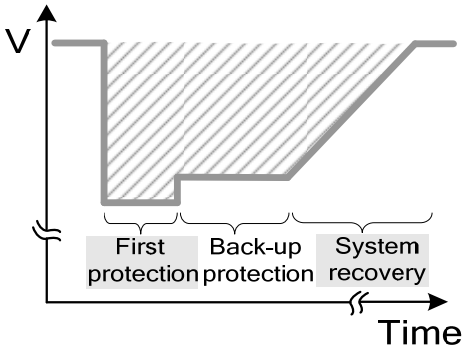

Figure 2.10. Non-disconnection profile.

In some cases, it is also demanded that the WPP supplies reactive current according to the severity of the fault. This injection helps the system in pushing up the voltage during the fault. The current injection level requirement during faults ranks from very high values in some countries, e.g., 0.9 pu at PCC [54], to other countries where it is not clearly specified, just it is mentioned that the WPP should collaborate as much as possible, e.g. [26].

2.6 Conclusions

The voltage plant control scheme is selected for the rest of the work, which is based on a slope control. Besides its characteristic, it is the most demanded scheme by the TSOs. Hence, being the selected plant AVR a proportional controller. Additionally, the requirements that apply for voltage control, including performance during faults (also called LVRT), are shown. These are collected from different grid codes and will drive the control design.

Chapter 3

Wind Power Plant Components

In this chapter, it is introduced an overview of the characteristics of the main WPP components involved in the voltage/reactive power control. The WPP is composed by many more components than the ones mentioned here, but the main focus of this work is to address the voltage performance, therefore only the main components that are part of the V and Q control are shown. Additionally, the single-line electrical diagram, communication layout of the selected WPP, and the control candidates are presented.

3.1 Introduction

The most common WTG used in the industry so far, is based on the DFIG type [55]. This type of WTG offers high output controllability with low amount of power converter. The DFIG converters only need to handle a fraction (0.25 – 0.30 pu) of the total power to achieve full control of the generator [56]. On the other hand, this low amount of installed power converters is the cause of lacking capacitive reactive power injection at high active power levels, which usually makes necessary the installation of extra reactive compensation equipments at substation level.

The most common reactive compensation equipments used in WPPs are the MSCs (static compensation) and the STATCOM (dynamic compensation) [57] - [59]. Moreover, the WPPs can include an OLTC system in the substation transformer to keep the MV of the plant close to its rated value, independently of the grid voltage and wind conditions [60], [61]. All these elements should be coordinated by the plant control to avoid counteractions.

3.2 Doubly Fed Induction Generator

The variable speed DFIG, see Figure 3.1, allows full control of generator active and reactive power using the rotor-connected frequency converter. Operating both with sub- and super-synchronous speed, the power can be fed both in and out of the rotor circuit.

The rotor-connected converter can employ various power dissipation solutions during severe transients, sometimes referred to as an active crowbar, which is located at the rotor terminals [62], [63], or as a chopper in the DC-link, R_{ch} in Figure 3.1.

The grid converter is used to regulate the voltage level of the DC-link, whereas the rotor converter regulates the P and Q at the stator terminals.

The WTG control calculates or receives power references from an external controller, (P_{ref}, q-$axis_{ref}$). Usually the P_{ref} is calculated by the speed control of the WTG, which also calculates the pitch angle reference (β_{ref}).

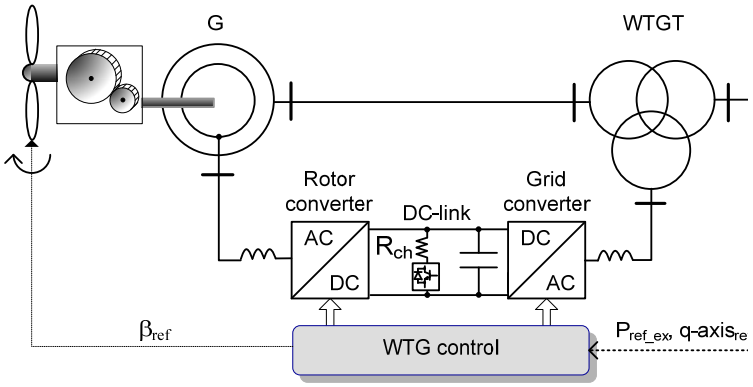

Figure 3.1. DFIG simplified single line electrical diagram.

The q-axis control loop could have different forms according to the reference sent by the plant control. The most common is that q-$axis_{ref}$ is set as "Q_{ref}" [64], [65]. Hence, being the WTG q-axis outer control a reactive power control (AQR). However, it can also take the form of a "V_{ref}", being the control loop a voltage control (AVR) [66], [67].

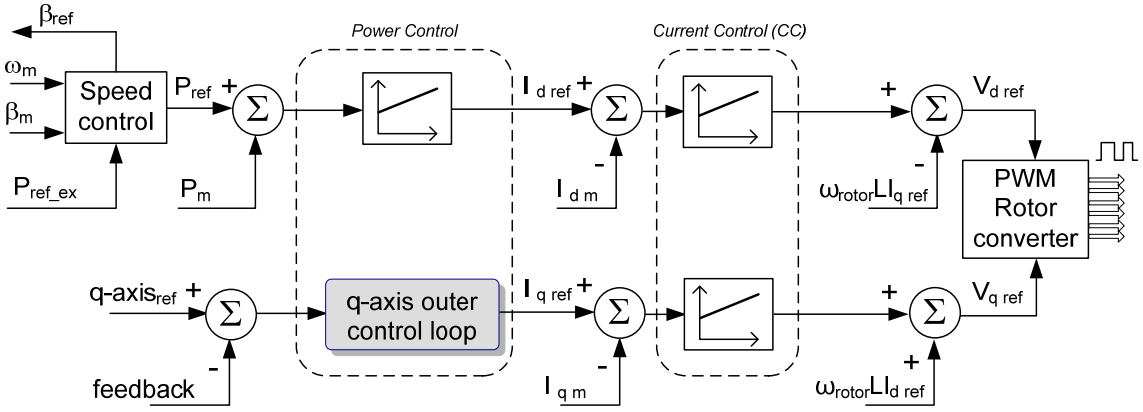

Figure 3.2. Simplified DFIG control diagram for the rotor-connected converter.

The simplified control of the rotor converter is depicted in Figure 3.2, where the active and reactive power are controlled using the d and q axis respectively [68] - [70].

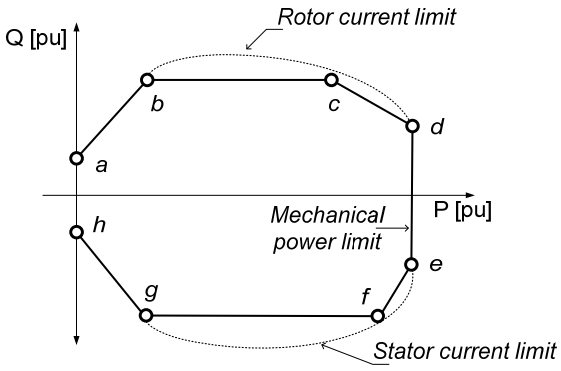

Figure 3.3. P-Q DFIG chart.

Figure 3.3 shows the P-Q chart of a DFIG machine. The P-Q chart programmed in the WTG is a consequence of the linearization of the WTG physical limits, i.e. mechanical and thermal (dotted lines in Figure 3.3), [71].

The control of the grid converter is not depicted here, since in this thesis it is not used for reactive power injection. It is used for keeping the DC-link voltage constant, by using a traditional d-q control aligned with the grid voltage.

3.3 Static Compensator

Flexible AC transmission systems based on voltage-source converter, such as STATCOM, are found increasing utilization in power systems because of their ability to provide improved performance for voltage support [72] - [77]. The single line diagram of the STATCOM for reactive power supply to the system is shown in Figure 3.4, where V_{LV} is the voltage of the bus-bar which is connected to, and V_{ST} is the controllable output voltage.

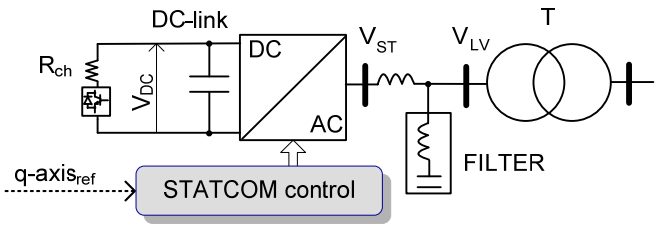

Figure 3.4. STATCOM simplified single line electrical diagram.

The DC-link voltage (V_{DC}) and the reactive power injection can be regulated by the d-axis current (I_d) and the q-axis current (I_q) respectively. The overall control scheme consists of two cascaded PI control loops, similar to what it is shown in Figure 3.2.

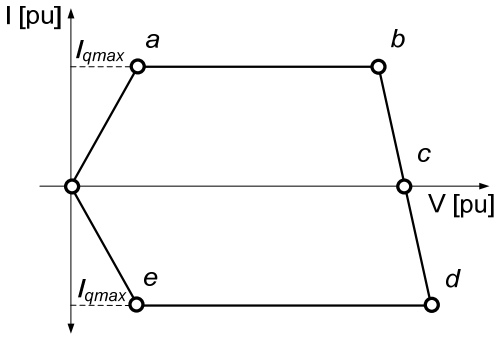

Figure 3.5. V-I STATCOM chart.

The outer control loops regulate independently the reactive power injection and the DC-link voltage of the STATCOM; whereas the inner current control loops generate the d-q voltage references [76], which are used by the PWM module to create the gate control signals to the converter to generate the desired voltage at the AC-side of the converter.

The STATCOM can be operated all over its full output current range even at very low system voltage levels. In other words, the output current can be maintained almost independently from the AC system voltage. The Q generation or absorption changes linearly with the system voltage. Figure 3.5 represents the typical V-I chart for a STATCOM [75]. Basically, the operation limits are defined by the maximum apparent current.

3.4 Mechanically Switched Capacitor Banks

The MSCs, used in this document, are to be connected to the MV bus-bar of the WPP.

The advantages of using MSC compared to other reactive power compensation equipment are: reasonably priced, less complex and fewer components in the design, and the disadvantages are: its output depends on the voltage level, the number of switching operations is limited to a few times per day, and the time between switching is rather long, thus it can be classified as a slow time response compensator.

The MSCs are connected to the MV bus-bar via a disconnector, a circuit breaker and a load switch. Additionally, MSCs include: a current limiting device, which is most likely a reactor, and a discharging resistor.

3.5 Remote Terminal Unit

Usually, a substation RTU monitors the field digital and analog parameters received from the different elements composing the substation, and transmits relevant data to communicate to other RTUs and control centers, as well as it is able to execute simple supervisory tasks related to protection. The gathering of direct-wired process information and its transfer to a higher level control system is one of the major tasks of the remote control application; RTUs usually communicate with other RTUs or dispatcher centers. The concentration of several functions on a central communication gateway reduces the number of required communication lines to higher control level. The RTU, used in this WPP, monitors the transformer tap position and the status of the capacitor breakers and contactors, and receives the switching commands to the capacitors, sent by the WPPC. The RTU will transfer these commands to the capacitor switches when the security and integrity checking has been done [78].

3.6 On-Load Tap Changer

OLTC system is a very common and effective tool for steady state voltage control. This system is considered a slow device, since it is actuated mechanically, and frequent regulations accelerate the wear of the moving parts. Basically, the OLTC modifies the ratio winding of the transformer [79], [80].

Since the allowed PCC voltage deviation is ± 10%, it is clear that an OLTC system will help avoiding the violation of the maximum and minimum generator voltage levels. Being this the reason why usually wind power plant transformer includes an OLTC and its voltage control. The OLTC voltage control commands the transformer tap changer, so that the controlled voltage, in this case the medium voltage (the OLTC measurement sensors are located at medium voltage side of the transformer) is practically constant, independently from the wind speed level and grid voltage conditions. An important requirement for tap control is, however, not only to keep the voltage profile but also to suppress the frequency of operations to the lowest possible (similar requirement than the MSCs). A compromise is needed, since these requirements basically contradict each other; frequent operations are usually needed to perform a high quality of voltage regulation.

3.7 Wind Power Plant Control

The wind power plant control (WPPC) receives the references and feedback (measurements), and outputs the turbines and STATCOM set-points, as well as the capacitor banks switching commands. This plant control includes a measurement device (see appendix B), which senses the currents and voltages at the PCC, and provides the feedback signals for control. This device samples at very high frequency values the output of the CTs and VTs, located at the PCC. This meter processes the signals by first calculating one cycle rms value of the signals, and then filtering for anti-aliasing. The plant control also includes, a dedicated computer which allocates the control and dispatcher algorithms, and a communication hub. This communication hub collects all the feedbacks, packs and sends all the necessary references for the correct operation of the WTGs, STATCOM and capacitor banks, using for that purpose the communication WPP Ethernet network and specific protocols.

The main purpose of the WPPC is to maintain the output of the plant as close to the required settings as possible. The basic method for maintaining the output is by means of a feedback controller. A feedback controller compares the actual production with the requested production, and instructs the controllable units by means of new set points.

The core control algorithms for a typical power plant are the active and reactive power loops, which can be actuated by different controllers: Q loop can be actuated by either a power factor, either a reactive power or a voltage control, and P loop can be actuated by either a frequency or an active power control. In Figure 3.6 voltage and frequency controls are used, which create the WTG references for the q and d axis, respectively.

Additionally, a grid fault detection logic scheme can be included (State Machine), which can be used to trigger the desired performance during faults (Fault mode), see Figure 3.6.

The following figure represents the simplified diagram of a wind power plant control.

The communication module represents the packing and protocol writing functions when sending the references, this action introduce delays in the system according to the selected hardware.

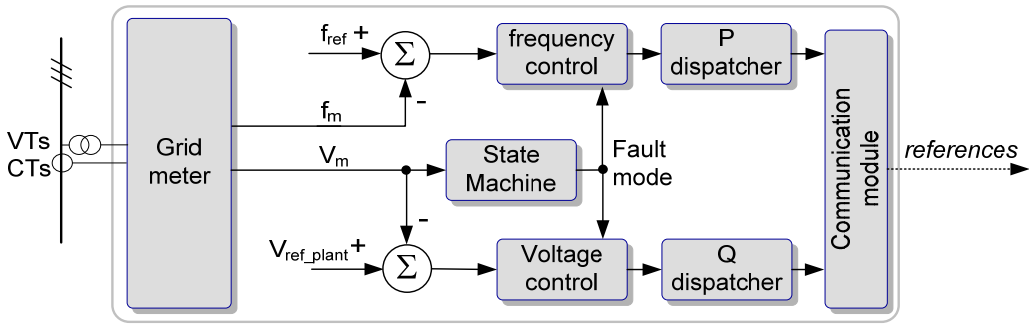

Figure 3.6. Wind power plant diagram overview.

3.7.1 Wind Power Plant Voltage Control

The voltage plant control used in this work is based on a proportional controller, also called slope control. This voltage controller causes the injection of reactive power proportionally to variation of voltage levels. Normally, the gain of the voltage controller (K_{slope}) and the plant voltage reference (V_{ref_plant}) are defined by the TSO.

The plant control gain, which is the inverse of the slope, can be defined as (3.1).

$$K_{slope} = \frac{1}{Slope} = \frac{\Delta Q_{PCC}}{\Delta V_{PCC}} \tag{3.1}$$

The references calculated by the plant voltage control to be sent to the dynamic reactive power actuators (WTGs and STATCOM), basically can be based on two forms:

- Reactive power references: if the plant control sends reactive power references, the WTGs should have implemented, as an outer q-control, a reactive power control (AQR).
- Voltage references: in this case the WTGs should have implemented a voltage control (AVR), to accommodate these references.

These two main concepts are based on the idea of a central and distributed (similar to the secondary voltage control scheme) voltage control systems, respectively.

3.8 Wind Power Plant Configuration

This section presents the single line electrical diagram and communication network of the WPP; moreover, some control options for the plant and WTG are presented.

3.8.1 Wind Power Plant Layout

The electrical single-line diagram of the considered WPP, with all the main components, is given in Figure 3.7.

In this figure, it can be seen how the main components are linked with a dotted line, representing the communication plant networks. This communication link is used by the plant control, among other things, to command the operation of the MSCs (On/Off), WTGs and STATCOM (References). The wind power plant is composed by 23 DFIG WTGs, which are distributed in 4 feeders, having: 6, 7, 6 and 4 units respectively.

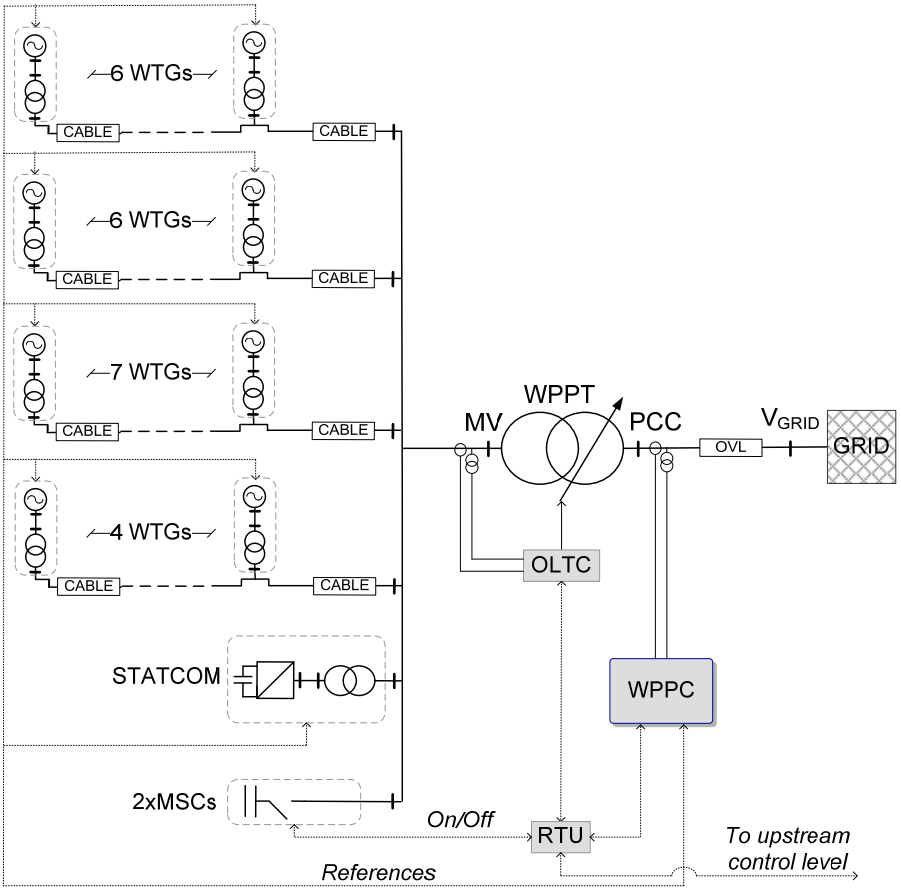

Figure 3.7. Single line diagram of the generic WPP.

These WTGs are connected through a step-up transformer to the collector bus (MV) by means of subterranean cables. The collector bus voltage is stepped up to the high voltage level, by means of the substation transformer (WPPT).

The main substation transformer includes an OLTC which is controlled locally. The high voltage terminal of this transformer is connected to the next substation through an overhead line (OVL). Upstream of this point, the whole electrical system is reduced to an equivalent grid, defined by its SCR and X/R.

3.8.2 Voltage Control Configuration

Following to what was exposed, several permutations according to the possible configurations of the plant and WTG control are presented. Every option offers different characteristics regarding time response and SCR sensitivity. The selection of one control configuration is needed and will be discussed in the following chapters.

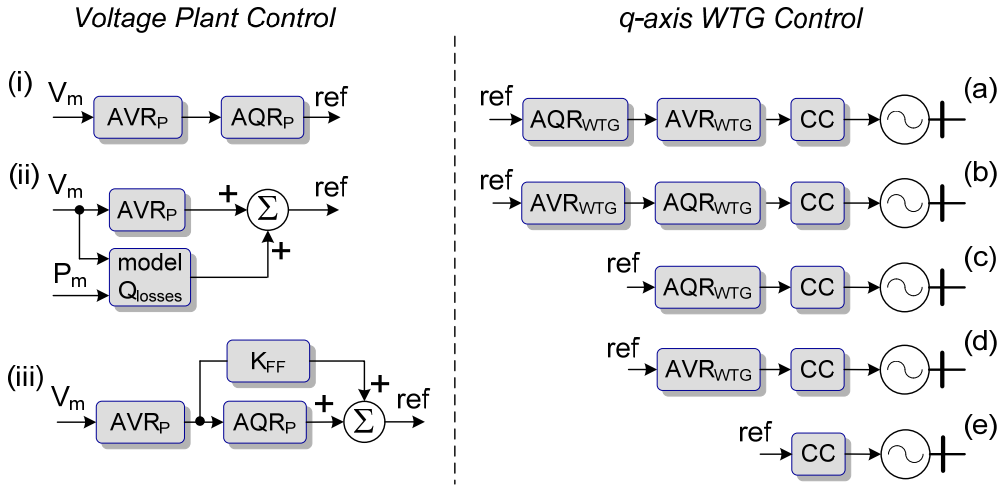

Figure 3.8. Candidate configurations regarding plant and WTG controls.

The scheme control options that include as a first WTG outer control loop an AVR, can be called distributed voltage control (options including (b) and (d) structures), whereas the other options can be classified as centralized voltage controls (options including (a), (c) and (e) structures).

It should be noticed that the voltage plant control has to compensate for the internal reactive power park losses, for such purpose option (i) includes an AQR, also this can be achieved by using a model of the park (ii), this model could be as simple as a quadratic function which can be adjusted by the voltage and the injected active power level at PCC. A feed-forward can be added to increase the time response of the control (iii).

Some of the previous schemes ((c) and (d)) have already been presented in the literature, but under different plant control concepts to what is considered here. Whereas most researchers are concerned with time delay reduction, none have presented the control selection according to the sensitivity to the grid impedance, [64] - [67], [81], [82], where the right combination of the plant and WTG control may play an important role. The sensitivity and robustness for different grid impedances are an important matter that should impact on the selection of the control scheme, and are at least as important as grid code fulfillment.

3.9 Summary

In this chapter it is presented the main components of a typical WPP related to reactive/voltage control. The chosen WTG technology is the DFIG, since it is the most extended in the market and used so far.

The main WPP components regarding voltage/reactive control are presented, which basically can be grouped according to their time response in: dynamic (with fast response), i.e. WTGs and STATCOM, and static (with a slow response), such as the OLTC and the MSCs.

Finally, the possible voltage control candidates for the WTG and plant, based on distributed and centralized concepts, are shown.

Chapter 4

Wind Power Plant Control Analysis for Small Disturbances

This chapter is devoted to create linear models of the WPP components for small signal voltage control analysis. Small signal analysis, using linear techniques, is suited for analyzing stability and control problems. This type of study gives valuable information about the stability margin of the system according to its gain. Based on these studies, preliminary design of the plant control can be done. Additionally, these simplified models can be used to evaluate the selection of the voltage control strategy to be used in the WPP, i.e., distributed or centralized.

4.1 Introduction

It is known that the voltage performance of a power plant depends on the grid impedance. Additionally, the stability of the controllers depends upon the grid impedance as the grid impedance is serial addition to the other main transformers. The driving point impedance at fundamental frequency, as viewed from the PCC location, is an important parameter in the voltage control loop since it determines how much the voltage can be changed when a certain amount of reactive current is injected to the system.

It is clear that for high system gains (small slope and SCR values) the system becomes more difficult to be controlled, moreover, the delays in the communication processes reduce the control stability margin when the gain of the system increases.

The tuning objective of the control, among other things is to achieve a response time of less than 1 s, an overshoot below 5 % (see Table I), and even more important to preserve stability for all realistically probable network conditions [38]. Therefore, the voltage regulator settings should be dictated by the most limiting operating condition, such as the system configuration with the lowest short-circuit power (contingency condition) [75]. However, this tuning may cause relatively long response for higher SCRs (normal operation), where the best performance of the system is most required. Delay time is a critical parameter, since it can be linked to the control hardware and software.

An appropriate tuning and selection of the voltage control allow the fulfillment of the design criteria in all the operation range: contingency operation (minimum SCR), normal operation (SCR percentile 95 %) and maximum SCR. In the present case, the SCR range is within 5 to 25.

4.2 Simplified Representation of the System for Control Studies

To provide further understanding of the voltage regulator parameters, the system strength, and delays on the system stability, root locus analysis should be performed, which provides the critical gains [84]. To do that, it is needed to represent the elements composing the system as transfer functions, whereas the pole-zero map can be easily extracted.

In the following sections, it is defined how the main elements can be represented by their simplified transfer functions.

4.2.1 WTG Model

The WTG model for voltage control has to be simplified in order it can be represented by a simple transfer function.

Having the WTG a d-q control, allows independent control of the reactive and active power injected at stator terminals. Thus, the components of the wind turbine related to mechanical performance, such as the drive train, the blades and the active power control loop can be neglected. The decoupling is considered ideal, hence, only the q-axes related components, which are affecting the reactive current injection, are represented.

The simplified WTG transfer functions, which include the terms related to reactive power and current control (PI_Q and PI_i respectively), generator transfer functions (G_1, G_4), converter transfer function (G_C) and feedback filters (F_i and F_Q), are depicted in Figure 4.1. The detailed description of the transfer functions can be found in [A.6.].

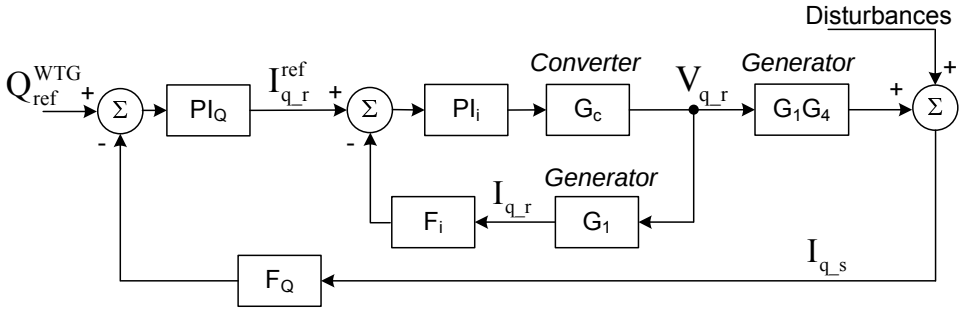

Figure 4.1. Simplified representation of the WTG for Q injection.

Since the system dynamic response is dictated by the poles closest to the origin, and for the sake of simplification and linearization, the obtained high order WTG transfer function can be simplified further. By doing so, the reactive power response of the WTG can be represented by a first order function (characterized by T_{WTG}), with the same bandwidth and gain as the high order transfer function, see (4.1).

The resulting transfer function is as follows (more details can be found in [A.6.]).

$$Turbine(s) = \frac{Q_{WTG}}{Q_{ref}^{WTG}} = \frac{PI_Q PI_i G_c G_1 G_4}{1 + F_i PI_i G_c G_1 + F_Q PI_i PI_Q G_c G_1 G_4} \approx \overbrace{\frac{1}{1 + sT_{WTG}}}^{Simplified\ \ function} \tag{4.1}$$

In this case, it is shown the transfer function of a WTG which includes an AQR. Similar process can be used when the WTG is using an AVR, see [A.1].

4.2.2 Grid Model

The impedances representing the grid are considered as an L_{GRID} and R_{GRID} system, thus the small capacitances are neglected. For small disturbances, we can assume the following approximation:

$$\left|\underline{V}+\underline{\Delta V}\right| = \sqrt{(V+\Delta V_d)^2+\Delta V_q^2} \approx V+\Delta V_d = V + R_{GRID}I_d + X_{GRID}I_q \tag{4.2}$$

Furthermore, the $R_{GRID}I_d$ term can be considered as a perturbation to the voltage control. Therefore, the gain of the grid, valid for small signal analysis, is obtained.

$$\Delta V \approx X_{GRID}I_q \tag{4.3}$$

4.2.3 Plant Control Model

The gain (K_{slope}) for the plant control is shown in (3.1). The plant control model has to include the time delays associated to the communication (T_{comm}) and sampling (T_s) processes. These are not negligible, and they could be in the range of hundred of milliseconds (according to the control hardware platform). The measurement system or "grid meter" can be represented by a first order function with a time constant T_m [1].

4.2.4 System Model

All the previous models have been linked together coherently according to the previous figures.

The exponential function representing the time delays should be linearized when doing the control analysis, e.g., by using Pade approximation.

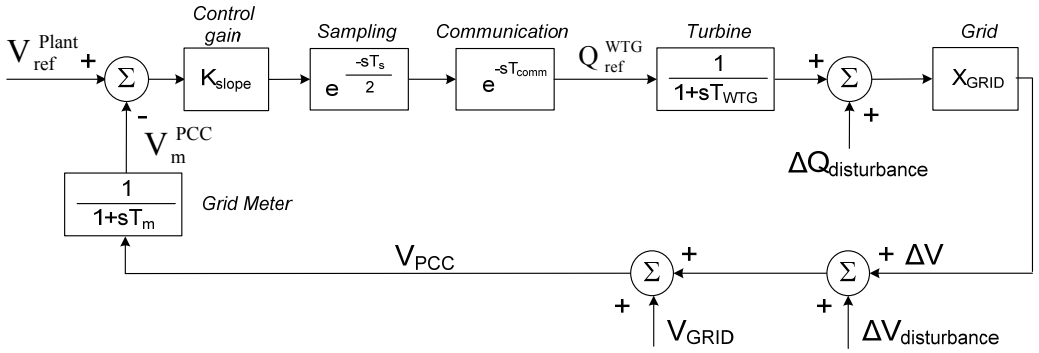

Figure 4.2. Simplified representation of the WPP, including the grid and voltage control.

This simplified model has some application boundaries. The use of this simplified model is not suitable for high SCRs where the current injection limitation of the converters or generator could be presented, and during low SCR conditions, where the assumption of a perfect decoupling between P-Q is not valid anymore [A.6.].

4.3 System Gain Analysis

Using the representation shown in Figure 4.2, it is possible to investigate the influence of the slope and SCR on the system stability. With high SCR, the grid becomes less sensitive to the plant operation, but also less dependent.

The open loop gain (K_T) is defined in (4.4).

$$K_T = X_{GRID} K_{slope} = \frac{X_{GRID}}{Slope} \tag{4.4}$$

By grouping together the communication and sampling times, the total time delay (T) can be defined.

$$T = 0.5T_s + T_{comm} \tag{4.5}$$

To extract the zero-pole map of the system, e^{-sT} is replaced with the Pade approximation, thus the linearization of $F(s)$ is obtained. Using the assumption of $T_m << T_{WTG}$, the following transfer function can be obtained.

$$F(s) = \frac{V_{PCC}}{V_{ref}^{Plant}} = \frac{K_T(1+sT_m)}{(1+sT_{WTG})+K_T e^{-sT}} e^{-sT} \approx \overbrace{\frac{K_T(1+sT_m)(1-s0.5T)}{(1+sT_{WTG})(1+s0.5T)+K_T(1-s0.5T)}}^{Linearized\ \ function} \tag{4.6}$$

The transfer function $F(s)$ is characterized by three parameters: the static gain K_T, the time constant T_{WTG}, and the dead time T. The parameters T and T_{WTG} are often called the apparent dead time and the apparent time constant, respectively. The ratio $dt = T/(T_{WTG}+T)$, is called the normalized dead time. This quantity can be used to characterize the difficulty of controlling a process. Generally speaking, processes with small dt are easy to control, and the difficulty in controlling the system increases as dt increases [84].

For the sake of illustration, the following typical data have been used throughout the document: T_m = 15 ms, T_{WTG} = 160 ms, and T = 150 ms (calculated by using T_{comm} = 100 ms and T_s = 100 ms).

By analyzing the pole location of the system, a clear picture can be done about the stability of the system for different control gains and SCRs. The following figure includes this relationship.

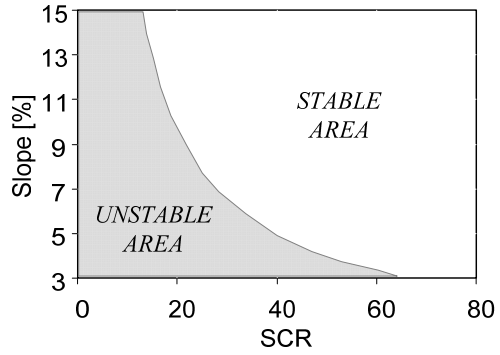

Figure 4.3. Stability area in terms of slope and SCR.

It is clear that for high system gains (small slope and SCR values), the system becomes more difficult to be controlled. In order to expand the stable area of the system, a lag compensator will be added to the plant control.

The tuning requirements for the control, i.e., the settling time and the overshoot, contradict each other. Higher gains will make the system faster, but at the same time the overshoot will be increased, in the other hand lower gains make the overshoot smaller but the time response is increased.

If the gain of the grid decreases, meaning that the SCR increases, one of the poles moves toward the right half plane, slowing the system. In the root locus figure (see Figure 4.4) the colored areas delimit the forbidden area for placing the poles of the system in order the control design criteria is fulfilled.

The settling time (t_s) is a vertical line which appears on the root locus plot at the pole locations, associated with the settling time value provided. This vertical line is exact for a second order system. Specifying the percent of overshoot (*OS*) in the continuous-time root locus causes two rays, starting at the root locus origin, to appear. These rays are the locus of poles associated with the percent value, using a second-order approximation too.

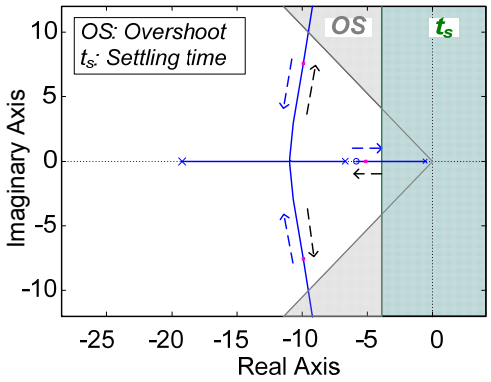

Figure 4.4. Root locus map of the system represented in Figure 4.2.

Therefore, when placing the poles of the system it can be defined a maximum gain (K_{max}, which is obtained due to the overshoot requirement), and a minimum one (K_{min}, which is obtained due to the settling time requirement) for fulfilling the design conditions. Moreover, it is possible to find the gain which makes the system unstable (K_{uns}).

$$K_{\min} < K_{slope} X_{GRID} < K_{\max} < K_{uns} \tag{4.7}$$

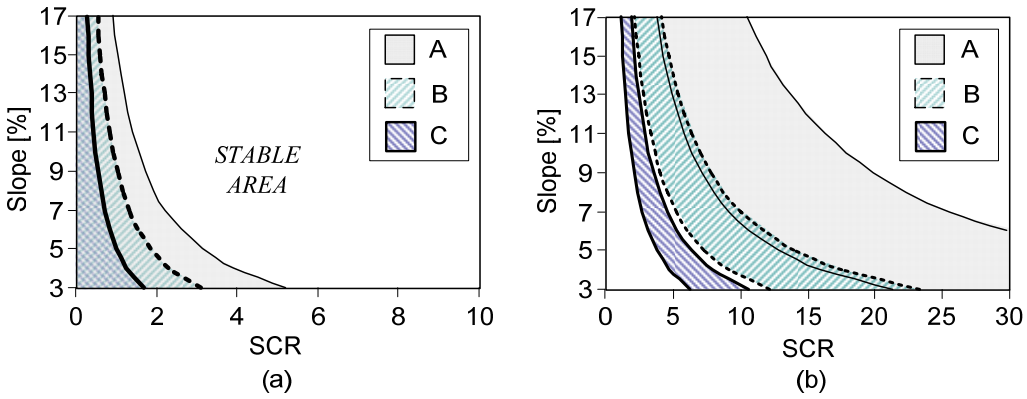

Figure 4.5. Stability (a) and design fulfillment (b) areas according to the SCR, for three set of control settings.

Figure 4.5 shows the stability area (Figure 4.5-(a)), and the fulfillment area of the design requirements (Figure 4.5-(b), within the colored surfaces), for three different control settings, which are calculated for three different SCRs, i.e., setting for curve A is optimized for a SCR equal to 5, curve B for 15, and curve C for 25. It can be observed that if the settings for case A or B are used, as it should be since these can ensure the stability operation within all the SCR range of interest, then the fulfillment area of the design requirements is quite reduced.

4.4 Central and Distributed Voltage Control

If the outer q-axis control loop of the WTGs is used as an AQR, two drawbacks are seen. Firstly, three set of control settings are needed to fulfill the design requirements for the whole SCR range of interest (between 5 and 25). Secondly, the fulfillment of the delay time (t_d) requirement could be physically impossible to achieve, regardless of the control, if the total sampling and communication control delays and WTG time response is bigger than the required t_d.

When the q-axis control loop of the WTGs is used as an AVR, the aforementioned two problems are solved. It is clear that changing the WTG q-axis control from being an AQR to an AVR, very fast system reactions are achieved for voltage disturbances. Besides, the fulfillment of the design requirements is extended to a wide range of SCRs, since the local voltage controllers are less dependant on the SCR.

This can be seen in the following figure, where the design fulfillment area is depicted (grey area in Figure 4.6) for a WPP where the WTGs are using an AVR. The system has been tuned for an optimal response when using a slope of 4% (marked with a dotted line in Figure 4.6) and SCR 5.

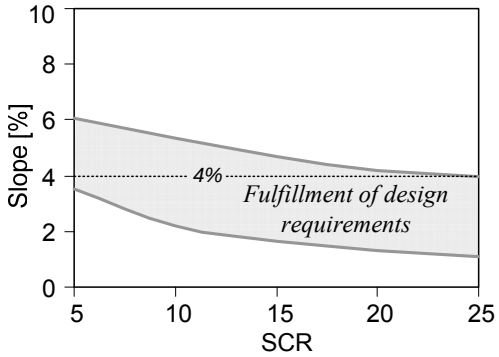

Figure 4.6. Design fulfillment area for a WPP with an AVR in the WTGs.

By looking into more details of the system transfer functions, it is possible to see where the main differences are. If the WTGs are controlled with an AQR, the aforementioned turbine transfer function is obtained (4.1).

$$Turbine(s) = \frac{Q_{WTG}}{Q_{ref}^{WTG}} \approx \frac{\mathrm{AQR_{WTG}}}{1+\mathrm{AQR_{WTG}}} \approx \frac{1}{1+sT_{WTG}} \tag{4.8}$$

It can be appreciated that the transfer function, which has been linearized, ideally is not depending on the grid gain.

Neglecting the sensors, time delays and WTG small time constants, and using the turbine transfer function shown in (4.8), the following structure representing the system is obtained (Figure 4.7).

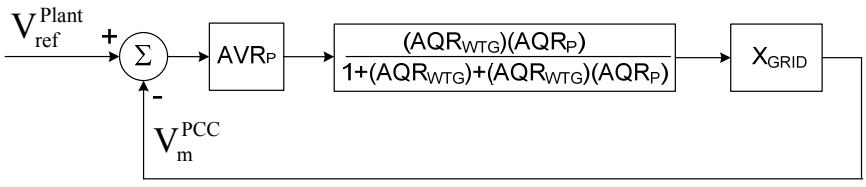

Figure 4.7. System representation when the WTGs include an AQR. Central scheme concept.

If the WTG includes an AVR, then the diagram depicted in Figure 4.8 is obtained, where X_{WPP} is the sum of the substation (X_{WPPT}) and WTG (X_{WTGT}) transformer positive impedances, and T_{cc} is the time constant of the first order transfer function between the rotor q-axis reference ($I_{q\_r}^{ref}$) and the reactive current in the stator (I_{q_s}).

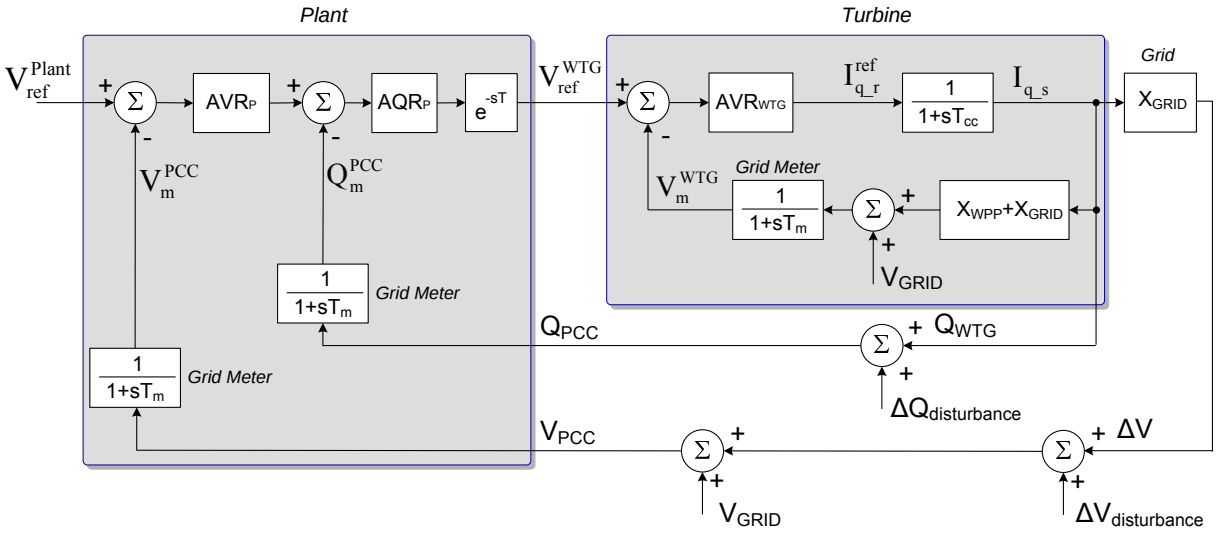

Figure 4.8. System representation for the WTGs with AVR.

The transfer function between the reactive current reference and the stator reactive current is defined in (4.9). More details can be found in [A.6.].

$$\frac{I_{q\_s}}{I_{q\_r}^{ref}} = \frac{PI_i G_c G_1 G_4}{1 + PI_i G_c G_1 F_i} \approx \left(\frac{M}{N(M + L_{\sigma s})}\right)\frac{1}{1 + sT_{cc}} \tag{4.9}$$

It should be pointed, that in Figure 4.8 the rotor control gains of the AVR_{WTG} has been translated to stator quantities by using:

$$AVR_{WTG} = \left(\frac{M}{N(M + L_{\sigma s})}\right) AVR_{WTG}^{rotor} \tag{4.10}$$

By neglecting the T_m and T_{cc} time constants, the turbine transfer function when including an AVR (the one shown in the Figure 2.4-(a)) is obtained (4.11).

$$Turbine(s) = \frac{Q_{WTG}}{V_{ref}^{WTG}} \approx \frac{\mathrm{AVR_{WTG}}}{1 + \mathrm{AVR_{WTG}}(X_{WPP} + X_{GRID})} = \frac{K_{PO}}{1 + sT_{PO} + K_{PO}(X_{WPP} + X_{GRID})} \tag{4.11}$$

By using Figure 4.8 and neglecting the small time constants, it is possible to obtain the structure depicted in Figure 4.9.

At first glance, it can be seen how the transfer function depicted in Figure 4.9 includes in the denominator a function of the X_{GRID}, which will make the system at the end less sensitive to X_{GRID} changes.

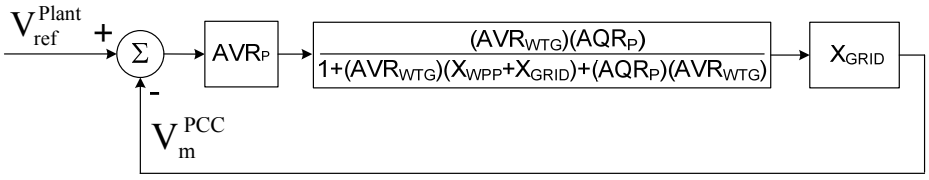

Figure 4.9. Simplified system representation for the WTGs with an AVR. Distributed voltage control scheme.

4.4.1 Sensitivity Analysis

The system sensitivity to a paremeter can be defined as the ratio of the percentage change in the system transfer function to the change of a parameter for a small incremental change. A sensitivity analysis is done to compare the influence of the X_{GRID} in the configurations depicted in Figure 4.7 (where its close loop transfer function is called $G_{central}$) and Figure 4.8 (where its close loop transfer function is called $G_{distributed}$).

If the influence of X_{GRID} is bigger in the $G_{central}$ than in the $G_{distributed}$, then its sensitivity term ($S^{X_{GRID}}$) will also be bigger. Thus, the condition shown in (4.12) needs to be verified.

$$S^{X_{GRID}}_{distributed} < S^{X_{GRID}}_{central} \tag{4.12}$$

Where the sensitivity of the previous transfer functions respect to X_{GRID}, is defined as follows:

$$S^{X_{GRID}}_{distributed} = \frac{\partial G_{distributed}}{\partial X_{GRID}} \frac{X_{GRID}}{G_{distributed}}, \quad S^{X_{GRID}}_{central} = \frac{\partial G_{central}}{\partial X_{GRID}} \frac{X_{GRID}}{G_{central}} \tag{4.13}$$

Thereby, obtaining the following results:

$$S^{X_{GRID}}_{distributed} = \frac{1 + \mathrm{AQR_{WTG}}(1 + \mathrm{AQR_P})}{1 + \mathrm{AQR_{WTG}}(1 + \mathrm{AQR_P} + \mathrm{AQR_P AVR_P} X_{GRID})} \tag{4.14}$$

$$S^{X_{GRID}}_{central} = \frac{1 + \mathrm{AVR_{WTG}}(X_{WPP} + \mathrm{AQR_P})}{1 + \mathrm{AVR_{WTG}}(X_{WPP} + X_{GRID} + \mathrm{AQR_P} + \mathrm{AQR_P} X_{GRID})} \tag{4.15}$$

For the sake of simplicity, similar gains of the plant reactive power control are used in both configurations, and also a gain of 1 is used for the AVR_P. By replacing the gains of the turbine transfer functions, AQR_{WTG} and AVR_{WTG} (1 and K_{PO} respectively), the following is obtained.

$$X_{WPP} < \frac{2}{\mathrm{AQR_P}} - \frac{1}{K_{PO}} + 3 \tag{4.16}$$

For a typical WPP, the X_{WPP} has a value of approximately 0.2 pu and the local WTG slope gain (K_{PO}) will be always bigger than 1, which confirms that (4.16) is, by far, always fulfilled. Hence, being more sensitive to X_{GRID} changes the central control configuration (WTG with AQR) than the distributed one (WTG with AVR).

4.4.2 Step Response

To validate the above conclusions, and using the aforementioned diagrams, the step responses, for a grid voltage change of 10% under different SCRs, are depicted.

The following figures show the step response of the system when the grid voltage is stepped down at time equal to 10 s. The curves show the WPP reactive power output when the WTG includes an AVR (AVR_{WTG}), and when includes an AQR (AQR_{WTG}), for the maximum and minimum SCR of interest. Both cases have been tuned for a SCR equal to 5.

It should be noticed that the curve AQR_{WTG_FF} is representing a similar plant control to the AQR_{WTG}, but with the addition of a feed-forward loop, with a maximum gain (K_{FF}) defined by the maximum allowed overshoot, see Figure 3.8.

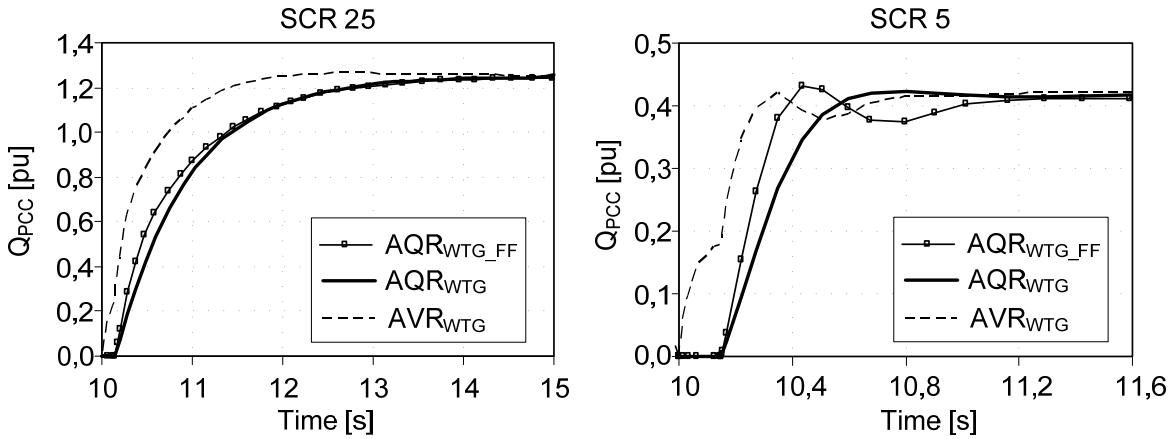

Figure 4.10. System step response of the diagram represented in Figure 4.8, where the turbine transfer function is replaced by (4.8) for the AQR_{WTG} curve, and (4.11) for the AVR_{WTG} curve. In the case of AQR_{WTG_FF} the plant control is provided with a fed-forward loop.

It can be checked that the WTG with an AVR has almost instantaneous response, and the t_d, t_r and t_s requirements are fulfilled for maximum and minimum SCR cases. However, for the case of the WTG with an AQR, t_d is not fulfilled, and t_r and t_s are only fulfilled for the "SCR 5" case. Additionally, it can be seen that, the impact of the SCR is much higher in the case of the WTG when using an AQR configuration.

It is clear that bypassing the AQR_P with a fed-forward, will easily make the system tend to overshoot. The AVR option is even more sensitive to this bypass than the AQR, since the WTG reference is calculated in terms of voltage, and is multiplied by the AVR_{WTG} gain (K_{PO}). Therefore, the feed-forward in a plant control which commands the WTGs with an AVR is not considered.

4.5 Conclusions

In this chapter, it is shown how the main elements of the wind power plant can be translated to a simple transfer function in order the pole-zero map can be extracted, making possible to select the gains that fulfill the design requirements. Moreover, it is discussed the benefits of using a distributed voltage control system by having the q-axis of the WTG actuated by an AVR. By doing so, very fast system response is achieved and the plant control is easier to tune, since the system dependency on the SCR is reduced compared to a WPP with an AQR in the WTGs. Therefore, the design of the WPP control will be based on a structure where the q-axis of the WTGs is controlled by an AVR.

Chapter 5

Control Design

This chapter deals with the design of the plant and WTGs voltage control. Furthermore, to understand and reach the appropriate control structure, possible interactions between different WPPs, and also between different voltage controllers within the WPPs, are analyzed. Finally, a new plant and WTG controls are proposed, which are based on a decentralized structure, but performs as a centralized one during steady-state.

5.1 Introduction

By placing a voltage control in the WTGs, which follows the voltage references sent by the plant control, the secondary voltage control concept is applied. The secondary voltage control concept is well known in the literature. The main thrust of the secondary voltage control scheme is to counteract in real time, reactive power flow changes in the system, by adjusting terminal voltage of generators system-wide. The amount of voltage adjustment is proportional to the voltage derivations at monitored buses [12], [85], and [86]. This concept can be applied to a wind power plant, where the pilot bus is located at the PCC bus, and the wind turbines include their own voltage controller.

As it was mentioned, slope voltage control is widely used in power system applications since it allows paralleling generators with individual voltage slope controllers without hunting phenomena or instability.

When there is high SCR, as in most of the cases in the transmission system, a slope controller will offer the best solution. Slope control provides a coordinated reactive power system, since the equilibrium point will be known for every voltage disturbance, independently of the controller time reaction and the Q compensator type. Therefore, it is easy to manage how the generators will share the reactive power injection for a certain voltage disturbance.

The control law that is applied for the slope concept can be defined, in a generic way, as follows:

$$Q_{ref} = Q_0 + \left(\frac{1}{Slope}\right)(V_{ref} - V_m) \tag{5.1}$$

Adding a certain offset to the slope controller (Q_0), or changing the voltage reference (V_{ref}), it is possible to regulate the Q injection of the plant.

5.2 Interaction between Different Slope Voltage Controllers

It is important to study the interactions that could occur between different slope controls of different WPPs located in the same area, and also it is of interest the control interaction inside the WPP, between the different generation units.

The following sections analyze these interactions.

5.2.1 Interaction between Wind Power Plants with Slope Voltage Control

When different WPPs are connected to the same point in the network, and they have to control the voltage at a remote location, different that the PoM* location, then current compounding can be used as SGs do [87]. This compounding can be done to have a better estimation of the voltage at the PCC.

However, this compounding could lead to instability if the settings of the control parameters are not properly chosen. To study this phenomenon, two cases are found to be representative enough. These two cases can be seen in Figure 5.1.

The WPPs can be linked tighter at the same bus-bar (Figure 5.1-(b)) or can be separated by some impedance, which could represent the OVL or even another transformer (Figure 5.1-(a)). Therefore, at some point of the system the WPPs are linked together, and evacuate the power through the same impedance (Z_{GRID}). The PCC is located within this Z_{GRID} impedance.

If there is no current compounding, the wind power plants will share the amount of reactive power to be delivered following their respective slope controls; this matter does not require more explanations.

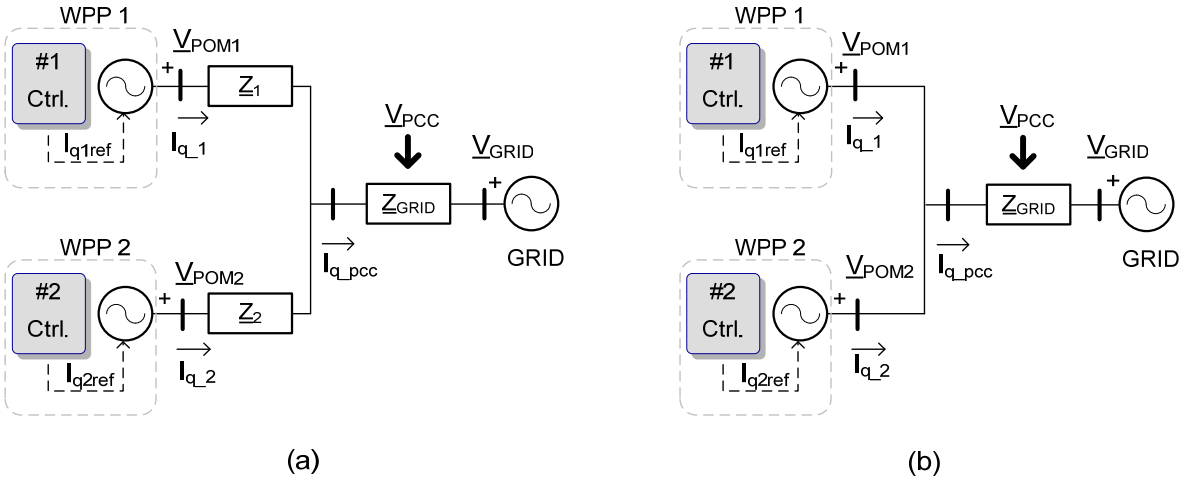

Figure 5.1. Two different interconnection configurations between different WPPs. Case A: the WPPs are connected through some impedances, and case B: they are directly coupled to the same bus-bar.

As it has been explained earlier, the WPP voltage control is represented with a gain (K_{SLOPE1}) and a time constant (T_1). If a compounding of the reactive current injected by the other plant is included in the control loop (K_{L1}), the following control structure is obtained.

* PoM is the point of measurement, which indicates the physical location of the CTs and VTs of the WPP, which normally is the same as the PCC, but in some cases could differ.

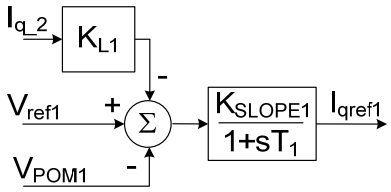

Figure 5.2. WPP slope control with current compounding from other WPP.

For the case represented in Figure 5.1-(a), the following steady state equation for the WPP1 control is obtained.

$$V_{ref1} - V_{POM1} = \left(\frac{1 + K_{SLOPE2} X_2 - K_{L1} K_{slope2} K_{slope1} (X_1 - K_{L2})}{1 + K_{SLOPE2} X_2 - K_{L1} K_{SLOPE2}} \right) \frac{I_{q\_1}}{K_{SLOPE1}} \tag{5.2}$$

Hence, it is expected instable operation for K_{L1} values close to:

$$K_{L1} = \frac{1}{K_{SLOPE2}} + X_2 \tag{5.3}$$

The current equilibrium point between these two WPPs is equal to:

$$\frac{I_{q\_1}}{I_{q\_2}} = \frac{K_1 (1 + K_2 (X_2 + K_{L1}))}{K_2 (1 + K_1 (X_1 + K_{L2}))} \tag{5.4}$$

For the case represented in Figure 5.1-(b), the following steady state equation for the WPP1 control is obtained.

$$V_{ref1} - V_{POM1} = \left(\frac{1 - K_{L1} K_{L2} K_{SLOPE2} K_{SLOPE1}}{1 - K_{L1} K_{SLOPE2}} \right) \frac{I_{q\_1}}{K_{SLOPE1}} \tag{5.5}$$

The system could be instable for a K_{L1} value close to:

$$K_{L1} = \frac{1}{K_{SLOPE2}} \tag{5.6}$$

The current equilibrium point between these two WPPs is equal to:

$$\frac{I_{q\_1}}{I_{q\_2}} = \frac{K_1 (1 + K_2 K_{L1})}{K_2 (1 + K_1 K_{L2})} \tag{5.7}$$

It should be noted that the stability of the plant depends on the control parameters of the nearby WPPs.

5.2.2 Slope Voltage Control Interaction inside the Wind Power Plant

Considering a wind power plant composed by a large amount of generators, and everyone having its own AVR, it is important to investigate the interaction between these controllers and the central plant control.

For studding this interaction, a generic system formed by two units (WTG1 and WTG2) and a central control (WPPC) is used. The central or plant control is placed to control the

voltage at the PCC, by commanding these two units. The single line diagram of this system is depicted in Figure 5.3.

The following equations show the control law applied to the individual controls.

$$WTG1 \Rightarrow (V_{ref} - V_1)K_1 = I_{q\_1} \tag{5.8}$$

$$WTG2 \Rightarrow (V_{ref} - V_2)K_2 = I_{q\_2} \tag{5.9}$$

$$WPPC \Rightarrow (V_{rated} - V_{PCC})K_{PCC} = I_{q\_PCC} \tag{5.10}$$

Note that in the above equations, the voltage reference (V_{ref}) is dictated by the plant control.

As it can be seen, these three controllers use different slope gains (K_1, K_2 and K_{PCC}) when controlling their local bus-bar voltage. This configuration offers a first and fast reaction to grid disturbances from the individual unit controls, and later it is compensated by the slowest central control unit. This central control unit sends voltage references to the units according to the central slope characteristics (K_{PCC}).

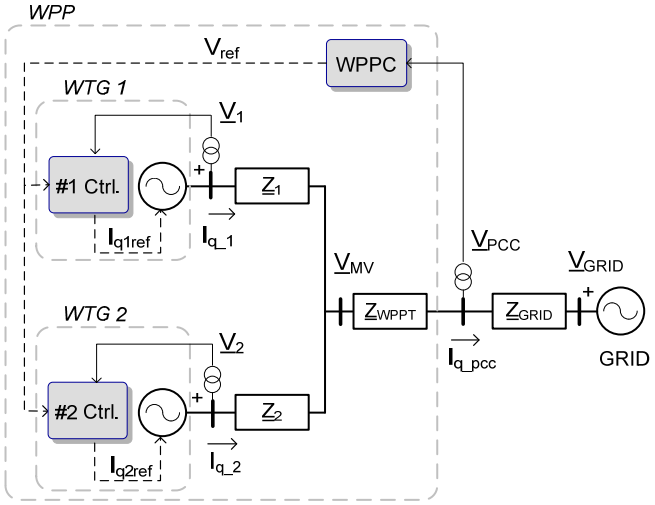

Figure 5.3. WPPC, secondary slope voltage control concept.

The characteristics of the controllers (WTG 1, WTG 2, WTG 1+2, and Ctrl PCC) and the system, for two different voltages (PCC V=0.9 pu and PCC V=1 pu), are depicted in Figure 5.4.

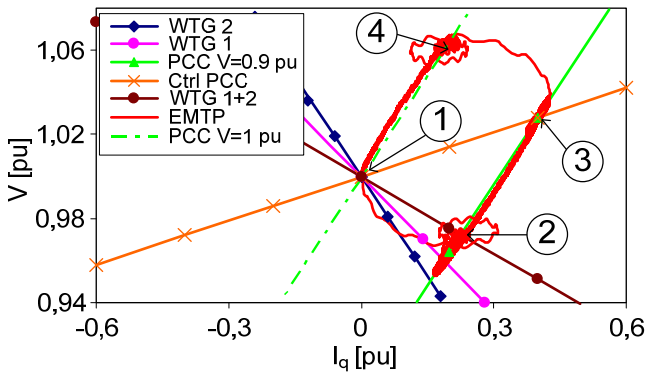

Figure 5.4. Characteristics of two generator units with slope voltage control and with a central control.

The equilibrium points are located in the intersection between the characteristic of the central control (Ctrl PCC) and the system one (PCC V). The trajectory between the equilibrium points is depicted in red color (EMTP), which is obtained from an EMTP simulation when stepping the grid voltage from 1 pu (point 1) to 0.9 pu (point 3) and back.

The followed I_q-V trajectory shows several interesting points. Due to the communication time delay between the central control with the local units, it can be seen how the first system reaction is to reach their local controller equilibrium point (point 2), then the reference from the central control arrives moving the equilibrium to point 3. After that, when the grid voltage is stepped back to 1 pu, it is possible to see similar reaction; first reaction from point 3 to point 4 is done by the local controls, and finally, point 4 is moved to 1 through the central control action.

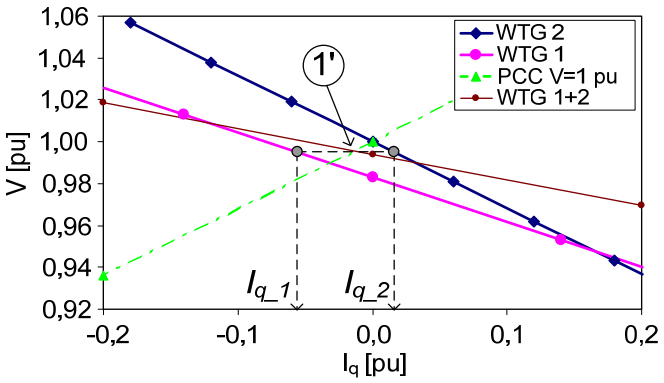

Figure 5.5. Active power effect in the equilibrium points.

Figure 5.5 shows how the resistance of the impedances Z_1 and Z_2, and active power injection can affect the previous equilibrium points. In this case, the WTG #1 and #2 are injecting the same active power level, but the resistance value connecting them to the PCC is different, $R_1 = 2R_2$. As it can be seen, the effect of this active power injection is to displace the previous equilibrium point 1 to a new position 1', making I_{q_1} inductive and I_{q_2} capacitive, for a grid voltage equal to 1 pu. This offset could lead to undesired behavior when having a centralized controller, since all the units should collaborate in the same reactive power direction. Additionally, it is clear that the amount of reactive power injection depends on the feeder position and wind speed.

5.3 Control Scheme Selection

According to the previous analysis, the permutations of the aforementioned control options (see Figure 3.8) have been evaluated. In all the cases, there is an outermost voltage control loop at PCC level, and in every case the plant controller specifies the references for the WTGs. These references are translated by the AQR_P to voltage or power references, according to the outer WTG control loop.

The use of a mathematical model of the park internal network, which must accurately compensate the VAr consumption inside park, in any case and circumstance, does not provide the advantage of removing one lag from the plant control (the integral part of the AQR_P). In essence, to have stable operation the plant control has to be slowed down to have at least 5-10 times lower bandwidth than the WTG outer control loop, being worthless to replace the close loop reactive power compensator by a predictive model.

The cases are characterized below, according to their SCR sensitivity and time response. According to this evaluation, schemes 4 and 9 have been selected as good control candidates

due to their fast response and low SCR dependency. Between these two candidates and based on the aforementioned characteristics option 4 is the favorite one.

TABLE II
COMBINATIONS FOR WTG AND PLANT CONTROL

Scheme	Plant control	WTG control	Time* response	SCR sensitivity	Comments
1	(i)	(a)	*slow-*	*high*	*Outer WTG control is dictated by an AQR.*
2	(i)	(b)	*fast-*	*low*	*Two closed loops for reactive power compensation.*
3	(i)	(c)	*slow*	*high*	*Faster than (a), one fewer layer control.*
4	(i)	(d)	*fast*	*low*	*Faster than (b), one fewer layer control.*
5	(i)	(e)	*slow*	*high*	*Faster than (a), two fewer layer controls.*
6	(ii)	(a)	*slow-*	*high*	*Outer WTG control is dictated by an AQR.*
7	(ii)	(b)	*fast-*	*low*	*Two closed loops for reactive power compensation.*
8	(ii)	(c)	*slow*	*high*	*Faster than (a), one fewer layer control.*
9	(ii)	(d)	*fast*	*low*	*Faster than (b), one fewer layer control.*
10	(ii)	(e)	*slow*	*high*	*Faster than (a), two fewer layer controls.*
11	(iii)	(a)	*slow*	*high*	*Two closed loops for reactive power compensation.*
12	(iii)	(c)	*slow+*	*high*	*Faster than same option with (i).*
13	(iii)	(e)	*slow+*	*high*	*Faster than same option with (i).*

5.4 Plant Control

According to the previous selection, the power plant structure can be designed. The proposed structure of the plant controller is shown in Figure 5.6, where the voltage plant controller (AVR_P) is extended with an inner plant reactive controller (AQR_P) to compensate for the internal reactive power losses that occur inside the plant. This controller ensures that the injected Q_{ref}^{Plant} at the PCC is the one dictated by the AVR_P in any circumstance.

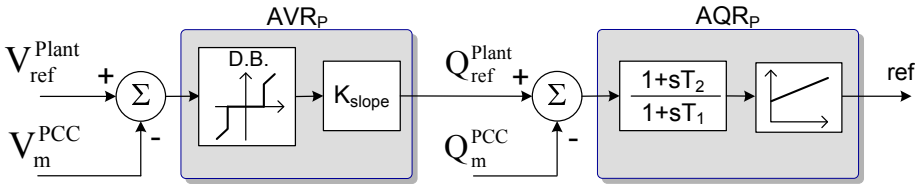

Figure 5.6. Plant control structure.

5.5 Wind Turbine Generator Control

The proposed WTG rotor converter q-axis control is shown in Figure 5.7, where the reactive current reference (I_{qref}) is generated according to the difference between the stator turbine terminal voltage, represented by V_m, and the V_{ref} sent by the WPPC. Therefore, the WTG outer control loop is a local voltage control, which can be adjusted by an external set-point.

The main difference with other secondary controls shown in the literature [66], [67], [81] is that this local voltage control will be active only during voltage transients.

In this voltage control, the WTG slope gain and time constant, K_{WTG} and T_3 respectively, are adjusted to provide fast reactions to voltage changes at generator terminals. The stator

* The time response is classified, from the slowest to the fastest, as follows: slow-, slow, slow+, fast-, fast

voltage variations are filtered with a differential pole filter with a time constant T_4, hence, only reacting to changes on the stator voltage but not to steady state voltage errors. Thus, removing the undesired voltage offset effect, caused for instance by the active power injection and the resistance of the cables and transformers, see Figure 5.5.

By using a differential filter, it is possible to affirm that this voltage control is only active during voltage transients, during steady-state the calculated reactive current reference (I_{qref}) is proportional to the one dictated by the plant control, and does not depend on the stator voltage, thus having all the units of the plant the same I_{qref}, being loaded equally in terms of reactive power injection.

The voltage control includes, as well, a protection against overvoltages, performed by the Overvoltage Protection, and an over-under voltage protection (LOGIC), see Figure 5.7. The protection LOGIC is as follows: the reference signals (V_{ref}) is frozen if: the measured voltage (V_m) is above the limits and the reference is capacitive increasing, or if it is below limits and the reference is inductive increasing.

The I_q limits are calculated according to the P-Q chart of the machine. The magnetization current of the generator (I_{mag}) is added to the loop, which is a function of the stator voltage.

The Decoupling term is calculated by using the diagram of the Figure 2.1, where it is possible to calculate the terms affecting the variation of the voltage at the PCC. It can be seen in (5.11), that the cause of this variation are the own WPP current injection (term 1), and the grid voltage changes (term 2).

$$\Delta V_{PCC} = \overbrace{X_{GRID}\left(\Delta I_{q\_WTG} - X_{WPP}(\Delta I^2_{WTG})\right) + R_{GRID}\left(\Delta I_{d\_WTG} - R_{WPP}(\Delta I^2_{WTG})\right)}^{1} + \overbrace{\Delta V_{GRID}}^{2} \tag{5.11}$$

If the grid voltage is kept constant ($V_{GRID} = cte$) then it is possible to calculate the reactive current (I_{q_WTG}) that will compensate for the voltage variations at the PCC, due to the flowing of active current. Thus, by replacing $\Delta V_{PCC} = 0$, (5.12) is obtained.

$$\Delta I_{q\_WTG} = \overbrace{\left(\frac{R_{GRID}R_{WPP} + X_{WPP}X_{GRID}}{X_{GRID}}\right)}^{K1}\Delta I^2_{WTG} - \overbrace{\left(\frac{R_{GRID}}{X_{GRID}}\right)}^{K2}\Delta I_{d\_WTG} \tag{5.12}$$

By using the calculated ΔI_{q_WTG} (called *Decoupling* in Figure 5.7) in the WTG voltage control, the plant control is released of compensating voltage changes due to WTGs active current flowing. Finally, the following voltage control can be depicted.

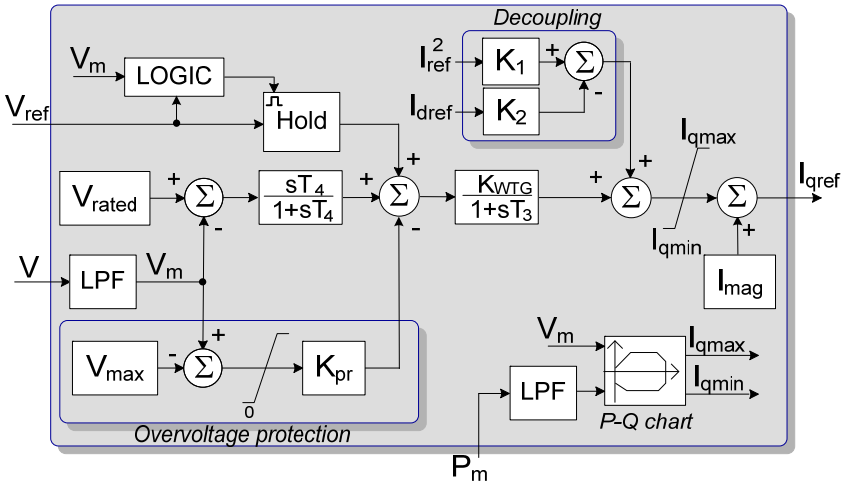

Figure 5.7. WTG voltage control.

One should realize, that the injected Q at the PCC is the same with and without the "*Decoupling*" term, since at the end the Q injected at the PCC is dictated by the AVR_P. Two main things can be achieved by placing this compensation inside the WTGs: more reliability, since in case the plant control is out of operation, the WTGs still do this compensation, and secondly, the bandwidth of the system is improved, since this compensation is done locally at WTG level, without using the "slow" plant control.

To avoid dependency on the grid parameters the term K_2 can be neglected (usually, is very small compared with K_1).

After neglecting the resistances, a value of X_{WPP} is obtained for K_1. X_{WPP} depends only on the project data, and is equal to (5.13), where N_{WTG} is the number of WTGs in the plant.

$$X_{WPP} = \frac{X_{WPPT}}{N_{WTG}} + X_{WTGT} \tag{5.13}$$

5.6 Conclusions

In this chapter a new decentralized voltage control scheme is presented, which offers a combination of the central and distributed control scheme characteristics.

The control concept used in this PhD work is based on the secondary slope voltage control. As voltage control is actuated by reactive power, it is possible to affirm that the voltage control design will cover an inner and fast reactive voltage control loop, located at turbine level, and an outer voltage control loop, located at the PCC, where it is intended to control the voltage.

The WTG voltage control is designed to be only active during transients to avoid the consequence of some undesired offset, caused by the active power flowing. Thus, having the advantages of a decentralized control (fast response), and removing its disadvantages (different Q offsets).

Additionally, the WTG voltage control is designed to include a compensation term for the variations of voltage due to the active power flowing, increasing the bandwidth and the reliability.

The selected plant control is based on a cascade control, with an outer voltage control and an inner reactive power control.

Chapter 6

Control and Integration of STATCOM, Mechanically Switched Capacitors and On-Load Tap Changer

This chapter describes the control integration of the STATCOM, MSCs and the OLTC. The STATCOM is integrated by means of a dispatcher module, located in the plant control, which uses the injected active power to level the STATCOM reactive power. The MSCs are installed and controlled to release the use of the converters during permanent disturbances. The OLTC system is voltage controlled locally, independently of the plant voltage control. The OLTC performance is improved by coordinating its control with the central substation control, this coordination includes the exchange of information about the status of the MSCs.

6.1 Introduction

Since most of the grid codes ask for having a voltage capability regulation within a minimum power factor of 0.95, the limited DFIG Q injection during high active power levels, implies that this requirement can not be fulfilled. To solve this situation, reactive power compensation equipment can be installed in the wind power plant.

The amount of extra VAr can be calculated by means of a load flow analysis for different active power production levels and grid voltages. The needed extra VAr can be supplied by a STATCOM (if fast response time to disturbances is required) or by MSCs (if no time or very slow response time is required), grid code play an essential role when selecting the compensation equipment. In the present case, the selection of the STATCOM is done based on grid code requirements related to fast time response to grid disturbances, and it is sized based on load flow calculations.

Voltage regulation including static converters, e.g., DFIG or STATCOM, is viewed primarily as a fast VAr source to counteract rapid and unexpected voltage disturbances [88]. To fulfill this condition, it is necessary to ensure that the converters will have sufficient VAr capacity to handle unpredictable disturbances at any moment; for this reason, the proposed WPP includes MSCs, thus keeping the dynamic capability of the converters to the maximum, and also reducing the switching converter losses. It should be noted that the operation of these switchable components is considered as a way to offset the operation level, and not as a voltage regulation itself.

Dynamic reactive resources are typically used to adapt to rapidly changing conditions on the transmission system, such as sudden loss of generators or transmission facilities. In contrast to switched static devices, which are typically used to adapt to slowly changing system conditions. An appropriate combination of both static and dynamic resources is needed to ensure reliable operation of the transmission system [29].

Moreover, OLTC systems are often employed in WPPs for offsetting the medium voltage level, and similarly to the MSCs, they can not be considered as a dynamic compensator.

6.2 STATCOM Control

The implemented STATCOM voltage control is similar to the one shown in Figure 5.7, with the particularity that the current limits are not dependant on the active power level (see Figure 3.5), and consequently the compensation terms related to active power and I_{mag} are not included.

The STATCOM is included in the loop as another WTG, which its primary function will be to supply reactive power whenever the WTGs do not suffice by themselves.

Other strategies for using the STATCOM in the plant, such as:

- STATCOM and WTGs equally loaded in reactive power at any moment.
- First STATCOM and second WTGs.

are not considered, the aim is to reduce the plant dependency on the STATCOM to the maximum. Other strategy could be chosen based on electrical losses and/or service hours requirements.

6.2.1 Dispatcher Function in the Plant Control

The strategy proposed in this document is based on using the STATCOM as the Q back-up for the system, to be used when the reactive power injected by the WTGs is not enough for grid code fulfillment. Therefore, the plant control should include a dispatching function to handle this operation.

The dispatcher has the functionality of splitting the references calculated by the plant control into the different elements composing the WPP according to the feedback received.

The following figure shows the dispatcher module in a schematic way, where the active power measured at the PCC (P_m^{PCC}) is filtered with a low pass filter (LPF) and used for calculating a K factor by means of a look-up table.

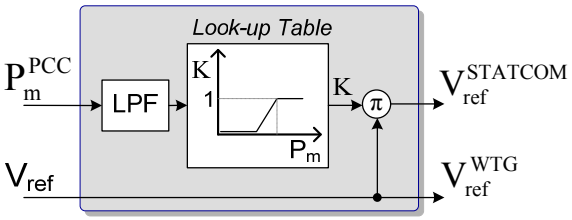

Figure 6.1. Dispatcher module.

The settings of the look-up table are obtained from the load flow analysis shown in section 6.4. Basically, the factor K remains zero below the active power level where the WTGs suffice by themselves, and where the WTGs need the support of the STATCOM, K is ramped to 1.

The gain factor (K) varies between 0 and 1, and multiplies the reference calculated by the control (V_{ref}), thereby, the reference for the STATCOM ($V_{ref}^{STATCOM}$) is obtained.

6.3 Mechanically Switched Capacitor Control

Typically, MSCs can be used to reduce looses due to Q transportation and/or for compensating permanent system disturbances, avoiding the use of dynamic compensators.

The proposed MSCs control strategy, is based on the idea that the steady-state operation of the Q injected by the converters has to be inside of a predefined range (which can be called steady-state converter operation band), thereby the step sizing of the capacitor banks, and its control are designed accordingly. A band of ± 0.1 pu has been chosen as a balance between the number of switching and the remaining converter capacity installed in the WPP.

The maximum size of the capacitor steps has to be equal to the size of the chosen converter operation band. One should realize that, the bigger the steady-state converter operation band, the lower the amount of MSC switching operations, but the bigger the energy losses due to the transportation of Q inside the plant and converter switching.

The integration of the capacitor control in the plant control is shown in Figure 6.2.

The output of the AQR_P is the total reference to be sent to the WPP components (V_{ref_total}). Before this reference is sent to them, it is altered by the capacitor control, which may subtract/add a fraction (ΔV_{Cap}, which can be considered a feed forward action) to the reference, if one of the capacitor steps is going to be connected/disconnected.

This is done to minimize the transient effect of the capacitor switching in the plant control. The effectiveness of this action is based on known system data, such as delay communication time. Error in this information will reduce the switching transient compensation performance.

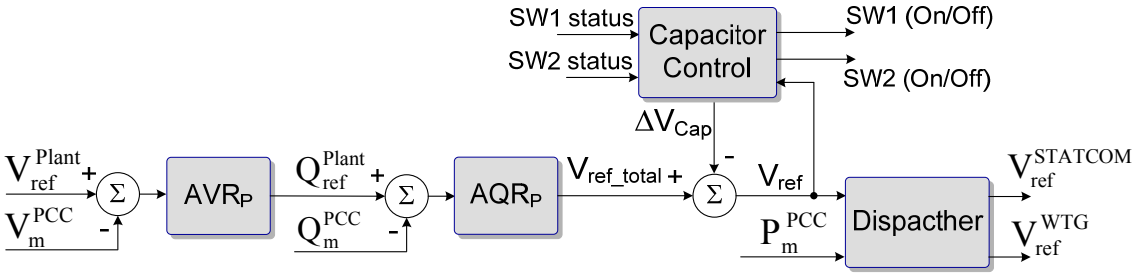

Figure 6.2. Plant voltage control, including the capacitor control.

The proposed capacitor control is depicted in Figure 6.3, and uses as an input the V_{ref} to calculate the needed reactive power (Q_{ref_cap}) by using (6.1), where K_{WTG} is the slope gain of the local voltage control of the WTGs and STATCOM (see Figure 5.7).

$$(1 - V_{ref})K_{WTG} \approx Q_{ref\_cap} \tag{6.1}$$

This Q_{ref_cap} reference is compared with some threshold value (Converter operation steady-state); if the reference is greater than this level, then the output is set to Q_{ref_cap}; otherwise it remains 0.

The Switching Logic module processes this signal, and decides which step to connect/disconnect based on some timer functions and the current status of the capacitors, the connection/disconnection commands are sent to the RTU. See appendix C for more details.

It should be noted that the discharging time of the capacitors (which normally is programmed in the capacitor switch) prevents the connection of the capacitor step without being discharged to a residual level; this discharging action usually takes 5-10 minutes.

The RTU processes the feedback of these discharging timers, and monitors other breakers status (i.e. main plant connection breakers) to decide whether or not to send the received connection commands to the capacitor switches.

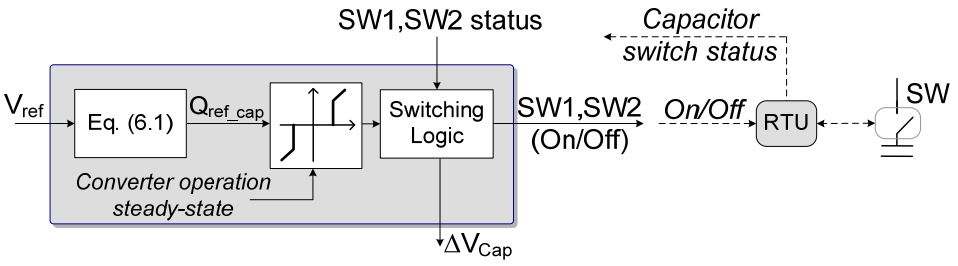

Figure 6.3. Proposed capacitor control.

Due to this lagging time, the plant control has to verify that the switches are able to follow the commands before they are sent, being needed to receive a feedback signal from the RTU, with this status information.

Finally, the outputs of the module are the step switching commands sent to the RTU, and the ΔV_{Cap}, which will offset the V_{ref_total}.

The effect of ΔV_{Cap} is to center the disturbance of the capacitor connection, thus decreasing the peak value of the capacitor connection transient. This ΔV_{Cap} is calculated based on (6.1), and uses the Q value of the capacitor step that is going to be connected/disconnected. Basically, the plant control starts decreasing/increasing the Q reference in a value equal to the Q supplied by the capacitor step (Q_{MSC}), before it is connected/disconnected, thus, this feed-forward action minimizes the Q impact of the connection/disconnection. See following figure.

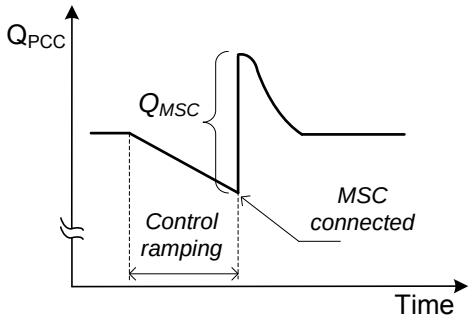

Figure 6.4. MSC connection process.

6.4 System Load Flow Analysis

The amount of VAr needed from the STATCOM can be calculated by means of a load flow analysis for different wind level productions and grid voltages.

Figure 6.5 shows the load flow analysis of the WPP depicted in Figure 3.7, for different Q operations of the WTGs. The curve lines show the load flow when the WTGs are operating at PF equal to 1 at stator terminals, for different grid voltage levels. Thus, the reactive power consumption of the WPP components, mainly the plant transformers, for different levels of active power injection and grid voltage levels can be evaluated.

The dotted red lines show the inductive and capacitive P-Q chart for a PF = 0.95.

The blue dot shows the intersection between the Q produced at the PCC and the PF = 0.95 capacitive requirement, when the turbines are operating at maximum capacitive reactive power. Beyond this active power level, the DFIGs are not able to fulfill the PF requirement by themselves. Therefore, this point determines when the STATCOM is starting to be needed to fulfill the PF = 0.95 requirement.

The green dot shows the maximum capacitive reactive power capability at the PCC when the WTGs are injecting their maximum capacitive reactive power at maximum active power injection. It can be used to determine the amount of VAr needed from the STATCOM.

The pink dot shows the maximum inductive reactive power capability at PCC when the WTGs are injecting their maximum inductive reactive power at maximum active power injection. Following to the load flow analysis, the amount of extra dynamic VAr needed from the STATCOM is chosen to be 0.25 pu of the total plant power.

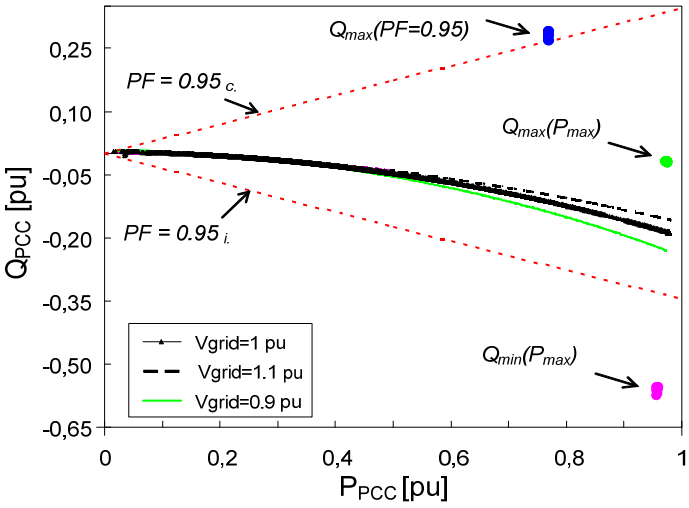

Figure 6.5. Load flow analysis of the wind power plant at PCC bus, for different WTG Q injections.

The following figure shows with a black line the combined operation of the DFIG and the MSCs (two steps are considered) for the capacitive area. For the inductive area, only the DFIG operation is considered. The dotted red line shows the chosen P-Q grid code requirements at PCC [26], and the dotted green lines show the P-Q profile obtained when the DFIGs are operating at 0.1 pu capacitive and inductive. The flat green line shows the P-Q obtained when the DFIGs are operating with a PF = 1, at generator terminals.

It can be seen in Figure 6.6, that at full power there is a lack of reactive power according to the requirement, but one should realize that the reactive power of the STATCOM is not included in this figure; therefore, the requirement can be fulfilled without any concern.

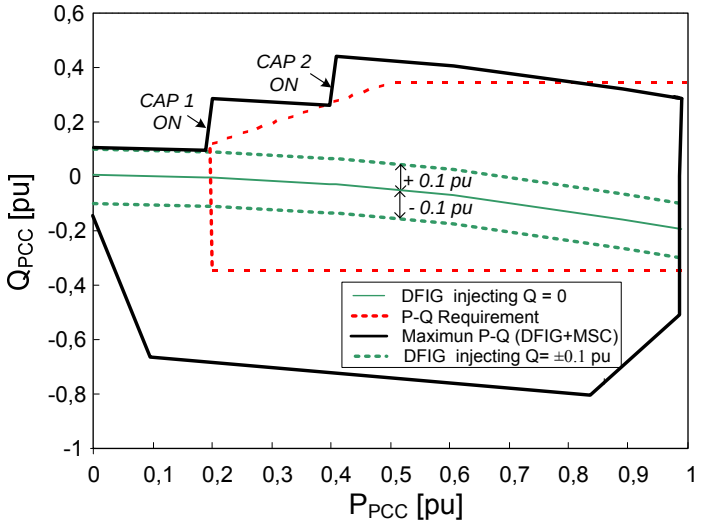

Figure 6.6. Wind power plant load flow analysis at the PCC including WTG and MSCs, and P-Q chart requirement.

6.5 Proposed On-Load Tap Changer Voltage Control

In this section, an OLTC strategy for a wind power plant is proposed, where the line drop compensator used in the tap control is dependant on the capacitor bank status. As a consequence of that, better voltage regulation and lower tap movement actions are expected.

The line drop compensation function is to regulate the voltage at a remote point along the feeder. This voltage is estimated by computing the voltage across a fictitious impedance (gain K_L in Figure 6.7). By removing the capacitor current (I_{q_c}) from the total MV current (I_{q_MV}), the line drop function estimates the voltage more accurately.

The reactive current injected by the MSCs is generated just at the MV bus-bar, thus is distorting the voltage drop related to the real distance to the converters, which the line drop should estimate.

The module called LOGIC (see Figure 6.7) includes the conditions to increase or decrease the tap position, and allocates a timer, which determines the duration of the voltage error exceeding the dead band value (D), which at the end will dictate the action to change the tap position. The timer is increased if the error is outside the dead band and it is reset if the error is within the dead band, either if there is a tap change or if the error oscillates above and below the dead band. Its operation is blocked in case that the voltage falls below some defined limits, (under-voltage blocking), and also when voltage or current exceeds another user defined limit (overvoltage or overcurrent blocking) [1], [89].

The DELAY module is used to prevent unnecessary tap changes in response to transient voltage variations or self-correcting voltage variations, and to introduce the desired time delay before a tap movement is commanded. The tap motor action is modeled as a pure delay with a time constant [3].

One simple solution to remove the reactive current produced by the MSCs, from the measured MV current without additional hardware requirements is to send to the OLTC control the switch status (SW_1 and SW_2) of the capacitor banks. This solution implies that the RTU exchanges the needed data with the tap control, about the capacitor switch status, using the existing communication link. Additionally, it is needed to add a simple algorithm inside the OLTC control, which will translate the received signals into the current injected by the connected capacitors (I_{q_C}). This current is calculated based on the rated capacitance of the capacitors and the measured voltage at medium side (V_{MV}).

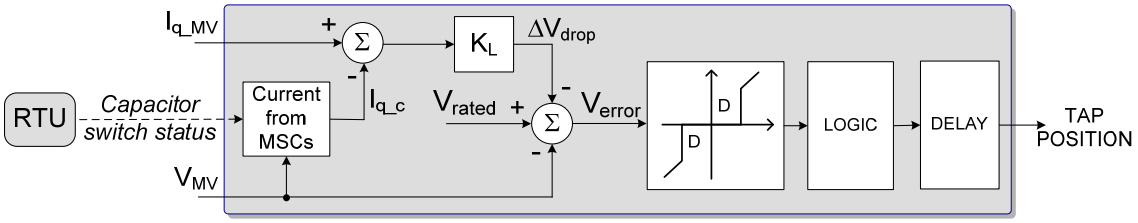

Figure 6.7. Proposed OLTC voltage control.

6.5.1 Interaction between the Plant and On-Load Tap Changer Controls

The voltage plant and voltage tap controllers can be considered ideally decoupled, for the following two main reasons: very different control time response, and the OLTC controls the voltage by changing the winding ratio, whereas the plant control is actuated by Q.

Basically, the tap controller is controlling the medium voltage side, by changing the transformer winding ratio, whereas the WPPC is controlling the voltage at the high side of the substation transformer, by injecting Q. Looking at the time response of these two controllers it

can be said that the WTGs and STATCOM are used for dynamic voltage control while the OLTC is used for steady-state voltage control.

Even that, since the OLTC and plant controls work independently, small interactions among the control actions are a natural consequence. Following sections study the interactions of the OLTC voltage regulator in the voltage plant control, and the voltage plant control in the OLTC voltage regulator [A.7.].

6.5.1.1 Effect of the On-Load Tap Changer Voltage Control on the Voltage Plant Control

A tap operation affects the medium bus voltage causing a consequent variation in the injected current at high voltage side of the transformer, which will cause at the end a variation in the voltage at the PCC. This is a clear counteraction between controllers, since an increment in the tap position to increase the MV will cause a decrement in the voltage at the PCC.

The coefficient which correlates the variation of the tap position (Δr) with the voltage variation at the PCC (ΔV_{PCC}) is shown in (6.2), where r reflects the tap position, being for the neutral position r equal to 1. The sub-index 0 reflects the previous value to the disturbance. See [A.7.] for more details.

$$\Delta V_{PCC} = -\left(\frac{r_0 X_{GRID} V_{PCC0}}{X_{WPPT} + r_0^2 X_{GRID}} \right) \Delta r \tag{6.2}$$

As it was expected, tap operations with high SCRs, and low transformer reactances are translated in higher voltage changes at the PCC.

For values close to rated, it can be said that this coefficient is lower in magnitude than 1.

6.5.1.2 Effect of the Voltage Plant Control on the On-Load Tap Changer Voltage Regulator

Additionally, it is important to analyze the effect of the plant voltage controller on the voltage at medium side, where the OLTC control is located. Equation (6.3) shows how a change in the PCC voltage is translated to the MV.

$$\Delta V_{MV} = \left(\frac{r - X_{WPPT} K_{slope}}{1 + X_{GRID} K_{slope}} \right) \Delta V_{PCC} \tag{6.3}$$

It can be said that low slope gains make the ratio between ΔV_{MV} and ΔV_{PCC} less dependant on the SCR, and higher slope gains make the ratio more dependant on the grid impedance.

For r values close to nominal and $X_{WPP} > X_{GRID}$, the coefficient which correlates the change in V_{PCC} and in MV, is bigger than 1 in absolute value. For more details see [A.7.].

6.6 Conclusions

In this chapter, it is proposed the integration and control of the MSCs, STATCOM and OLTC. The MSCs are controlled by a novel capacitor control, which is integrated in the plant controller, allowing the reduction of the capacitor switching transients and limiting the converter operation for reactive power injection during steady-state. Moreover, the coordination of the STATCOM, WTGs and capacitor banks can be done in such way that the "steady-state" reactive power usage of the converters is less than a desired band of 0.1 pu, which is a compromise between switching converter losses and capacitor switching operations.

The STATCOM is coordinated with the rest of the WTGs by using a new dispatcher function, which uses the settings obtained from the load WPP flow analysis.

In the proposed OLTC control, the current injection from the capacitor banks is removed from the line drop, thus the voltage performance is improved, and the amount of tap operations is reduced. To implement this concept, the proposed OLTC voltage control has to be coordinated with the plant control to receive the information of the MSCs switch status.

Chapter 7

Simulations and Analysis of the Results

The principal purpose of this chapter is to present some of the most representative simulation results, and to analyze the performance of the whole WPP during small disturbances in the grid. The performance of the proposed controls, for the WTG, OLTC, MSCs and WPP, are shown in details.

7.1 Introduction

The WPP shown in Figure 3.7, which includes the aforementioned controllers, has been tested through EMT simulations. The WPP is tested under different SCRs and active power injection scenarios. For transient response analysis, the full WPP is modeled (simulations with the time frame in seconds), and for the long term performance, an aggregated model of the WTGs is used due to computational reasons (simulations with the time frame in hours).

The sizing of the MSCs and STATCOM is based on the previous load flow calculations.

The WPPC slope gain of the plant voltage control is chosen to be 4 % in all the simulated cases, and the modeled plant layout and data are based on an existing installation.

7.2 Model Validation

In order to validate some of the simulation models, some tests were performed in a real WPP. The real WTG, used for validation purposes, includes an AQR, thus the WTG model has been programmed according to the same AQR. The same real WPP layout is used in the simulations.

Figure 7.1 shows the step response comparison between the model and the real WTG. It can be checked that the Q step response of the real WTG is similar to the simulated one. The performance of the simulated model correlates with the real measurements. It is expected that this validation can be extended to the WTG model which uses the proposed AVR.

Moreover, the simplified grid model (Thevenin equivalent) is verified by stepping the reactive power injected of the WPP up and down, and comparing the voltages obtained at the PCC in the real and in the simulated grid model. The model is fed with the real measured active and reactive power data.

Unfortunately, during the tests no bigger changes than 1% in the voltage at PCC were allowed by the TSO, so this validation only includes small changes in the voltage.

Following figure shows the Q comparison when stepping the Q_{ref} of a WTG. The Q reference (ref) is stepped up (Figure 7.1-(a)) and down (Figure 7.1-(b)). The real (real) and the simulated (sim) Q are represented in the figures.

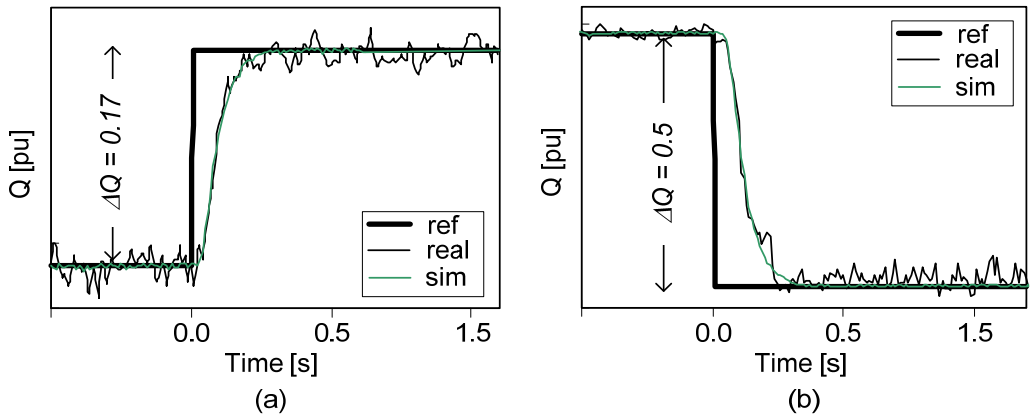

Figure 7.1. Q step results of the model and the real WTG.

Following figure shows the voltage step result comparison at PCC. The green curve is the model performance (sim), and the black one is the real measurement (real).

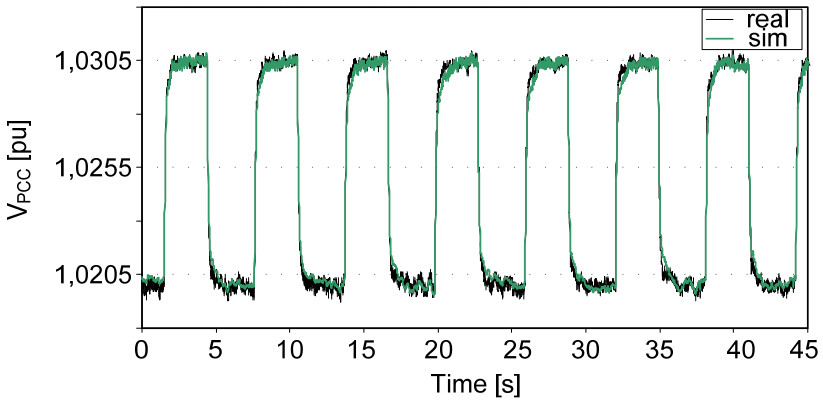

Figure 7.2. PCC voltage step result comparison of the model and the real grid.

7.3 On-Load Tap Changer Analysis Performance

Some simulations have been done to check the performance of the proposed OLTC control. In these simulations it is used two OLTC control configurations for comparing the performance. One control is not using the MSC current for decoupling purposes (called "normal") and the other one is using the MSC current for decoupling the line drop compensator (called "improved").

In the simulated cases, the SCR is equal to 5, the K_L is 8 %, and the active power injection of the plant is kept constant to a level of 0.7 pu. The voltage of the grid (V_{GRID}) is stepped up and down 0.1 pu.

The following figures show the grid voltage (V_{GRID}), the tap position (Tap position), the voltage at medium side (V_{MV}), and the voltage at WTG level (V_{LV}) for both cases (normal and improved).

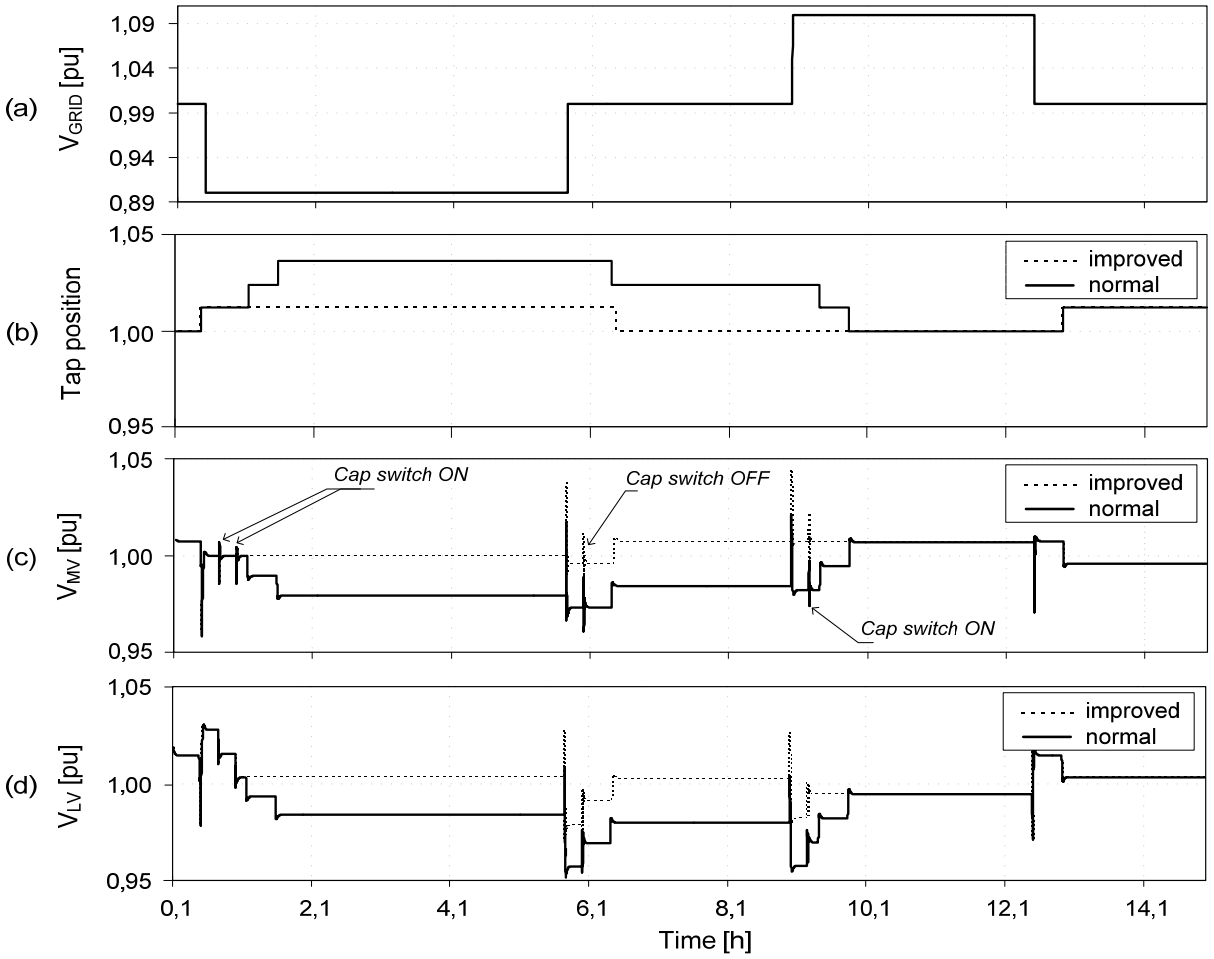

Figure 7.3. Comparison of two OLTC control configurations.

It can be observed how the tap changer compensates for the changes in the grid voltage. Using the scheme shown in Figure 6.7, the calculated ΔV_{drop} allows a better estimation of the voltage. It can be seen how the number of tap operations is reduced considerably (Figure 7.3-(b)) and the voltage at WTG terminals is closer to the nominal value (Figure 7.3-(d)), when the proposed OLTC control is used.

7.4 Step response of the Wind Power Plant

The grid voltage has been steeped up and down, under different SCRs and different active power level injections.

Figure 7.4 shows the voltage and reactive power at the PCC, when the grid voltage is stepped up (Figure 7.4-(b)) and down (Figure 7.4-(a)) 0.05 pu.

Figure 7.5 shows the voltage level at the PCC, the voltage references (V_{ref}) sent to the WTGs and STATCOM, the reactive power reference of the plant (Q_{ref}) and the measured at the PCC (Q_{PCC}), when the voltage of the grid is stepped down 0.1 pu.

In Figure 7.6, it is shown the voltage performance of the WPP at the PCC (V_{PCC}), when the plant control is shut down (no references sent to the WTGs, STATCOM and MSCs, and the OLTC is out of operation).

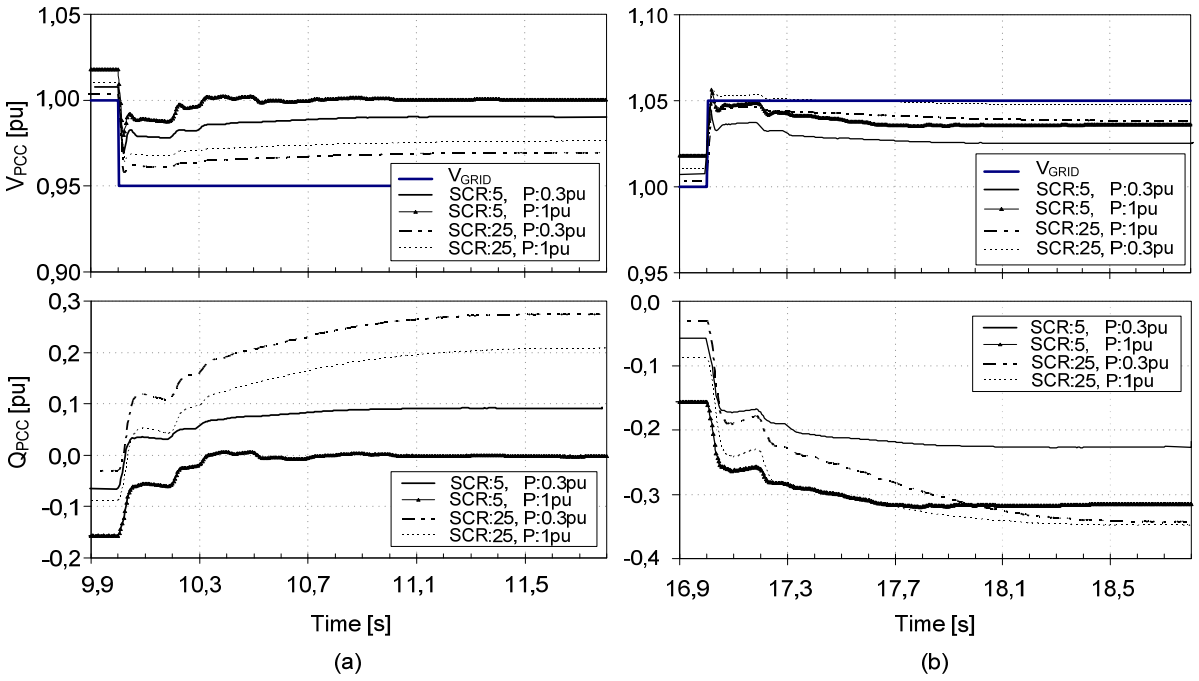

Figure 7.4. WPP step response for different SCRs and active power levels.

In Figure 7.4, it can be observed that the system offers a very fast reaction to PCC voltage changes. The summary of the step response in relation to the design indexes can be found in the last section of this chapter.

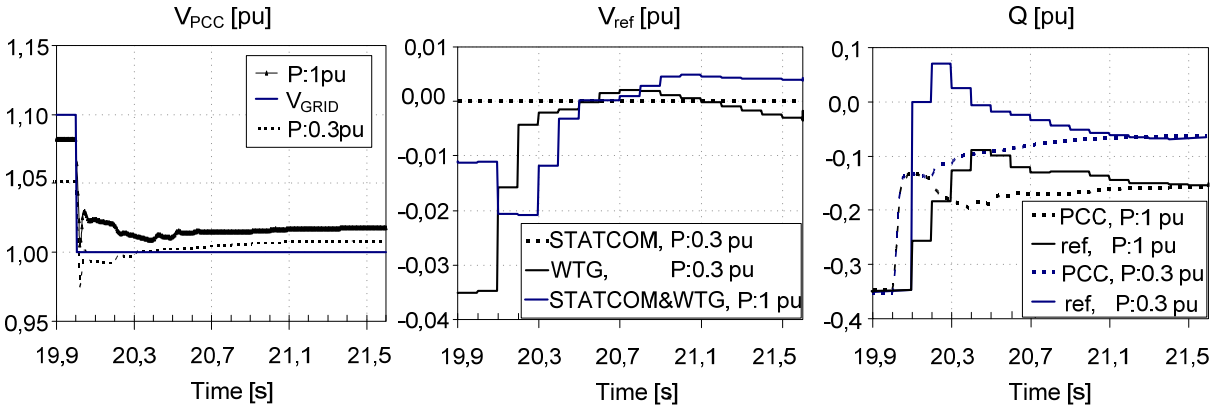

Figure 7.5. WPP response for SCR 5, and grid voltage step of 10%.

It can be observed in Figure 7.5-(V_{ref}), how the reference sent to the STATCOM is zero when the active power level at the PCC is 0.3 pu, at this active power level the DFIG WTGs are able to inject the required Q by themselves. For an active power level of 1 pu, the dispatcher K factor makes the STATCOM to have the same reference than the WTGs.

Additionally, it can be observed in Figure 7.5-(Q) that the lower the injected active power, the lower the injected Q by the WTGs and STATCOM is. This is due to the reactive power losses in the plant, which are related to the active power flow.

The curve named as Comp is representing the performance when the WTGs are including the Decoupling term (see Figure 5.7), and the curve No comp represents the performance when this term is disabled.

The aggregated WTG is injecting the active power shown in the Figure 7.8.

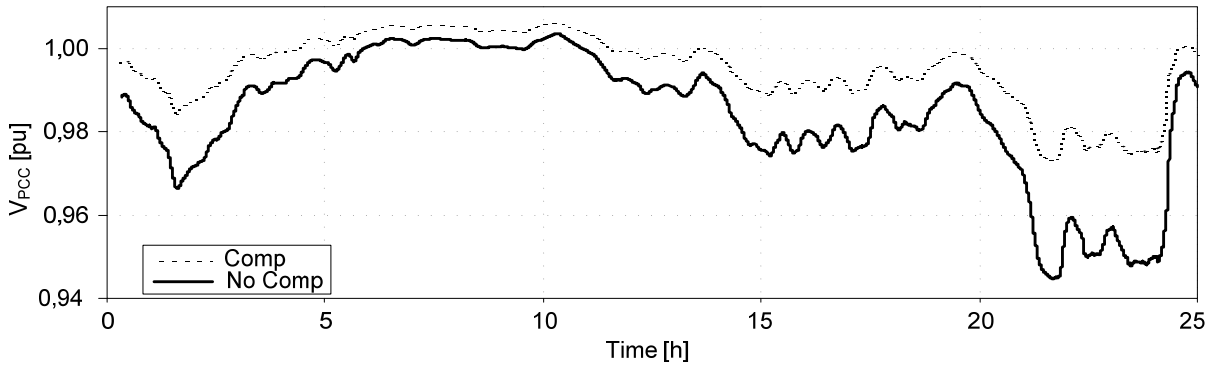

Figure 7.6. WPP performance when the central control is disabled, for a SCR 5. It is depicted the performance when the WTGs include the decoupling term (Comp) and when do not (No Comp).

7.5 Capacitor Step Switching Performance

In Figure 7.7, it is shown the transient effects of the capacitor switching in the voltage and reactive power at the PCC. Two different cases are simulated, and in both cases it is shown the performance when the function which calculates the ΔV_{Cap}, is activated ($\Delta V_{Cap\ ON}$) and when is not ($\Delta V_{Cap\ OFF}$). When it is activated, it can be seen how the transients are centered on the previous Q and V values.

In Figure 7.7-(a), one capacitor is connected with a SCR of 5, a grid voltage of 0.95 pu and with a WPP active power level injection of 1 pu. In Figure 7.7-(b), one capacitor is disconnected with a SCR of 10, a grid voltage of 1 pu and the WPP active power level injection is set to 1 pu.

The voltages at the PCC bus (V_{PCC}), and the Q injected at the PCC (Q_{PCC}) are plotted for every simulated case.

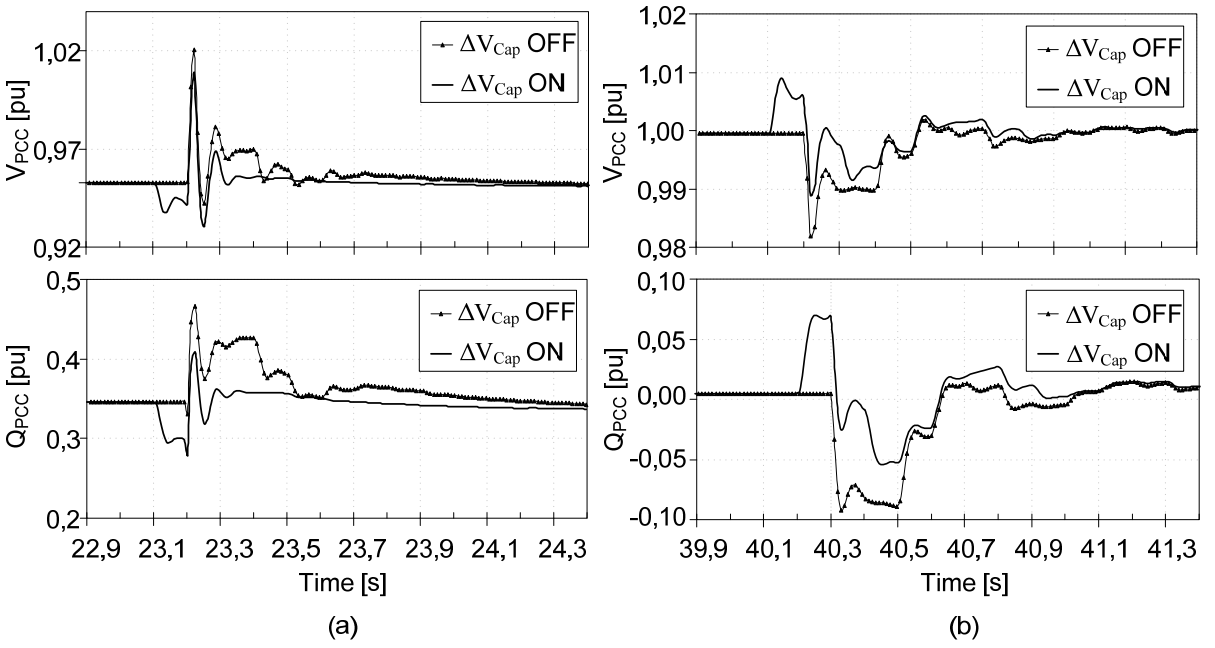

Figure 7.7. Capacitor switching transients: Case A: switching in 1 capacitor. Case B: switching out 1 capacitor.

7.6 Full system Analysis Performance

The performance of the plant under different conditions is shown in the following figures. The used line drop compensation gain (K_L) is 4 %.

In Figure 7.8 the aggregated WTG is programmed to inject the active power measured at the PCC of a real WPP, and the voltage of the grid is kept constant and equal to 1 pu.

It can be appreciated how the capacitors are switched in and out (Figure 7.8-(b)), to keep the steady-state reactive power converter action of the plant within 0.1 pu.

In the following figure, the injected active power at PCC (PCC), the injected reactive power of the WTGs, STATCOM and capacitors (Figure 7.8-(b)), and the voltage at WTG, STATCOM, and capacitor terminals (MV side of the transformer) are depicted (Figure 7.8-(c)).

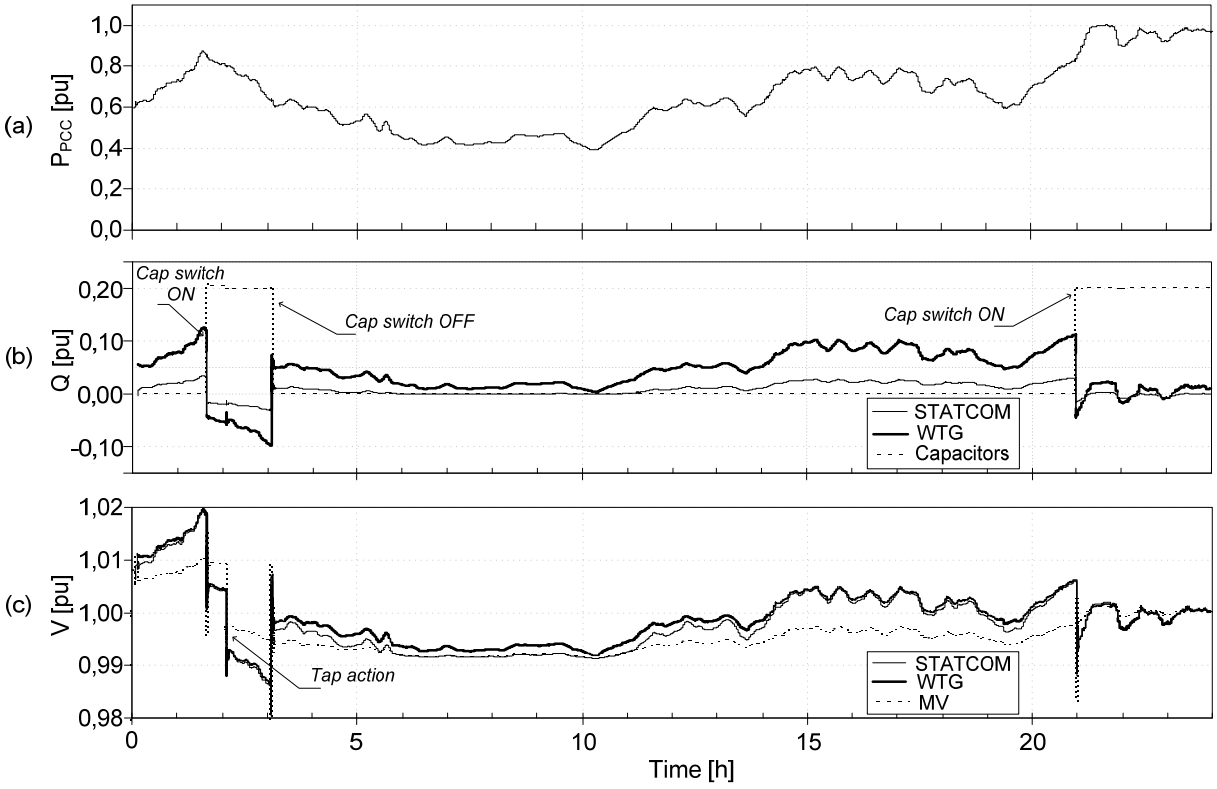

Figure 7.8. Simulation of a real time series injection of active power. V_{GRID} = 1 pu = cte., SCR = 5.

In Figure 7.9, the aggregated WTG is programmed to inject a constant active power equal to 0.7 pu, but in this case the voltage of the grid is stepped up and down 0.05 pu (Figure 7.9-(b)).

In the following figure, the injected reactive power from the WTG, STATCOM, and capacitors (Figure 7.9-(a)), and the measured voltages at the grid, PCC and MV buses (Figure 7.9-(b)), are depicted.

It can be seen, how the plant control connects and disconnects the capacitor banks, in order the amount of used reactive power from the converters is kept below a desired operation band of 0.1 pu. It should be mentioned, that this operation band has been found as a compromise to avoid excessive switching operations of the capacitors and reduce losses due to the converter usage.

The simulations show that the OLTC system control can run independently of the plant voltage control without any hunting phenomena.

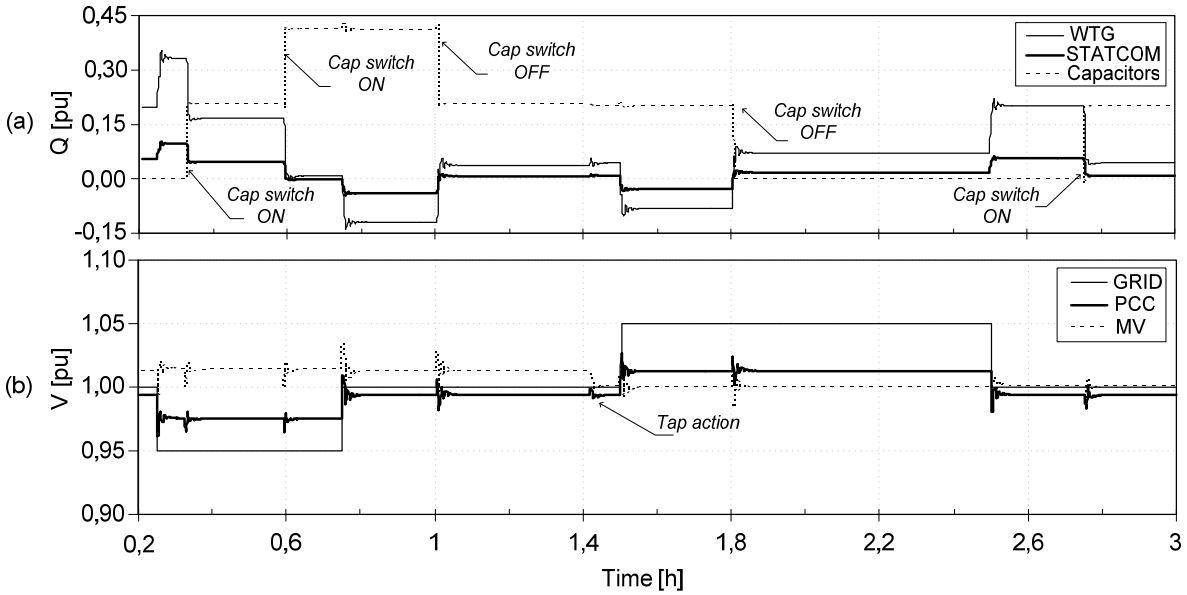

Figure 7.9. Voltage of the grid is stepped up and down 5 %, P = 0.7 pu = cte. SCR = 5.

7.7 Conclusions

In this chapter, it is shown some small signal simulation results where the performance of the system can be analyzed.

The proposed capacitor controller is successfully integrated in the plant controller, allowing the reduction of the capacitor switching transients, and limiting the converter operation for reactive power injection during steady-state perturbations. Moreover, the coordination of the STATCOM, WTGs and capacitor banks is done in such way that the "steady-state" reactive power usage of the converters is less than a desired band of 0.1 pu (see Figure 7.8 and Figure 7.9). Additionally, the proposed feature for the OLTC control shows an improved performance (see Figure 7.3).

The decentralized voltage implemented in the WTGs shows that the reliability of the system can be improved (see Figure 7.6). Finally, it can be said that the designed controls are performing according to the design specifications (see Figure 7.4).

The following tables summarize some of the simulation results obtained previously.

TABLE III
SUMMARY OF THE SIMULATED CASES FOR OLTC

CASE	Slope [%]	K_L [%]	SCR	Tap operations
Normal	4	8	5	*3*
Improved	4	8	5	*7*

TABLE IV
EVALUATION OF THE WPP STEP RESPONSE

P [pu]	SCR	Overshoot [%]	t_d [s]	t_r [s]	t_s [s]
0.3	5	*0*	*0.02*	*0.31*	*0.81*
1.0	5	*1*	*0.02*	*0.31*	*0.91*
0.3	25	*0*	*0.02*	*0.80*	*1.16*
1.0	25	*0*	*0.02*	*0.81*	*1.29*

Chapter 8

Control Operation during Large Disturbances

This chapter is related to the particular operation of the DFIG and WPP during faults. The performance of the DFIG is analyzed, and compared with the SG during faults. Additionally, it is proposed a DFIG control during severe faults, in order maximum reactive current injection at PCC is obtained. The WPP control during faults is also explained.

8.1 Introduction

The method used some years ago, disconnection of wind power generation after a network fault or having a great amount of reactive power consumption during post-fault periods, due to re-magnetization of the generator, is no longer acceptable by the grid operators. The reasons for these requirements are mainly two: possibility of voltage collapse in the recovery time after the fault, due to high reactive power consumption, and loss of synchronism if there is a massive wind power disconnection.

The replacement of traditional SGs by the new wind power plants, makes the TSOs to establish harder requirements during disturbance conditions, i.e. what it is desirable is that the WPPs perform in similar way as the SGs which are being replaced. In these grid codes, it is not explicitly specified how the active current should perform during faults; however, usually the reactive current injection is described, and should be inversely proportional to the voltage level during the fault. Nevertheless, the active current plays an important role to reach the desired reactive current at the PCC, especially during very low voltage conditions.

The DFIG response time during faults is another point of interesting discussion. Even it is not a controllable action, the high and fast demagnetization current of the stator, which follows almost instantaneously to the fault, can and should be considered as a reactive current injection supporting the grid voltage. This fault reactive current is capacitive.

This demagnetization reaction is similar to what can be seen in machines where the stator is directly coupled to the grid, such as the SGs or the inductions machines.

8.2 Doubly Fed Induction Generator Performance during Faults

The converters of the DFIG allow the control of the injected currents during faults, thus avoiding the WTG disconnection, moreover making possible the fulfillment of the grid codes regarding LVRT [90].

During grid faults, the DFIG uses the converter attached to the rotor to over-magnetize the generator, thus injecting reactive current to the electrical network, as the grid codes ask for. Thereby, and during fault periods, the WTG converters emulate the excitation of the SGs providing high levels of reactive current injection to the system.

Usually, the converter connected to the rotor, is controlled during short-circuits in a manner that makes the I_q injection to follow the grid code requirements [91], and I_d injection to follow the active power reference (P_{ref}), which is the output of the speed controller. It should be mentioned that during faults the priority is given to Q over P, among other things, this is needed if high values of I_q are requested by the TSOs.

The role of the speed controller is to allow maximum power tracking for every wind speed and together with the pitch system, to ensure that the generator rotational speed is between limits. During fault periods, and since I_q has priority to fulfill grid codes, usually I_d will fill the remaining value between I_q and the maximum converter current (I_r), see (8.2).

The grid connected converter is used for the DC-link voltage control; getting the voltage level of the DC-link between margins will avoid the disconnection of the WTG [92].

For faults causing high short-circuit currents, the rotor converter stops switching; the converter enters in blocking state to protect itself against high currents, losing the controllability of the rotor excitation. During this period, it is expected to have uncontrolled power going into the DC-link, causing the increase of the DC-link voltage. Therefore, the protective action of the chopper during these events is needed.

When the fault current level is under some pre-set threshold level, the converters resume the switching, enabling the generator to supply a predefined value of reactive current according to the remaining stator voltage. Normally, this reactive current level is specified by the local grid codes [25], [93]. If the fault location is sufficiently remote from the generator terminals, the converters will not be blocked, controlling the currents in every instant, therefore not presenting almost any current transient phenomena.

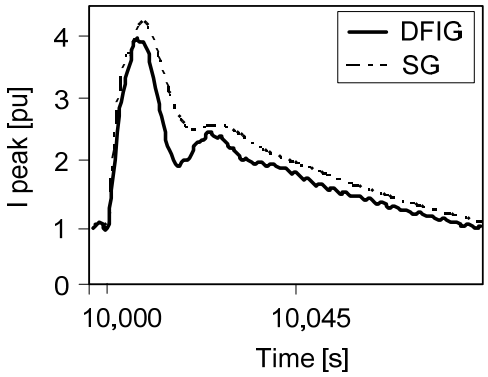

Figure 8.1. Short-circuit current envelope of a DFIG and a SG tuned for showing similar performance than a DFIG, for a three phase fault.

The DFIG with chopper protection, dissipates significant power on the rotor side during severe faults, therefore shortens the decay times and reduced peak currents are expected than for squirrel cage induction or synchronous generators [94] - [97]. In essence, the active rotor circuit depletes the generator magnetization much faster than SG excitation can do. This

causes the DFIG stator short-circuit current contribution to exhibit a very low AC component; this could make the protection coordination of the system to not operate correctly [A.5.].

One of the main differences between the traditional SG and the DFIG is the variable rotational speed range, allowed by the operation of the rotor converter. This variable slip of the DFIG has a direct impact on the short-circuit current frequencies, and an indirect impact on the peak values of the short-circuit currents, due to the chopper action.

Basically, it can be said that the short-circuit behavior of the DFIG is similar to a SG with very high time constants in the rotor circuit, thus they can be represented as a conventional SG [A.5.]. Reliable models of the WTGs in the industry standard simulation tools are needed, unlike conventional generators, the DFIG performance during faults is not standardized. A recent work in this direction has been presented in [A.3.].

The presented equivalence allows the tuning of a SG to have similar performance as a DFIG during severe faults, where the converter is blocked. Thus, making possible to use IEC [98] and other standards to evaluate the DFIG short-circuit performance.

Figure 8.1 shows the short-circuit current envelopes during a bolted three phase fault, at the MV side of the WTG (primary side of the WTG transformer). The curve labeled as DFIG shows the performance of a WTG based on a DFIG, and the curve labeled as SG shows the performance of the SG which has been tuned for having similar response than the DFIG.

8.3 Wind Power Plant Control during Faults

Since the plant control response is “slow”, hundreds of milliseconds in time reaction, there will be no centralized control action on the injected current at the PCC during faults. The LVRT control is performed solely by the WTGs and STATCOM controls.

The grid meter, located in the plant control, detects the fault and triggers a state machine (see Figure 3.7), which basically freezes the controllers during the fault to avoid saturation and undesired post-fault performance [29]. All the references sent by the plant control are frozen as soon as the fault is detected, when the fault is cleared, and after some predefined recovery time, the controllers will be unfrozen and re-initialized.

In the following figures, it is shown the comparison performance of the WPP when the state machine freezes the controllers (SM active) and when do not (SM not active).

In the simulated case, a 3-phase is applied causing the voltage at PCC (V_{PCC}) to decrease to 0.2 pu, the chosen SCR is 5.

It can be observed how by freezing the controllers during the fault period makes the fault recovery process smother. Moreover, the post-fault transient is longer when the state machine is not activated.

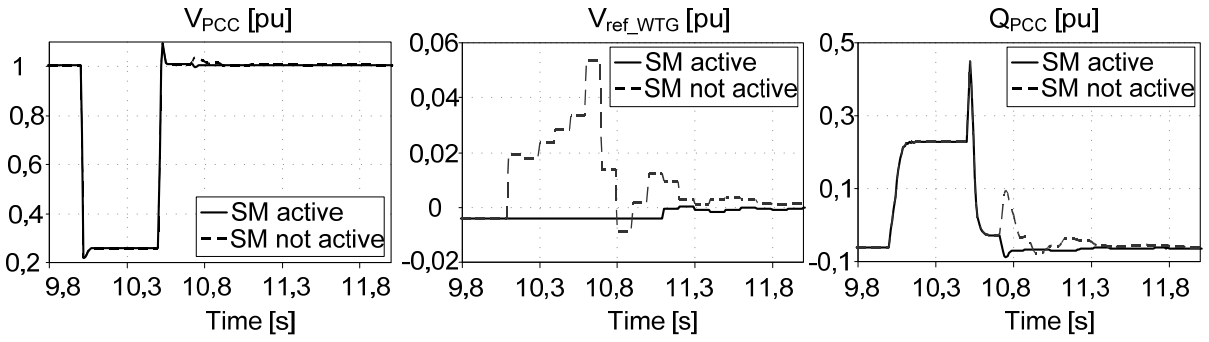

Figure 8.2. WPP performance during a fault, with and without LVRT state-machine implemented.

8.4 Proposed Wind Turbine Generator Control during Faults

Attention should be drawn to the importance of the particular d-q ratio between the injected currents during short-circuits to fulfill the grid codes requirements related to LVRT. The lower the voltage at PCC, the greater the influence of the ratio in the I_q measured at the PCC. The I_q measured at the PCC during very low voltage events, is drastically influenced by the injected I_d from the WTGs [A.4.]. Therefore, to keep the desired I_q at the PCC a new WTG control strategy is defined for very low voltage events (below 0.25 pu at generator terminals), making possible to reach high levels of I_q injection at the PCC, as most of the grid codes are asking for.

Basically, this control changes from injecting the I_d according to the speed control, to a new calculated reference according to the impedances seen from the generator to the fault, obtaining the desired d-q ratio at PCC.

The control implementation, for calculating the optimal active current reference (I_{d_ref}), can be simplified, neglecting the coefficients that include the impedance data of the grid and the faulted branch. Hence, making possible the use of an off-line data solely based on the available project data. See (8.1), being Z_{WPP} the impedance from generator terminals to the PCC ($\underline{Z}_{WPP} = R_{WPP} + jX_{WPP}$). More details can be found in [A.4.].

The voltage at PCC (V_{PCC}) can be estimated by the WTG using the minimum rms value, measured at the generator terminals during the event.

$$I_{d\_ref} = \frac{R_{WPP}}{X_{WPP}}\left(I_{q\_ref} - \frac{V_{PCC}}{|\underline{Z}_{WPP}|}\right) \tag{8.1}$$

The process of calculating the current references is as follows. In any case, the reactive rotor current reference (I_{q_ref}) is calculated by using the grid operator requirements regarding LVRT, generally speaking a look-up table will set the I_q reference according to the remaining voltage in the stator.

If the stator voltage (V_s) is below some threshold value ($V_{activation}$) then, I_{d_ref} is calculated by using (8.1), see Figure 8.3, where the switch will be in position (I). By using this equation it is possible to ensure an optimal I_q at the PCC [A.4.].

If the stator voltage is above the activation limit, then I_d is calculated by using the speed control, see Figure 8.3, where the switch will be in position (II).

$$I_r^2 = I_{q\_ref}^2 + I_{d\_ref}^2 \tag{8.2}$$

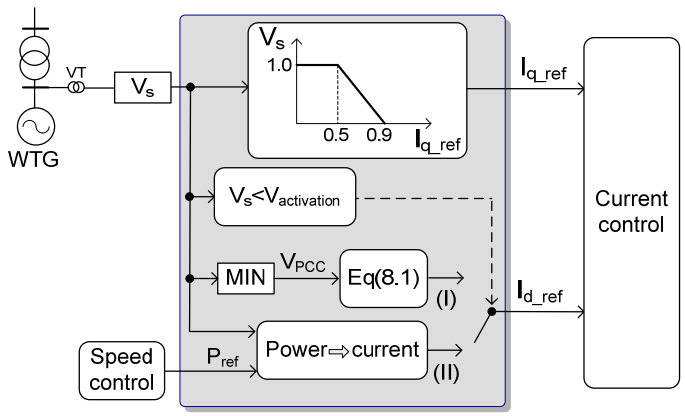

Figure 8.3. Diagram of the proposed WTG LVRT control.

A simple representation of the LVRT control implementation is shown in Figure 8.3. It can be easily observed, that during disturbances the reactive current reference, calculated by the voltage control, is bypassed and recalculated by a direct look-up table. The current control is the same as it was depicted in Figure 3.2.

In Figure 8.4, it is shown the performance of the WPP when a 3-phase fault located in the system makes the voltage at the PCC to decrease 90% of its rated value. Two different cases are shown.

Figure 8.4-(a) shows the WTG using the control algorithm shown in (8.1), and Figure 8.4-(b) shows when the WTGs inject the I_d according to the P_{ref}. The fact that during severe faults the stator voltage is quite low makes, in case (b), the injected I_d to follow (8.2). Hence, the I_d calculated by the power reference has to be decreased and accommodated to the maximum current of the converter.

The d-q currents depicted in Figure 8.4, I_q and I_d are the quadrature, and direct current respect to the voltage vector at the point where they are measured (at WTG level and at PCC level), and they are calculated following IEC 61400-21 [99].

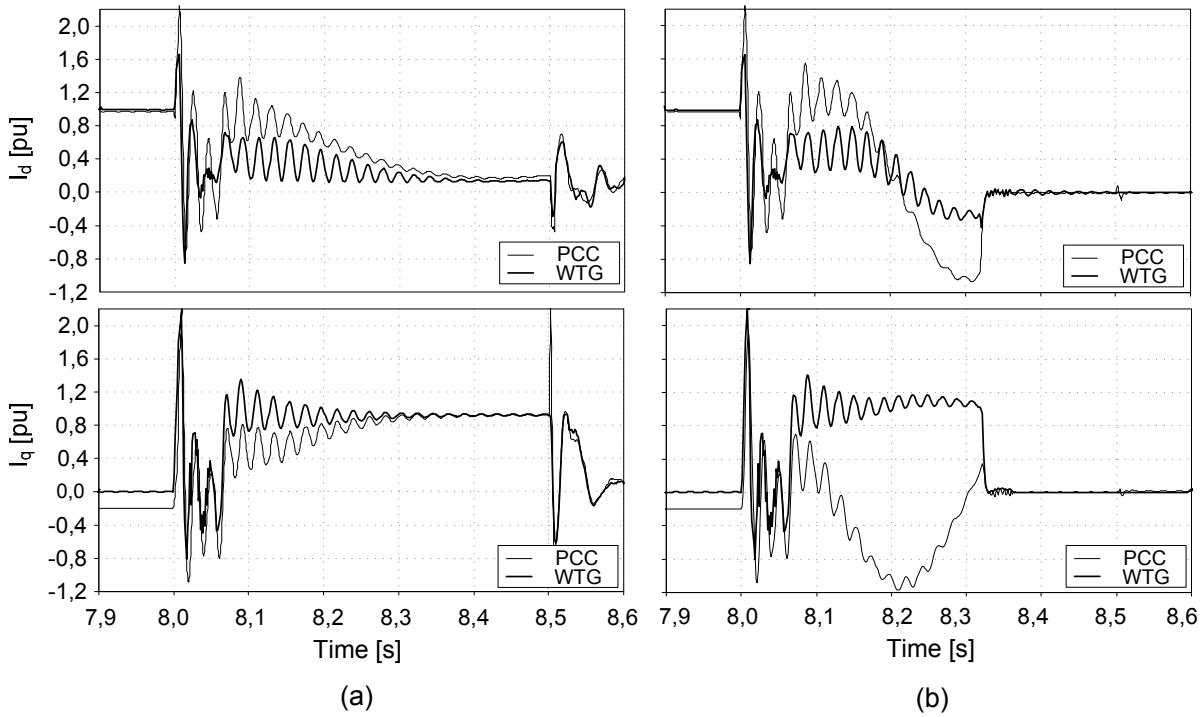

Figure 8.4. I_d and I_q measured at the PCC and generator terminals, for the two different LVRT controls. Case A: proposed control. Case B: I_d calculated according to $P_{ref.}$

It can be checked how in the case (a), which has the optimal I_d injection control, the I_q injected at the PCC keeps its maximum value, however in the case (b) the I_q gets even inductive values at the PCC. In both cases, the d-q currents at WTG level are following the desired references calculated by the WTG control, having I_q high values at generator terminals. Nevertheless, in the case (b) it can be checked how at PCC, the injected I_q is far away of what is required by the TSO.

This clearly shows the needed of an appropriate control of I_d during severe faults.

8.5 Conclusions

In this chapter, it is explained the DFIG performance during grid faults, and how the slip of the generator can affect the short-circuit currents, making a difference of this technology with the traditional SGs. Even, if the SGs exhibit very different short-circuit currents than the DFIG, SGs can be easily tuned for showing the same performance, thus making extensive the use of short-circuit standards, defined in the industry mainly for the SGs and induction generators, to the DFIG technology.

Furthermore, a new current control is presented for the DFIG, to maximize the reactive level current injection at the PCC during faults which cause very low voltage levels at PCC. Finally, it is presented how the plant control operates during faults; basically, it freezes all the controllers when the fault is detected, and when the fault is clear, and after some waiting time, the plant resumes the voltage control.

Chapter 9

Wind Power Plant with a VAr Reserve System

The amount of dynamic VAr, available most of the operation time, makes the WPP a good candidate to include VAr reserve management systems. In this chapter, two different ways of implementing a VAr management system are proposed and analyzed. It is an advantage of this control that the wind power plant itself may, due to its intrinsic overrated reactive power capacity, supply sufficient reactive power in order to uphold a given grid voltage level. By utilizing the intrinsic overrated reactive power capacity additional devices, such as for example SVCs and STATCOMs, can be avoided at other locations of the grid. As previously mentioned, such a reactive power reserve may be provided by the wind power plant itself, since the amount of reactive power installed for most active power working points exceeds the demand required by the grid operator. This overrated reactive power capacity is a consequence of sizing wind turbine facilities for maximum active power level.

9.1 Introduction

VAr reserve concept can be applied to a wind power plant in a manner similar to the SVC or STATCOM [75], [100]. This can be done since the amount of available reactive power in most of the active power working points increases the demand required by the grid operator. This is a consequence of sizing the reactive power plant for maximum active power level.

In the following figure, it is depicted the P-Q chart that includes the total WPP dynamic VAr sources (STATCOM and WTGs), and the P-Q grid code requirement.

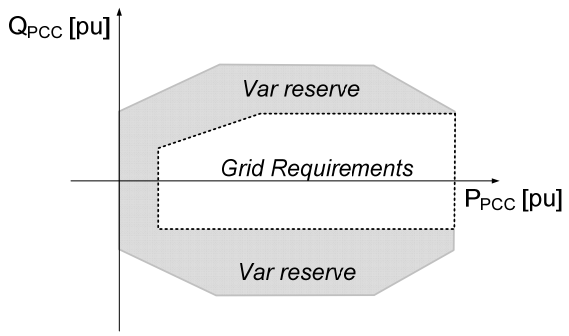

Figure 9.1. WPP installed dynamic VAr and grid code requirement P-Q charts.

The available amount of extra reactive power (VAr reserve) in the considered WPP is depicted in Figure 9.1, where the white area corresponds to the reactive power demands of the grid operator, and the grey area corresponds to the extra available dynamic reactive power. This extra fast-VAr capacity (given by the installed converters) can and should be used whenever the plant is below some active power levels, as it is happening most of the time in a WPP, thus helping the system restoration after events. Moreover, this VAr reserve concept is important for the system since the amount of reactive reserves at generating stations is a measure of the degree of voltage stability [4].

9.2 Wind Power Plant VAr Reserve Management

In this section, it is described two ways of implementing the reserve concept for a wind power plant; see Figure 9.2-(a): case A, and Figure 9.2-(b): case B.

In both cases, the maximum Q available is the maximum installed, the difference between these two cases is related to the management system to reduce this Q to its rated value, where the rated value is the one required by the grid operator.

Case A is based on offsetting the AQR_P reference with a Q_0, see Figure 9.3-(a). This Q_0 is activated when the injected reactive power is greater than the rated one (grid code requirement), and its function is driving back the injected reactive power to the rated value. The Q_0 is calculated in order the injected Q is driven slowly from point 1 to 2, see Figure 9.2-(a), waiting for the system to compensate for the voltage change by using passive components located nearby the WPP, such as OLTC, MSCs or MSRs. Use of tap-changing transformers is rather spread way of controlling node voltages. The whole voltage profile of the distribution grid is shifted up or down depending on the tap movement. MSCs and MSRs affect mainly the voltage of the node to which they are connected [5].

The control option used in the case A is suitable whenever no communication is available to the next substation.

To implement the case B concept, it is needed a communication link with the upwards substation, or to another central dispatcher. In this case, the WPP control translates the amount of extra VAr to a suitable reference for the tap changer or for other passive reactive power compensators (Ref_ex). Thus, no continuous reduction of Q is done in the WPP output; instead the WPPC forces to change the system characteristic by activating other passive components through a reference, getting a reduction in the injected Q after the reference is followed.

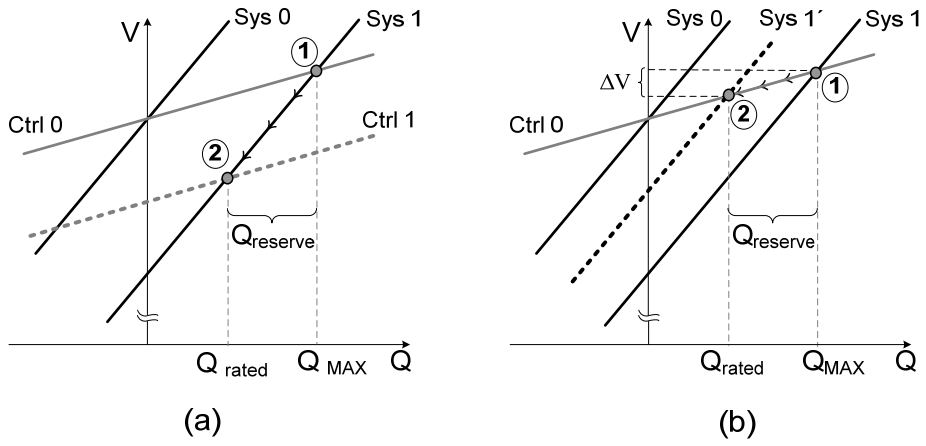

Figure 9.2. System and control characteristics for case A and B. Case A: Offsetting the control. Case B: Creating a ΔV reference.

The previous figures represent the characteristics of the two mentioned options. In these figures, it is depicted how the system will react for a step in the grid voltage. The grid characteristic changes from Sys 0 to Sys 1.

In the case A, the VAr control will offset slowly the Q_{ref}, changing the control characteristics from Ctrl 0 to Ctrl 1. In the Case B, the WPP injects the maximum Q installed, and the control calculates the ΔV reference to be sent upwards. When the system characteristic is changed (form Sys 1 to Sys 1'), then the Q is reduced accordingly, following the control characteristics, in essence it is reduced only when the voltage at PCC is increased.

Q_{MAX} is the maximum capability installed on the WPP, and Q_{rated} is the grid code requirement (dotted line in Figure 9.1.)

With these controls, the WPP will not reduce its Q output if no regulation capacity is left in the system (i.e., it could be that all the other elements are out or already connected).

The structures of the plant control with the implemented reserve VAr concept for the cases A and B are shown in the following figures.

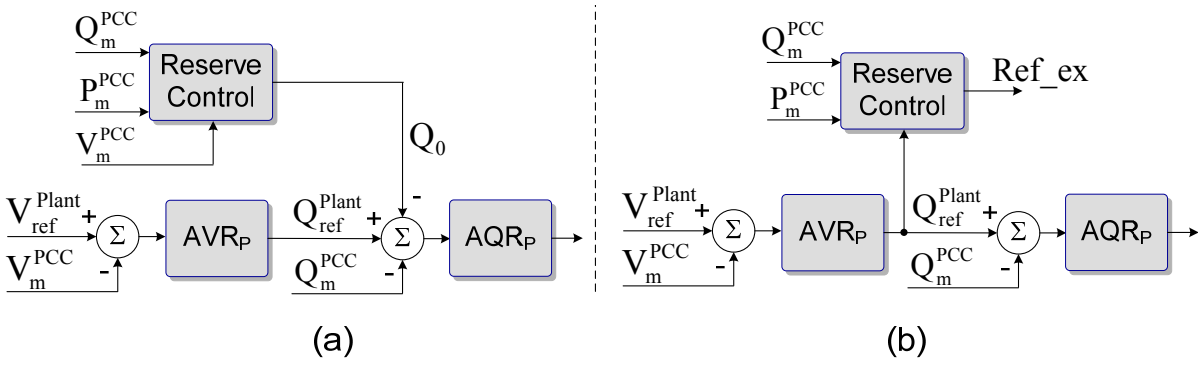

Figure 9.3. Plant control diagram including VAr reserve options. Case A: offsetting the input of the AQR_P, and case B: sending a reference to the upstream control layer.

9.2.1 Case A: Offsetting the AQR_P Reference

In the case A (Figure 9.4), the Q_{ref} calculated by the AVR_P is offset by the VAr control, in order the reactive power measured gets below the rated value. This kind of control should be applied whenever the communication with the upwards substation or high control layer is not possible.

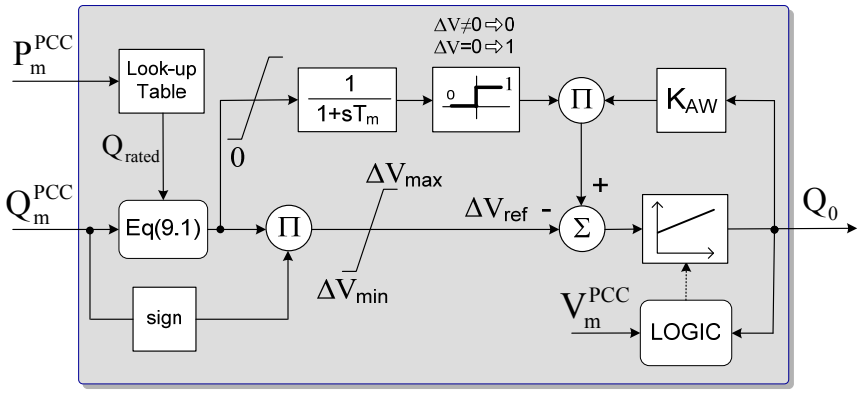

Figure 9.4. Reserve control for case A.

The bandwidth of the reserve control has to be smaller than the AQR_P. The K_{AW} function is to drive the Q_0 to zero when the Q_m is equal or below the rated Q.

The LOGIC module allocates the supervisory algorithm to detect changes in the grid. This module will freeze the PI regulator in case some predefined voltage changes at PCC

(ΔV) are measured. Moreover, the LOGIC module will unfreeze the PI regulator when the voltage at PCC (V_m^{PCC}) changes in opposite direction relative to the voltage influence of Q_0. Therefore, this LOGIC module will ensure that the WPP will not remove Q from the system if no reaction to the first reduction of Q is observed. Thus, this is an indirect way of gaining information about the availability of the other devices in the nearby area, and their capability of counteracting this Q reduction.

Basically, the LOGIC module allows a maximum voltage change (ΔV) for every reactive power reduction step, and only when the system reacts to this voltage variation, the control allows another change of ΔV. For that reason, Q_m is translated to a voltage level, ΔV_{ref}, by using (9.1). Thereby, it is possible to define the maximum change in voltage that the reserve control can drive in every step.

As depicted in Figure 9.4 the active power measured at the PCC (P_m^{PCC}) is used to calculate Q_{rated}. The Q_m^{PCC} together with the Q_{rated} are used to calculate the desired ΔV which will be fed to the PI regulator after going through a hard limiter. The PI regulator will drive ΔV to zero by outputting a Q_0 in order to off-set the AQR of the plant. The calculated ΔV is passed through a filter (with a time constant T_m) and whenever ΔV is greater than zero, K_{AW} is disabled by multiplying it by zero. On the other hand, when ΔV is equal to or below zero the K_{AW} is activated by reducing Q_0 to zero.

9.2.2 Case B: Creating a Reference

In the case B, the Reserve Control calculates a reference (Ref_ex). The VAr control function is to translate the Q_{ref}^{Plant} into an appropriate signal for the upstream control level, meanwhile the Q_{ref}^{Plant} is greater than the Q_{rated} in absolute value.

The calculated reference can be in different forms, e.g., move up/down the tap position, ΔV_{ref} or ΔQ_{ref}. Therefore, moving from point 1 to 2 indicates that the system characteristic is changed, by e.g., tap changer action or capacitor connection in the nearby area.

As an example, the reference ΔV_{ref} can be calculated as it is shown below, where the Q_{rated} is calculated by using a look-up table similar to Figure 9.1.

$$\text{Ref\_ex} = \Delta V_{ref} = \frac{(Q_m^{PCC} - Q_{rated})}{K_{SLOPE}} \tag{9.1}$$

9.3 Simulation Results and Analysis

Figure 9.5 represents the diagram of the simulated cases. The WPP is connected to the sub-transmission system, where some loads could be presented. Two loads, see (9.2), are connected to the respective buses of the OVL, representing small costumer consumptions (characterized by the following indexes a = 1, b = 2) [1].

$$L1 = L2 = P + \underline{j}Q = 0.3 + \underline{j}0.1 \quad [pu] \tag{9.2}$$

For the Case A, there is no communication link between the RTUs, and for the Case B the communication link is operative, and will be used for commanding the OLTC#2. The simulation results show the performance of the reserve controls for case A (see Figure 9.6) and case B (see Figure 9.7), when they are implemented in the WPP control.

In the Case B, the WPP is sending references to the tap changer control of the next substation, which is connected at the end of the OVL, whereas in the Case A there is no communication link between RTUs.

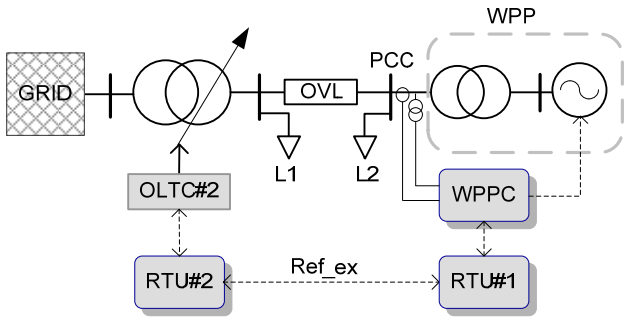

Figure 9.5. Simplified diagram of the simulated cases.

Figure 9.6 and Figure 9.7 show for the case A and B, a comparison when the tap control of the next substation is operative and can be changed (Tap ok), and when is out of operation (Tap out), i.e. either it is not working or it has reach the maximum position.

In these figures are depicted the tap position of the next substation (Tap postion#2), the Q at PCC (Q_{PCC}), and the voltage of the grid and at the PCC. Finally in the case A, it is also shown the offsetting signal (Q_0).

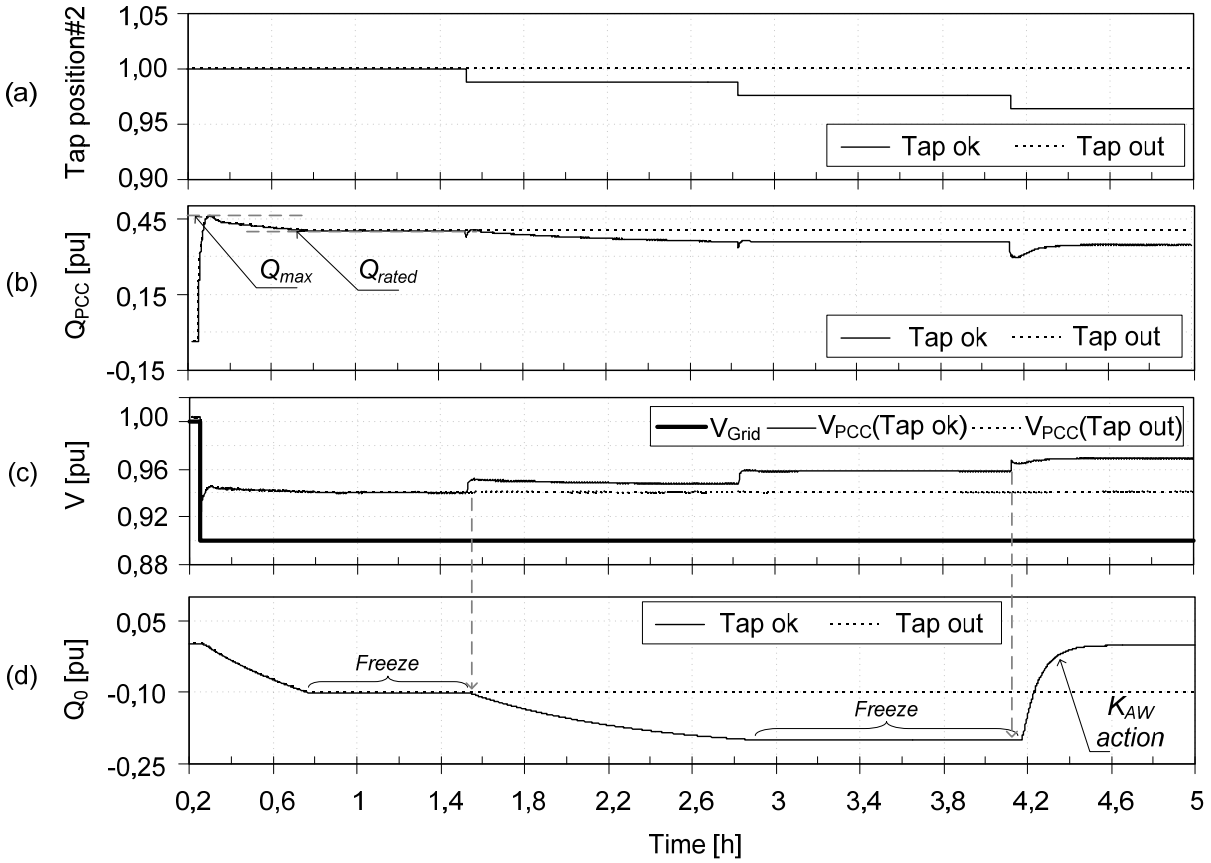

Figure 9.6. Simulation results for the case A.

It can be seen how in the case A (Figure 9.6), the WPP will inject its maximum available reactive power into the power supply grid, if a measured grid voltage falls below a predetermined grid voltage level.

When the controller detects that the injected reactive power exceeds a rated reactive power level the amount of reactive power is reduced, and the reactive power controller subsequently waits for the system to react to this small reactive power reduction. After a certain time, a tap changer of the next substation changes its transformer ratio (Figure 9.6-(a)), increasing the voltage of the feeder. This is sensed by the reactive power controller which will allow a further reduction of the injected reactive power. The reduction of injected reactive power is continued until the rated level is reached (Figure 9.6-(b)).

If the tap changer of the next substation is not operative, only the first reactive power reduction is allowed, since no change in the grid voltage can be sensed by the reactive power controller. Thus, in this scenario the LOGIC keeps Q_0 continuously frozen.

Finally, it can be observed that the K_{AW} action will drive the Q_0 to zero when the Q injected gets below the Q_{rated} (Figure 9.6-(d)).

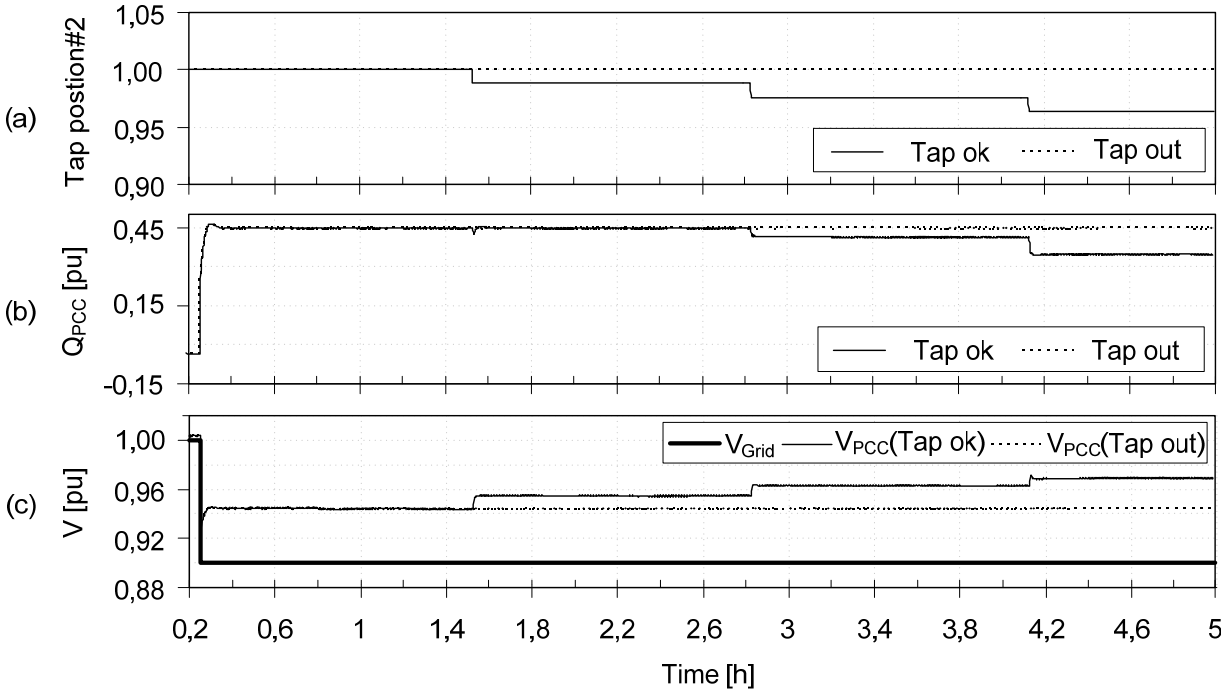

Figure 9.7. Simulation results for the case B.

In the case B (Figure 9.7), it can be seen that when the tap changer of the next substation is operative (Tap OK), it will follow the reactive power control references increasing its winding ratio (Figure 9.7-(a)), and the reactive power injected into the power supply grid is reduced as a consequence of this voltage increasing (Figure 9.7-(b)).

The AVR will reduce its Q_{ref}^{Plant} in accordance with the new voltages (Figure 9.7-(c)), and the reactive power is reduced in accordance with a new equilibrium working point once the tap has moved. Obviously, when the tap changer is out (Tap out), the reactive power is not reduced since no changes in the voltages are produced.

It can be seen how in the two presented control options (case A and B), the WPP stop reducing the Q injected when the system is not able to compensate this WPP Q reduction (Tap out cases), see Figure 9.6-(b) and Figure 9.7-(b).

9.4 Conclusions

In conclusion, this chapter explains how a reactive power reserve concept can be applied to a WPP. Instead of slowly reducing the reactive power injected, as other devices will do without knowing if the nearby system compensators are able to compensate for this reduction [29], the presented idea proposes two methods for implementing the reactive power reserve concept. One method is based on a reduction of the reactive power, by sending references to the next higher control level, whereas the other method is based on a reduction of the reactive power driven by a supervisory control, which allows a reduction of the reactive power in predefined voltage steps. The latter only applies if the system can not be communicated with the nearby compensators.

Chapter 10

Conclusions

This work has examined and proposed a control strategy for voltage control in a WPP, composed of DFIG type wind turbines. It has been shown how a WPP with DFIG WTGS can comply with some of the most demanding requirements regarding voltage performance if the right controls are implemented, and moreover, it can add some extra value to the system by using the WPP as a VAr reserve.
This chapter presents the summary and the conclusions of the work done.

10.1 Summary

In this project, the process of designing a wind power plant, composed of DFIGs, STATCOM and MSCs, for voltage control is shown. The selected control structure is based on a decentralized system, since it offers very fast system response to grid disturbances, and lower sensitivity to the grid impedance, making this decentralized system a good candidate when the expected SCR of the grid can change broadly, due to contingencies in the grid. Additionally, this control structure releases the central control of having grid impedance estimation techniques or adaptive controls.

By using a decentralized structure, the most demanding indexes regarding voltage control can be fulfilled. The presented decentralized control is using the advantages of the decentralized control (fast response reaction to grid voltage disturbances and low SCR dependency), and also, the advantages of a central control (equally reactive power loading in every WTG).

During severe grid transients, and due to the slowness of the central plant, the current injection control is fully done locally at WTG level.

The performance of the reactive current injection at the PCC can be optimized by having a dedicated control of the active current during faults, which none of the grid operators have put some much attention so far.

The lack of reactive power supplied by the DFIG compared to what it is required by the TSOs, is overcome by installing reactive power compensator, i.e. a STATCOM unit. To release the operation of the converters during steady-state disturbances, MSCs are installed in the WPP, which due to their characteristics they are appropriate for permanent disturbances compensation. The plant control includes the logic to switch in/out the MSCs, in such way that the usage of the converters for reactive power injection during steady-state is kept below a desired value of 10 %.

The STATCOM is coordinated with the rest of the WTGs by a dispatcher function, allocated in the plant control. The settings of the dispatcher are calculated by means of a WPP load flow analysis; these settings are depending on the active power injected at the PCC.

Normally, WPP transformer includes an OLTC system, since usually the allowed voltage range of operation defined by the TSO is ranging from ±10% of its rated value, and considering that the point of connection is separated from the WTG stator terminals by two transformers, it is clear that an OLTC system will help to keep the stator voltage close to its nominal value. It is proposed to coordinate the OLTC system with the main substation control, thereby the OLTC line drop compensation can estimate much better the voltage at a remote location inside the WPP, the information exchanged is the connection status of the MSCs. Therefore, by having this information, the current injected from the MSCs can be removed from the total measured current at MV.

All the previous elements need to be coordinated by a central control; otherwise counteraction can occur between them.

Finally, due to the WPP reactive power sizing is done for maximum active power level, it is expected that a big amount of reactive power remains unused most of the time due to the wind power generation characteristics; to change this, a VAr reserve concept system is proposed and applied, therefore the grid can be benefit from this extra reactive power for most of the active power levels.

10.2 Main contributions

The main contributions presented in this work are the following ones:

- Small signal analysis of a WPP with DFIG wind turbines, for voltage control purposes. This includes the detailed representation of the DFIG WTG as transfer functions. Hence, the system stability, in terms of SCR and control gains, can be analyzed, providing a tool to choose the most suitable strategy for voltage control and grid code fulfillment.

- Development of a distributed control for a WPP, including the design of the local and central controllers. The analysis of the interaction, between the different voltage controls of the WTGs, allows the design of the proposed controllers.
  It has been found that a distributed proportional voltage control is a suitable option when low SCR sensitivity and fast time reaction are needed. However, the decentralized structure, which requires voltage controls to be programmed in the WTG, offers a disadvantage if compared with a central control, which requires the WTG to allocate a reactive power control. The local voltage control of the WTG is influenced by the active power flow and the relative position on the feeder, causing the loading of the WTGs, in term of reactive power injection, to be unequally, and even sometimes with different signs. The proposed control uses the advantages of both concepts, i.e. equally loading (central control), and fast reaction to disturbances (decentralized control).

- All the elements that are included in the WPP, which collaborates in the reactive/voltage control, need to be coordinated. Thus, the integration in the plant control of the MSCs, STATCOM and OLTC is studied.
  - A novel strategy for dispatching the STATCOM is created, which is based on previous load-flow analysis of the WPP. Having the STATCOM the same voltage control implemented as the WTGs, the STATCOM can easily be integrated in the system.
  - A strategy for the connection/disconnection of the MSCs is proposed, which is focused on releasing the reactive power operation of the converters to a predefined level, and at the same time avoiding excessive switching in the capacitors.

  - An OLTC control is proposed. It has been found that the reactive current of the MSCs badly influences the line drop compensator of the OLTC, therefore a decoupling system has been proposed.

- The DFIG performance during faults has been analyzed and compared with traditional SGs. It has been found that the DFIG operation during severe faults, where the protective action of the chopper is activated, can be easily represented by an adequately tuned SG.
  During severe faults, the reactive current at the PCC can be drastically influenced by the active current, hence to increase the reactive power level at the PCC a new dedicated control for active current during fault is proposed, which is using an off-line data based on the WPP data. Summarizing, the following two points are proposed:
  - Representation of a conventional SG as a DFIG for short-circuit studies.
  - A new WTG LVRT control for severe faults, which allows having an optimal reactive current at PCC.

- To extract the maximum benefits of the installed converters, which most of the time remains unused, a VAr reserve concept is applied to the WPP. Two different ways for the implementation are proposed and analyzed. As a difference with traditional VAr reserve regulators, the proposed controls are based on an effectively reduction of the injected reactive power according to the system capability to cope with this reduction.

10.3 Future work

Most of the objectives stated in the problem definition have been met. However, many improvements still remain to be made for the integration of the WPP in the system. Future work should be pointed in the following direction:

- Analysis of more advanced dispatching methods for STATCOM and WTGs.

- Interaction of the WPP with more realistic grid models, where other generators SGs are presented. This study should be focused more on the outside world of the WPP.

- Other MSCs switching strategies, based on losses minimization.

- Analysis of the overloading capabilities of the converters installed and its use for voltage control.

- Other fault control strategies considering the overloading of the converters.

10.4 Author's Publication List

[A.1.] Jorge Martínez, Philip C. Kjær, Pedro Rodriguez, Remus Teodorescu, "Comparison of Two Voltage Control Strategies for a Wind Power Plant". Accepted for publication in IEEE Power & Energy Society 2011. Power Systems Conference and Exposition. March 20-23, 2011, Phoenix, USA.

[A.2.] Jorge Martínez, Philip C. Kjær, Pedro Rodriguez, Remus Teodorescu, "VAr Reserve Concept Applied to a Wind Power Plant". Send for publication to

IEEE Power & Energy Society: 2011. Power Systems Conference and Exposition. March 20-23, 2011, Phoenix, USA.

[A.3.] Jorge Martínez, Philip C. Kjær, Pedro Rodriguez, Remus Teodorescu, "Short Circuit Signatures from Different Wind Turbine Generator Types".
Presented in: 2009 Power System Relaying Committee, Power Engineering Society, IEEE, College Station, Texas.
http://www.pes-psrc.org/c/C17/TAM%20Session%200409%20Vestas%20Fault%20Current%20Signatures%20of%20DFIG%20Wind%20Turbines%20Garcia.pdf
Accepted for publication in IEEE Power & Energy Society 2011. Power Systems Conference and Exposition. March 20-23, 2011, Phoenix, USA.

[A.4.] Jorge Martínez, Philip C. Kjær, Pedro Rodriguez, Remus Teodorescu, "Active current control in wind power plants during grid faults".
Published in: WIND ENERGY, (2010), DOI: 10.1002/we.394

[A.5.] Jorge Martínez, Philip C. Kjær, Pedro Rodriguez, Remus Teodorescu, "Parameterization of a synchronous generator to represent a doubly fed induction generator with chopper protection for fault studies".
Published in: WIND ENERGY, (2010), DOI: 10.1002/we.406

[A.6.] Jorge Martínez, Philip C. Kjær, Remus Teodorescu, "DFIG Turbine Representation for Small Signal Voltage Control Studies".
Published in: 12th International Conference on Optimization of Electrical and Electronic Equipment (OPTIM), 2010 Issue Date: 20-22 May 2010, page(s): 31 - 40

[A.7.] Jorge Martínez, Philip C. Kjær, Pedro Rodriguez, Remus Teodorescu, "Design and Coordination of a Capacitor and OLTC control for a Wind Power Plant of DFIG Wind Turbines".
Sent for publication to WIND ENERGY. Manuscript number is WE-10-0106.

[A.8.] Jorge Martínez, Philip C. Kjær, Pedro Rodriguez, Remus Teodorescu, "Centralized Slope Voltage Control for a DFIG Wind Power Plant with STATCOM".
Sent for publication to IEEE Transactions on Sustainable Energy. Manuscript number is TSTE-00113-2010.

[A.9.] Jorge Martínez, Philip C. Kjær, Pedro Rodriguez, Remus Teodorescu, "Design and Analysis of a Slope Voltage Control for a DFIG Wind Power Plant".
Accepted for publication in IEEE Transactions on Energy Conversion with small changes. Manuscript number is ID TEC-00256-2010

10.5 Author's Pending Patent List

A. Control Method for an OLTC System

B. Method for Creating a VAr Reserve in a WPP

C. Method for Controlling the MSCs in a WPP

D. Dispatching Strategy for a Reactive Power Compensator

E. Method for WTG Control

F. Method for Controlling the Current Injection During Faults

Bibliography

[1] "*Reactive Power Control in Electric Systems*", Edited by Timothy J. E. Miller, John Wiley & Sons, New York, 1982.

[2] Rabiee A., Parniani M., "*Optimal reactive power dispatch using the concept of dynamic VAR source value*". Power & Energy Society General Meeting, 2009. PES '09. IEEE Publication Year: 2009, Page(s): 1 – 5.

[3] P. Kundur, "*Power System Stability and Control*", 1994 McGraw-Hill, Inc. ISBN 0-07-035958-X.

[4] Feng Dong, Chowdhury, B.H., Crow, M.L., Acar, L., "*Improving voltage stability by reactive power reserve management*", Power Systems, IEEE Transactions on Volume: 20, Issue: 1, Publication Year: 2005, Page(s): 338 – 345.

[5] "*Wind Power in Power Systems*", Edited by T. Ackermann, 2005 John Wiley & Sons, Ltd ISBN: 0-470-85508-8 (HB).

[6] Avramovic, B., Fink, L.K., "*Real-time reactive security monitoring*", Power Systems, IEEE Transactions on Volume: 7, Issue: 1, Publication Year 1992, Page(s): 432 – 437.

[7] Rubenstein, A. S., Walkley, W. W., "*Control of Reactive Kva with Modern Amplidyne Voltage Regulators*", Power Apparatus and Systems, Part III. Transactions of the American Institute of Electrical Engineers Volume: 76, Issue: 3, 1957, Page(s): 961–968.

[8] M. Stacey, E. Lemak, T., Gyugyi, L., Cease, T.W. Edris, A., "*Development of a ±100 MVAr static condenser for voltage control of transmission systems*", Power Delivery, IEEE Transactions on Volume: 10, Issue: 3, Publication Year: 1995, Page(s): 1486 – 1496.

[9] System Dynamic Performance Subcommittee, "*Power System Engineering Committee Static VAr compensator models for power flow and dynamic performance simulation*" Transactions on Power Systems, IEEE Volume: 9, Issue: 1, Publication Year: 1994, Page(s): 229–240.

[10] Khalilinia, H., Ghaisari, J., "*Improve Sub-Synchronous Resonance (SSR) damping using a STATCOM in the transformer bus*", EUROCON '09. IEEE Publication Year: 2009, Page(s): 445 – 450.

[11] Mutale J., Strbac G., "*Transmission network reinforcement versus FACTS: an economic assessment*", Power Systems, IEEE Transactions on Volume: 15, Issue: 3 Publication Year: 2000, Page(s): 961 – 967.

[12] Al-Majed, S.I., "*Secondary Voltage Control: Enhancing Power System Voltage Profile*", Power and Energy Conference, 2008, PECon 2008, IEEE 2nd International, 1–3 Dec. 2008, Page(s): 1218–1221.

[13] Taylor, C.W., "*Line drop compensation, high side voltage control, secondary voltage control-why not control a generator like a static VAr compensator?*", Power Engineering Society Summer Meeting, 2000. IEEE Volume: 1: 2000, Page(s): 307–310.

[14] Lefebvre H., Fragnier D., Boussion J.Y., Mallet P., Bulot M., "*Secondary coordinated voltage control system: feedback of EDF*", Power Engineering Society Summer Meeting, 2000. IEEE Volume: 1 Publication Year: 2000, Page(s): 290 – 295.

[15] A. Conejo, M. Aguilar, "*A nonlinear approach to the selection of pilot buses for secondary voltage control*", IEE proceedings – Power System Control and Management, Conf. Publi. No. 421, 1996, Page(s): 191 – 195.
[16] Richardot O., Viciu A., Besanger Y., Hadjsaid N., Kieny C., "*Coordinated Voltage Control in Distribution Networks Using Distributed Generation Transmission and Distribution Conference and Exhibition*", 2005/2006 IEEE PES Publication Year: 2006, Page(s): 1196 – 1201.
[17] Corsi S., "*Wide Area Voltage Regulation & Protection*", PowerTech, 2009 IEEE Bucharest Publication Year: 2009, Page(s): 1 – 7.
[18] http://www.ewea.org/
[19] V. Akhmatov, "*Experience with Voltage Control from Large Offshore Windfarms: the Danish Case*", WIND ENERGY, 11 Feb 2009, Page(s): 692 – 711.
[20] I. Erlich, U. Bachmann, "*Grid Code Requirements Concerning Connection and Operation of Wind Turbines in Germany*", IEEE Power Engineering Society General Meeting, 12-16 June 2005, Vol.2, Page(s): 1253 – 1257.
[21] Arulampalam A., Ramtharan G., Jenkins N., Ramachandaramurthy V.K., Ekanayake J.B., Strbac G., "*Trends in Wind Power Technology and Grid Code Requirements*". International Conference on Industrial and Information Systems, ICIIS 2007, 9–11 Aug. 2007, Page(s): 129 – 134.
[22] https://www.entsoe.eu/
[23] Dienst uitvoering en toezicht elekriciteit. Netcode. Technical report, 2003.
[24] P.O.12.2, "*Connected Installations to the Transmission Spanish System: Minimum Requirements for Design and Security*", Red Electrica de España, Grid Code Requirements for installations connected to the transmission system in Spain.
[25] P.O.12.3, "*Requirements during voltage dips for the installations in the group of renewable energy*", Royal Decree 436/2004, REE, July 2004, Grid Code Requirements for Voltage Dips in Spain.
[26] National Grid Electricity Transmission: "*Guidance Notes for Power Park Developers*", 2008.
[27] Alberta Electric System Operator (AESO), "*Wind Power Facility, Technical Requirements*", Alberta, November 2004.
[28] Hydro–Quebéc, "*Technical Requirements for the Connection of Generation Facilities to the Transmission Systems*", Quebéc, Canada.
[29] Romegialli G., Beeler H., "*Reactive compensation. Problems and concepts of static compensator control*", Generation, Transmission and Distribution, IEE Proceedings C Volume: 128, Issue: 6, Year: 1981, Page(s): 382 – 388.
[30] S. Narita, M. Hamman, "*Multi-computer Control of System Voltage and Reactive Power on Real-time Basis*", IEEE Transactions on Power system. Vol. PAS-92, no. 1, 1973.
[31] 20 USA–FERC-661–A–2005–12–12, Final Rule on Interconnection for Wind Energy, Order No. 661–16.
[32] Australia, NEEMCO, 2007–03–15.
[33] National Electricity Amendment (Technical Standards for Wind Generation and other Generator Connections) Rule 2007 No. 2–26.
[34] Canada, CanWEA, 2006–06–09–DRAFT, Canadian Wind Interconnection Working Group – (CWIWG).
[35] IEEE Std. 421.5–1992, "*IEEE Recommended Practice for Excitation System Models for Power System Stability Studies*".
[36] Tsu-Tian Lee, Jin-Tsong Jeng, Ching-Long Shih, "*Using neural networks to improve gain scheduling techniques for linear parameter-varying systems*", International Workshop on Advanced Motion Control, 1996. AMC '96-MIE. Proceedings, 1996 4th, Volume 1, 18–21 March, Page(s): 299 – 304.

[37] Belanger J., Scon G., Andersson T., Torseng S., "*Gain Supervisor, for Thyristor Controlled Shunt Compensator*", CIGRE Proceedings of the 31'Session 1984, paper 3841.
[38] Li Chun, Jiang Qirong, Xu Jianxin, "*Investigation of voltage regulation stability of static synchronous compensator in power system*" PES Winter Meeting, 2000. IEEE, vol.4, Publication Year: 2000, Page(s): 2642 – 2647.
[39] L. Asiminoaei, R. Teodorescu, F. Blaabjerg, and U. Borup, "*Implementation and test of an online embedded grid impedance estimation technique for PV inverters*", Industrial Electronics, IEEE Transactions on, 2005, vol. 52, Page(s): 1136 – 1144.
[40] M. Tsukamoto, S. Ogawa, Y. Natsuda, Y. Minowa, and S. Nishimura, "*Advanced technology to identify harmonics characteristics and results of measuring*", Proc. of HQP, 2000, vol. 1, Page(s): 341 – 346.
[41] M. C. Di Piazza, P. Zanchetta, M. Sumner, and D. W. P. Thomas, "*Estimation of load impedance in a power system*", Proc. of HQP, 2000, vol. 2, Page(s): 520 – 525.
[42] J. P. Rhode, A. W. Kelley, and M. E. Baran, "*Line impedance measurement: a non-disruptive wideband technique*", Proc. of IAS, 1995, vol. 3, Page(s): 2233 – 2240.
[43] Kennedy J., Fox B., Morrow D.J., "*Distributed generation as a balancing resource for wind generation*", Renewable Power Generation, IET Volume: 1 , Issue: 3, Publication Year: 2007, Page(s): 167 – 174
[44] Robert G., Prestat B., "*Conformity evaluation method of power plants performance for grid stability*", Power Systems Conference and Exposition, 2004. IEEE PES Publication Year: 2004, vol.2, Page(s): 1109 – 1112.
[45] Robert G., Planque J.L., "*Robust Digital Automatic Reactive Power Regulator for Hydro Power Plants*", International Conference on Clean Electrical Power, 2007. ICCEP '07. Publication Year: 2007, Page(s): 175 – 179.
[46] CIGRE TF 38.02.17. "*Advanced Angle Stability Controls*", CIGRE, Brochure, April 2000.
[47] C. W. Taylor, "*Power System Voltage Stability*", McGraw-Hill, 1994.
[48] https://pscad.com/index.cfm?
[49] Fila, M., Taylor G.A., Hiscoc, J., Irving M.R., Lang P., "*Flexible voltage control to support Distributed Generation in distribution networks*", Universities Power Engineering Conference, 2008. UPEC 2008. 43rd International, Publication Year: 2008, Page(s): 1 – 5.
[50] Eirgrid-2007–01–01, Grid Code, Version 2.01.
[51] Nordel-2006–11–11, Nordel Connection Code Wind Turbines 13.
[52] France-Arrete-2003-07-04, 4. July 2003 relating to the technical specification of design and operation for connection with the public network of transport of an electric generating station of power, NOR: INDI0301719A.
[53] IEEE Std. 421.2–1990, "*IEEE Guide for Identification, Testing, and Evaluation of the Dynamic Performance of Excitation Control Systems*".
[54] http://www.nerc.com/filez/standards/Project2008-01_Voltage_and_Reactive_Planning_and_Control.html.
[55] EWEA organization, "Integrating Wind Developing Europe's Power Market for the Large-Scale Integration of Wind Power". February 2009. http://www.ewea.org/fileadmin/ewea_documents/documents/publications/reports/TradeWind_Report_01.pdf.
[56] Wei Qiao, Harley R., Venayagamoorthy G., "*Coordinated reactive power control of a large wind farm and a STATCOM using heuristic dynamic programming*" Power & Energy Society General Meeting, 2009. PES '09. IEEE Publication Year: 2009, Page(s): 493 – 503.
[57] Wei Qiao, Venayagamoorthy G.K., Harley R.G., "*Real-Time Implementation of a STATCOM on a Wind Farm Equipped with Doubly Fed Induction Generators*", Industry

Applications Conference, 2006. 41st IAS Annual Meeting. Conference Record of the 2006 IEEE Volume: 2, Page(s): 1073 – 1080.

[58] Muyeen S.M., Ali M.H., Takahashi R., Murata T., Tamura J., "*Stabilization of Wind Farms Connected with Multi Machine Power System by Using STATCOM*", Power Tech, 2007 IEEE Lausanne, Page(s): 299 – 304.

[59] W. Qiao, R. G. Harley, and G. K. Venayagamoorthy, "*Effects of FACTS devices on a power system which includes a large wind farm*", Proc. IEEE PES Power Syst. Conf. Expo. 2006, Atlanta, GA, Page(s): 2070 – 2076.

[60] Liew S.N., Strbac G., "*Maximising penetration of wind generation in existing distribution networks Transmission and Distribution*", IEE Proceedings- Volume: 149, Issue: 3, Publication Year: 2002, Page(s): 256 – 262.

[61] Li Wang, Tai–Her Yeh, Wei–Jen Lee, Zhe Chen, "*Analysis of a commercial wind farm in Taiwan Part II: Different current-limit reactors and load tap changers on system performance*", Industrial & Commercial Power Systems Technical Conference - Conference Record 2009 IEEE, Publication Year: 2009, Page(s): 1 – 8.

[62] Liwei Wang, Sina Chiniforoosh, and Juri Jatskevich, "*Simulation and Analysis of Starting Transients in Rotor-Chopper-Controlled Doubly-Fed Induction Motors*" 2008 IEEE Electrical Power & Energy Conference.

[63] Pannell G., Atkinson D. J., Zahawi B., "*Minimum-Threshold Crowbar for a Fault-Ride-Through Grid-Code-Compliant DFIG Wind Turbine*", Energy Conversion, IEEE Transactions on Volume: 25, Issue: 3, Publication Year: 2010, Page(s): 750 – 759.

[64] G. Tapia, A. Tapia, and J. Ostolaza, "*Proportional-Integral Regulator-Based Approach to Wind Farm Reactive Power Management for Secondary Voltage Control*", IEEE Transactions on Energy Conversions, Vol.22, No.2, June 2007.

[65] J. Rodriguez Amenedo, S. Arnalte, and J. Burgos, "*Automatic generation control of a wind farm with variable speed wind turbines*", IEEE Transactions on Energy Conversion, vol. 17, 2002, Page(s): 279 – 284.

[66] El Moursi M., Joos G., Abbey C., "*A Secondary Voltage Control Strategy for Transmission Level Interconnection of Wind Generation*", Transactions on Power Electronics, IEEE, Volume 23, Issue 3, May 2008, Page(s):1178 – 1190.

[67] El Moursi M., "*A novel line drop secondary voltage control algorithm for variable speed wind turbines*", WIND ENERGY, published online 2010.

[68] R. Pena, J. Clare, and G. Asher, "*Doubly Fed Induction Generator Using Back-to-back PWM Converters and its application to Variable-speed Wind Energy Generation*", Proc. Inst. Elect. Eng., Electric Power Applications, vol. 143, no. 3, May 1996, Page(s): 231 – 241.

[69] Ren-jie Ye, Hui Li, Zhe Chen, Qiang Gao, "*Comparison of Transient Behaviors of Wind Turbines with DFIG considering the Shaft Flexible Models*", ICEMS 2008. International Conference on Electrical Machines and Systems, Publication Year: 2008, Page(s): 2585 – 2590.

[70] Shuhui Li, Haskew T.A., "*Analysis of Decoupled d-q Vector Control in DFIG Back-to-Back PWM Converter*", Power Engineering Society General Meeting. IEEE Publication Date: 24-28 June 2007, Page(s): 1 – 7.

[71] Torsten Lund, Poul Sørensen, "*Reactive Power Capability of a Wind Turbine with doubly Fed Induction Generator*", Wind Energy 2007, Wiley Interscince.

[72] Hammad and A.E, "*Analysis of Power System Stability Enhancement by Static Var Compensators*", IEEE Trans. Power Syst., vol. E–1, no. 4, 1986, Page(s): 222 – 227.

[73] Wei Qiao, Harley R.G., "*Power Quality and Dynamic Performance Improvement of Wind Farms Using a STATCOM*", Power Electronics Specialists Conference, 2007. PESC 2007. IEEE 2007, Page(s): 1832 – 1838.

[74] J. Martinez, J. Navarro, "*Behavior Improvement during Faults of Fixed Speed Stall Control Induction Generator Wind Turbines*", WIND ENERGY 2009, 12, Page(s): 527 – 541.

[75] Hingorani N., Gyugyi L., "*Understanding Facts*", IEEE Press Series on Power Engineering. IEEE Press: Piscataway, New Jersey, 2000, 432. Page(s): 194 – 197.

[76] Gerardo Escobar, Aleksandar M. S and Paolo Mattavelli, "*An Adaptive Controller in Stationary Reference Frame for D-Statcom in Unbalanced Operation*", IEEE Transactions on Industrial Electronics, vol. E–51, no. 2, Apr. 2004, Page(s): 401 – 409.

[77] Tyll, H.K., "*FACTS technology for reactive power compensation and system control*", Transmission and Distribution Conference and Exposition: Latin America, 2004 IEEE/PES Publication Year: 2004, Page(s): 976 – 980.

[78] GEEnergy, http://www.gepower.com/prod_serv/products/substation_automation/en/index.htm

[79] G. Celli, E. Ghiani, M. Loddo, F. Pilo, "*Voltage Profile Optimization with Distributed Generation*", Power Tech, 2005 IEEE Russia: 2005, Page(s): 1 – 7.

[80] Bonhomme A., Cortinas D., Boulanger F., Fraisse J. L. "*A new voltage control system to facilitate the connection of dispersed generation to distribution networks*", 2001. Part 1, CIRED. 16th International Conference and Exhibition on Electricity Distribution (IEE Conf. Publ. No. 482) Volume: 4, 2001.

[81] Jens Fortmann, Michael Wilch, Friedrich W. Koch, István Erlich, "*A Novel Centralized Wind Farm Controller Utilizing Voltage Control Capability of Wind Turbines*", 16th PSCC, Glasgow, Scotland, July , 2008, Page(s): 14 – 18.

[82] R. de Almeida, E. Castronuovo, and J. Pecas Lopes, "*Optimum Generation Control in Wind Parks When Carrying out System Operator Requests*", IEEE Transactions on Power Systems, vol. 21, 2006, Page(s): 718 – 725.

[83] George Ellis, "Control System Design Guide", 2004 Elsevier academics press, ISBN 0-12 – 237461 – 4.

[84] Karl J. ström, Tore Hägglund, "*Advanced PID Control*" Princeton university press.

[85] Stankovic A., Ilic M., Maratukulam D., "*Recent Results in Secondary Voltage Control of Power Systems*", Transactions on Power Systems, IEEE, Volume 6, Issue 1, Feb. 1991, Page(s): 94 – 101.

[86] Gehao Sheng, Yadong Liu, Dapeng Duan, Yi Zeng, Xiuchen Jiang, "*Secondary Voltage Regulation Based on Wide Area Network*", Power & Energy Society General Meeting, 2009. PES '09. IEEE 26-30 July 2009, Page(s):1 – 7.

[87] Murdoch A., Sanchez-Gasca J. J., D'Antonio M. J., Lawson R. A., "*Excitation control for high side voltage regulation*", PES Summer Meeting, 2000. IEEE Volume: 1 2000, Page(s): 285 – 289.

[88] Gyugyi Laszlo, "*Reactive compensation. Control of shunt compensation with reference to new design concepts*", Generation, Transmission and Distribution, IEE Proceedings C Volume: 128, Issue: 6, 1981, Page(s): 374 – 381.

[89] GE Energy, www.GEindustrial.com/Multilin, "*Transformer Tap Change Controller: DTR*".

[90] Morren J, de Haan SWH, "*Ridethrough of Wind Turbines with Doubly-fed Induction Generator during a Voltage Dip*", IEEE Transactions on Energy Conversion 2005, Vol. 20, Page(s): 435 – 441.

[91] Erlich I., Wrede H., Feltes C., "*Dynamic Behavior of DFIG-Based Wind Turbines during Grid Faults*", Power Conversion Conference - Nagoya, 2007. PCC '07 Publication Year: 2007, Page(s): 1195 – 1200.

[92] Johan Morren, Sjoerd W. H. de Hann, "*Short-Circuit Current of Wind Turbines With Doubly Fed Induction Generator*", IEEE Transactions on Energy conversion, Vol. 22, No. 1, March 2007.

[93] E.ON Netz GmbH, "*Grid Connection Regulations for High and Extra High voltage*". http://www.pvupscale.org/IMG/pdf/D4_2_DE_annex_A-3_EON_HV_grid__connection_requirements_ENENARHS2006de.pdf.
[94] Nasser D. Tleis: "*Power Systems Modeling and Fault Analysis*", Elsevier Publishing Company. 2008, ISBN–13: 978–0–7506–8074–5.
[95] I. Boldea and S.A. Nasar: "*Electric machine dynamics*", MacMillan Publishing Company. July 1986, ISBN-10: 0029480302.
[96] Krause et al: "*Analysis of Electrical Machinery*", IEEE Press 1994, ISBN 0–7803–1101–9.
[97] Bernad Adkins, Ronald G. Harley: "*The General theory of Alternating current Machines: Application to Practical Problems*". Chapman and Hall Publishing Company.
[98] IEC 60909-0 First edition 2001-07, "*Short-circuit currents in three-phase a.c. systems*" – Part 0.
[99] IEC 61400-21, Edition 2007, "*Measurement and assessment of power quality characteristics of grid connected wind turbines*".
[100] Lixin Bao, Zhenyu Huang, Wilsun Xu "*Online voltage stability monitoring using VAr reserves*", PES, IEEE Vol.: 18, Issue: 4, 2003, Page(s): 1461 – 1469.

Appendixes

Appendix A

PI with line drop compensation and Slope control step response
By using the following conditions, both controls show a similar response in the frequency of interest.

$$K_{PO} = \frac{1}{K_L}, \quad K_P T_i << 1, \quad T_{PO} = T_i\left(\frac{1}{K_L} + K_P\right) \qquad \text{A.1}$$

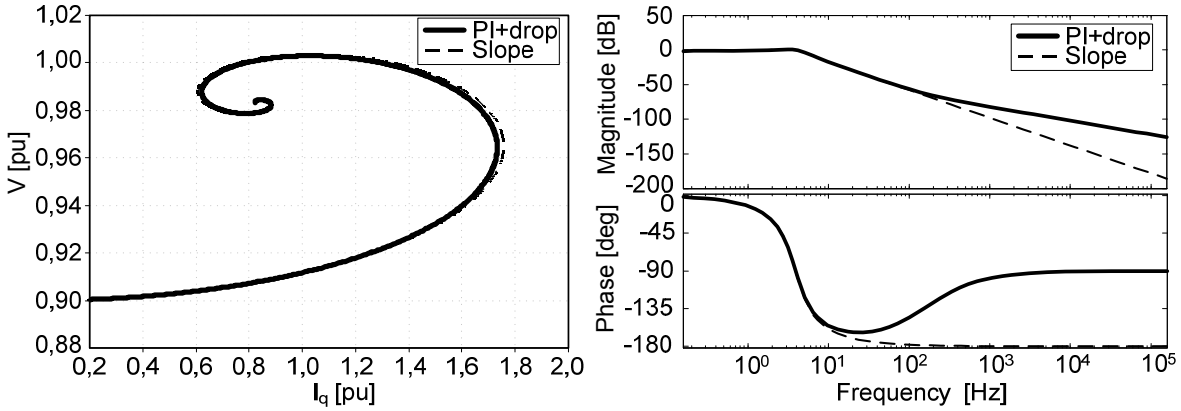

Figure 10-1. Slope and PI with drop compensation control comparison.

Step Voltage Response Classification

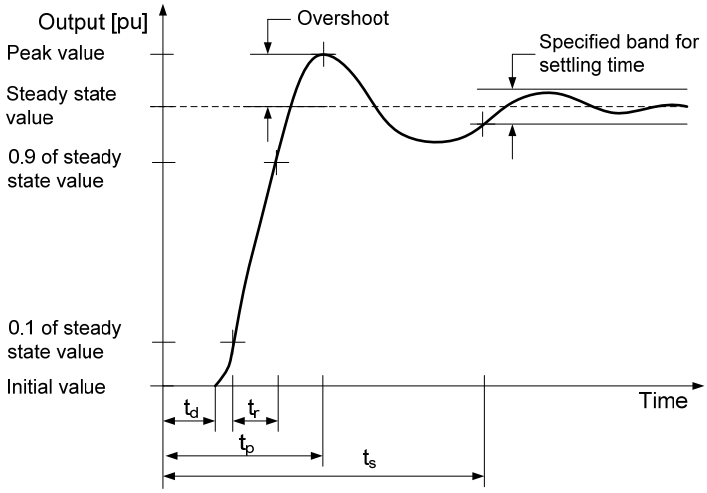

Figure 10-2. IEEE std. for a typical transient response of a feedback control system to a step change in input [53].

Appendix B

Project Data:

TABLE V
WTG, SYSTEM, STATCOM DATA

	Parameter	Value	Unit
WTG	S_{WTG}	2100	[kVA]
	V_{LV}	0.69	[kV]
	Electrical frequency	50	[Hz]
	Stator Resistance	0.006	[pu]
	Rotor Resistance	0.009	[pu]
	Mutual Inductance	3.422	[pu]
	Stator Inductance	0.072	[pu]
	Rotor Inductance	0.101	[pu]
	S step-up transformer 0.69:20kV	2100	[kVA]
	Z step-up transformer	0.08	[pu]
SYSTEM	Number of WTGs	23	
	X_{OVL}	0.0181	[pu]
	R_{OVL}	0.0089	[pu]
	C_{OVL}	0.0051	[pu]
	L_{OVL}	10.2	[km]
	X_{WPPT}	0.1191	[pu]
	R_{WPPT}	0.0049	[pu]
	S_{WPPT}	55000	[kVA]
	Winding Connection WPPT	D-Yn	
	Medium voltage level	20	[kV]
	High voltage level	115	[kV]
STATCOM	$S_{STATCOM\ trafo}$	14000	[kVA]
	V_{LV}	0.69	[kV]
	Electrical frequency	50	[Hz]
	S step-up transformer 0.69:20kV	15000	[kVA]
	Z step-up transformer	0.09	[pu]

TABLE VI
DISPATCHING LOOK-UP TABLE

P_m [pu]	K
0.00	0
0.45	0
0.65	1
1.00	1

TABLE VII
P-Q DFIG AND V-I STATCOM CHART COORDINATES

	Point	P	Q	Unit in WTG base
WTG	A	0.00	0.10	[pu]
	B	0.10	0.60	[pu]
	C	0.70	0.60	[pu]
	D	1.00	0.20	[pu]
	E	1.00	-0.30	[pu]
	F	0.85	-0.60	[pu]
	G	0.10	-0.60	[pu]
	H	0.00	-0.15	[pu]
	Point	**V**	**I**	**Unit in STATCOM base**
STATCOM	A	0.30	1.00	[pu]
	B	0.92	1.00	[pu]
	C	1.00	1.00	[pu]
	D	1.08	-1.00	[pu]
	E	0.30	-1.00	[pu]

Measurement system:
The following figure shows the diagram of the measurement system of the plant, implemented in the simulations.

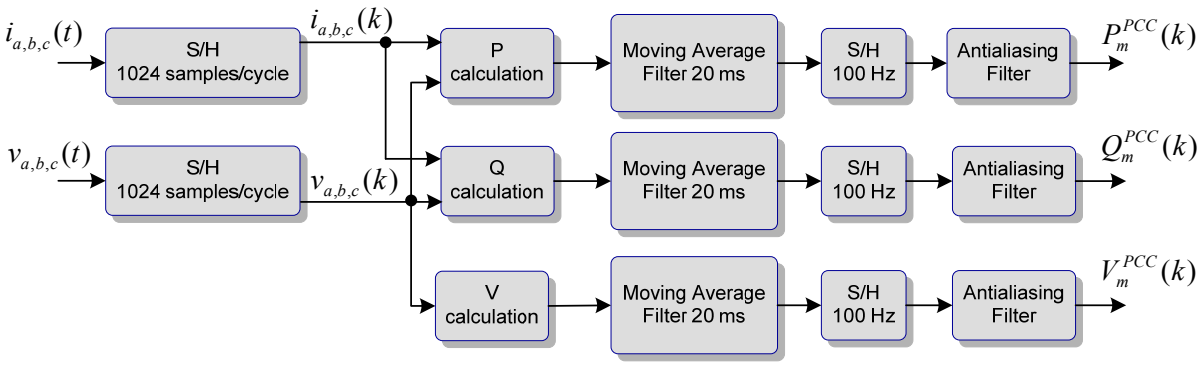

Figure 10-3. Measurement system representation

Appendix C

Capacitor Control Logic:

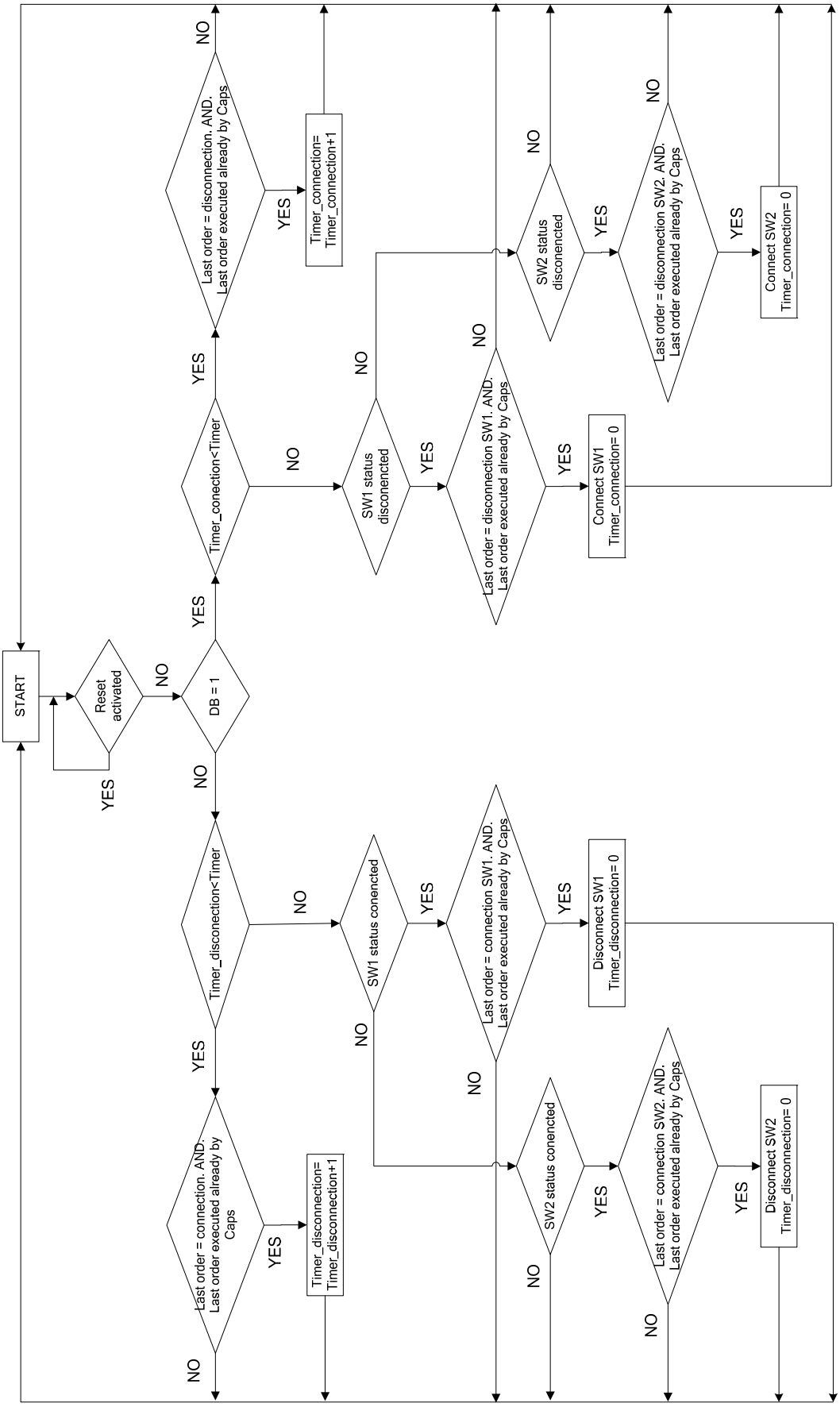

Figure 10-4. Capacitor control logic module

Publications

A.1

"Comparison of Two Voltage Control Strategies for a Wind Power Plant"
Jorge Martínez, Philip C. Kjær, Pedro Rodriguez, Remus Teodorescu.

Comparison of Two Voltage Control Strategies for a Wind Power Plant

Jorge Martínez, Philip C. Kjær, Pedro Rodriguez, Member, IEEE, Remus Teodorescu, Senior Member, IEEE.

***Abstract*—Larger percentages of wind power penetration translate to more demanding requirements from grid codes. Recently, voltage support at the point of connection has been introduced by several grid codes from around the world, thus, making it important to analyze this control when applied to wind power plants.**

This paper addresses the analysis of two different voltage control strategies for a wind power plant, i.e. decentralized and centralized voltage control schemes.

The analysis has been performed using the equivalent and simplified transfer functions of the system. Using this representation, it is possible to investigate the influence of the plant control gain, short circuit ratio, and time delays on the system stability, as well as the fulfillment of the design requirements.

The implemented plant voltage control is based on a slope voltage controller, which calculates the references to be sent to the wind turbines, according to the slope gain and the difference between the reference and measured voltage at the point of connection.

The results show that for a system where the time delay between the central control and the actuators is not negligible, the performance of a decentralized voltage control is better than the centralized one in terms of time reaction, disturbance rejection, and short-circuit ratio (SCR) dependency. However, for a system with reduced time delay (10 ms) the centralized scheme can have a performance similar to the decentralized one, in the SCR range of interest.

***Index Terms*—wind turbine generator, power system, wind power plant, voltage control.**

I. Nomenclature

AC	Alternate Current
AVR	Automatic Voltage Regulator
AQR	Automatic Reactive Power Regulator
COMM	Communication
CC	Current Control
CT, VT	Current and Voltage Transformer
DC	Direct Current
DFIG	Doubly Fed Induction Generator
M	Mutual Reactance
MV	Medium Voltage
N	Stator to rotor turns ratio
P, Q	Active and Reactive power
PCC	Point of Common coupling
PI	Proportional and Integral control
TSO	Transmission System Operator
s	Laplace term
SCR	Short Circuit Ratio
V, I	Voltage, Current
X, R	Reactance, Resistance
WTG	Wind Turbine Generator
WPPC	Wind Power Plant Control
WTG	Wind Turbine Generator
WTGT	Wind Turbine Generator Transformer
Z	Impedance

Subscripts

m	Measured
ref	Reference
d, q	Direct and Quadrature components
σs	Stator leakage

II. Introduction

The traditional electrical grid, in which the power is produced at centralized power plants, and delivered to the customers through transmission and distribution networks, is greatly challenged by the deregulation of the power system and the connection of wind power generation**.** It is clear that if wind power replaces power from conventional generators, it will no longer be possible to control the node voltages adequately, and it will become necessary that wind power plants also contribute to voltage control.

In the recent years, some voltage capability regulation has been introduced in some of the grid codes around the world. Utilizing the reactive power capability regulation of the wind turbine generators (WTGs) is a natural consequence to further enhance the interaction between the grid and the wind power plant (WPP). DFIG and full-scale converter WTGs can provide smooth reactive power regulation to the grid by means of its electronic converters.

However, there are some limitations related to the voltage control operation of a WPP, e.g. wind power plants comprise a large amount of small generation units, which need to be fully controlled and monitored. This large computational effort makes the plant control to have a slow response nature

J. Martínez is with VESTAS Wind Systems, Power plant R&D, DK, (corresponding author e-mail: jomga@ vestas.com).

P. C. Kjaer is with VESTAS Wind Systems, Power plant R&D, DK, (e-mail: pck@ vestas.com).

R. Teodorescu is with Aalborg University, DK, (e-mail: ret@iet.aau.dk).

P. Rodriguez is with Aalborg University, DK, (e-mail: prodriguez@ee.upc.edu).

(hundreds of milliseconds). The communication control delay between the wind turbine generators and the wind power plant controller is a source of possible instability when adjusting the controllers with the wrong parameters.

Time-delay has been a common phenomenon to overcome whenever we close a feedback loop for the purpose of controlling any system. In the majority of the publications dealing with delays in controlled systems related to power plants, fuzzy-based and predictive controls were proposed [1]-[2]. Some predictive control techniques, such as the internal model control (IMC) and the Smith predictor control were presented to cope, among other things, with time-delay systems. Both incorporate the plant model to cancel the plant dynamics.

Since the plant model incorporated in these control schemes is not the plant itself, it is difficult to perfectly reflect the actual behavior of the plant. The possible difference of the actual plant from the model gives rise to mismatch between the plant and the controller. A certain Smith predictor and IMC control schemes are stable only when there is insignificant mismatch, i.e. an arbitrarily small difference in the time delays makes the system unstable. Additionally, Smith predictor is difficult to be implemented when the system to be controlled presents some nonlinearities, such as the input saturation [3].

For plants with significant but not too large time delays, and very well defined plant variation, both techniques can be an attractive alternative to the plain PID controller, presupposing that the complete controller including the predictor is optimized. However, when the primary controller is of the PI type, more profit can be obtained by providing it with a derivative part than by augmenting it with a Smith predictor or IMC systems [4].

In addition, another challenge presented when doing voltage control in power systems, is the high dependency of the grid impedance, which changes constantly. A high voltage network is an exceedingly complex system, whose defining parameters are continuously subject to change. These changes cannot be foreseen.

The dynamic behavior of the voltage control is a function of the system impedance. This means that the time response and, thus the stability of the control are dependant on the system impedance. For this reason, normally the control is optimized for the maximum expected system impedance, avoiding instability in any case. Voltage step responses with the same regulator but at different system strength show that the control can not be applicable to all the systems; the weaker the system, the greater tendency to instability is. It can be found that the weakest system has higher DC gain and wider bandwidth, consequently with faster response but less phase margin.

One option to overcome this SCR dependency, and achieve enhanced performance, is to use a gain supervisor. The gain supervisor can promise faster response for normal system configuration without having to worry about instability for degraded conditions [5]. Such function, however, should be regarded as protection, which is milder on the power system than a trip, rather than control strategy. This protection cannot ensure fast response during emergencies [6]. It is also noticeable that, usually, these methods use special hardware dedicated devices, and typically involve large mathematical calculations.

These techniques are hardly implemented and accepted to control the wind power plants, since firstly; grid operators want to have deterministic behavior of the plant to make the system planning analysis, and secondly computational wise they are high demanding.

The aforementioned shortcomings, i.e. time delay and fulfillment of the design criteria in a wide range of SCR, become a challenge when designing the voltage control of the wind power plant. All these aspects need a special consideration when trying to emulate the conventional voltage performance of traditional power plants.

III. System Diagram

The system to be studied is composed by a wind power plant, of *n* DFIG turbines distributed in several feeders, connected to a grid, which is characterized by its SCR. The plant uses a voltage controller (WPPC) to command the reactive power of the WTGs to obtain the desired voltage at the point of common coupling (PCC), which is the point where the power has to be delivered according to the grid codes.

The following figure is used to represent the main elements of the system. The dotted line represents the communication network of the plant.

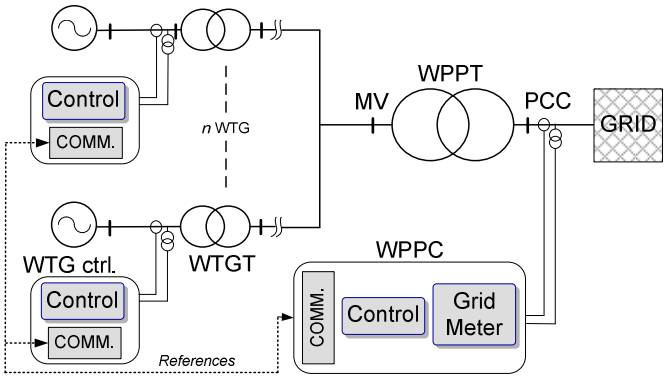

Fig. 1. Simplified system diagram.

Clearly, it is possible to classify the system in the following three groups:

- WTGs: mainly, the generator, converters, and their controllers.
- Collector and grid system: these are covering the main electrical impedances of the system, e.g. the substation transformer (WPPT), and the equivalent grid impedance (GRID).
- Plant control: it is the WPPC, which includes the measurement device (grid meter), the computer allocating the control algorithms, and also the communication hub, which is packing, sending and collecting all the references and relevant information

from the WTGs.

It is known that the voltage performance of a power plant depends on the grid impedance. Additionally, the stability of the controllers depends upon the grid impedance, as the grid impedance is serial addition to the other main transformers. The driving point impedance at fundamental frequency, as viewed from the PCC location, is an important parameter in the voltage control loop since it determines how much the voltage can be changed when a certain amount of reactive current is injected to the system.

It is clear that for high system gains (small slope and SCR values) the system becomes more difficult to be controlled, moreover, the delays in the communication processes reduce the control stability margin when the gain of the system increases.

The design criteria of the control, among other things, is to achieve a response time (t_r) of less than 1 s, an overshoot below 5 %, a settling time (t_s) lower than 2 s, and a delay time (t_d) lower than 0.2 s [7], [8], and, even more important, to preserve stability for all realistically probable network conditions [6]. Therefore, the voltage regulator settings should be dictated by the most limiting operating condition, such as the system configuration with the lowest short circuit power (contingency condition) [9]. However, this tuning may cause relatively long response for higher SCRs (normal operation), where the best performance of the system is most required. An appropriate tuning and selection of the voltage control scheme allows the fulfillment of the design criteria in all the operation range; contingency operation (minimum SCR), normal operation (SCR percentile 95%) and maximum SCR. In the present case, the SCR range is within 5 to 25.

IV. Plant Control

The selected plant voltage control, for this study, is based on a proportional control, also called slope control. Slope voltage control is widely used in power system applications since it allows paralleling generators with individual voltage slope controllers without hunting phenomena or instability. When there is high SCR, as in most of the cases in the transmission system, a slope controller will offer the best solution. Slope control provides a coordinated reactive power system, as the equilibrium point will be known for every voltage disturbance, independent of the time reaction of the controller and the *Q* compensators. Therefore, it is easy to manage how the generators will share the reactive power injection for a certain voltage disturbance.

Taking into consideration the aforementioned advantages, a pure PI will unlikely be used as a voltage control; instead, the PI can be used in combination with a feedback of its output (PI with line drop compensation, see Fig. 2-(b)), which offers a similar response in the frequency of interest than a proportional or slope control (Fig. 2-(a)). These two control schemes are predominant in power system voltage control, as it can be observed in the IEEE std. [10].

Therefore, in the following sections of this work, PI with line drop control could be used instead of slope or proportional control.

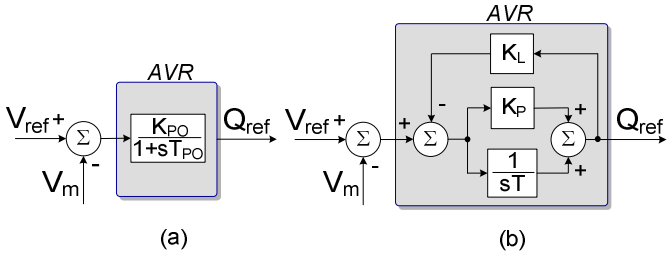

Fig. 2. (a): Slope or proportional control. (b): PI with line drop compensation.

The control law that is applied for the slope concept can be defined, in a generic way, as follows:

$$Q_{ref} = Q_0 + \left(\frac{1}{Slope}\right)(V_{ref} - V_m) \tag{1}$$

Adding a certain offset to the slope controller (Q_0) or changing the voltage reference (V_{ref}), it is possible to regulate the Q injection of the plant.

The slope gain can be defined as follows:

$$K_{slope} = \frac{100}{Slope\ [\%]} = \frac{\Delta Q}{\Delta V} \tag{2}$$

Usually, the slope is given by the TSO. Throughout this work, a slope of 4% is considered [7].

The references to be sent to the reactive power actuators (WTGs), calculated by the plant control, basically can be based on two forms:

- Reactive power references: if the plant control sends reactive power references, the WTGs should have implemented, as an outer q-control, a reactive power control (AQR).
- Voltage references: when sending voltage references the WTGs need to have implemented a voltage control (AVR), to accommodate these references.

These two forms of calculating the actuator reference (voltage or reactive power), reflect the idea of a central and distributed voltage control system, respectively.

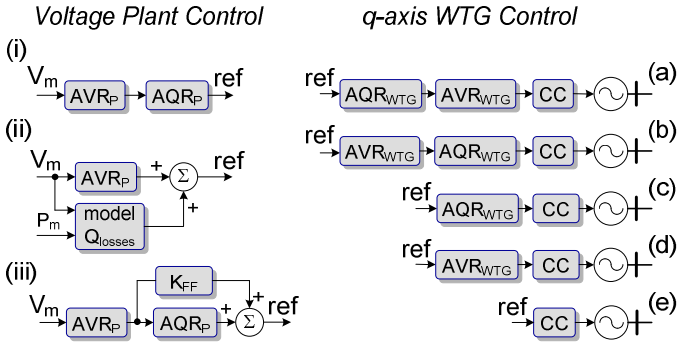

Fig. 3. Candidate configurations regarding plant and WTG control.

According to the possible configurations of the plant and

WTG outer-loop q-axes control, several permutations are presented (see Fig. 3).

Every option offers different characteristics regarding time response and SCR dependency.

The scheme control options, which include an AVR as a q-axis WTG outer control loop, can be classified as distributed voltage control schemes (options including *(b)* and *(d)* structures), whereas the other options can be classified as centralized voltage control schemes (options including *(a)*, *(c)* and *(e)* structures).

It should be noted that the plant voltage control has to compensate for the internal reactive power park losses. For such purpose, option *(i)* and *(iii)* includes an AQR, and option *(ii)* includes a model of the park, which can be adjusted by the voltage and the injected active power level.

In option *(iii)*, a feed-forward is added, which can increase the time response of the control.

The use of a mathematical model of the park internal network, which must accurately compensate VAr consumption inside park in any case and circumstance, does not provide the advantage of removing one lag from the plant control (the integral control of the AQR). In essence, to have stable operation the plant control has to be slowed down to have at least 5-10 times lower bandwidth than the WTG.

For the outer WTG loop control, options *(a)* and *(b)* are neglected, since it is not needed to have so many nested controls, when the WPP has already a *Q* compensator. These options can be considered if no plant control is installed in the WPP. Option *(e)* is also rejected, since high bandwidth in the WTG response is not needed, when the system includes high delays.

Hence, only options *(c)* and *(d)* are considered. These WTG control schemes ((c) and (*d*)) have been previously presented in literature, but under different plant control concepts than what is considered here. Whereas most researchers are concerned with time delay reduction, none have presented the control selection according to the sensitivity to the grid impedance [11]-[14], where the right combination of the plant and WTG control may play an important role. The sensitivity and robustness for different grid impedances are an important matter that should impact on the selection of the control scheme, and are at least as important as grid code fulfillment.

V. Centralized and Decentralized Voltage Control

A central voltage control system is formed when the outer plant control is composed by an AVR and the outer control of the actuators (WTG) is not an AVR.

Whereas, a decentralized voltage control is obtained when the outer control loop of the actuators is formed by an AVR. By placing a voltage control (AVR) in the outer WTG q-axis control, which follows the voltage references sent by the plant control, the secondary voltage control concept is applied. The secondary voltage control concept is well known in the literature. The main thrust of the secondary voltage control scheme is to counteract, in real time, reactive power flow changes in the system, by adjusting terminal voltage of generators system-wide. The amount of voltage adjustment is proportional to the voltage derivations at monitored buses [15]-[17]. This concept can be applied to a wind power plant, where the pilot bus is located at the PCC bus, and the wind turbines include their own voltage controller.

This voltage controller will cause the injection of reactive power proportionally to variation of voltage levels; thus, it supports the grid voltage recovering process after disturbances [8].

VI. System Analysis

To provide further understanding of the voltage regulator parameters, system strength, and delays on the system stability, root locus analysis should be performed, which provides the critical gains. To achieve that, it is needed to represent the elements composing the system as transfer functions, thereby the pole-zero map can be easily extracted. When placing the poles of the system, it can be defined a maximum gain (K_{max}, which is obtained due to the overshoot requirement) and a minimum one (K_{min}, which is obtained due to the settling time requirement) for fulfilling the design conditions. Moreover, it is possible to find the gain which makes the system unstable (K_{uns}).

$$K_{\min} < K_{slope} X_{GRID} < K_{\max} < K_{uns} \tag{3}$$

The conventional method to control a nonlinear system is to design a linear controller using a linearized model of the system dynamics at a desired operating point. Thus, the initial design and tuning of the plant voltage controller is done based on some simplifications and linearization processes (4), which can be considered true for small voltage changes, and in systems where the *X/R* ratio is high, i.e. transmission and sub-transmission levels.

$$Q \approx I_q \ , \quad Z \approx X \ , \ \Delta V \approx X_{GRID} I_q \tag{4}$$

The plant control receives the references and feedback (measurements) and calculates the turbine set-points. The plant AVR control architecture is represented as a gain (K_{slope}), following (2).

The grid meter, which provides the feedback signals for control, samples at very high frequency the output values of the CTs and VTs, located at the PCC. This meter processes the signals by first calculating one cycle *rms*, then filtering for anti-aliasing. The grid meter can be represented by a first order transfer function, with a time constant (T_m) [18].

The communication delays (T_{COMM}) and control sampling (T_s) effect of the WTG and the WPPC, can be represented together as an exponential delay function, with a time constant T ($T= T_{COMM} + 0.5T_s$).

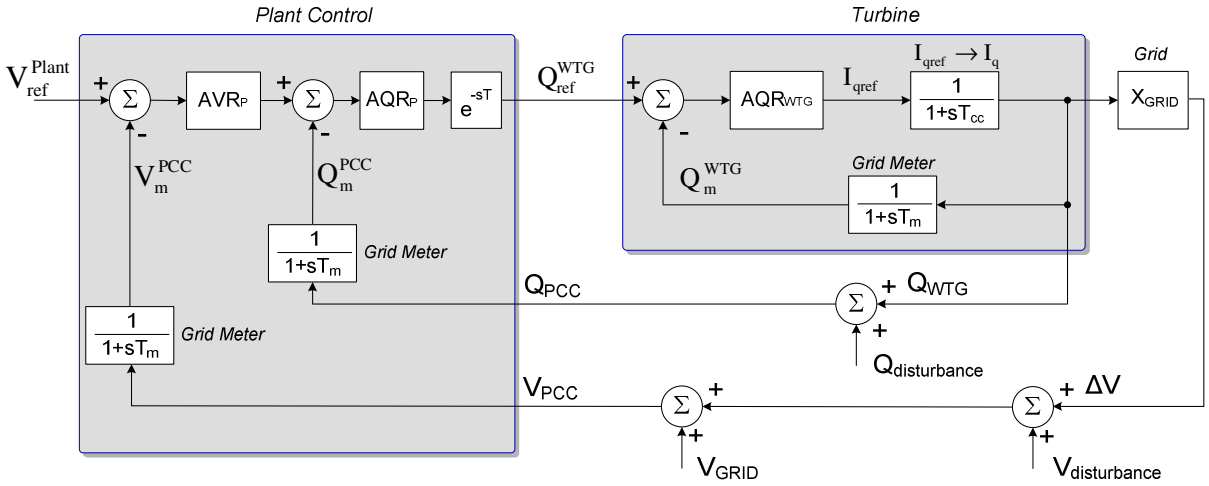

Fig. 4. Centralized voltage control scheme. System representation for the WTGs with an AQR.

The exponential function should be linearized when doing the control analysis, e.g. by using Pade approximation

A. Centralized Voltage Control Strategy

If the WTGs are controlled with an AQR, the following turbine transfer function is obtained, which is considering a perfect control decoupling between the q-d axes [19].

$$Turbine(s) = \frac{Q_{WTG}}{Q_{ref}^{WTG}} \approx \frac{1}{1 + sT_{WTG}} \tag{5}$$

It should be noted that the turbine transfer function is ideally independent from the grid impedance.

By linking together the different components, Fig. 4 is obtained, which is representing the case of the centralized voltage control system.

In a DFIG, the AQR controls the stator Q by commanding the rotor current, thus the rotor control gains (AQR_{WTG}^{rotor}) are translated to the stator side (AQR_{WTG}) [19]. Hence, for the DFIG WTG type the following is used:

$$AQR_{WTG} = \frac{1}{N}\left(\frac{M}{M + X_{\sigma s}}\right) AQR_{WTG}^{rotor} \tag{6}$$

Fig. 5-a shows the stability area, and Fig. 5-b shows the fulfillment area of the design requirements (within the colored surfaces), for three different control settings, and T=0.15 s. The settings are optimized for different SCRs, i.e. setting for curve A is optimized for a SCR equal to 5, curve B for 15, and curve C for 25. It can be observed that if the settings for case A or B are used, as it should be, since these can ensure the stability operation within all the SCR range of interest, then the fulfillment area of the design requirements is quite reduced.

If the outer q-axis control loop, of the WTGs, is used as an AQR, two drawbacks are seen. Firstly, three set of control settings are needed to fulfill the design requirements for the whole SCR range of interest (between 5 and 25). Secondly, the fulfillment of the time delay (t_d) requirement could be physically impossible to achieve, regardless of the control tuning, if the total sampling and communication control delays are bigger than the required t_d. It should be remarked that, the bigger the time delay (T) the bigger the influence of the SCR in the design constraints.

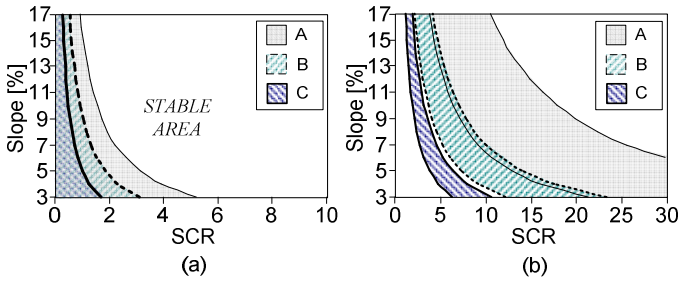

Fig. 5. (a) Stability, and (b) design fulfillment areas according to the SCR, for three set of control settings for a centralized voltage control scheme, and T=0.15 s.

The following figure shows the root-locus for the centralized voltage control system for two different time delays, T=0.15 s and T=0.01 s.

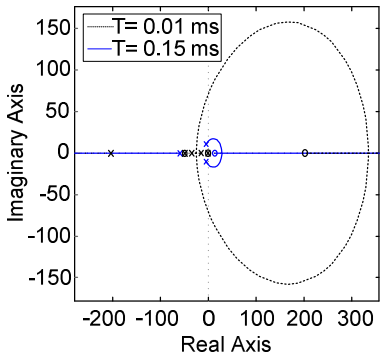

Fig. 6. Root-locus for the centralized system, for two different time delays.

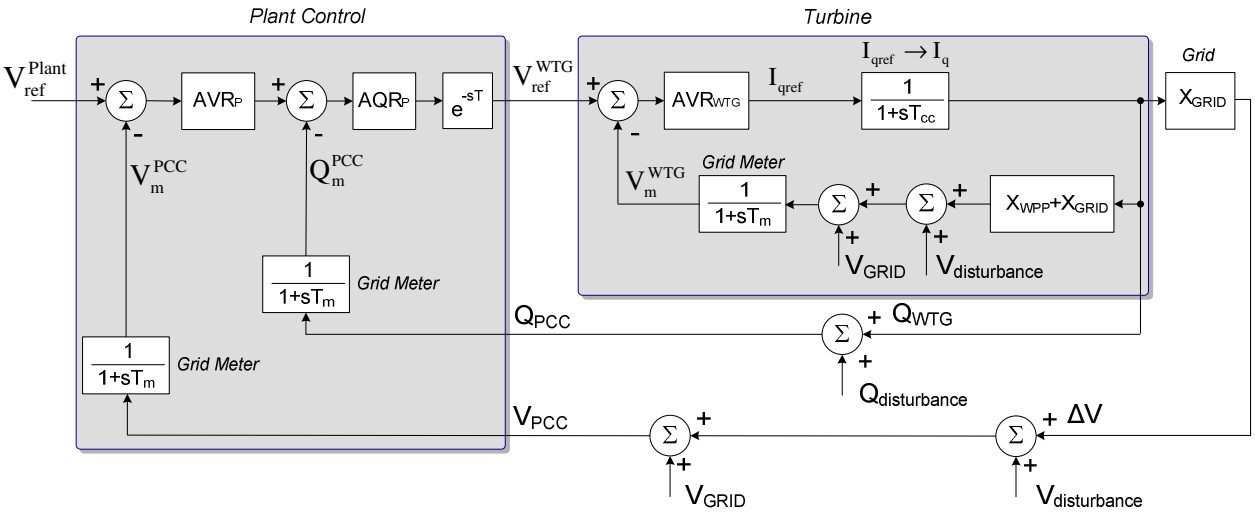

Fig. 7. Decentralized voltage control scheme. System representation for the WTGs with AVR.

The system with a delay of T=0.01 s shows a root trajectory which allows bigger gains without instability problems.

B. Decentralized Voltage Control Strategy

When the q-axis control loop of the WTGs is used as an AVR, the aforementioned two drawbacks are solved. Moreover, the fulfillment of the design requirements is extended to a wide range of SCRs, since the local voltage controllers are less dependant on the SCR. This can be seen in the following figure, where the design fulfillment area is depicted (grey area in Fig. 8) for a WPP where the WTGs are using an AVR, and T=0.15 s. The AVR of the WTG is a slope controller, similar to what is depicted in Fig. 2, to avoid counteraction with the rest of the WTGs in the plant.

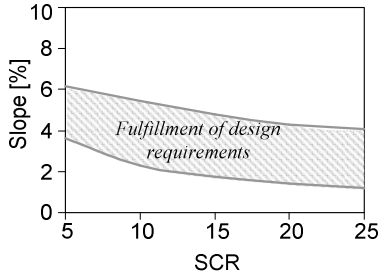

Fig. 8. Design fulfillment area for a WPP with decentralized voltage control scheme and T=0.15 s.

By looking into further details of the system transfer functions, it is possible to see where the main differences are. Fig. 7 shows the system diagram for the decentralized case, where X_{WPP} represents the positive impedance of the WPP and WTG transformers.

By neglecting the T_m and T_{cc}, the turbine transfer function, when including an AVR, is obtained (7).

$$Turbine(s) = \frac{Q_{WTG}}{V_{ref}^{WTG}} \approx \frac{K_{PO}}{1 + sT_{PO} + K_{PO}(X_{WPP} + X_{GRID})} \tag{7}$$

At first glance, it can be seen how the transfer function (7) includes in the denominator a function of the X_{GRID}, which will make the system at the end less sensitive to X_{GRID} changes.

VII. Sensitivity Analysis

The system sensitivity to a paremeter can be defined as the ratio of the percentage change in the system transfer function to the change of a parameter for a small incremental change. A sensitivity analysis is done to compare the influence of the X_{GRID} in the configurations depicted in Fig. 4 (where its close loop transfer function is called $G_{central}$), and Fig. 7 (where its close loop transfer function is called $G_{distributed}$).

If the influence of X_{GRID} is bigger in the $G_{central}$ than in the $G_{distributed}$, then its sensitivity term ($S^{X_{GRID}}$) will be also bigger. Thus, the condition shown in (8) needs to be checked.

$$S_{distributed}^{X_{GRID}} < S_{central}^{X_{GRID}} \tag{8}$$

The sensitivity of the previous transfer functions with respect to X_{GRID}, are defined as follows:

$$S_{distributed}^{X_{GRID}} = \frac{\partial G_{distributed}}{\partial X_{GRID}} \frac{X_{GRID}}{G_{distributed}}, \quad S_{central}^{X_{GRID}} = \frac{\partial G_{central}}{\partial X_{GRID}} \frac{X_{GRID}}{G_{central}} \tag{9}$$

Hence, obtaining the following results:

$$S_{distributed}^{X_{GRID}} = \frac{1 + AQR_{WTG}(1 + AQR_P)}{1 + AQR_{WTG}(1 + AQR_P(1 + AVR_P X_{GRID}))} \tag{10}$$

$$S_{central}^{X_{GRID}} = \frac{1 + AVR_{WTG}(X_{WPP} + AQR_P)}{1 + AVR_{WTG}(X_{WPP} + X_{GRID} + AQR_P(1 + X_{GRID}))} \tag{11}$$

For the sake of simplicity, similar gains for the plant reactive power control are used, and also a gain of 1 is used for the AVR_P. By replacing the gains of the turbine transfer

functions, AQR_{WTG} and AVR_{WTG} (1 and K_{PO} respectively), the following is obtained.

$$X_{WPP} < \frac{2}{AQR_P} - \frac{1}{K_{PO}} + 3 \tag{12}$$

For a typical WPP, the X_{WPP} has a value of approximately 0.2 pu, and the local WTG slope gain (K_{PO}) will be always bigger than 1, which confirms that (12) is, by far, always fulfilled. Hence, being more sensitive to X_{GRID} changes the central control configuration (WTG with AQR) than the decentralized one (WTG with AVR).

VIII. Step Response

To validate the above conclusions, and using the aforementioned diagrams, the step responses for a grid change of 10% under different SCRs, are depicted.

Fig. 9 shows the step response of the system when the grid voltage is stepped down at time equal to 10 s. The curves show the WPP reactive power output when using the decentralized scheme (called AVR_{WTG}), and the central scheme control (called AQR_{WTG}), for the maximum and minimum SCR of interest. Both schemes are using an optimized tuning for a SCR equal to 5.

It should be noticed that the curve AQR_{WTG_FF} is representing the plant control option (*iii* in Fig. 3), which is the same that AQR_{WTG} but including a feed-forward loop, with a gain (K_{FF}) defined by the maximum allowed overshoot, see Fig. 9.

It is clear that bypassing the AQR_P with a feed-forward loop, will easily make the system tend to overshoot. The decentralized option (AVR_{WTG}) is even more sensitive to the feed-forward loop than the centralized one, since the WTG reference is calculated in terms of voltage, and is multiplied by the AVR_{WTG} gain (K_{PO}). Consequently, the feed-forward in a plant control which commands the WTGs with an AVR is not considered.

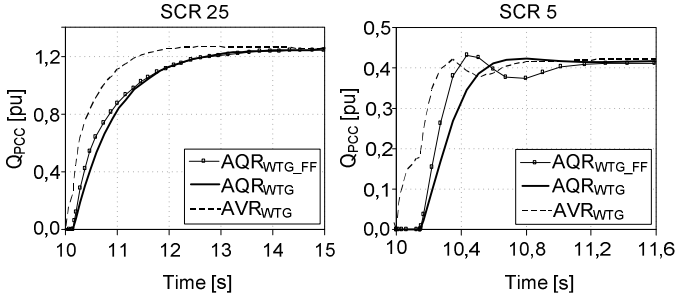

Fig. 9. System step response, of the diagrams represented in Fig. 8 and Fig. 4, for a T= 0.15 s.

It can be checked that the WTG with an AVR has almost instantaneous response, and the t_d, t_r and t_s are fulfilled for both SCR cases. However, for the case of the WTG with an AQR, t_d is not fulfilled in any of the cases, and t_r and t_s are only fulfilled for the case of a SCR 5. It can be seen that, the impact of the SCR is much higher in the centralized control configuration.

Considering an ideal case, where the delay (T) is 0.01 s, the following step responses, for the centralized (AQR_{WTG}) and decentralized (AVR_{WTG}) cases, are depicted, for two different SCRs (5 and 25).

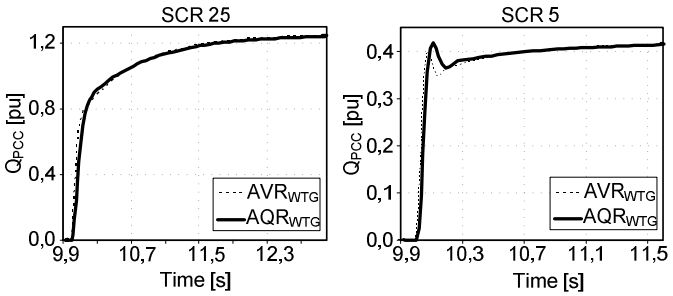

Fig. 10. Step response of the diagrams represented in Fig. 8 and Fig. 4, for a T= 0.01 s.

It should be noticed that to obtain similar response for the centralized and the decentralized schemes, within the SCR of interest, the delay (T) has been reduced from 0.15 to 0.01 (a factor of 15). It is worth mentioning that the decentralized scheme also gets extended its SCR design fulfillment range after the time delay is reduced.

IX. Disturbance Rejection

The capability of the centralized and decentralized schemes for disturbance rejection is analyzed in this section. Disturbances related to the reactive power ($Q_{disturbance}$) can be associated, e.g., to active power fluctuations and sudden disconnection of WTGs. The transfer function relating this disturbance with the V_{PCC} is shown in (13).

Disturbances related to the voltage ($V_{disturbance}$) can be associated, .e.g., to active power fluctuations and grid voltage changes. The transfer function relating this disturbance with the V_{PCC} is shown in (14). The grid meters are not included for the sake of simplification.

$$V_{PCC}(s) = \frac{X_{GRID}}{1 + C_i(s)\left(1 + AVR_P X_{GRID}\right)} Q_{disturbance}(s) \tag{13}$$

$$V_{PCC}(s) = \frac{1 + C_i(s)}{1 + C_i(s)\left(1 + AVR_P X_{GRID}\right)} V_{disturbance}(s) \tag{14}$$

Where, for the centralized and the decentralized schemes C_Q and C_V should be used, respectively.

$$C_{i=Q}(s) = \overbrace{\frac{1+sT_1}{1+sT_2}\frac{sT_i + K_P}{sT_i}}^{AQR_P} \overbrace{\frac{1}{1+sT_{WTG}}}^{Turbine} \overbrace{e^{-sT}}^{delay} \tag{15}$$

$$C_{i=V}(s) = \overbrace{\frac{1+sT_1}{1+sT_2}\frac{sT_i + K_P}{sT_i}}^{AQR_P} \overbrace{\frac{K_{PO}}{1+sT_{WTG} + K_{PO}(X_{WPP} + X_{GRID})}}^{Turbine} \overbrace{e^{-sT}}^{delay} \tag{16}$$

Fig. 11 shows the V_{PCC} performance, for the decentralized (AVR_{WTG}) and centralized (AQR_{WTG}) schemes, when a step disturbance is applied to the system; reactive power disturbance in Fig. 11-a ($Q_{disturbance}$), and voltage disturbance in Fig. 11-b ($V_{disturbance}$).

The disturbances are introduced at 10 s, with a magnitude of 1 pu. The used time delay (T) is 0.15 s.

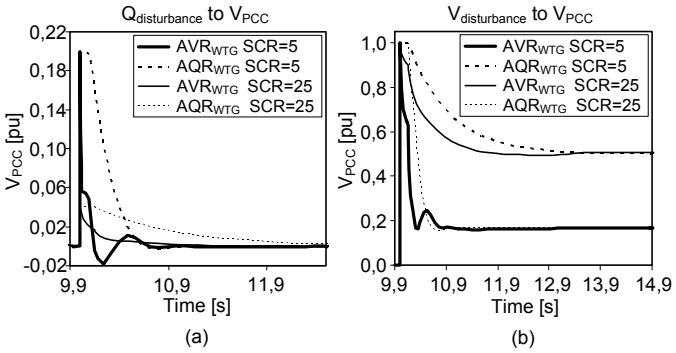

Fig. 11. (a) Q disturbance, and (b) V disturbance response for the centralized (AQR_{WTG}) and decentralized (AVR_{WTG}) cases, using T=0.15 s.

In steady state, the effect on the V_{PCC} caused by $Q_{disturbance}$ is zero, due to the action of the AQR_P. However, the effect on the V_{PCC} caused by the $V_{disturbance}$ is not completely removed (as it was expected) due to the slope control concept, see (17), Fig. 11-b, and Fig. 12-b.

$$V_{PCC} \underset{s\to 0}{=} \frac{1}{1+K_{slope}X_{GRID}}V_{disturbance} \tag{17}$$

It can be checked that the disturbance rejection capability of the decentralized controller is much better than the centralized one. Additionally, it can be appreciated that the lower the SCR the bigger the influence of the Q disturbance in the voltage at the PCC.

Finally, it is depicted the disturbance performance for the case where the time delay (T) is 0.01 s.

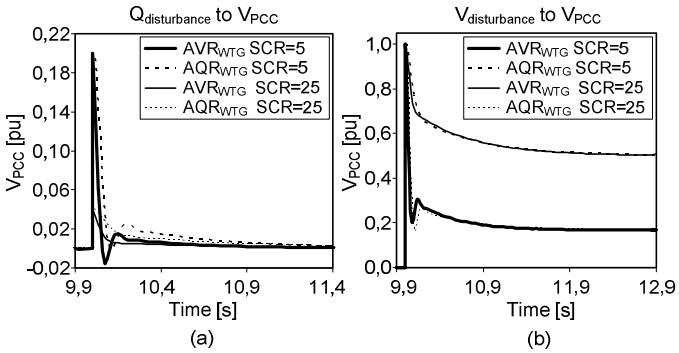

Fig. 12. (a) Q disturbance, and (b) V disturbance response for the centralized (AQR_{WTG}) and decentralized (AVR_{WTG}) cases, using T=0.01 s.

For the case where the time delay is 0.01 s, the disturbance rejection capability of both schemes is quite similar.

X. Conclusions

It is shown that for a wind power plant where the delay between the plant control and the WTGs is not negligible (150 ms), the decentralized scheme performs better in terms of typical design requirements (i.e. time delay, time response and overshoot), moreover the low dependence on grid impedance eliminates the need of gain scheduling for covering a wide range of SCR. Thus, the decentralized control is a good candidate for voltage control in presence of communications delays. Hence, by having the q-axis of the WTG actuated by an AVR, very fast system response is achieved and the plant control is easier to tune since the system dependence on the SCR is reduced, compared with a WPP which uses an AQR in the WTGs.

It can also be concluded that, the centralized scheme can reduce its dependence on the grid impedance by reducing the communication delay. It has been found that if a reduced delay time value is used (10 ms), similar responses can be achieved with both schemes, within the SCR range of consideration.

XI. References

[1] S. Narita and M. Hamman, "Multi-computer Control of System Voltage and Reactive Power on Real-time Basis", IEEE Transactions on Power system. Vol. PAS-92, no. 1, 1973.

[2] Tsu-Tian Lee; Jin-Tsong Jeng; Ching-Long Shih, "Using neural networks to improve gain scheduling techniques for linear parameter-varying systems", Advanced Motion Control, 1996. AMC '96-MIE. Proceedings. 1996 4th International Workshop on, Volume 1, 18-21 March 1996 Page(s): 299 - 304 vol.1.

[3] Abe, N.; Yamanaka, K., "Smith predictor control and internal model control - a tutorial"; SICE 2003 Annual Conference Volume: 2 Publication, 2003, Page(s): 1383 - 1387 Vol.2 IEEE Conferences.

[4] Evaluation and tuning of robust PID controllers Lennartson, B.; Kristiansson, B.; Control Theory & Applications, IET Volume: 3, Issue: 3 Digital Object Identifier: 10.1049/iet-cta: 20060450 Publication Year: 2009, Page(s): 294 – 302.

[5] Belanger J., Scon G., Andersson T., Torseng S. "Gain Supervisor, for Thyristor Controlled Shunt Compensator". CIGRE, 1984 Proceedings of the 31'Session, paper 3841.

[6] Li Chun; Jiang Qirong; Xu Jianxin, "Investigation of voltage regulation stability of static synchronous compensator in power system" PES Winter Meeting, 2000. IEEE, Publication Year: 2000, Page(s): 2642 - 2647 vol.4.

[7] National Grid Electricity Transmission: "Guidance Notes for Power Park Developers", 2008.

[8] IEEE Std. 421.2-1990, "IEEE Guide for Identification, Testing, and Evaluation of the Dynamic Performance of Excitation Control Systems".

[9] Hingorani NG, Gyugyi L., "Understanding Facts". IEEE Press Series on Power Engi-neering. IEEE Press: Piscataway, New Jersey, 2000; 432. Page(s): 194-197.

[10] IEEE Std. 421.5-1992, "IEEE Recommended Practice for Excitation System Models for Power System Stability Studies".

[11] El Moursi, M.; Joos, G.; Abbey, C., "A Secondary Voltage Control Strategy for Trans-mission Level Interconnection of Wind Generation", Power Electronics, IEEE Transactions on, Volume 23, Issue 3, May 2008 Page(s):1178 - 1190.

[12] El Moursi, M., "A novel line drop secondary voltage control algorithm for variable speed wind turbines", WIND ENERGY, published online 2010.

[13] Jens Fortmann Michael Wilch, Friedrich W. Koch, István Erlich, "A Novel Centralized Wind Farm Controller Utilizing Voltage Control Capability of Wind Turbines", 16th PSCC, Glasgow, Scotland, July 14-18, 2008.

[14] G. Tapia, A. Tapia, and J. Ostolaza, "Proportional-Integral Regulator-Based Approach to Wind Farm Reactive Power Management for

Secondary Voltage Control". IEEE Transactions on Energy Conversions, Vol.22, No.2, June 2007.
[15] Stankovic, A.; Ilic, M.; Maratukulam, D., "Recent Results in Secondary Voltage Control of Power Systems", Power Systems, IEEE Transactions on, Volume 6, Issue 1, Feb. 1991 Page(s):94 - 101.
[16] Gehao Sheng; Yadong Liu; Dapeng Duan; Yi Zeng; Xiuchen Jiang, "Secondary Voltage Regulation Based on Wide Area Network", Power & Energy Society General Meeting, 2009. PES '09. IEEE 26-30 July 2009 Page(s):1 - 7.
[17] Al-Majed, S.I., "Secondary Voltage Control: Enhancing Power System Voltage Profile", Power and Energy Conference, 2008. PECon 2008. IEEE 2nd International, 1-3 Dec. 2008 Page(s):1218 – 1221.
[18] P. Kundur, "Power System Stability and Control", page 362, 1994 McGraw-Hill, Inc. ISBN 0-07-035958-X.
[19] Martínez, J.; Kjer, P.C.; Teodorescu, R., "DFIG turbine representation for small signal voltage control studies"; International Conference on Optimization of Electrical and Electronic Equipment (OPTIM), 2010 12th Publication Year: 2010 , Page(s): 31 – 40.

XII. APPENDIX

For the case represented in Fig. 4, and using an $AQR_{P,}$ defined with a time constant (T_i), an a AVR_P with a slope gain of K, the following roots are extracted, which can be used for plotting the stability impact shown in Fig. 8.

$$s_{1,2} = -\frac{(0.5TT_i + KX_{GRID} + T_{WTG}T_i + 1)}{(T_{WTG}TT_i - 1 - KX_{GRID})} \pm \sqrt{TT_i(TT_i + 4KX_{GRID} - 4T_iT_{WTG} + 4) + 8KX_{GRID}(T_{WTG}T_i + 1 + T_i) + 4T_{WTG}T_i(T_{WTG}T_i + 2) + 4 + 8T_i} \quad (19)$$

A.2

"VAr Reserve Concept Applied to a Wind Power Plant"

Jorge Martínez, Philip C. Kjær, Pedro Rodriguez, Remus Teodorescu.

VAr Reserve Concept Applied to a Wind Power Plant

Jorge Martínez, Philip C. Kjær, Pedro Rodriguez, Member, IEEE, Remus Teodorescu, Senior Member, IEEE.

***Abstract*—Larger percentages of wind power penetration translate into more demanding requirements from the grid codes; for example voltage support at the point of connection has been introduced recently by several grid codes from around the world, making it important to analyze this control when applied to wind power plants.**

This paper proposes two different VAr reserve control strategies for a wind power plant.

The amount of dynamic VAr available most of the operation time, makes the wind power plant (WPP) a good candidate to include a VAr reserve management system. Two different ways of implementing a VAr management system are proposed and analyzed.

Such a reactive power reserve may be provided by the wind power plant since the amount of reactive power installed for most active power working points exceeds the demand required by the grid operator. Basically, this overrated reactive power capacity is a consequence of sizing wind turbine facilities for maximum active power level. The reactive power losses, due to active power transportation inside the plant (normally two transformers), and P-Q wind turbine characteristics define the P-Q reserve chart.

By utilizing the intrinsic overrated reactive power capacity, additional devices, such as for example SVCs and STATCOMs, can be avoided in other locations of the grid.

***Index Terms*—wind turbine generator, VAr reserve, wind power plant, voltage control.**

I. Nomenclature

AC	Alternate Current
AQR	Automatic Reactive Power Regulator
AVR	Automatic Voltage Regulator
DFIG	Doubly Fed Induction Generator
MSC	Mechanical Switch Capacitor
MSR	Mechanical Switch Reactor
MV	Medium Voltage
OLTC	On-Line Tap Changer
OVL	Over Head Line
P, Q	Active and Reactive power
PCC	Point of Common coupling
PF	Power Factor
PI	Proportional and Integral control
RTU	Remote Terminal Unit
TSO	Transmission System Operator
s	Laplace term
SCR	Short Circuit Ratio
SVC	Static VAr Compensator
V, I	Voltage, Current
WPP	Wind Power Plant
WPPC	Wind Power Plant Control
WTG	Wind Turbine Generator
Z	Impedance

Subscripts

m	Measured
ref	Reference

II. Introduction

The traditional electrical grid, in which the power is produced at centralized power plants, and delivered to the customers through transmission and distribution networks, is greatly challenged by the deregulation of the power system and the connection of wind power generation**.** It is clear that if wind power replaces power from conventional generators, it will no longer be possible to control the node voltages adequately, and it will become necessary that wind power plants also contribute to voltage control.

In the recent years, some voltage regulation capability has been introduced in some of the grid codes around the world [1]-[4]. Utilizing the reactive power capability regulation of the wind turbine generators (WTGs) is a natural consequence to further enhance the interaction between the grid and the wind power plant (WPP). DFIG and "full-scale converter" WTGs can provide smooth reactive power regulation to the grid by means of their electronic converters.

The VAr reserve concept can be applied to a wind power plant in a manner similar to the SVC or STATCOM [5], [6]. This can be done, because the amount of available reactive power in most of the active power working points exceeds the demand required by the grid operator. This is a consequence of sizing the reactive power plant for maximum active power level. This is of special relevancy, because the amount of hours that the wind power plants are operating at maximum active power is quite low compared with traditional power plants.

The reactive power provision for the WPP is to be considered as a voltage requirement. As it was mentioned, the

J. Martínez is with VESTAS Wind Systems, Power plant R&D, DK, (corresponding author e-mail: jomga@ vestas.com).

P. C. Kjaer is with VESTAS Wind Systems, Power plant R&D, DK, (e-mail: pck@ vestas.com).

R. Teodorescu is with Aalborg University, DK, (e-mail: ret@iet.aau.dk).

P. Rodriguez is with Aalborg University, DK, (e-mail: prodriguez@ee.upc.edu).

voltage control will be actuated by the reactive power. The reactive power capability offered by the plant is often translated in terms of power factor. The most typical requirement for power factor is ± 0.95. However, this requirement is quite dependent on the specifics of the grid, For example, there are cases where 0.90 capacitive is required, e.g. Canada (CanWEA), Germany (VDN).

The main goals of the reactive and voltage control are the stabilization of the node voltage, and avoidance of violation of the maximum and minimum voltage levels. Therefore, the reactive power sources in the system should continuously provide enough reactive power to keep the voltage close to its rated value, moreover the system should be able to cope with unexpected disturbances, making necessary to have a provision of reactive power in case these disturbances happen.

The voltage stability of a power system can be understood as the ability to maintain steady acceptable voltages in the considered buses of the system under normal operating conditions, and after being subjected to a disturbance. One of the main factors causing voltage instability is the inability of the power system to meet the demand for reactive power [7]. Voltage instability occurs when the power system is unable to provide the required reactive power to meet the load demands that may lead to uncontrolled operation, cascading outages, and consequently may lead to a voltage collapse.

The spinning reactive reserve activated during a contingency should be recovered, so that the minimum reserves are maintained and the system is always ready for the next contingency [8].

The provision and planning of the needed reactive power is a challenging work of the grid operator, which also normally indicates which kind of voltage control should be used for every node of the transmission and sub-transmission system.

The VAr reserve and its management control are important matters, than can guarantee that the system does not move towards voltage collapse as demand changes, or under sudden contingencies [9]. Despite of the preparations and planning by the TSOs, the combination of generation unavailability, and limited transmission capability, coupled with unanticipated circumstances, could result in shortages of generation sources for reactive supply, that could affect the security of the electric grid [8]. Thus, it is important for the electrical grid that power plants can offer maximum available reactive power if needed.

The amount of reactive reserves at generating stations is a measure of the degree of voltage stability [10].

III. WPP System Diagram

The electrical single-line diagram of the considered WPP, with all the main components, is given in Fig. 1.

In this figure, it can be seen how the main components are linked with a dotted line, representing the communication plant networks. This communication link is used by the plant control, amongst other things, to command (References) the operation of the MSCs (On/Off), WTGs and STATCOM.

The wind power plant is composed by DFIG WTGs, which are distributed in feeders. These WTGs are connected through a set-up transformer to the collector bus (MV) by means of a subterranean cable. This collector bus is stepped up to the high voltage level, by means of the substation transformer (WPPT). The main substation transformer includes an OLTC which is controlled locally. The high voltage terminal of this transformer is connected to the next substation through an overhead line (OVL).

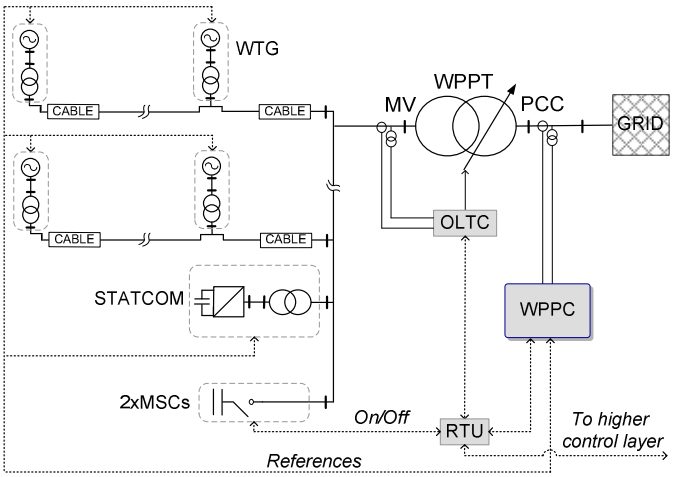

Fig. 1. Generic WPP system diagram

The elements composing the WPP are described below.

STATCOM and MSCs are installed in the plant, to help the WTGs to fulfill the grid code related to reactive power injection.

Usually, a substation RTU monitors the field digital and analog parameters received from the different elements composing the substation, and transmits relevant data to communicate to other RTUs and control centers, aditionally it is able to execute simple supervisory tasks related to protection. The gathering of direct-wired process information and its transfer to a higher level control system is one of the major tasks of the remote control application. The RTU, used in this WPP, monitors the transformer tap position and status of capacitor breakers and contactors, and receives the switching commands to the capacitors sent by the WPPC (wind power plant control). The RTU will transfer these commands to the capacitor switches when the security and integrity checking have been done [11].

The WPPC basically, includes an AVR as the outer control loop, and an AQR as the inner loop, which compensates the reactive power losses of the plant. The selected plant AVR, for this study is based on a proportional control, also called slope control. Slope voltage control is widely used in power system applications since it allows paralleling generators with individual voltage slope controllers without hunting phenomena or instability [12].

The OLTC system controls the voltage at MV side of the plant, and aims to keep the MV side of the plant to a constant level independently of the wind speed and grid voltage conditions.

Another point is that the OLTC and MSC are considered slow or steady-state regulators, since these devices are actuated mechanically, and frequent regulations accelerate the wear of the moving parts. Basically, the OLTC modifies the winding ratio of the transformer by moving the tap, and the MSC connects capacitance to the system through a mechanical switch.

IV. WPP P-Q Characteristics

In the present study, DFIG WTG type is used. The P-Q DFIG chart programmed in the WTG is a consequence of the physical limits of the WTG (i.e. stator and rotor overcurrent) [13].

Fig. 2-(a) shows the P-Q charts of a DFIG WTG (white area), and the DFIG together with a STATCOM (white and grey area).

Fig. 2-(b) shows the Q provided by the MSCs installed in the WPP (typically two MSC steps).

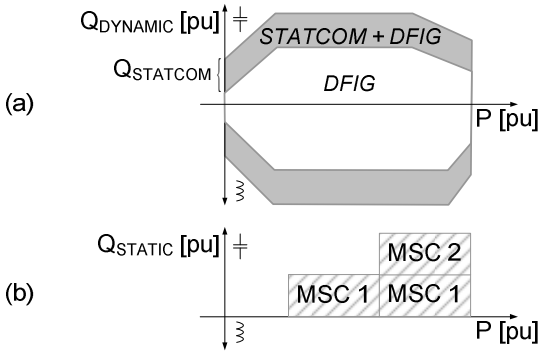

Fig. 2. (a) DFIG and STATCOM P-Q chart. (b) MSC P-Q chart.

Supposing a perfect reactive power losses compensation of the internal plant transformers, by means of the MSCs. This can be depicted in Fig. 3 can be depicted, which shows the reactive power obtained at the PCC, according to the injected active level.

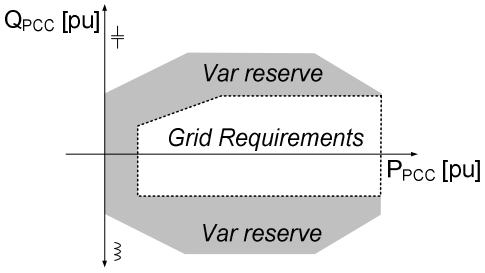

Fig. 3. WPP installed dynamic VAr and grid code requirement P-Q charts.

The available amount of dynamic reactive power (STATCOM and WTGs) in the WPP at the PCC, is depicted in Fig. 3, where the white area corresponds to the reactive power demands of the grid operator [2], and the grey area corresponds to the extra available dynamic reactive power. This extra dynamic-VAr capacity (grey area in Fig. 3), given by the installed converters, can and should be used whenever the plant is below some active power levels, as it is happening most of the time in a WPP, thus helping the system restoration after events.

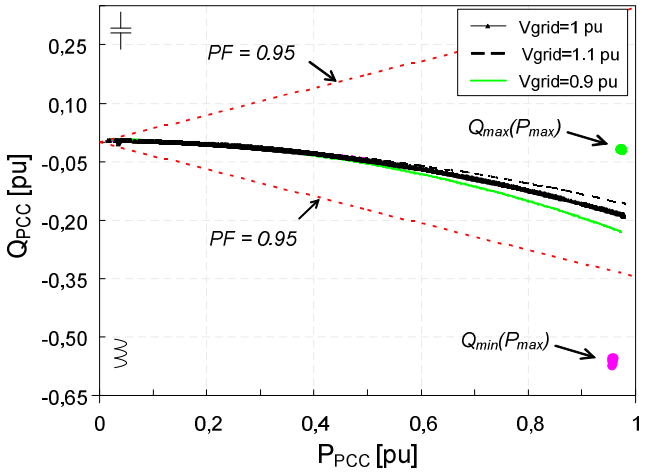

Fig. 4. Load flow analysis of the wind power plant at the PCC bus, for PF=1, maximum, and minimum Q provided by the WTGs.

The amount of VAr needed from the STATCOM can be calculated by means of a load flow analysis for different wind level productions and grid voltages.

Fig. 4 shows the load flow analysis of the WPP depicted in Fig. 1, (without the MSCs and STATCOM) for different Q operations of the WTGs.

The curve lines show the load flow when the WTGs are operating at PF equal to 1 at stator terminals, for different grid voltage levels. Thus, the reactive power consumption of the WPP components for different levels of active power injection and grid voltage levels can be evaluated.

The dotted red lines show the inductive and capacitive P-Q chart for a PF = 0.95.

The green dot shows the maximum capacitive reactive power capability at the PCC, when the WTGs are operating at their maximum capacitive reactive power at P=1 pu. It can be used to determine the amount of VAr needed from the STATCOM.

The pink dot shows the maximum inductive reactive power capability at PCC, when the WTGs are injecting their maximum inductive reactive power at P=1 pu.

According to this, the amount of VAr needed from the STATCOM is chosen to be 0.25 pu of the total plant power.

By using the yearly energy profile of an existing WPP, Fig. 5-(a) can be depicted, where the time distribution of the power injected to the grid is shown. This distribution is different from year to year, but it can be used to extract a generic conclusion.

It is worth mentioning that the operation time when the active power is zero has not been included.

Additionally, the available extra dynamic reactive power (Q reserve), according to the selected grid code is shown in Fig. 5-(b).

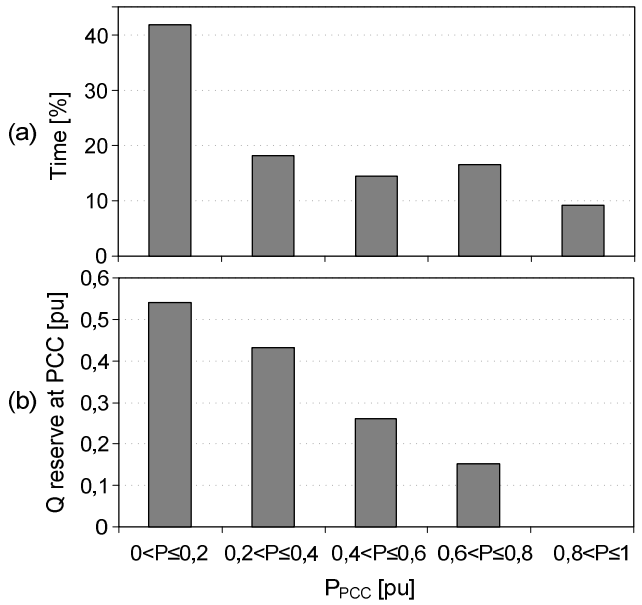

Fig. 5. (a) WPP time power distribution, (b) Q reserve according to the installed reactive power and grid code requirement.

It can be seen, that at least 90% of the time, it is possible to extract from the WPP an additional 0.15 pu reactive power.

V. Proposed VAr Management Systems

A continuously variable reactive power source is a relatively costly system in comparison with fixed shunt compensators. For this reason, the division of the task between the different compensator systems must be exactly planned.

Therefore, it is the task of the converters to stabilize the network by means of rapid changes in reactive power, whereas other sources can cover the need for VAR resulting from changes in load flow, which are relatively slow changes. By means of their voltage controllers, and because of their short reaction time, the converters keep the network voltage constant, with the result that other sources are not even activated. The danger then arises that, even for stationary network operation, the converters are loaded to the limit of their capacity, whereas other slow time reaction VAR sources remain unused [14], thereby, the importance of using a management system for the VAr reserve.

In this section, two ways (case A and B) of implementing the reserve VAr concept in a wind power plant are proposed. In both cases, the WPP disturbance response is not limited by the Q asked by the grid code; instead, it is limited by the actual P-Q chart.

The difference between the proposed two schemes is related to the VAr management system, which will take charge of reducing the injected Q whenever its value is higher than the level asked by the grid code (value which will be called "rated" throughout the rest of the document).

Case A is based on offsetting the output of the plant reactive control reference with a calculated Q_0, see Fig. 7. This Q_0 starts to be used when the injected reactive power is greater than the rated one, and its function is to drive back the injected reactive power to the rated value. This is done in small steps, and only after the system has compensated for the previous step, it is allowed to proceed further. Thereby, the control waits for the system to recover for the voltage change caused by the reserve control, forcing the system to use passive components located nearby the WPP, such as OLTC, MSCs or MSRs.

Case B needs a communication link with the upstream substation or to another central dispatcher able to follow external references. In this case, the WPP reserve control translates the amount of extra VAr to a suitable reference (see Fig. 9) for the tap changer, or for another passive reactive power compensator (Ref_ex). Thus, no continuous reduction of Q is done in the WPP output; instead the WPPC forces to change the system characteristic by activating other passive components through a reference, resulting in a consequent reduction in the injected Q after the reference is followed.

After the reference is followed, the voltage at PCC will be closer to its rated value, thus having a reduction in the injected Q by means of the AVR action.

With both control schemes, the WPP will not reduce its Q output if no regulation capacity is left in the system (i.e., if the reference is not followed, it could be that all the other Q-V compensators in the nearby area are out of operation, or already used to their maximum extent).

A. Case A

This kind of control should be applied whenever the communication with the upstream substation or high control layer is not possible.

The following figure represents the characteristics of the control (Ctrl.) and system (Sys), when the system is subjected to a step in the grid voltage. Initially, the grid characteristic changes from Sys 0 (point 0: pre-disturbance) to Sys 1 (point 1: just after the disturbance).

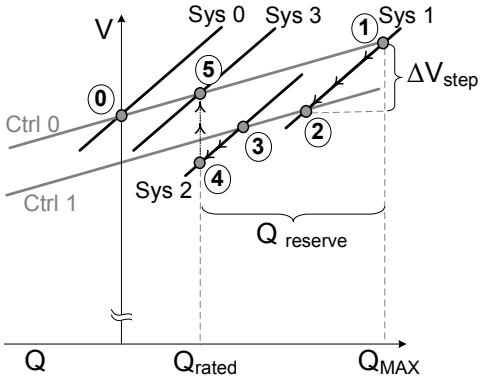

Fig. 6. System and control characteristics. Case A: Offsetting the control.

The reserve control will offset slowly the output of the plant voltage control (from point 1 to 2, and from 3 to 4), changing the control characteristics, e.g. Ctrl 0 changes to Ctrl 1. After decreasing the voltage of the system, by the Q_0 action (from point 1 to 2), the nearby compensators will react changing the system characteristics, from Sys1 to Sys 2 (from point 2 to 3).

This process continues until the Q_{rated} is reached (point 5). See Fig. 6.

The WPP injects the maximum installed reactive power if needed (Q_{MAX}), and the reserve control calculates the needed offset to drive back the WPP operation to its rated reactive power (Q_{rated}, dotted line in Fig. 3).

The offset (Q_0) is calculated in order for the injected Q to be driven slowly, and in small predefined steps (ΔV_{step}), according to a maximum allowed voltage step.

The control structure of the plant control with the implemented reserve VAr concept is shown in the following figure. The Q_{ref}^{Plant} calculated by the AVR is offset by the reserve control in order that the measured reactive power gets below the rated value.

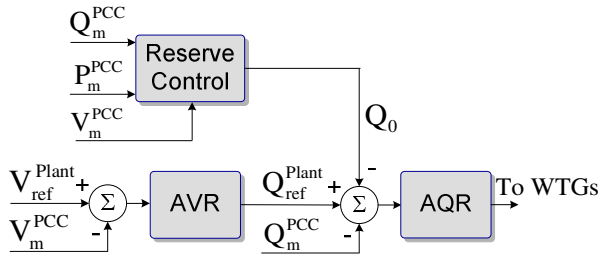

Fig. 7. Plant control case A: offsetting the input of the AQR.

Fig. 8 shows the detailed implementation of the reserve control.

The bandwidth of the reserve control has to be smaller than the AQR to avoid control hunting. The K_{AW} function is to drive the Q_0 to zero when the Q_m is equal or below the rated Q.

The LOGIC block allocates the supervisory algorithm to detect changes in the grid. This block will freeze the PI regulator in case some predefined voltage changes at the PCC (ΔV) are measured. Moreover, the LOGIC block will unfreeze the PI regulator when the voltage at the PCC (V_m^{PCC}) changes in the opposite direction relative to the voltage influence of Q_0.

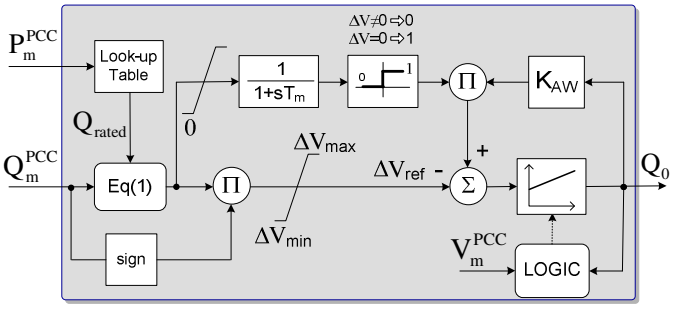

Fig. 8. Reserve control for case A.

The LOGIC block will ensure that the WPP will not remove Q from the system if no reaction to the first reduction of Q is observed. Thus, this is an indirect way of gaining information about the availability of the other devices in the nearby area, and their capability of counter-acting this Q reduction.

Basically, the LOGIC block allows a maximum voltage change (ΔV) for every reactive power reduction step, and only after the system reacts to this voltage variation, the control will allow another voltage change (ΔV).

For that reason, Q_m is translated to a voltage reference (ΔV_{ref}), by using (1), making possible for the control to define the maximum change in the PCC voltage, that the reserve control can drive in every step.

As depicted in Fig. 8, the active power measured at the PCC (P_m^{PCC}) is used to calculate Q_{rated}, by means of a look-up table containing the dotted line of Fig. 3.

The Q_m^{PCC} together with the Q_{rated} is used to calculate the desired ΔV, which will be fed to the PI regulator.

The PI regulator will drive ΔV to zero, by outputting a Q_0, which offsets the AQR output of the plant.

The calculated ΔV is passed through a filter (with a time constant T_m), and whenever ΔV is greater than zero, K_{AW} is disabled by multiplying it by zero. On the other hand, when ΔV is equal to or below zero, the K_{AW} is activated, hence reducing Q_0 to zero.

B. Case B

In this case, the reserve control calculates a reference (Ref_{ex}). The reserve control function is to translate the excess of Q_m^{PCC} into an appropriate signal for the upwards control level, meanwhile it is greater than the Q_{rated} in absolute value.

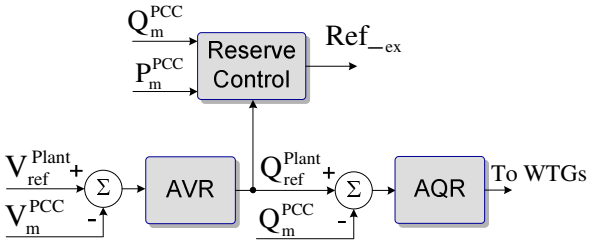

Fig. 9. Plant control case B: creating a reference to the following control layer.

The calculated reference can be in different forms, e.g. moving up/down the tap position, ΔV_{ref} or ΔQ_{ref}.

In Fig. 10, when moving from point 1 to 2 means that the system characteristic is changed; by e.g. tap changer action or capacitor connection in the nearby area.

The WPP can inject the maximum installed Q (if needed), and calculates the ΔV reference to be sent upwards.

When the system characteristic is changed from (Sys 1) to (Sys 2), according to the sent reference (Ref_{ex}), the voltage at the PCC reduces its difference with the rated value, consequently the injected Q is reduced following the AVR action. In essence, the Q is reduced only when the voltage at PCC changes to a closer rated value.

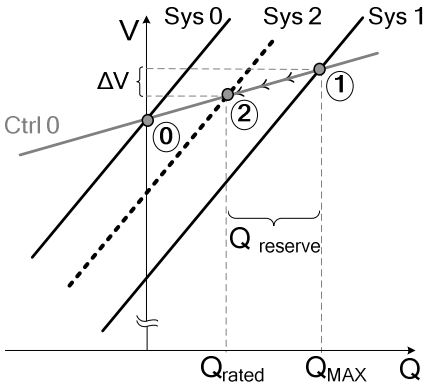

Fig. 10. System and control characteristics. Case B: Creating a ΔV reference.

As an example, the reference ΔV_{ref} can be calculated as it is shown below, where the Q_{rated} is calculated by using a look-up table similar to Fig. 3.

$$\mathrm{Ref}_{-ex} = \Delta V_{ref} = \frac{Q_m^{PCC} - Q_{rated}(P_m^{PCC})}{K_{SLOPE}} \quad (1)$$

VI. Simulation Results and Analysis

Fig. 11 represents the diagram of the simulated cases. The WPP is connected to the sub-transmission system, where some loads could be presented (L1 and L2). Upstream of this point, the whole electrical system is reduced to an equivalent grid, defined by its SCR and X/R.

Two loads are connected to the respective buses of the OVL, which represents small costumer consumptions. In the absence of specific information, the most commonly accepted static load model is to represent active power as constant source and reactive power as constant impedance (i.e., the following indexes are used to represent the loads a=1, b=2) [7].

The OLTC control has been modeled according to [15].

$$L1 = L2 = P + jQ = 0.3 + j0.1\ [\mathrm{pu}] \quad (2)$$

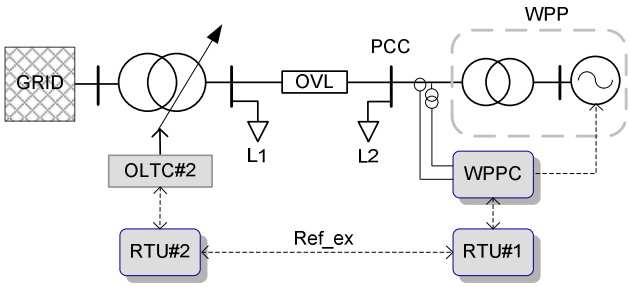

Fig. 11. Simplified diagram of the system for the simulated cases.

The simulation results show the WPP performance for a grid voltage drop of 0.1 pu, when the schemes A (see Fig. 12) and B (see Fig. 13) are implemented. Both schemes, including the cases where the OLTC#2 is not operative (Tap out), and when it is fully operative (Tap ok), are simulated.

In these figures are shown the tap position of the next substation (Tap#2 position), the Q at PCC (Q_{PCC}), the voltage of the grid (V_{GRID}) and at the PCC (V_{PCC}), and finally, for the case A, the offsetting signal (Q_0) is shown.

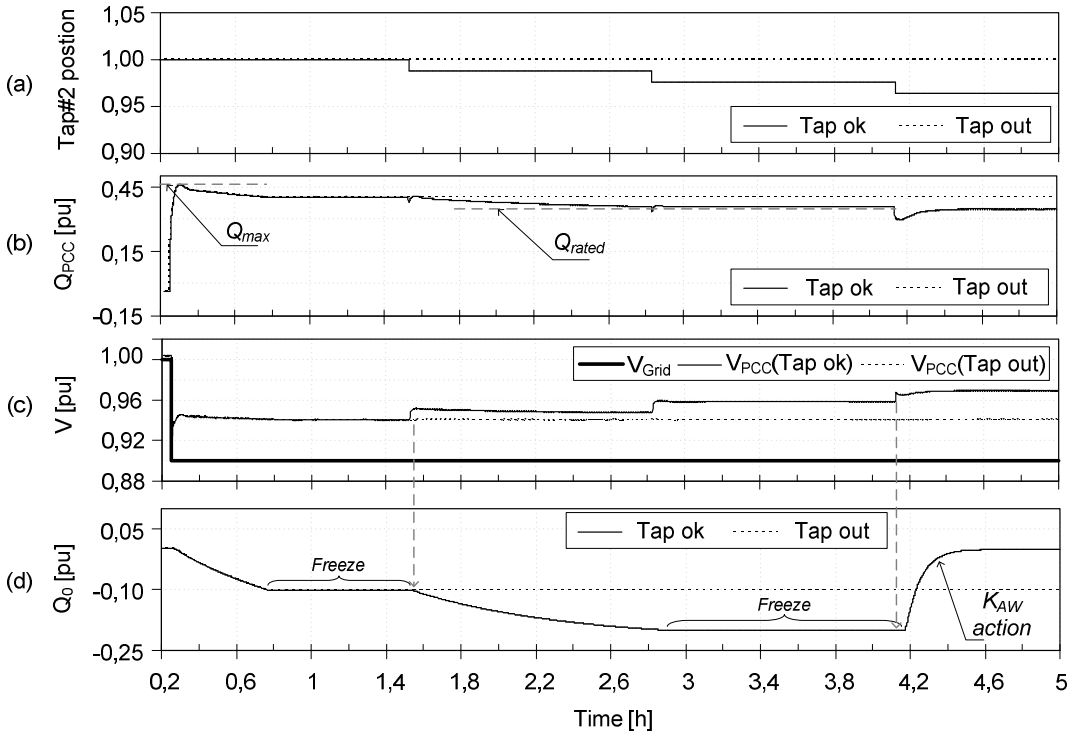

Fig. 12. Simulation results for the case A.

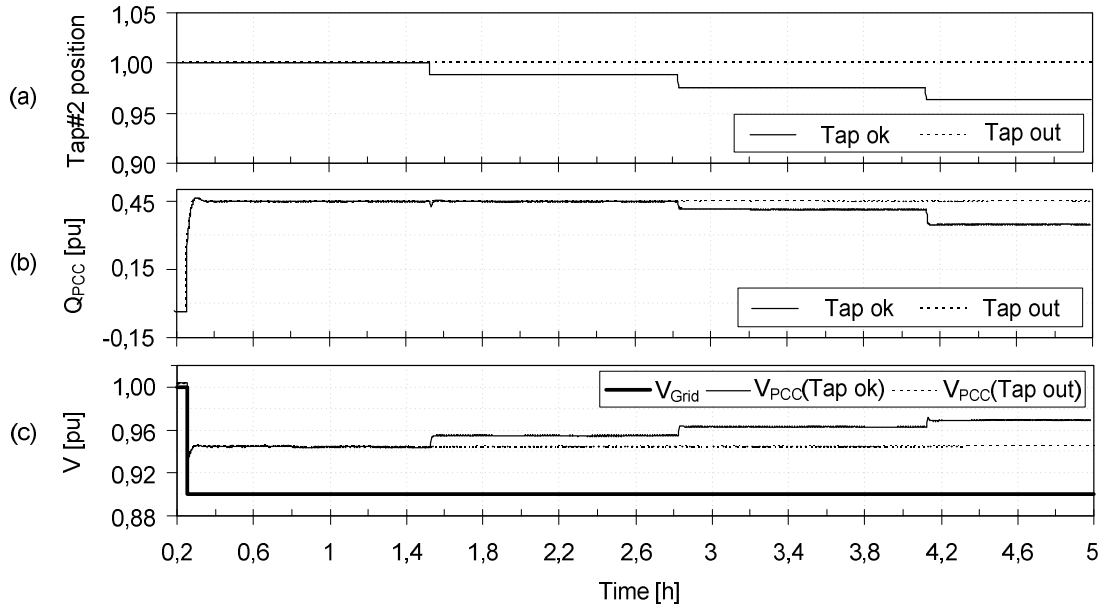

Fig. 13. Simulation results for the case B

A. Simulation Results: Case A

It can be seen how in the case A, the WPP will inject its maximum available reactive power into the power supply grid if the measured grid voltage falls below a predetermined grid voltage level, see Fig. 12-(c). When the controller detects that the injected reactive power exceeds a rated reactive power level, the amount of reactive power is reduced, and the reactive power controller subsequently waits for the system to react to this small reactive power reduction, see Fig. 12-(b).

After a certain time, the tap of the next substation moves (Fig. 12-(a)), changing the transformer ratio, and increasing the voltage of the feeder. This is sensed by the plant reserve control, which will allow a further reduction of the injected reactive power. The reduction of injected reactive power is continued until the rated level is reached. See Fig. 12-(d).

If the tap changer of the next substation is not operative (Tap Out curves), only the first reactive power reduction is allowed, since no change in the grid voltage can be sensed by the reactive power controller. Thus, in this scenario the LOGIC module keeps Q_0 continuously frozen. See Fig. 12-(d).

It can be observed that the K_{AW} action drives the Q_0 to zero when the Q injected gets below the Q_{rated}. See Fig. 12-(d).

B. Simulation Results: Case B

In the Case B, it can be seen that when the tap changer of the next substation is operative (Tap OK), it will follow the reactive power control references increasing its winding ratio (Fig. 13-(a)), and the reactive power injected into the power supply grid is reduced as a consequence of this voltage increasing, see Fig. 13-(b).

The AVR will reduce its output in accordance with the new voltage level (Fig. 13-(c)), thus, the reactive power is reduced in accordance with a new equilibrium working point, once the tap has moved. Obviously, when the tap changer is not operative (Tap out), the reactive power is not reduced, since no changes in the voltages are produced.

VII. Conclusions

This paper presents the implementation of VAr reserve management system to wind power plants.

WPP energy-time profile characteristic makes WPP a perfect candidate for such control. It is possible to say that WPPs are often below their rated active power, hence having unused reactive power compensation equipment most of the time.

Additionally, two different reactive power reserve management systems are proposed. Both control schemes are tested by means of simulations.

The proposed VAr reserve system management schemes use the maximum capability reactive power of the WPP. Moreover, instead of slowly reducing the reactive power injected without knowing if the nearby system compensators are able to compensate for this, as normally other VAr compensators do [5], two systems are suggested where by indirect (case A) or direct (case B) methods, the reduction of Q is done according to the availability of the nearby reactive-voltage compensators.

One method (case B) is based on a reduction of the reactive power by sending references to the next higher control level, whereas the other method (case A) is based on a reduction of the reactive power, driven by a supervisory control, which allows a reduction of the reactive power in predefined voltage steps. The last one is only preferred if the system can not be communicated with the nearby compensators.

VIII. References

[1] P.O.12.2, "Connected Installations to the Transmission Spanish System: Minimum Requirements for Design and Security", Red Electrica de

España, Grid Code Requirements for installations connected to the transmission system in Spain.

[2] National Grid Electricity Transmission: "Guidance Notes for Power Park Developers", 2008.

[3] Alberta Electric System Operator (AESO), "Wind Power Facility, Technical Requirements", Alberta, November 2004.

[4] Hydro-Quebéc: Technical Requirements for the Connection of Generation Facilities to the Transmission Systems, Québec, Canada.

[5] Hingorani NG, Gyugyi L., "Understanding Facts". IEEE Press Series on Power Engineering. IEEE Press: Piscataway, New Jersey, 2000; 432. Page(s) 194-197.

[6] Lixin Bao; Zhenyu Huang; Wilsun Xu "Online voltage stability monitoring using VAr reserves", PES, IEEE Vol.: 18, Issue: 4, 2003, Page(s): 1461 – 1469.

[7] P. Kundur, "Power System Stability and Control", 1994 McGraw-Hill, Inc. ISBN 0-07-035958-X.

[8] Trehan, N.K.; "Ancillary services-reactive and voltage control" Engineering Power Society Winter Meeting, 2001. IEEE Volume: 3, Publication Year: 2001, Page(s): 1341 - 1346 vol.3.

[9] Zalapa, R.R. Cory, B.J.; "Reactive reserve management" Generation, Transmission and Distribution, IEE Proceedings- Volume: 142, Issue: 1 Publication Year: 1995, Page(s): 17 – 23.

[10] Feng Dong; Chowdhury, B.H.; Crow, M.L.; Acar, L. "Improving voltage stability by reactive power reserve management" Power Systems, IEEE Transactions on Volume: 20 , Issue: 1, Publication Year: 2005 , Page(s): 338 – 345.

[11] GEEnergy, http://www.gepower.com/prod_serv/products/substation_automation/en/index.htm.

[12] Martínez, J.; Kjer, P.C.; Teodorescu, R., "DFIG turbine representation for small signal voltage control studies"; International Conference on Optimization of Electrical and Electronic Equipment (OPTIM), 2010 12th Publication Year: 2010, Page(s): 31 – 40.

[13] Torsten Lund, Poul Sørensen, "Reactive Power Capability of a Wind Turbine with doubly Fed Induction Generator". Wind Energy 2007, Wiley Interscience.

[14] Romegialli, G.; Beeler, H.; "Reactive compensation. Problems and concepts of static compensator control" Generation, Transmission and Distribution, IEE Proceedings C Volume: 128, Issue: 6, Year: 1981, Page(s): 382 – 388.

[15] Calovic, M.S.; "Modeling and Analysis of Under-Load Tap-Changing Transformer Control Systems" Power Apparatus and Systems, IEEE Transactions on Volume: PAS-103, Issue: 7, Publication Year: 1984, Page(s): 1909 – 1915.

A.3

"Short Circuit Signatures from Different Wind Turbine Generator Types"
Jorge Martínez, Philip C. Kjær, Pedro Rodriguez, Remus Teodorescu.

Short Circuit Signatures from Different Wind Turbine Generator Types

Jorge Martínez, Philip C. Kjær, Pedro Rodriguez, Member, IEEE, Remus Teodorescu, Senior Member, IEEE.

Abstract— **Modern wind power plants are required and designed to ride through faults in the network, subjected to the fault clearance and following grid code demands. Beside voltage support during faults, the wind turbine fault current contribution is important for relay protection settings.**

The following wind turbine generator during faults have been studied: (i) induction generator, (ii) induction generator with variable rotor resistance (iii) converter-fed rotor (often referred to as DFIG) and (iv) full scale converter.

To make a clear comparison and performance analysis during 3-phase faults, and the consequent effects on substation protections, the aforementioned configurations have been simulated using PSCAD/EMTDC, with the same power plant configuration, electrical grid and generator data.

Additionally, a comparison of these wind turbine technologies with a conventional power plant, with a synchronous generator, has been simulated.

This paper addresses the difficulties that distance or overcurrent relays can experience when they are used in wind power plants. Whereas the short circuit contribution from power plants with synchronous generators can be calculated on the basis of the machine parameters alone, for wound rotor asynchronous and full scale generators power plants, the converters or rotor circuitry representation have to be taken into account for short circuit current studies and relay settings.

Index Terms—**Wind turbine generator, power system, faults, doubly fed generator, full scale converter, short circuit currents, distance relays.**

I. Nomenclature

C	Capacitor
CB	Circuit Breaker
CT	Current Transformer
DC,AC	Direct Current, Alternate Current
DFIG	Doubly Fed Induction Generator
FSC	Full Scale Converter
G	Generator
IG	Induction Generator
IGR	Induction Generator with Rotor resistances
LV	Low Voltage
P, Q	Active, Reactive power
PCC	Point of Common Coupling
PI	Proportional and Integer
S	Apparent power
SG	Synchronous Generator
SCR	Short Circuit Ratio
SET, SCL	Substation, Short Circuit Level
V, I	Voltage, Current
OVL	Overhead Line
WPP, WTG	Wind Power Plant, Wind Turbine Generator
WPPT	Wind Power Plant Transformer
WTGT	Wind Turbine Generator Transformer
ω	Angular frequency
X, R	Inductance, Resistor
Z	Impedance

Subscripts

a, b, c	Three phase quantities
d, q	Direct and quadrature axes
ref	Reference
m	Measured

Manuscript September 10, 2010.

J. Martínez and P. C. Kjaer are with VESTAS Wind System.

R. Teodorescu and P. Rodriguez are with Aalborg University.

II. Introduction

With increasing penetration of wind power generation, the requirements for the connection of WPP to the electrical grid are defined by the new and emerging grid connection codes. The grid connection requirements vary in different parts of the world, but they have some common aims like permitting the development, maintenance and operation of a coordinated, reliable and economical transmission or distribution system. The new requirements generally demand that wind farms provide ancillary services to support the network in which they are connected [1]-[2]. Wind turbine technology is evolving from the direct connected IG or DFIG to the FSC with either IG or SG, where better controllability of the current output can be achieved.

These different technologies used in WPPs provide very different short circuit current signatures, which should influence the protection settings of the WPP. Whereas the fault current in case of a SG can be calculated based on the generator parameters and the impedance to the fault, this can not be done with some of the wind turbine technologies, i.e., the DFIG and IGR technologies, as a consequence of the dissipated energy in the rotor excitation during faults, and in the case of the FSC technology the stator is connected to the grid via AC/DC DC/AC converters. These WTGs are controlled during faults in a manner that leads to a behavior quite different from the SGs.

III. WIND TURBINE GENERATOR TYPES

Most of the wind turbines employ one of the electric-mechanical energy conversion schemes depicted in Fig. 1, 2, 3 and 4. In the following, a brief explanation about these technologies can be found.

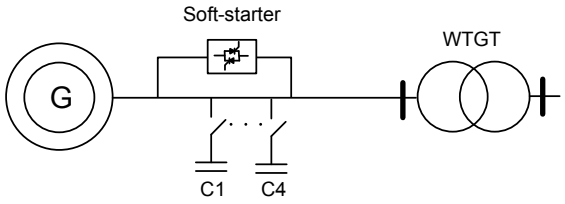

Fig. 1. IG; fixed speed cage induction generator.

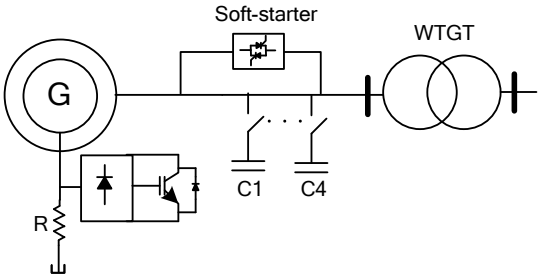

Fig. 2. IGR; variable speed wound rotor asynchronous generator with variable rotor resistance.

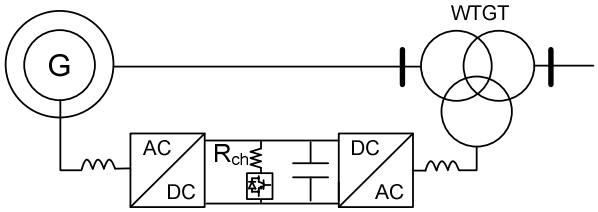

Fig. 3. DFIG; variable speed doubly fed generator.

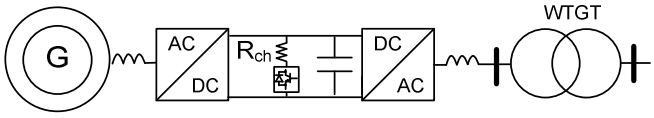

Fig. 4. FSC; variable speed full scale conversion.

A. IG

The fixed-speed squirrel-cage induction generator, Fig. 1, requires a soft starter for being connected to grid, and employs capacitor banks (in this case 4 steps are represented) for power factor correction to compensate the generator reactive power consumption. The generator electrical torque is not directly controlled.

B. IGR

The variable rotor resistance wound rotor asynchronous generator is a variable speed generator, Fig. 2, and allows adaptation of the generator torque-slip curve to wind conditions, in order to maximize the energy extraction. The effective rotor resistance (R) is controlled by a power electronic circuit involving a chopper switch. By adjusting the duty cycle of the switch, the effective resistance applied to the rotor circuit can be dynamically controlled. Therefore, the torque can be controlled to achieve the desirable performance [3].

Soft starter and power factor correction circuitry are still needed, as for the case of IG.

A simple diagram of the controller is shown in Fig. 5, where it can be seen how the duty cycle of the switch is calculated based on two cascade PI controllers. A look-up table, with the generator speed as an input, is used to generate the active power reference.

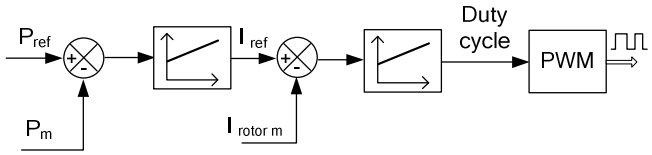

Fig. 5. IGR simplified diagram controller.

C. DFIG

The variable speed doubly-fed generator, Fig. 3, allows full control of generator active and reactive power using the rotor-connected frequency converter. Its rating is in the order of 0.3 pu. Operating both with sub- and super-synchronous speed the power can be fed both in and out of the rotor circuit. The rotor connected converter can employ various power dissipation solutions (sometimes referred to as active crowbar located in the rotor terminals or chopper located in the DC link bus bar: R_{ch}). The simplified control of the rotor converter is depicted in Fig. 6, where the active and reactive power are controlled using the d and q axes respectively.

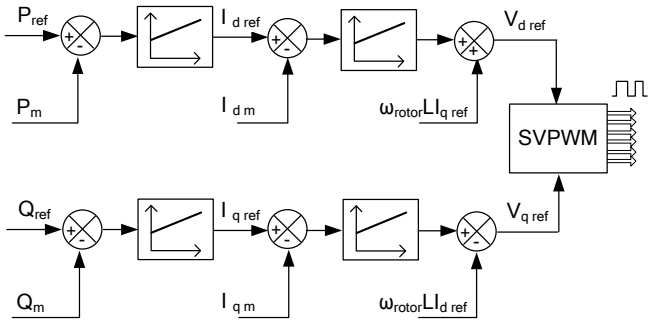

Fig. 6. DFIG simplified diagram controller

D. FSC

With full scale (1 pu) back to back power converter, the generator (this could be IG or SG) is effectively decoupled from the grid. Generator power can be dissipated in the converter DC link by means of a brake resistor (R_{ch}), see Fig. 4. Reaction to the grid faults will be dependant on the grid converter rating and its control. In Fig 7 it can be seen a simplified diagram of the control of the converter connected to

the grid-side, which is the one of interest.

The d axis loop controls the DC-link voltage level, and the q axis loop controls the reactive power supplied to the grid.

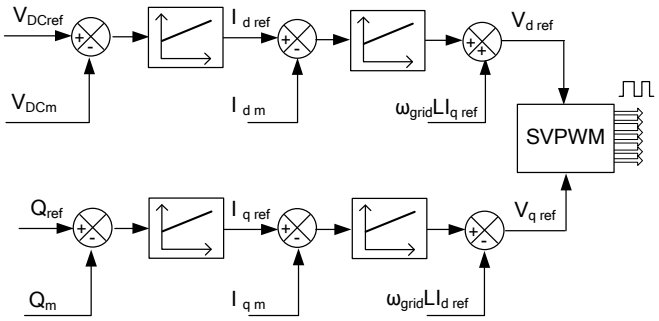

Fig. 7. FSC simplified diagram controller

IV. Case Setup

The following cases have been simulated in PSCAD version 4.2.1 with a simulation time step of 50 μs. The same base set-up case has been used with the four different WTG models mentioned in section III. See Fig. 8.

In every case, the WTGs composing the WPP are represented as an aggregated one. This aggregated WTG is connected through its set-up transformer to the collector bus by means of a subterranean cable. This collector bus is step-up to the high voltage level, by means of the substation transformer, WPPT in Fig. 8. The high voltage terminal of this transformer is connected to the next substation through an overhead line. Upstream of this point the whole electrical system is reduced to an equivalent, defined by its SCR and angle.

The subterranean feeder cables are modeled as a PI equivalent with an X/R ratio of a 240 mm^2 section cable and a total impedance of 1 % (Z_{cable}). The OVL is modeled as a PI equivalent, with the characteristic X/R ratio of a 150 mm^2 section OVL, and with a total impedance of 2 % (Z_{OVL}). The substation and WTG transformers are modeled with 12 % and 8 % impedance and an X/R ratio of 24 and 10 respectively. See more data simulation details in the appendix tables.

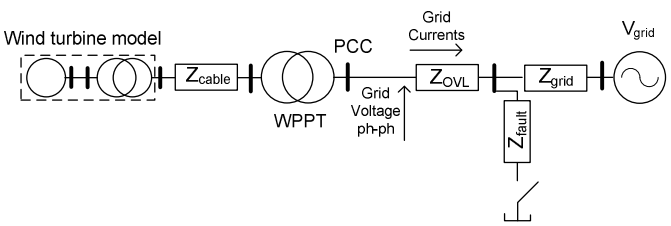

Fig. 8. Simulated base-case system diagram.

The grid is represented by an equivalent Thevenin circuit with a SCR of 10 and a grid angle of 75 degrees (Z_{grid}). The impedance to the fault (Z_{fault}) is calculated accordingly to make a voltage divider with the desired ratio. The fault is applied after the OVL, following the scheme depicted in Fig. 8.

V. Protection Short Circuit Current Coordination

Modern wind power plants are required and designed to ride through faults in the transmission and distribution networks, subjected to fault clearing.

Fig. 9 represents a typical OVL protection system for a WPP with a radial connection, where a distance relay (21), which basically would trip for faults up to a certain distance away from a substation but not beyond that point, and an earth directional overcurrent (67N) protection relay are used. ANSI device numbers are used for the representation of the relays [4].

In Fig. 9 only the relay functions at PCC related to OVL protection have been plotted.

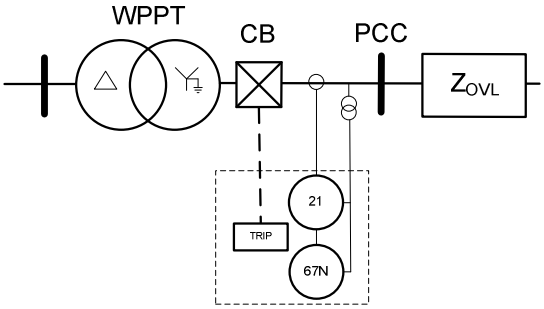

Fig. 9. OVL current protection diagram.

VI. Simulation Results

In the following, each of the generator types, shown in section III, has been subjected to a simulated 3-phase bolted short circuit. The test circuit used in the simulations is shown in Fig. 8. In all of the following simulations the residual voltage at PCC is 0.1 pu, the pre-fault active power is 1 pu, and power factor 1 at WTG terminals. The fault is cleared after 500 ms.

In the following simulations, 3-phase short circuits are applied at time 0 seconds. The voltages and currents seen at PCC during the simulations are shown.

In all the simulated cases, the current and voltage waveforms have been processed using a sixteen samples cycle, full cosine cycle filter, as it is particularly suited for protective digital relaying, while extracting the fundamental, the filter rejects all harmonics including the decaying exponential [5].

The following figures show the instantaneous 3-phase values of the real (blue color line) and processed data (red color line), as well as the envelope of the instantaneous 3-phase values of the real (solid blue line) and processed data (dashed red line) of the voltages and currents at PCC. The used indexes for the instantaneous and the envelope of the instantaneous data in the figures are: $_{abc}$ and $_{envelope}$ respectively.

A. IG

As the squirrel-cage induction generator is uncontrolled, it sources a large reactive current and demagnetizes based on generator and grid impedances. Upon the recovery of the line voltage, the re-magnetization of the generator will sink a large reactive current. See Fig. 10.

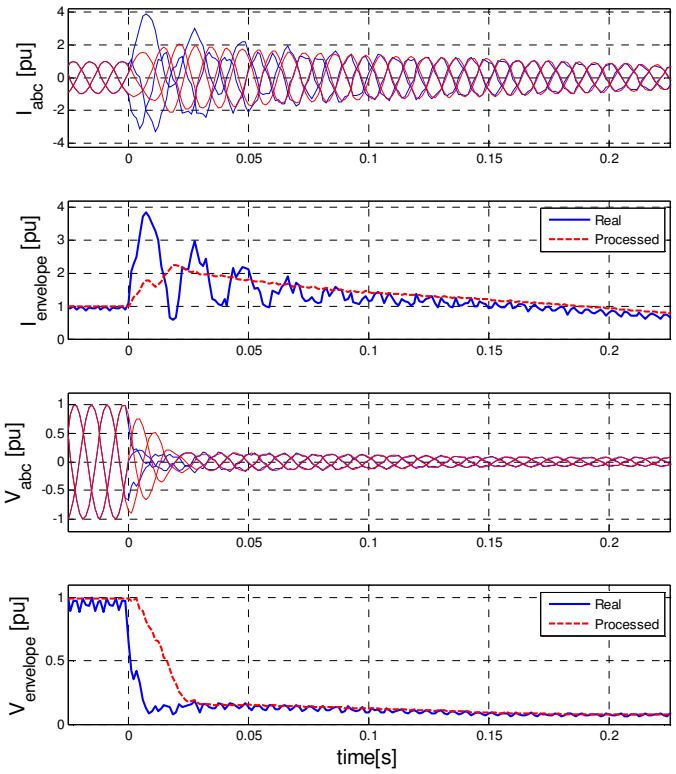

Fig. 10. 3-phase fault, IG case.

B. IGR

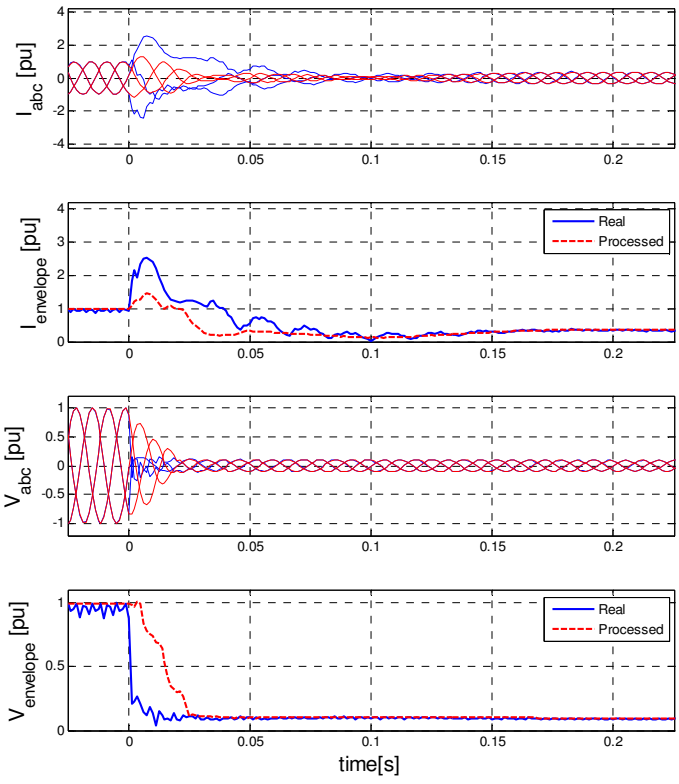

Fig. 11. 3-phase fault, IGR case.

Upon the rise of the stator current, the rotor current will exceed its reference value, I_{ref} in Fig. 5, and the power electronic switch is continuously off, leading to the maximum rotor resistance value, necessary for limiting the rotor current. This causes a rapid dissipation of energy as the generator demagnetizes.

The resulting stator currents exhibit a much lower AC component than in the case of the squirrel cage induction generator.

Once the rotor current falls below its reference value from pre-fault operation, the power electronic switch can actively modulate the effective rotor resistance again, and can bring the current back to its reference value (subject to limitations by stator voltage range restrictions). See Fig. 11.

C. DFIG

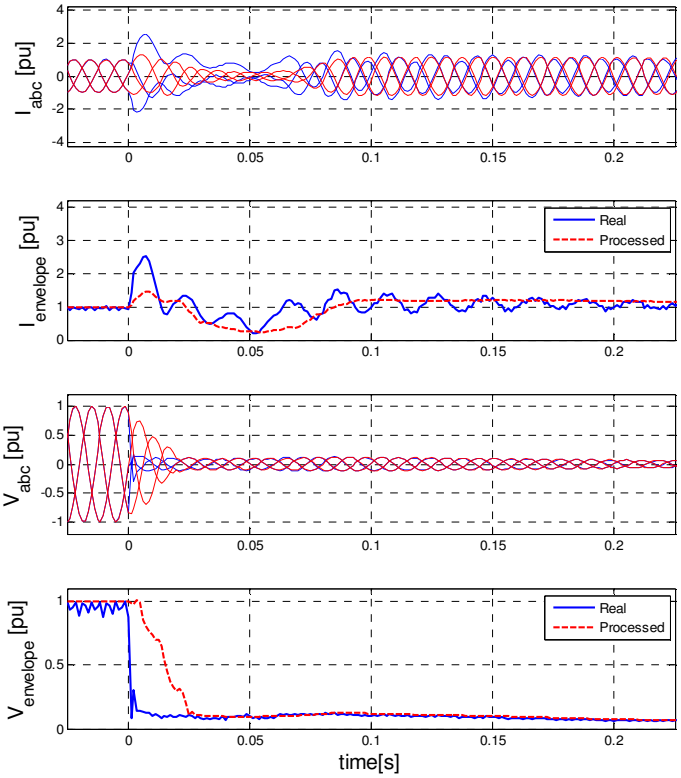

Fig. 13. 3-phase fault, DFIG case.

DFIG technology can present different short circuit current response depending on the fault severity. Usually, for severe faults the rotor converter can be blocked during certain time to protect itself against high currents. Upon the rise of the stator current, the rotor current forces the rotor connected converter to block and its diodes to freewheel, which charges the DC link rapidly.

The brake chopper maintains the DC voltage level by turning on the DC link chopper in full conduction mode (no chopping). Once the rotor currents fall below their protection levels, the rotor-connected converter resumes switching and the rotor windings are subjected to a controlled voltage, which will cause the injection of reactive current according to the stator voltage level.

The I_q reference is calculated according to the stator voltage (V_{LV}) and usually it is defined by the grid codes, see Fig. 12. Thus, the WTG supports the grid voltage recovering process

[6-8]. The I_q injected during the fault can be seen in Fig. 18.

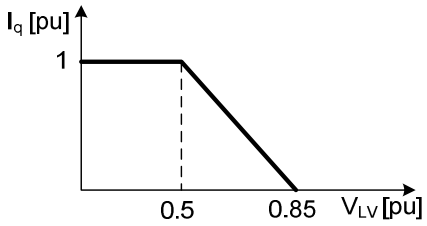

Fig. 12. I_q reference according to the stator voltage.

D. FSC

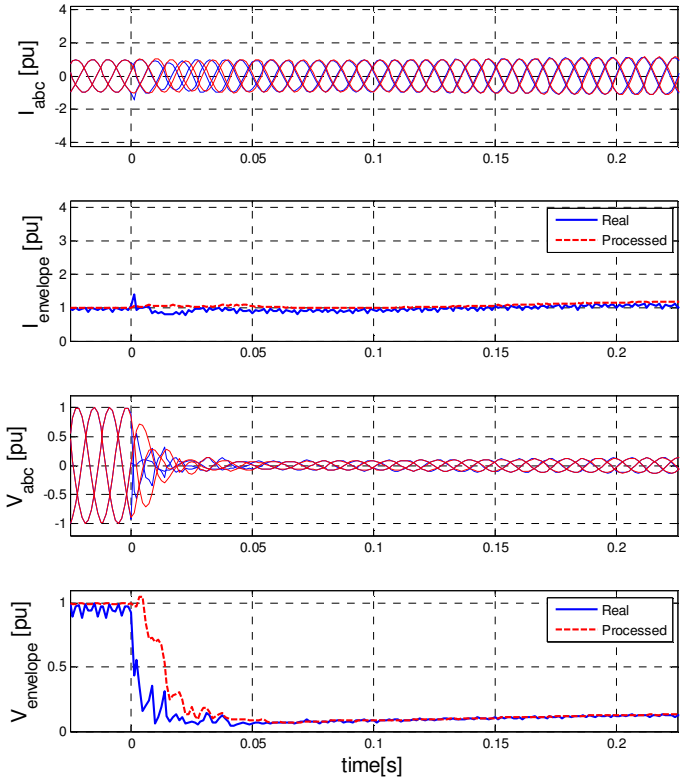

Fig. 14. 3-phase fault case FSC.

The grid connected converter could have several behaviors depending on the sizing of the electronics, control capabilities and fault severity, i.e. the following two cases are presented: (i) blocks its switching upon over-current limit, and then resumes switching action to produce 1 pu or other reactive current level, (ii) blocks switching during the entire fault period [9].

Only the case (i) is shown in Fig. 14, due to the fact that the fault simulated is located at PCC, far away from converter terminals, having in between the converter terminals and fault location: the subterranean cable, the OVL, the WTG and the WPP transformers impedances, therefore, reducing the risk of reaching high peak current values.

As can be seen in Fig. 18 the FSC will inject 1 pu I_q, as fast as the control is ready (it can be said that the transient is a control transient and not a electromagnetic transient, lasting only several ms), according to the reference calculated upon the stator level (V_{LV}). See Fig. 12.

E. SG

In this case, a synchronous generator with round rotor and one damping circuit has been tuned to have similar response than the short circuited generator used in the other cases [10].

This has been done to compare the previous cases with a conventional power plant with a synchronous generator.

The SG shows during the fault, see Fig. 15, a fundamental frequency oscillatory component, due to interaction with the rotor field, and a unidirectional component caused by the fundamental frequency induced in the rotor. Generator and grid inductances will dictate the rotor and stator current decay times.

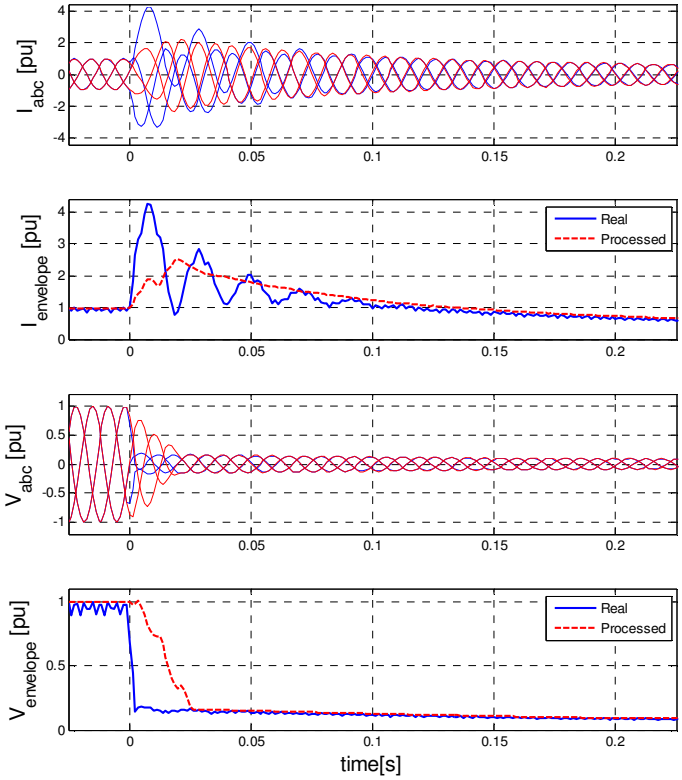

Fig. 15. 3-phase fault, SG case.

VII. Impedances to the Fault and Maximum Peak Current Values

A list of the different maximum peak values obtained in the simulated cases are depicted in table 1, as well as a comparison of these peak values with the one obtained for the SG.

TABLE I
MAXIMUM SHORT CIRCUIT PEAK CURRENTS

	IG	DFIG	IGR	FSC	SG
I_{peak} [pu]	*3.9*	*2.5*	*2.5*	*1.4*	*4.2*
I_{peak} relative to SG [pu]	*0.93*	*0.61*	*0.61*	*0.33*	*1.00*

Voltages and currents extracted from the previous cases have been processed using the sixteen samples cycle, full cosine cycle filter algorithm [11]. With these values, the

different impedances to the fault (Z_d = V/I) are calculated and shown in Fig. 16.

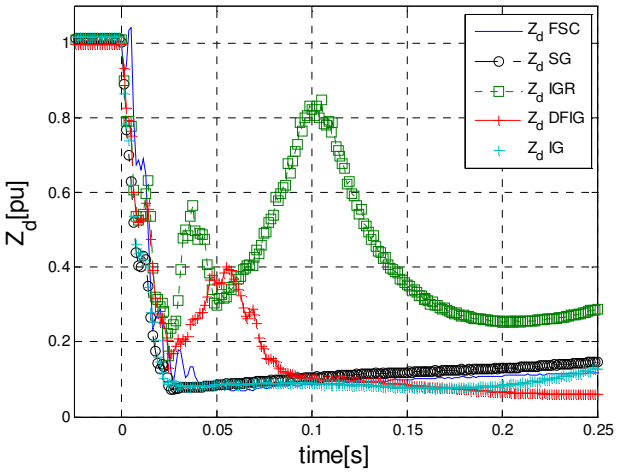

Fig. 16. Impedance to the fault for the different WTGs.

VIII. Analysis of the Results

As the waveforms in the previous graphs demonstrate, the short circuit contribution from different turbine technologies, using the same generator but different circuitry attached to the rotor or stator, vary widely.

Generally speaking;

a) The IG and the SG behave similarly, as they both preserve the rotor field well into the duration of the fault. Therefore, they exhibit very similar current to the fault, showing high peak currents and high AC current component.

b) The IGR and the DFIG both dissipate significant power on the rotor side during faults, and therefore shorten the rotor decay times, which implies the following: reduced peak currents, and lower AC current components. This low AC component could lead to a bad function of the distance relays when classifying the zone where fault is located (as it can be seen in Fig. 16). Using differential relays should be considered instead of distance relays. Moreover, this low AC component could be a problem for the breaker operation when trying opening currents at non zero crossing and saturation of the CTs should be a concern as well.

c) The FSC separates itself by virtually no difference between nominal and short circuit current amplitude. Short circuit current will be dependant on control and converter sizing. This technology exhibit low and short duration peak current during faults. In any case, the use of overcurrent relays could be a concern if the grid connected converter is blocked and consequently there is no current injection to the fault, or if it is not blocked and injects currents close to the rated value without any transient.

IX. Conclusions

WPPs comprise very different technologies compared to the SG power plants. The four most common wind turbine technologies (all of them using the same main electrical components: generator and transformer) and a SG with the same equivalent generator impedances have been subjected to a 3-phase fault at the PCC showing that they exhibit very different short circuit current signatures.

The consequences of having quite different short circuit behavior than the SGs are shown when using distance or overcurrent protection relays.

DFIG and IGR technology could lead to a malfunction of distance relays when detecting the zone where the fault is located, due to the low AC component in the injected short circuit currents, see Fig. 16. FSC technology could lead to problems when adjusting the overcurrent relays due to low short circuit peak values, additionally a permanent blocking of the converter will affect the correct distance relay operation too. See Table I.

Therefore, when there are not enough available data of the WTG circuitry and controls to make a proper short circuit study, the following combinations should be treated very carefully: DFIG-distance protection, IGR-distance protection and FSC-overcurrent protection.

For the DFIG, IGR and FSC, the circuitry attached to the rotor or stator of the generator and its control are influencing heavily the behavior during faults. Different control for same topology (same circuitry) could lead to different short circuit behavior, having the consequence that different manufacturers offering same topology could present different short circuit response.

As a conclusion, the WTG circuitry and its control should be represented correctly when studying short circuit currents from wind power plants, even in the cases of the DFIG or IGR where the converters represent only a small fraction of the total power. This shows the need of a standardization process for the WTG representation during faults and the importance of collecting the right data for short circuit studies for all WTG technologies.

X. Appendix

TABLE II
ELECTRICAL DATA OF WIND TURBINE

Parameter	Value	Unit
S_{base}	2100	[kVA]
V_{base}	0.69	[kV]
Electrical frequency	50	[Hz]
Stator Resistance	0.006	[pu]
Rotor Resistance	0.009	[pu]
Mutual Inductance	3.422	[pu]
Stator Inductance	0.072	[pu]
Rotor Inductance	0.101	[pu]
S step-up transformer 0.69:20kV	2100	[kVA]
Z step-up transformer	0.08	[pu]

TABLE III
ELECTRICAL DATA OF THE SYSTEM

Parameter	Value	Unit
X_{cable}	0.65	[%]
R_{cable}	0.83	[%]
C_{cable}	1.66	[%]
X_{OVL}	1.81	[%]
R_{OVL}	0.89	[%]
C_{OVL}	0.51	[%]
X_{WPPT}	11.91	[%]
R_{WPPT}	0.49	[%]
X_{GRID}	9.66	[%]
R_{GRID}	2.58	[%]
High voltage level	115	[kV]

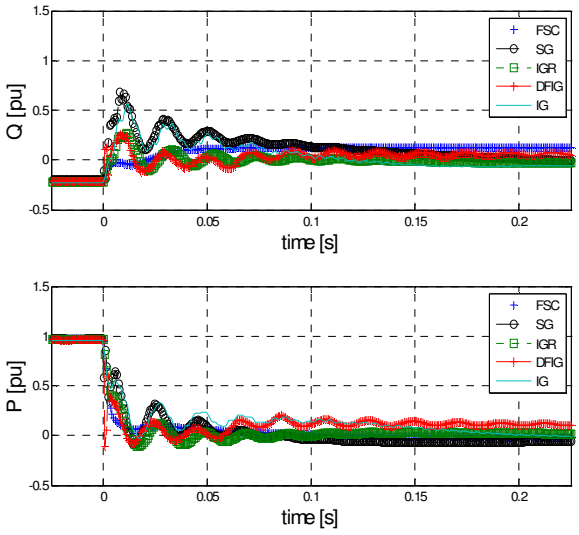

Fig. 17. P and Q at PCC for the different WTGs.

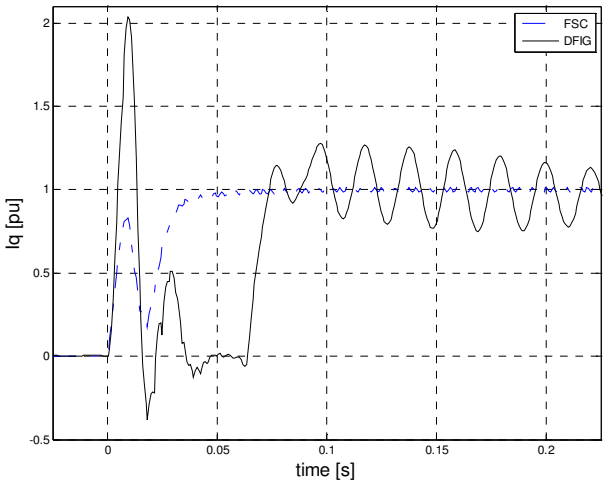

Fig. 18. Iq injected at LV for the FSC and DFIG.

XI. References

[1] P.O.12.3, "Requisitos de respuesta frenta a huecos de tension de las instalaciones de produccion de regimen especial", Royal Decree 436/2004, Red Electrica de Espana, July 2004, Grid Code Requirements for Voltage Dips in Spain.

[2] I. Erlich, U. Bachmann, "Grid Code requirements concerning Connection and Operation of Wind Turbines in Germany". IEEE Power Engineering Society General Meeting, 12-16 June 2005; 1253-1257 Vol.2.

[3] Liwei Wang, Sina Chiniforoosh, and Juri Jatskevich, "Simulation and Analysis of Starting Transients in Rotor-Chopper-Controlled Doubly-Fed Induction Motors" 2008 IEEE Electrical Power & Energy Conference.

[4] Applied Protective Relaying 1979 by Westinghouse Electric Corporation, 2nd Printing, "Appendix II, Electrical Power System Device Numbers and Functions" as adopted by IEEE standard and incorporated in American Standard C37.2-1970 and -2008.

[5] E.O Schweitzer III and Daqing hou, "Filtering for Protective Relay", 19th Annual Westerm Protective Relay Conference, Spokane, Washington, October 20-22, 1992.

[6] Johan Morren, Sjoerd W. H. de Hann, "Short-Circuit Current of Wind Turbines With Doubly Fed Induction Generator", IEEE Transactions on Energy conversion, Vol. 22, No. 1, March 2007.

[7] Morren J, de Haan SWH. "Ridethrough of Wind Turbines With Doubly-fed Induction Generator during a Voltage Dip". IEEE Transactions on Energy Conversion 2005; 20: 435–441.

[8] Ling Peng; Yongdong Li; Francois, B. "Dynamic behavior of doubly fed induction generator wind turbines under three-phase voltage dips". Power Electronics and Motion Control Conference, 2009. IPEMC '09. IEEE 6th International 17-20 May 2009 Page(s):620 - 626

[9] Conroy, J.F.; Watson, R. "Low-voltage ride-through of a full converter wind turbine with permanent magnet generator; Renewable Power Generation, IET Volume 1, Issue 3, September 2007 Page(s):182 - 189

[10] I.Boldea and S.A. Nasar: "Electric Machine Dynamics". Mac Millan Publishing Company. (July 1986), ISBN-10: 0029480302

[11] W.A. Elmore, C.A. Kramer, and S.e. Zocholl, "Effects of Waveform distorsion on Protective Relays". IEEE Transactions on Industrial Applications, Vol.29, No.2, March/April 1993, pp. 404-411.

A.4

"Active current control in wind power plants during grid faults"
Jorge Martínez, Philip C. Kjær, Pedro Rodriguez, Remus Teodorescu.

WIND ENERGY
Wind Energ. (2010)
Published online. DOI: 10.1002/we.394

RESEARCH ARTICLE

Active current control in wind power plants during grid faults

Jorge Martínez[1], Philip C. Kjær[1], Pedro Rodriguez[2] and Remus Teodorescu[2]

[1] Vestas Wind Systems R&D, Power System Analysis Global Research, Arhus N, Denmark
[2] Ålborg University, Denmark

ABSTRACT

Modern wind power plants are required and designed to ride through faults in electrical networks, subject to fault clearing. Wind turbine fault current contribution is required from most countries with a high amount of wind power penetration. In order to comply with such grid code requirements, wind turbines usually have solutions that enable the turbines to control the generation of reactive power during faults. This paper addresses the importance of using an optimal injection of active current during faults in order to fulfil these grid codes. This is of relevant importance for severe faults, causing low voltages at the point of common coupling. As a consequence, a new wind turbine current controller for operation during faults is proposed. It is shown that to achieve the maximum transfer of reactive current at the point of common coupling, a strategy for optimal setting of the active current is needed. Copyright © 2010 John Wiley & Sons, Ltd.

KEYWORDS

wind turbine generator; faults; doubly fed induction generator; short-circuit currents; low-voltage ride through; grid code

Correspondence

J. Martínez, Vestas Wind Systems R&D, Power System Analysis Global Research, Arhus N, Denmark.
Email: jomga@vestas.com

Received 19 September 2009; Revised 8 December 2009; Accepted 31 January 2010

NOMENCLATURE

j	complex number
G	generator
X, R	reactance and resistance
P, Q, S	active, reactive and apparent power
T	torque
V, I	voltage, current
d, q	direct and quadrature
ref.	reference
mech.	mechanical
elec.	electrical

ABBREVIATIONS

AC	alternate current
DC	direct current
DT	distribution transformer
DFIG	doubly fed induction generator
LV	low voltage
LVRT	low-voltage ride through
OVL	overhead line
PCC	point of common coupling
RC	rotor converter
rms	root mean square
SCR	short-circuit ratio
VT	voltage transformer
WPP	wind power plant
WTG	wind turbine generator

1. INTRODUCTION

With increasing penetration of wind power generation[1], the requirements for the connection of wind power plants (WPPs) to the electrical grid are defined by new and emerging grid connection codes. The grid connection requirements vary in different parts of the world, but they have a common aim: to permit the development, maintenance and operation of a coordinated, reliable and economical transmission or distribution system. The new requirements generally demand that WPPs provide ancillary services to support the network in which they are connected.[2,3]

The method used some years ago, disconnection of wind power generation after a network fault or having a great amount of reactive power consumption during faults and post-faults, due to remagnetization of the generator, is no longer acceptable for grid operators, e.g. EON or REE from Germany and Spain, respectively. The reasons for these requirements are mainly two: possibility of voltage collapse in the recovery time after the fault, due to high reactive power consumption, and loss of synchronism if there is a massive wind power disconnection.

During grid faults, there is an imbalance between mechanical power absorbed by the wind turbine and electrical power injected into the grid. This imbalance in power is transformed into rotational speed increase.

Currently, most wind turbine generators (WTGs) can reduce very fast the mechanical power absorbed by the wind turbine by means of changing the angle of the blades; therefore, disconnection due to overspeed problems are not present anymore. During faults, the doubly fed induction generator (DFIG) will use the converter attached to the rotor to overmagnetize the generator, and thus injecting reactive current into the electrical network, as the grid codes ask for.

2. MAXIMUM REACTIVE CURRENT INJECTION AT POINT OF COMMON COUPLING

Most WPPs are connected through overhead lines (OVLs) to distribution or transmission systems, having a similar scheme to the one represented in Figure 1. For the sake of simplicity, an aggregated WTG is used to represent the whole WPP. Usually the point of common coupling (PCC) is located in bus number 5 or 4.

When a fault is located close to bus number 6 or 5, the system can be represented and simplified as is shown in Figure 2. In the figure, $\vec{Z}$ is the impedance from the WTG terminals to the PCC (equivalent impedance from bus number 1 to 5 in Figure 1), $\vec{Z}_F$ is the impedance to the fault from the PCC bus, and $\vec{Z}_G$ is the equivalent impedance of the grid at the PCC.

The following equations are extracted using the system represented in Figure 2:

$$\vec{V}_{PCC} = K_G\vec{V}_G + K_{wf}\vec{V}_{WTG} \tag{1}$$

$$\vec{V}_{WTG} = E_S(\cos(\alpha) + \sin(\alpha)\,j) \tag{2}$$

$$\vec{V}_G = v_G \tag{3}$$

where α is the angle between vectors $\vec{V}_{PCC}$ and $\vec{V}_{WTG}$.

Supposing that the impedances $\vec{Z}$, $\vec{Z}_F$ and $\vec{Z}_G$ have the same angle, then

$$\vec{Z}_F = K_2\vec{Z}_G \tag{4}$$

$$\vec{Z} = K_1\vec{Z}_G \tag{5}$$

$$\vec{Z} = R + Xj \tag{6}$$

$$K_G = \frac{\vec{Z}_F\vec{Z}}{\vec{Z}_G\vec{Z} + \vec{Z}_F\vec{Z} + \vec{Z}_G\vec{Z}_F} = \frac{K_2K_1}{K_1 + K_1K_2 + K_2} \tag{7}$$

$$K_{wf} = \frac{\vec{Z}_F\vec{Z}_G}{\vec{Z}_G\vec{Z} + \vec{Z}_F\vec{Z} + \vec{Z}_G\vec{Z}_F} = \frac{K_2}{K_1 + K_1K_2 + K_2} \tag{8}$$

where the parameter K_1 is related to the short-circuit ratio (SCR) between the WPP and the grid, and the parameter K_2 is related to the distance of the fault to the PCC or basically the remaining voltage at the PCC.

I_q and I_d are the quadrature current and direct current (DC) with respect to the voltage vector at the point where they are measured, and they are calculated following IEC 61400-21.[4]

In order to calculate the I_q value at the PCC (I_{q_PCC}), the next equations are used:

$$\vec{S}_{PCC} = P_{PCC} + Q_{PCC}\,j = \vec{V}_{PCC}\vec{I}_S^{\,*} = \vec{V}_{PCC}\left[\frac{\vec{V}_{WTG} - \vec{V}_{PCC}}{\vec{Z}}\right]^* \tag{9}$$

$$I_{d\_PCC} = \frac{P_{PCC}}{|\vec{V}_{PCC}|} \tag{10}$$

$$I_{q\_PCC} = \frac{Q_{PCC}}{|\vec{V}_{PCC}|} \tag{11}$$

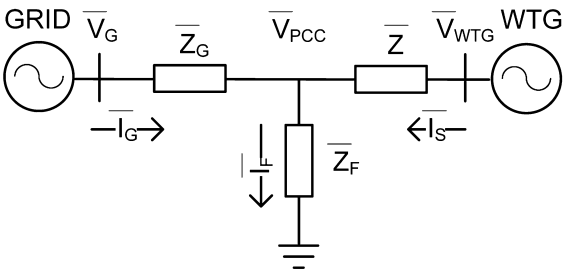

Figure 2. Simplified system diagram.

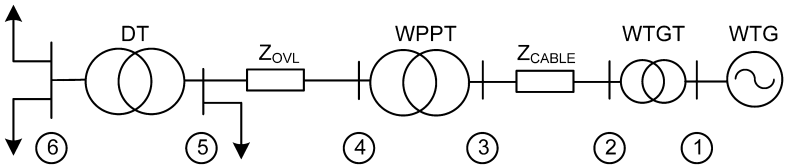

Figure 1. Simplified connection diagram of a WPP.

The amplitude of the WTG terminal voltage can be calculated using equation (12), where I_{q_WTG} is the I_q measured at the WTG terminals:

$$E_S = \frac{I_{q\_WTG}Z^2 + v_G K_G (R\sin(\alpha) + X\cos(\alpha))}{X(1-K_{wf})} \quad (12)$$

For calculating the maximum injection of the reactive current at the PCC, equation (20) is used, which is derived form the previous equations, obtaining thus the optimal current injection angle (α_{opt}):

$$\alpha_{opt} = \arctan\left(\frac{R}{X(2K_{wf}-1)}\right) \quad (13)$$

Using the optimal angle [equation (13)], the I_d that has to be injected at the WTG terminals (I_{d_WTG}) is obtained:

$$I_{d\_\mathrm{WTG}} = \frac{R}{X}\left(I_{q\_\mathrm{WTG}} \pm \frac{v_G K_G}{\sqrt{Z^2 + 4X^2(K_{wf}^2 - K_{wf})}}\right) \quad (14)$$

Equation (14) has two solutions. The second term in the equation will be negative when $2K_{wf} < 1$, and this is our case since K_{wf} is almost proportional to the remaining voltage at the PCC, and since this control will be used for voltages below 0.5 pu, $2K_{wf}$ will be always below 1.

2.1. Practical example

In this practical example, the diagram depicted in Figure 2 and the data $X = 0.25$ pu, $X/R = 6.5$, $K_1 = 15$ and $K_2 = 0.1$ are used.

The following case is presented to highlight the differences in the reactive current injected at the PCC when using this new control strategy.

In Figure 3, two curves can be seen, representing the I_q injected by the WTG as a function of the I_q measured at the PCC. The curve 'I_{q_PCC}' is obtained when the WTG is injecting a I_d that follows a constant ratio value; $I_{d\_WTG} = I_{q\_WTG}\cos(70°)$. The other curve, '$I_{q\_PCC\_opt}$', is calculated when using equation (14) in obtaining the I_d injection; $I_{d\_WTG} = I_{d\_WTG\_opt}$.

The vertical axis of the graph is the reactive current injected by the wind turbine, and the horizontal one is the resulting reactive current measured at the PCC.

When using equation (14) for the I_d calculation, it can be seen that the reactive current value at the PCC is maximized for any reactive current generated by the wind turbine.

In Figure 4 is depicted the injected I_d by the WTG as a function of the injected I_q by the WTG. In one case, the injected I_d is following a constant ratio; $I_{d\_WTG} = I_{q\_WTG}\cos(70°)$, curve '$I_{d\_WTG}$' and the other curve, '$I_{d\_WTG\_opt}$', are calculated using equation (14).

2.2. Influence of the grid parameters on I_{q_PCC} injection

The diagram in Figure 2 has been used in studying I_{q_PCC} when varying the different parameters of the system.

- In Figure 5, the parameter K_2 is varied, and $X/R = 6.5$, $X = 0.25$, $K_1 = 10$ and $I_{d\_WTG} = I_{q\_WTG}\cos(70°)$ are kept constants.
- In Figure 6, the parameter K_1 is varied, and $X/R = 6.5$, $X = 0.25$, $K_2 = 0.1$ and $I_{d\_WTG} = I_{q\_WTG}\cos(70°)$ are kept constants.

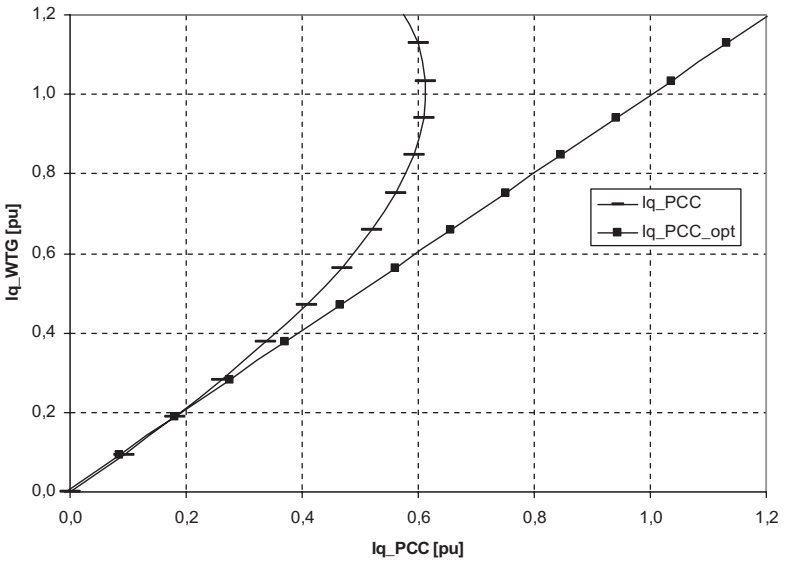

Figure 3. I_q at PCC for optimal and non-optimal I_d controls.

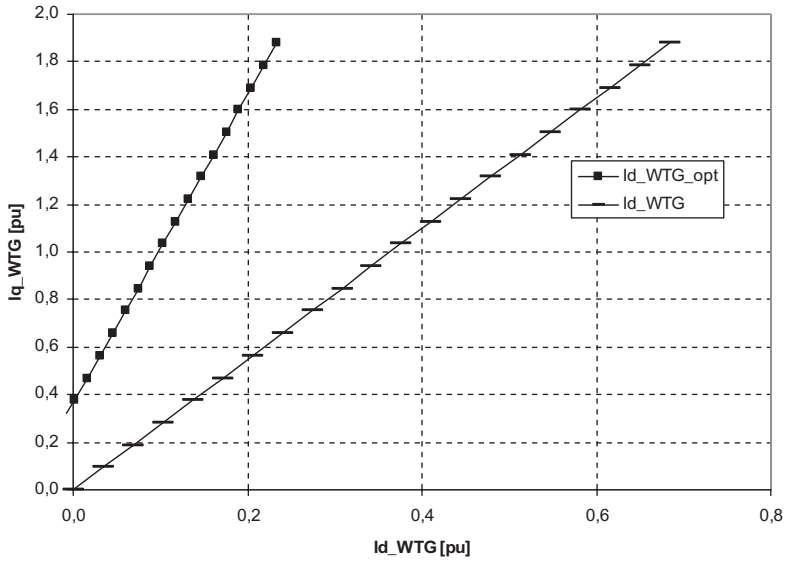

Figure 4. I_d at the WTG using optimal and non-optimal I_d controls.

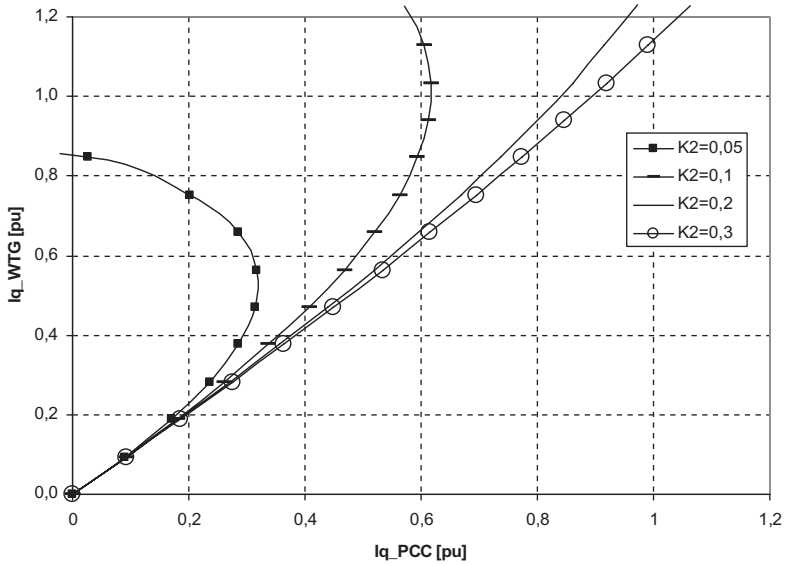

Figure 5. I_q at the PCC for different K_2 values.

- In Figure 7, the parameter X is varied, and $X/R = 6.5$, $X = 0.25$, $K_2 = 0.1$, $K_1 = 10$ and $I_{d\_WTG} = I_{q\_WTG} \cos(70°)$ are kept constants.
- In Figure 8, the parameter X/R is varied, and $X = 0.25$, $K_2 = 0.1$, $K_1 = 10$ and $I_{d\_WTG} = I_{q\_WTG} \cos(70°)$ are kept constants.

As a conclusion of the previous graphs, it is possible to say that the parameters that influence the most the I_q measured at the PCC are the total impedance to the PCC, the remaining voltage at the PCC and the X/R ratio of the total impedance to the PCC.

Higher impedance values from the WTG to the PCC and lower voltages at the PCC make necessary a strategy for the I_d injection at the WTG terminals in order to achieve higher I_q levels at the PCC.

3. STUDIED CASE

Data of a real WPP have were used to analyze the performance of the DFIG during three-phase faults with the new control scheme. Simulations in the PSCAD program were carried out to show the relevance of the

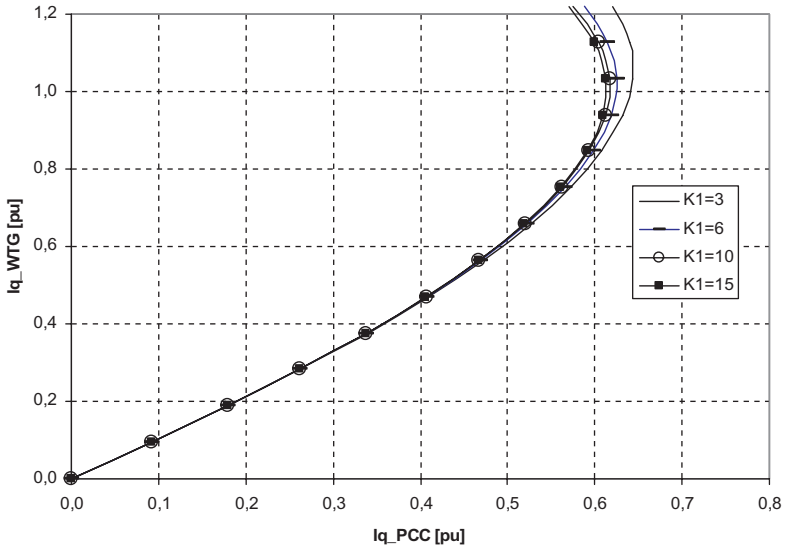

Figure 6. I_q at the PCC for different K_1 values.

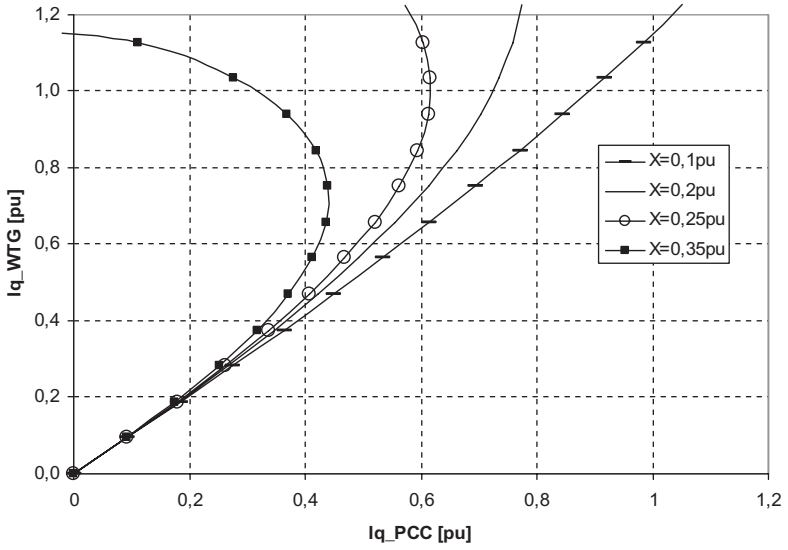

Figure 7. I_q at the PCC for different X values.

I_{d_WTG} injection in order to fulfil the grid codes when asking for a high amount of reactive current at the PCC during low-voltage (LV) events.

The studied case was formed by a WPP of 25 DFIGs connected through a cable collector system to the main substation transformer, which is connected with an OVL to the PCC.

The DFIGs were modelled as an aggregated single WTG, as can be seen in Figure 9. The collector system of the WPP consisted of four radial underground feeders with up to seven or six WTGs on a single feeder. The four feeders were collected at the 22 kV substation and fed into a 55 MVA, 132/22 kV transformer. The cables and the OVL were modelled using an equivalent section. The grid was modelled as an ideal voltage source in series with an equivalent impedance, which represents the SCR of the grid. The impedance to the fault (Z_{fault}) was calculated accordingly to produce the desired voltage level at the PCC.

The whole setup of the case can be seen in Figure 9, where three-phase faults were applied at the PCC in order to check the performance against the low-voltage ride through (LVRT) grid code requirements using the new and the existing control for I_{d_WTG}.

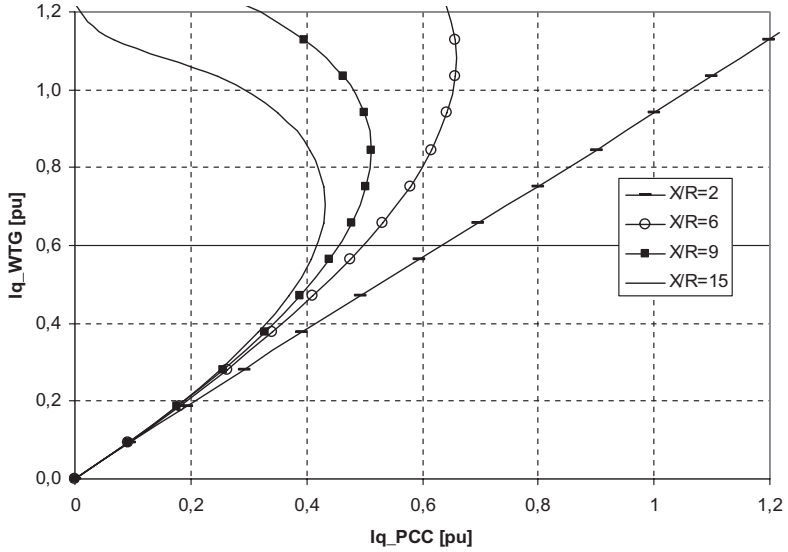

Figure 8. I_q at the PCC for different X/R values.

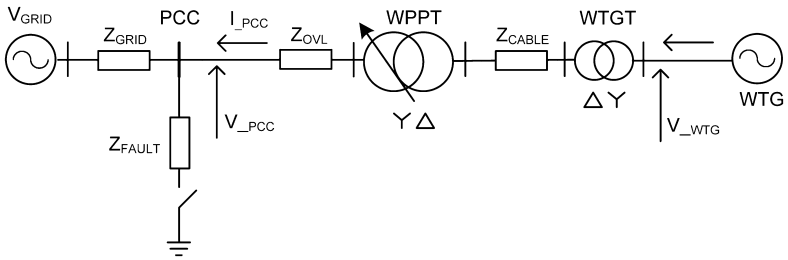

Figure 9. Diagram of the simulated case.

Table I. Data of the WPP components.

	X (%)	X/R
Z_{GRID}	9.8	6
Z_{OVL}	1.2	3.3
WPPT	10.9	24
Z_{CABLE}	1.4	1.1
WTGT	7.6	9.8

The impedance and X/R ratio of every component in Figure 9 are depicted in Table I.

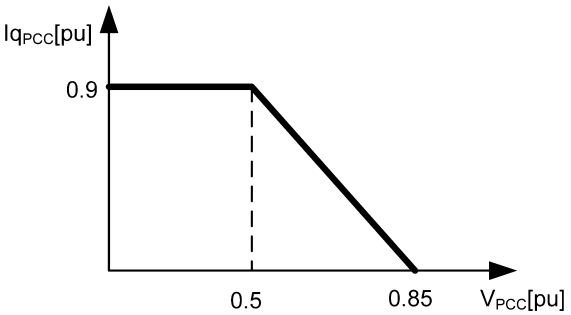

Figure 10. Requirement for the injected reactive current as a function of the voltage at the PCC.

3.1. Grid code requirements for LVRT

The grid code P.O. 12.3 of REE[5] covers the requirements for WPPs to ensure the right operation of the system during faults and LV events.

The PCC is defined as the point of connection to the transport or distribution grid where the energy is evacuated.

The requirement says that during faults and post-faults (voltage recovery periods), the WPPs should remain connected to the grid. Besides, during faults, the WPP installation should contribute to the system with the maximum reactive current possible for every voltage level, as is depicted in Figure 10. No active current consumption is allowed, except during the first 150 ms of the fault and post-fault times.

3.2. DFIG technology

The variable speed doubly fed generator (see Figure 11) allows full control of the generator active and reactive powers using the rotor-connected frequency converter. Its rating is in the order of 0.3 pu. Operating both in the sub- and the super-synchronous speed, the power can be fed in and out of the rotor circuit. The rotor-connected circuit can employ various power dissipation means during fault periods, sometimes referred to as active crowbar when it is located in the rotor terminals or chopper when it is located in the DC link bus bar (R_{ch} in Figure 11).[6,7]

In the DFIG, the converter connected to the rotor is controlled during short circuits in a manner that makes I_q current injection following grid code requirements and I_d injection following the active power reference (P_{ref}) from the power controller, which is the control that allows maximum power tracking for every wind speed and, together with the pitch system, ensures that the generator rotational speed is between limits.

If the maximum current level of the converter is reached during fault periods and since I_q has priority to fulfil grid codes, I_d will fill the gap between I_q and the rated converter current.

The grid connected converter (GC in Figure 11) is used for DC link bus bar voltage control since getting the voltage level of the DC link between margins will avoid disconnection of the WTG.[8]

3.3. Control implementation in the WTG

The proposed changes in the WTG controller allow maximum I_q injection at the PCC by means of the estimated impedance from generator terminals to the PCC and the voltage fault level at the PCC.

Since I_d is related to the active power injected by the WTG, any change in the original I_d control has to take into account the impact into the mechanical WTG system. However, since this new control will be applied for faults causing very LV levels at generator terminals, it is expected that there will be almost no active power flowing into the grid; therefore, the affection to the mechanical system, compared with the previous control, will be almost the same.

Using the assumptions $v_G = 1$, $K_G \approx V_{PCC}$ and $K_{wf} << Z$, equation (14) can be simplified in order to achieve a simpler implementation in the WTG controller; thus, equation (15) is obtained.

$$I_{d\_WTG} \approx \frac{R}{X}\left(I_{q\_WTG} - \frac{V_{PCC}}{Z}\right) \tag{15}$$

The impedance Z, from generator terminals to the PCC, could be estimated in different ways. Since this controller is going to be used for low voltages at the PCC, the error in the Z value was mitigated compared with the term I_{q_WTG}.

In this control implementation, the data available for the project were used to calculate the theoretic Z value. Some deviance, with the real Z, was expected due to the tolerances in the data and different loading temperatures, but as it was mentioned before, the affection to the total I_{d_WTG} was negligible.

Simulations can be seen in Figure 20, in Section 4.2, where an error of ±10% is introduced in the Z and X/R terms.

The voltage at the PCC (V_{PCC}) will be calculated using the minimum root mean square (rms) value measured at the LV side of the WTG during the event.

Using equation (15) for calculating the I_d rotor current reference, I_{d_ref}, the I_{q_ref} that is possible to inject for different grid conditions [equation (16)] can be calculated without exceeding the rated current I_s of the rotor converter (RC):

$$I_s^2 = I_{q\_ref}^2 + I_{d\_ref}^2 \tag{16}$$

$$I_{q\_ref} = \frac{R^2 V_{PCC} \pm \sqrt{I_s^2 Z^2 (X^4 + R^2 X^2) - X^2 R^2 V_{PCC}}}{Z^3} \tag{17}$$

A positive sign is used for the second term in equation (17) in order to get the maximum I_q injection.

Figure 12 shows an example of I_{d_ref} and I_{q_ref} obtained for different voltage levels at the PCC and different inductances (X) when using $I_s = 1$ pu and $X/R = 6.5$.

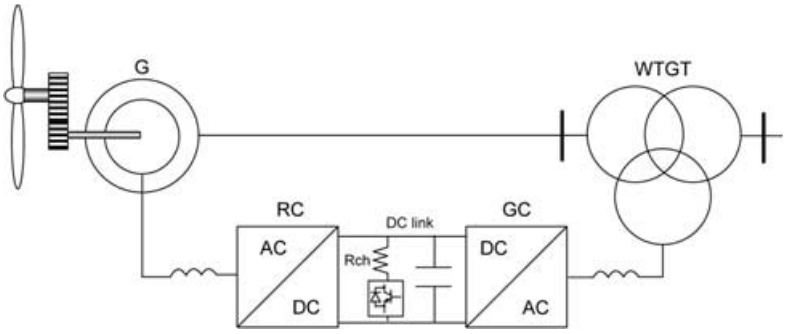

Figure 11. DFIG, variable speed doubly fed generator diagram.

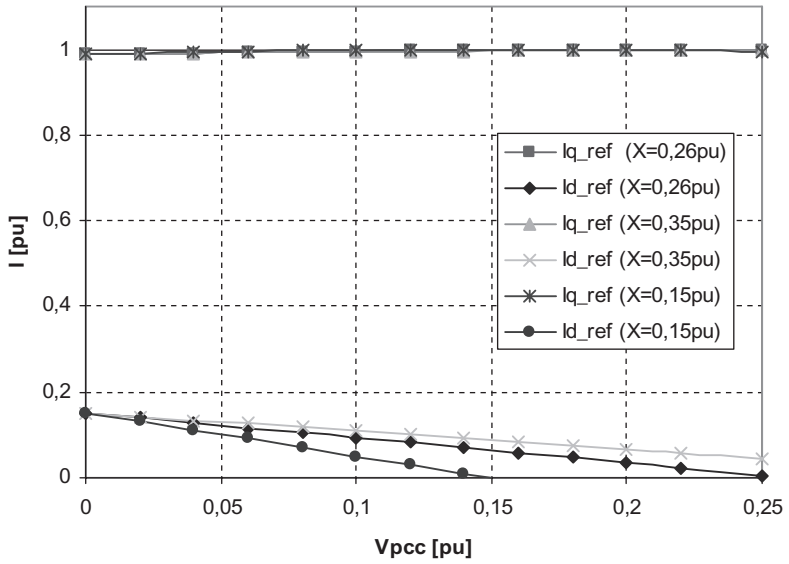

Figure 12. Current references *d-q* using the proposed controller.

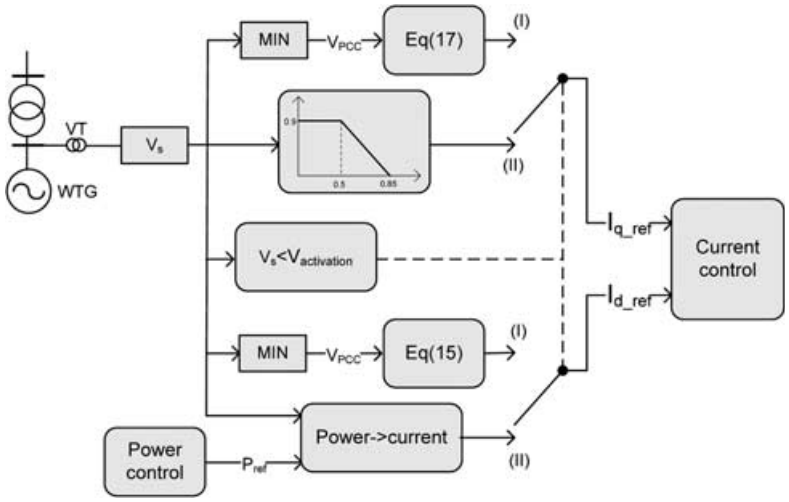

Figure 13. Diagram of the proposed controller.

A simplified diagram of the proposed controller implemented in the WTG is depicted in Figure 13.

The voltage measured at the LV side of the WTG was processed for rms calculation in the block called 'V_S'. Afterwards, this voltage was used for calculation depending on whether the optimal I_d control is going to be activated (position I) or not (position II).

In the present case, 0.2 pu was used as the triggering level.

I. If V_s was below 0.2 pu, then the references for I_q and I_d were calculated using equations (15) and (17), and the V_{PCC} used in these equations was calculated in the block called 'MIN', where the minimum rms voltage was detected during the event.

II. If V_s was above 0.2 pu, then the reference for I_q was calculated according Figure 11, and the reference for I_d was calculated following the power controller reference (P_{ref}). This power reference was translated into a current reference in the block 'Power → current'.

4. SIMULATION CASES

The simulation test setup can be seen in Figure 9. In the simulations, three-phase faults at the PCC, of 0.5 s duration, were applied at a time equal to 8 s. The faults

simulated will cause the voltage at the PCC to decrease to 10% of the rated value.

The fault was applied for two different control cases: control that uses the I_d reference calculated by the P_{ref} (case A: present control performance) and control based on the diagram in Figure 13 (case B: proposed control performance).

The currents and voltages at the PCC and at the WTG generator terminals were plotted in order that a clear comparison of the performance can be done.

Mechanical and electrical torques were plotted as well for both cases in order to make it possible to check the assumption of low impact in the electrical torque when using the new control compared with the original control scheme.

For case B, as it was explained in Section 4.3, the impedance value Z and X/R were introduced off-line since these data are known from the project of the WPP. In order to check the influence of possible deviances in the off-line data values with the real ones, four more cases were simulated. For these cases, a value deviance of ±10% with the real ones was introduced in the WTG controller.

Positive values of I_d and I_q indicate WTG injection of active and reactive powers, respectively.

4.1. Present control performance

Results of the present control performance are shown in this section (Figures 14–16).

4.2. Proposed control performance

Results of the proposed control performance are shown in this section (Figures 17–20).

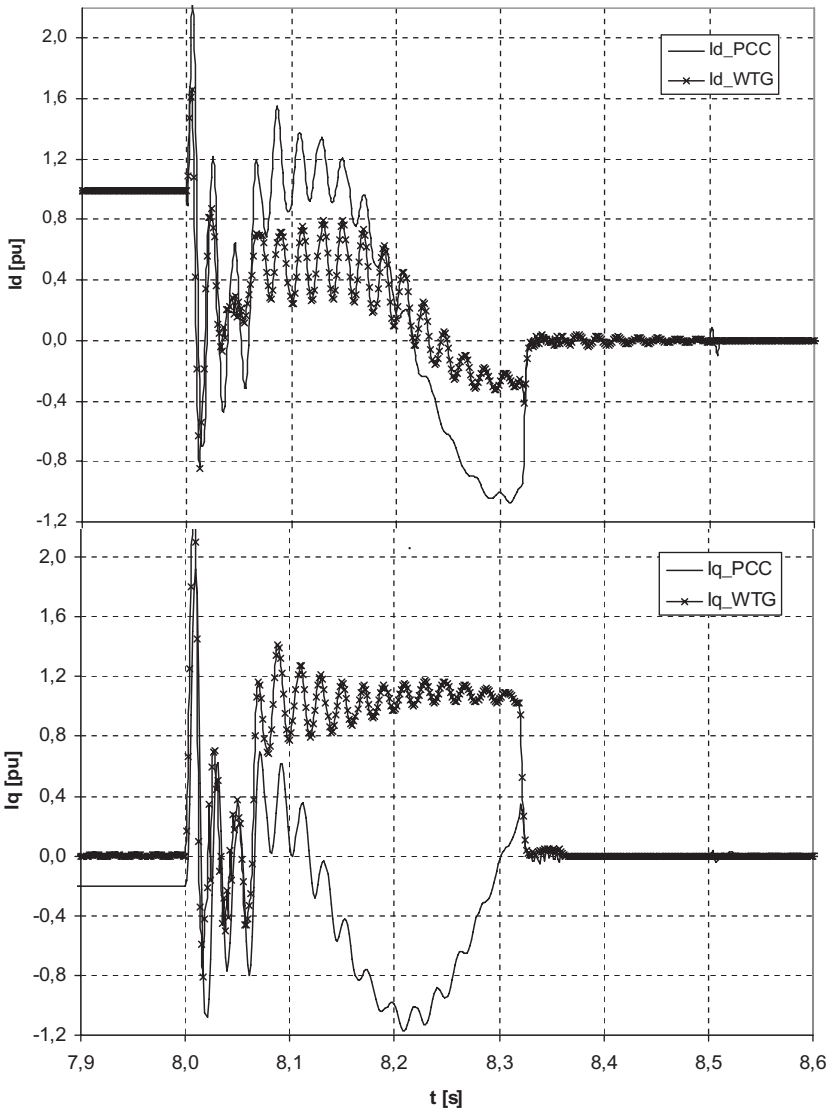

Figure 14. I_d and I_q at the WTG and PPC.

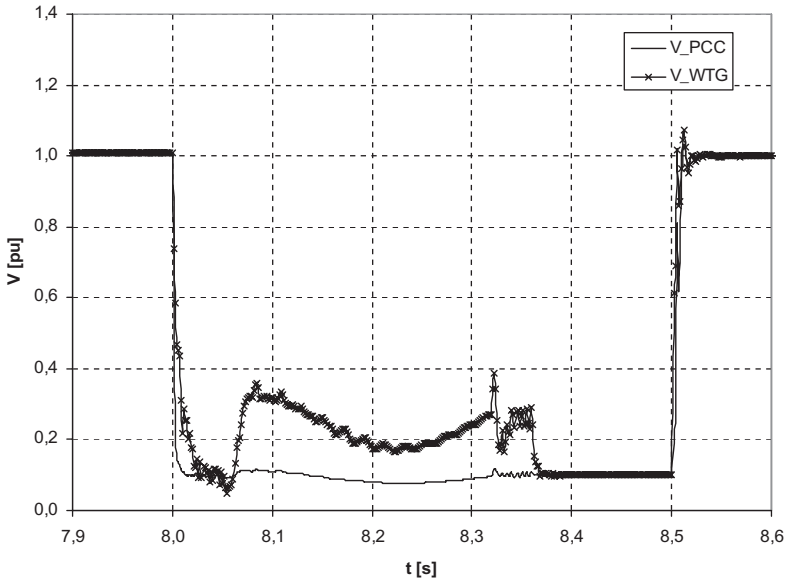

Figure 15. Voltages at the WTG and PPC.

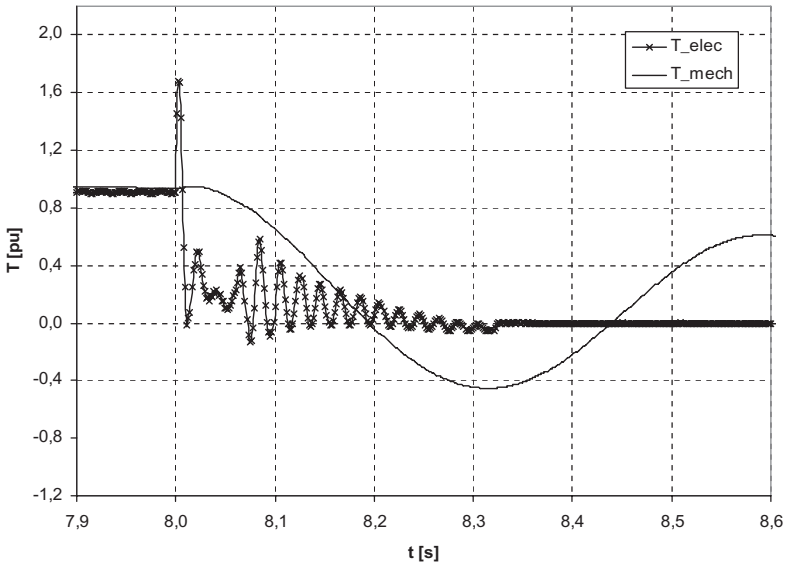

Figure 16. Mechanical and electrical WTG torques.

For this specific case, off-line data can be used since the deviance effects in the I_q injection at the PCC were acceptable.

4.3. Analysis of the results

Figure 14 shows the value of the active and reactive currents at the PCC and WTG without the new current control, and Figure 17 shows the value of the active and reactive currents at the PCC and WTG with the proposed current control.

With this new current control can be seen (Figure 17) how the injected I_q by the WTG was maximized at the PCC, and therefore the fulfilment of the grid codes regarding LVRT is possible.

In Figures 16 and 19 can be compared how the resulting torque with the new controller was very similar to the one achieved by the old one, and thus not stressing, more than previously, the mechanical system.

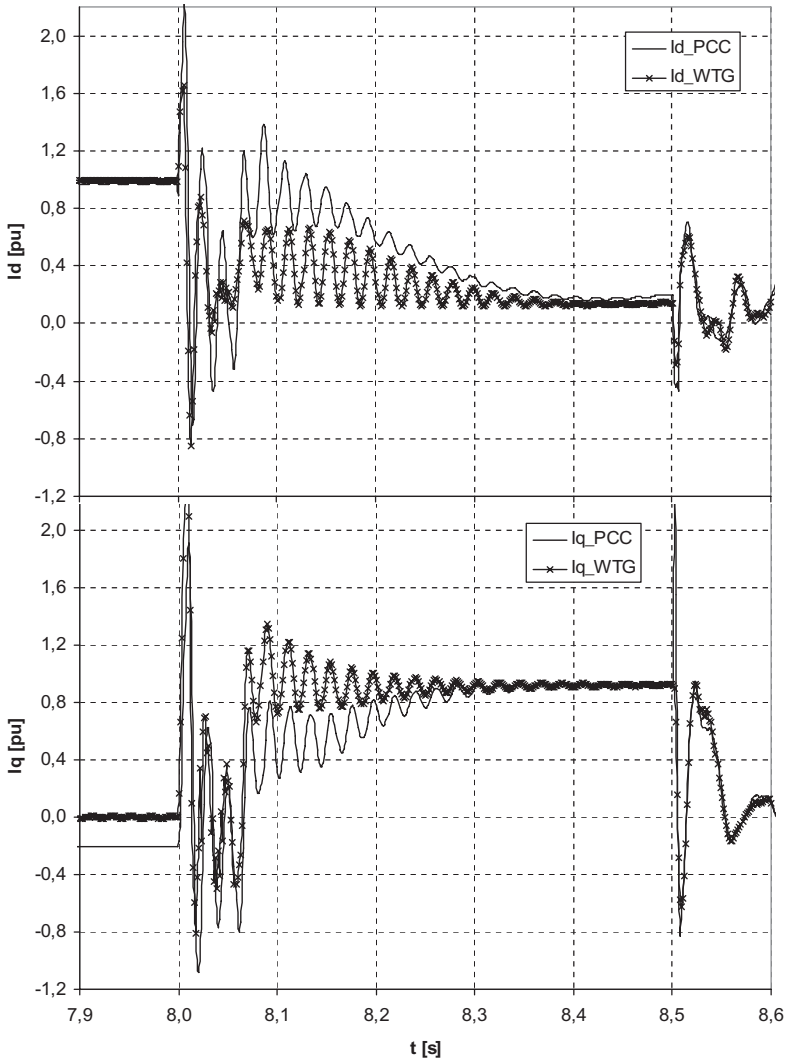

Figure 17. I_d and I_q at the WTG and PPC.

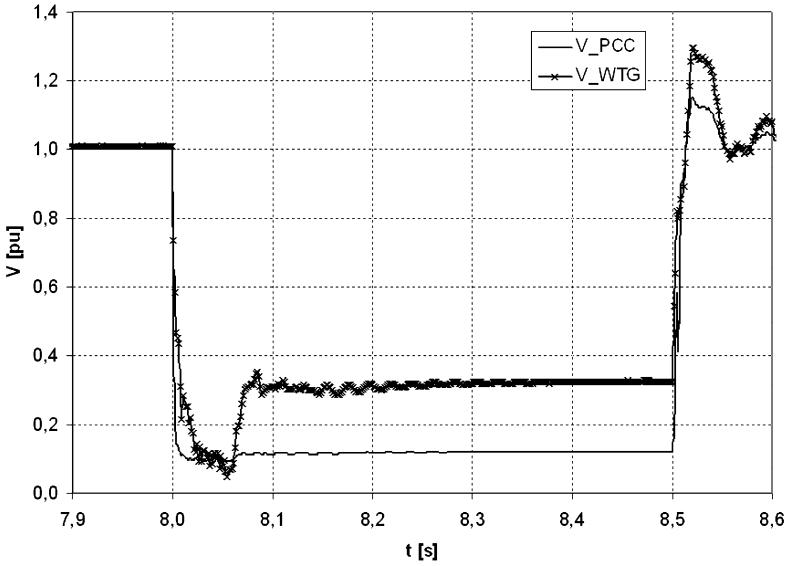

Figure 18. Voltages at the WTG and PPC.

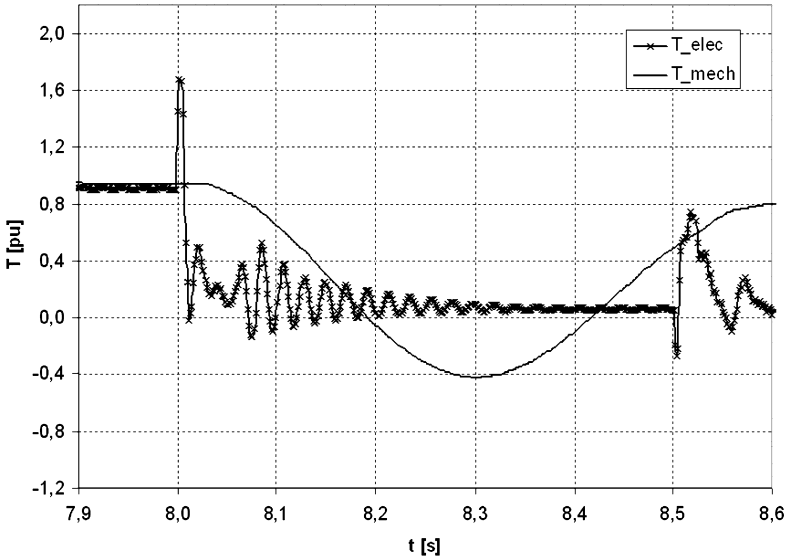

Figure 19. Mechanical and electrical WTG torques.

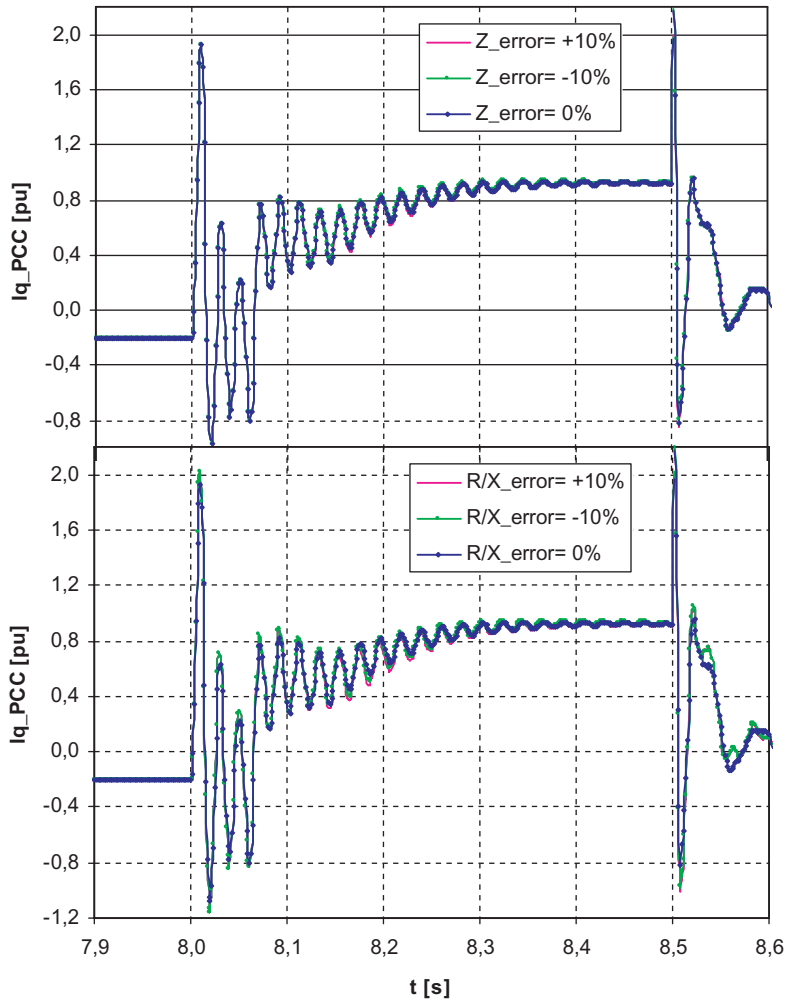

Figure 20. I_q and I_q at the PCC for different errors of the Z value introduced in the control.

5. CONCLUSIONS

The I_q measured at the PCC for grid conditions with high impedance levels from generator terminals to the PCC and during LV events will be influenced drastically by the I_d injected by the WTG. Therefore, to keep control of the I_q at the PCC, a new WTG control strategy was defined for LV events, thus reaching high levels of I_q injection at the PCC, as most of the grid codes are asking for.

The control implementation for calculating the current references can be simplified neglecting the coefficients that include the impedance data of the grid and the fault, making possible the use of an off-line data *Z*, based on the available project data.

In conclusion, attention should be drawn to the importance of the particular ratio between *d* and *q* injected current during short circuits to fulfil the grid code requirements related to LVRT.

APPENDIX

$$I_{d\_PCC} = -\frac{\begin{array}{c}-v_G K_G E_S (X\sin(\alpha) + R\cos(\alpha)) + \\ 2v_G K_G R E_S K_{wf}\cos(\alpha) + v_G^2 K_G^2 R + E_S^2 K_{wf} R (K_{wf} - 1)\end{array}}{Z^2\sqrt{v_G^2 K_G^2 + 2v_G K_G K_{wf} E_S\cos(\alpha) + K_{wf}^2 E_S^2}} \tag{A1}$$

$$I_{q\_PCC} = -\frac{\begin{array}{c}v_G K_G E_S (R\sin(\alpha) - X\cos(\alpha)) + \\ 2v_G K_G X E_S K_{wf}\cos(\alpha) + v_G^2 K_G^2 X + E_s^2 K_{wf} X (K_{wf} - 1)\end{array}}{Z^2\sqrt{v_G^2 K_G^2 + 2v_G K_G K_{wf} E_S\cos(\alpha) + K_{wf}^2 E_S^2}} \tag{A2}$$

REFERENCES

1. EWEA organization. Integrating wind developing Europe's power market for the large-scale integration of wind power. [Online]. Available: http://www.ewea.org/fileadmin/ewea_documents/documents/publications/reports/TradeWind_Report_01.pdf. (Accessed February 2009)
2. Erlich I, Bachmann U. Grid code requirements concerning connection and operation of wind turbines in Germany. *IEEE Power Engineering Society General Meeting*, Vol. 2, 12–16 June 2005; 1253–1257.
3. Arulampalam A, Ramtharan G, Jenkins N, Ramachandaramurthy VK, Ekanayake JB, Strbac G. Trends in wind power technology and grid code requirements. *International Conference of the Industrial and Information Systems, 2007* (*ICIIS 2007*), 9–11 August 2007; 129–134.
4. IEC 61400-21. Measurement and assessment of power quality characteristics of grid connected wind turbines, 2007.
5. P.O.12.3. Requirements during voltage dips for the installations in the group of renewable energy. Grid code requirements for voltage dips in Spain. Royal Decree 436/2004, REE, July 2004.
6. Morren J, de Haan SWH. Short-circuit current of wind turbines with doubly fed induction generator. *IEEE Transactions on Energy Conversion* 2007; **22**: 174–180.
7. Morren J, de Haan SWH. Ride through of wind turbines with doubly-fed induction generator during a voltage dip. *IEEE Transactions on Energy Conversion* 2005; **20**: 435–441.
8. Li S, Haskew TA. Analysis of decoupled d-q vector control in DFIG back-to-back PWM converter. *Power Engineering Society General Meeting, 2007*. IEEE publication date: 24–28 June 2007; 1–7.

A.5

"Parameterization of a synchronous generator to represent a doubly fed induction generator with chopper protection for fault studies"

Jorge Martínez, Philip C. Kjær, Pedro Rodriguez, Remus Teodorescu.

WIND ENERGY
Wind Energ. (2010)
Published online. DOI: 10.1002/we.406

RESEARCH ARTICLE

Parameterization of a synchronous generator to represent a doubly fed induction generator with chopper protection for fault studies

Jorge Martínez,[1] Philip C. Kjær,[1] Pedro Rodriguez[2,3] and Remus Teodorescu[2]

[1] VESTAS Wind System, Power Plant R&D, Denmark
[2] Aalborg University, Institute of Energy Technology, Denmark
[3] Technical University of Catalonia, Electrical Engineering, Spain

ABSTRACT

This paper addresses the representation of the wound rotor asynchronous generators by an equivalent synchronous generator, valid for short circuit current calculations.

Modern wind power plants are required and designed to ride through faults in the network, subjected to fault clearing. Accurate knowledge of the wind turbine short circuit current contribution is needed for component sizing and protection relay settings during faults within the wind power plant collector system or in the external networks.

When studying fault currents and protection settings for wind power installations, the industry standard is to employ software packages where generators are represented by their equivalent synchronous generator operational impedances. Hence, it is of importance to represent non-synchronous wind generators by an equivalent synchronous generator.

KEYWORDS

Wind turbine generator; operational impedances; simulation; doubly fed induction generator; short circuit currents; synchronous generator

Correspondence

Jorge Martínez, Vestas Wind Systems R&D, Power System Analysis Global Research, Arhus, Denmark.
E-mail: jomga@ vestas.com

Received 28 September 2009; Revised 26 February 2010; Accepted 04 April 2010

NOMENCLATURE

AC	alternate current
DC	direct current
DFIG	doubly fed induction generator
EMT	electromagnetic transient
f	frequency
GC	grid converter
IG	induction generator
IGR	induction generator with rotor resistances
IGBT	insulated gate bipolar transistor
L, R, C	inductance, resistance, and capacitance
RC	rotor converter
s	laplace term
SG	synchronous generator
SCR	short circuit ratio
T_0,T_s,T'	open, stator, and rotor circuit time constants
T,G	transformer and generator
V, I	voltage, current

X''	subtransient reactance
X'	transient reactance
X	reactance
WTG	wind turbine generator
λ	flux
ω	speed

SUBSCRIPTS

r, s, m	rotor, stator and mutual
f	field
σ	leakage
ch	chopper
d, q	direct and quadrature

1. INTRODUCTION

DFIG technology is widely used in the wind industry. The variable speed and the reduced size of the power converters, normally 25% of the generator power but high controllability, offer a very competitive market solution.

Since wind power is growing drastically, reaching high percentages of penetration into the power system becomes necessary to have a representation of the DFIG technology in standard simulation programs. When simulating the DFIG, especially during faults, the most prudent method would be to use EMT simulation programs, employing a simulation model of the complete wound rotor asynchronous machine, based on the equivalent circuit diagram depicted in Figure 1. This can be done if the parameters and control circuitry are available, but it is not always possible to get this detailed data. Whenever this is the case, an EMT program employing a simulation model of the SG, with its parameters fitted to match the DFIG under specified fault conditions, can be used. If a static short circuit calculation program is used, e.g., ASPEN, ETAP or SKM, then the SG parameters can be entered. However, different SG parameters may be required for different fault studies.

Whereas the short circuit contribution from SGs can be calculated on the basis of the machine parameters alone, the wound rotor asynchronous generators vary their rotor circuits during faults and this has to be taken into account.

In the DFIG, the converter connected to the rotor is controlled during short circuits in a manner that makes these generators perform rather differently than SGs and their excitations normally do. In essence, the active rotor circuit depletes the generator magnetization much faster than SG excitation can do. This causes the DFIG stator short circuit current contribution to exhibit a very low AC component. This excitation control, being non-linear, increases the complexity of making the translation into operational impedances.

For severe faults, the rotor converter stops switching; the converter enters in blocking state to protect itself against high currents, losing the controllability of the rotor excitation. During this period, it is expected to have uncontrolled power going into the DC-link, causing the increase of the DC-link voltage. As a consequence, the protective action of the chopper during these events is needed.

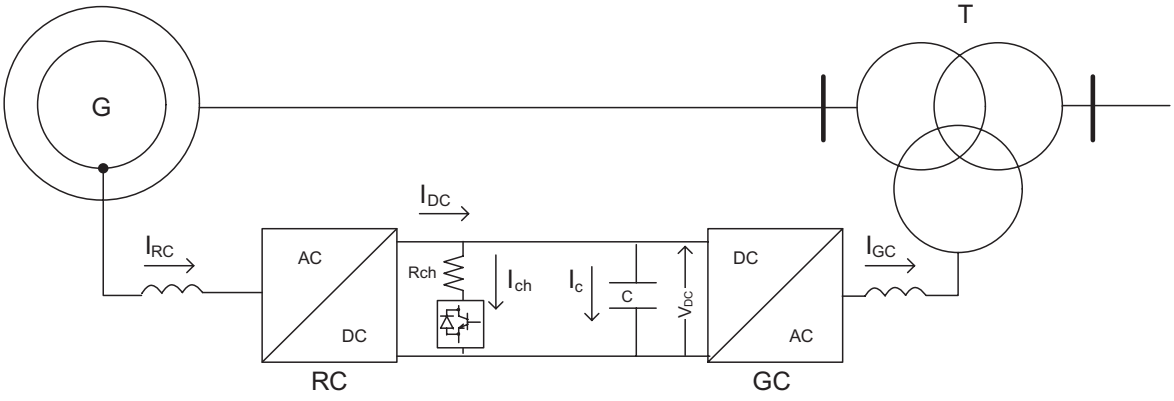

Figure 1. DFIG electrical single line diagram.

The DFIG with chopper protection dissipates significant power on the rotor side during faults, therefore, shortens the decay times and reduced peak currents are expected than for squirrel cage induction generators and synchronous generators.

2. DFIG BEHAVIOUR DURING FAULTS

In the DFIG technology, one converter, RC, is connected to the rotor of generator controlling the excitation of the generator and is connected via DC-link to another converter, GC, which controls the voltage level of this DC-link.[1] Usually, as a protective regulation unit, a chopper R_{ch}, is installed in the DC-link. See Figure 1.

During grid fault periods and depending on the short circuit current level, the converters could enter into blocking state, meaning that they would stop the switching of the IGBTs. When the fault current level is under some pre-set threshold level, the converters resume the switching, enabling the generator to supply a predefined value of reactive current according to the remaining stator voltage. Normally, this reactive current level is specified by the local grid codes.[2] If the fault location is sufficiently remote from the generator terminals, the converters will not be blocked, controlling the currents in every instant and, therefore, not presenting almost any current transient phenomena.

2.1. Slip influence in the short circuit currents

In this section, the slip influence in the short circuit currents is evaluated. DFIG machines have variable speed. The rotational speed range of the generators varies depending on the wind turbine manufacturer, but it is mainly in the range of ±15% of the synchronous speed.

One of the main differences between the SG and the DFIG is the variable rotational speed range, allowed by the operation of the rotor converter.

In order to check the slip influence in the short circuit current peak value, the space vector equations (1) and (2) are used, which are obtained from Figure 2.[1–3]

Figure 2 shows in synchronous reference frame the steady state representation of DFIG with the excitation of the rotor circuit $\underline{V_r}$. The non-saliency in the stator and rotor windings makes no difference between d-q axes.

$$\underline{V_s} = (R_s + L_s s)\underline{I_s} + L_m s\underline{I_r} + j\omega_s\left(L_s \underline{I_s} + L_m \underline{I_r}\right) \tag{1}$$

$$\underline{V_r} = (R_r + L_r s)\underline{I_r} + L_m s\underline{I_s} + j\omega_s slip\left(L_r \underline{I_r} + L_m \underline{I_s}\right) \tag{2}$$

where

$$L_s = L_m + L_{s\sigma} \tag{3}$$

$$L_r = L_m + L_{r\sigma} \tag{4}$$

$$slip = \frac{\omega_s - \omega_r}{\omega_s} \tag{5}$$

The stator flux is defined as follows.

$$\underline{\lambda_s} = L_m \underline{I_r} + L_s \underline{I_s} \tag{6}$$

By using equations (1), (2), and (6) and replacing $\underline{V_r} = 0$ and slip = 0, it is possible to obtain the $L_s(s)$ of the squirrel cage induction machine. By analogy with the synchronous machines is called the operational inductance of the induction

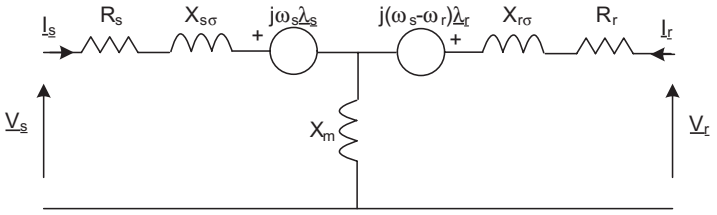

Figure 2. DFIG representation.

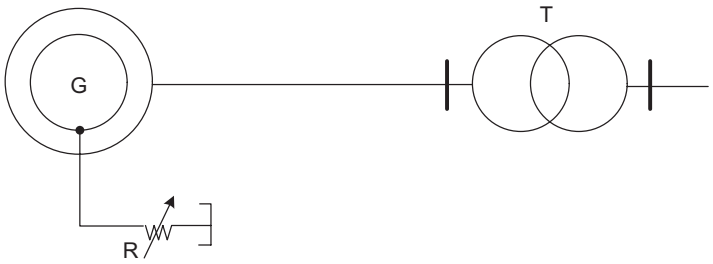

Figure 3. IGR single line diagram.

machine. The DFIG operational inductance can be obtained in the same way by using the slip ≠0 and since the rotor can be considered short-circuited by the chopper during severe faults $\underline{V_r} = 0$, see Figure 3.

By using $V_{qs} = 0$ and $I_{qs} = 0$ for calculating I_r and then replacing it in equation (6), it is possible to obtain equation (7).

$$\lambda_{ds}(s) = \left(L_s - L_m^2 \frac{L_r s^2 + R_r \omega_s s + slip^2 L_r \omega_s^2}{L_r^2 s^2 + 2R_r L_r \omega_s s + \left(R_r^2 + slip^2 L_r^2\right)\omega_s^2} \right) I_{ds} - \left(\frac{V_{dr}\left(R_r \omega_s^2 + L_r \omega_s s\right) + V_{qr}\left(\omega_s^2 L_r slip\right)}{L_r^2 s^2 + 2R_r L_r \omega_s s + \left(R_r^2 + slip^2 L_r^2\right)\omega_s^2} \right) M \tag{7}$$

Further, by replacing $\underline{V_r} = 0$, equation (8) can be obtained.

$$L_s(s) = L_s - L_m^2 \frac{L_r s^2 + R_r \omega_s s + slip^2 L_r \omega_s^2}{L_r^2 s^2 + 2R_r L_r \omega_s s + \left(R_r^2 + slip^2 L_r^2\right)\omega_s^2} \tag{8}$$

Therefore, equation (8) can be used to evaluate the slip influence in the peak currents when a sudden three-phase short circuit occurs. From the initial value theorem, $L(s)$ at initial time ($time \to 0$, $s \to \infty$) becomes L'_s, which can be termed the transient inductance of the DFIG machine.

$$L'_s = Lim_{s\to\infty} L_s(s) = \frac{L_r L_s - L_m^2}{L_r} \tag{9}$$

Regrouping equation (8) in terms of leakage inductances:

$$L'_s = L_{s\sigma} + \frac{L_m L_{r\sigma}}{L_m + L_{r\sigma}} \tag{10}$$

And thus, the transient reactance of the machine is obtained.

$$X'_s = \omega_s L'_s = X_{s\sigma} + \frac{X_m X_{r\sigma}}{X_m + X_{r\sigma}} \tag{11}$$

By looking at equation (11), it can be checked that the slip variation does not affect the machine short circuit peak current value, $X'_{s(slip\neq 0)} = X'_{s(slip=0)}$, since the transient reactance (11) does not depend on the machine slip, having the same value; the transient inductance of the DFIG machine and the induction machine.

In the other hand, the slip is reflected in the frequency of the injected stator currents (f_{sc}) during the fault. The value of this frequency can be seen in equation (12),[4]

$$f_{sc} = (1 - slip) f_{grid} \tag{12}$$

These different possible frequencies of the stator short-circuit current affect the time instant that corresponds to the first and subsequent peaks of the short-circuit current. This variable short circuit current frequency makes a clear difference with the short circuit current of the SG, which its main AC short circuit component has the same frequency as the grid, having the first short circuit current peak at half cycle of the grid frequency.

In order to show the impact on this variable short circuit current frequency, the following cases are simulated in PSCAD program. The DFIG is modelled as it is represented in Figure 1.

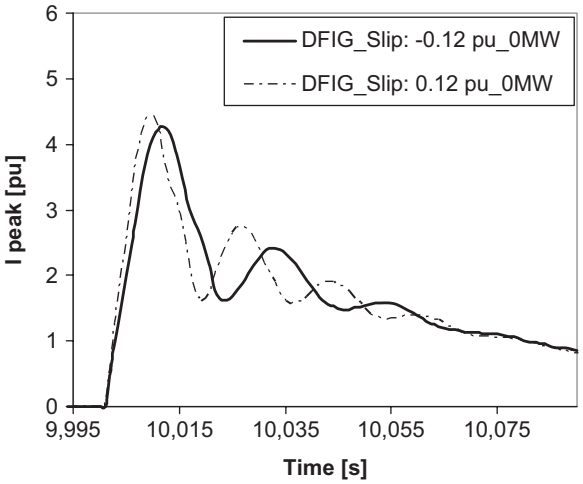

Figure 4. Short circuit current envelopes of DFIG for different slips and same power injections.

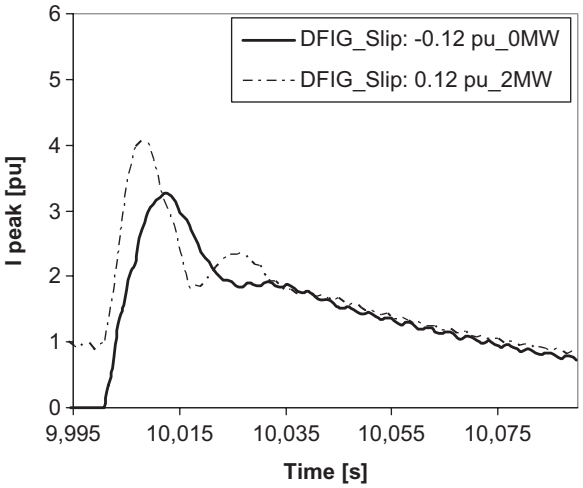

Figure 5. Short circuit current envelopes of DFIG with zero and maximum active power injection.

Figure 4 shows a simulation of a DFIG subjected to a three-phase fault for two different slips, in both cases the active and reactive pre-fault power production are set to zero. For these cases, the modulation index of the DC-link chopper during the fault has been fixed to the maximum value. The maximum modulation index ensures the chopper resistance to its rated value regardless of the DC-link voltage level. Therefore, the same resistor value is attached to the rotor during these faults, even for two different slips.

The dotted line shows the DFIG that initially is operating at a slip that corresponds to a maximum active power production, slip: 0.12 pu, its rotational speed is above synchronous speed.

This rotational speed makes the first peak of the current occur before the usual half cycle of the grid frequency. Conversely, the continuous line in the graph shows the DFIG that initially is operating at a slip that corresponds to the minimum active power production, slip: –0.12 pu, its rotational speed is below synchronous speed; therefore, the instant of the first peak of the current occurs after half cycle of the grid frequency.

In Figure 4, one can observe the differences in the short circuit current frequency, as it was mentioned in the previous paragraph, and a smaller value in the short circuit current peak of the DFIG when operating at sub-synchronous speed. This is due to the exponential decay time pattern followed by the short circuit currents.[5] Lower frequencies imposed in the short circuit currents will show higher damping in the peak current values.

Figure 5 shows a simulation of a DFIG subjected to a three-phase fault for two different cases. In these cases the modulation index is not fixed and it is calculated by the WTG control depending on the DC-link voltage level, as it happens in the reality.

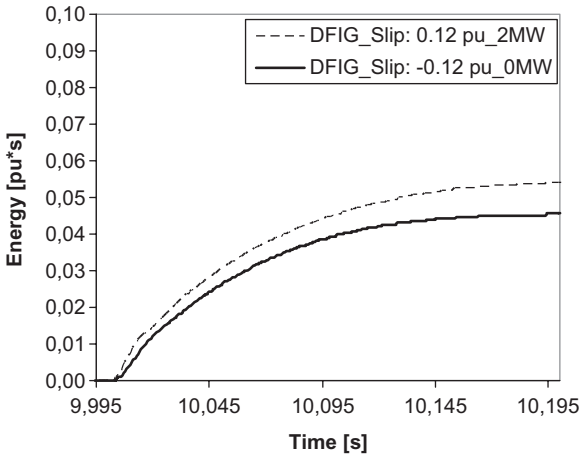

Figure 6. Energy dissipation in the DC-link chopper during a three-phase fault for zero and maximum active power injection.

The dotted line shows the case where the generator is rotating at rated slip, slip: 0.12 pu, and full active power production, and the continuous line shows the generator that is at zero active power production and at lower rotating speed, slip: –0.12 pu.

Very different peaks in short-circuit currents can be seen from these two curves depicted in Figure 5. These differences can be explained by the different chopper modulation indexes presented in these two cases, which is translated to a different equivalent resistances connected to the rotor during the faults.

The modulation indexes are different since the rise of the current entering into the DC-link depends on the frequency of the short circuit currents. Higher frequency in the short circuit currents will raise the DC-link voltage in a faster way, therefore more power needs to be dissipated in the chopper, see Figure 6, leading to an equivalent smaller chopper resistance.

Therefore, the slip of the DFIG has a direct impact on the short circuit current frequencies and an indirect impact on the peak values presented in the short circuit currents, due to the chopper action of the converter.

After this brief explanation about the DFIG short circuit behaviour, the rest of the sections in this paper are focused on finding the synchronous equivalent, which matches with the DFIG topology that produces maximum short circuit current injection.

3. EQUIVALENT ASYNCHRONOUS REPRESENTATION OF DFIG

In order to start with the calculation of the equivalent impedances, the induction generator is used as a starting point due to the similarity with the DFIG generator structure.

For short circuit studies, the following assumptions can be taken to simplify the topology of the DFIG with chopper protection:

a) Chopper action keeps V_{DC} level constant during the fault period.
b) No energy transfer to the grid through the grid converter. Grid converter is blocked during the fault.
c) Just after the fault, the rotor converter is blocked as well. Only the diode bridge is operational during the fault.

Based on the above assumptions, the next conclusions are extracted:

- Using assumption (a), the current flow into the DC-link capacitors is zero, $I_c = 0$.
- Using assumptions (a) and (b), only current through the chopper resistance (R_{ch}) is flowing during the fault, $I_{DC} = I_{ch.}$
- Using assumption (b), active current from the GC is zero, $I_{GC} = 0$.

Under the above conditions, the DFIG can be represented as an IG with an equivalent extra variable resistance attached to the rotor during the fault, see Figure 3, allowing the suppression of the converters, thus reducing the complexity of the DFIG topology.

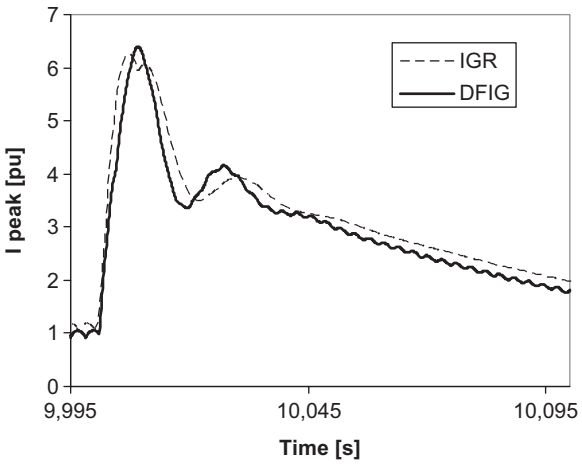

Figure 7. Short circuit current envelopes of the DFIG and its equivalent IGR for rated active power injection.

3.1. Value of the equivalent resistance attached to the rotor

In the DFIG, the instantaneous chopper resistance value depends on the value of the modulation index applied by the control to the chopper IGBTs. Therefore, as can be seen in Figure 3, the equivalent resistance attached to the rotor in the IGR should be controlled, during the fault period, in a way that becomes time dependant.

But when using EMT models, the parameterization of the SG has to be done neglecting this time dependency of the chopper resistance, and supposing that the resistance attached to the rotor is constant during the whole fault period. This has to be done in this way, as it is not possible to enter variable resistance values into the field and damping winding data, since EMT programs representing SGs use a constant value for these inputs. As a consequence of doing that, some mismatching will be presented in the generator time constants and short circuit current peaks; due to the used total rotor resistance is not the real one during the fault period.

The chosen equivalent resistance (R) connected at the IGR rotor terminals is formed by the full chopper resistance, R_{ch} in Figure 1, which is the element in the converter where most of the energy is dissipated during the fault. The losses in the converter, IGBTs and diodes, during the fault can be neglected.

Choosing this value for the equivalent resistance gives a good approach for the short circuit peak value obtained. This is because the configuration at the beginning of the fault will be very similar between the DFIG and the IGR with this constant resistance attached to the rotor. At the beginning of the fault, the generator current contribution to the fault is the highest one; therefore, more energy has to be dissipated in the DC-link to keep the voltage level constant, having the full chopper resistance almost continuously connected.

To validate all the assumptions listed, a simulation of a three-phase bolted fault is applied at the generator stator terminals of the DFIG and the IGR, see Figure 7.

In the pre-fault time the generators are injecting rated active power. Since for the IGR no capacitors for reactive power compensation are included in the stator terminals, the reactive power consumption by the IGR is 0.45 pu. The DFIG reactive power is set to 0.35 pu, which is the maximum reactive power consumption without exceeding its rating at full active power production.

4. SG PARAMETRIZATION AS DFIG

When using EMT SG models, the data for the electrical impedances should be supplied into the model, or translated from X'', X', X, T''_0, and T'_0 values. These constants define the inductance and resistance winding values of the model.

Calculating IG equivalent impedances and time constants can be found in the literature.[6–8] These equations can be adapted by adding the attached resistance to the rotor terminals (R) to the generator rotor resistance value (R_r), thus transforming the IG into an IGR.

The transient reactances of the equivalent SG are calculated as follows:

$$X'_d = X_{s\sigma} + \frac{X_m X_{r\sigma}}{X_m + X_{r\sigma}} \tag{13}$$

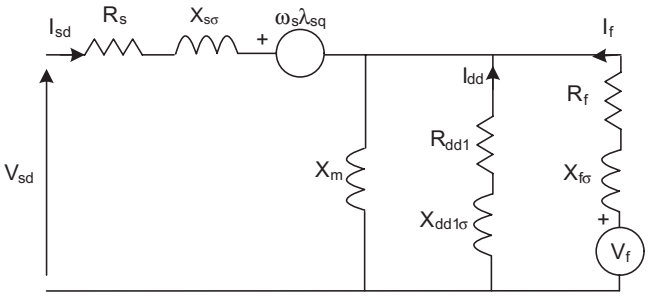

Figure 8. SG, d axe representation with 1 damper circuit.

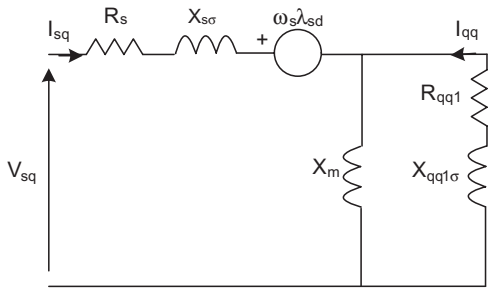

Figure 9. SG, q axe representation with 1 damper circuit.

$$X'_q = X'_d \tag{14}$$

The open circuit transient time constants of the equivalent SG are calculated as follows:

$$T'_{d0} \approx \frac{X_m + X_{r\sigma}}{2\pi f R_r} \tag{15}$$

$$T'_{q0} = T'_{d0} \tag{16}$$

Figure 8 and Figure 9 show in d-q stationary reference frame the steady state representation of a round rotor SG with one damping circuit.

The differences of the IG having one rotor circuit, where no winding damping is presented, can be solved by setting the T''_0 to very low values. This will cause the damping resistance value R_{dd1} [see equation (18)] to be very high, thus making the SG damping branch neglectable.

A recommendation from the authors for T''_0 value can be found in equation (17).

$$T''_{q0} \approx 0.001 T'_{q0} \tag{17}$$

Following typical SG equations, (18) and (19) are extracted from[9]

$$T''_{d0} \approx \frac{1}{2\pi f_{grid} R_{dd1}} \left(X_{dd1} + \frac{X_m X_{f\sigma}}{X_m + X_{f\sigma}} \right) \tag{18}$$

$$T''_{q0} = T''_{d0} \tag{19}$$

For the same reason of having one equivalent rotor circuit, the subtransient reactance (X'') should be set to a value similar to the transient reactance (X') to avoid computational problems when using electrical simulation programs.

The most common representation of the IGR is without subtransient impedance term, only if the generator has deep double cage bars[6] another branch should be used in the equivalent circuit, and consequently, an equivalent subtransient values of X'' and T''_0 could be calculated accordingly.

5. SIMULATION CASES

5.1. Simulations setup

The simulation test setup can be seen in Figure 10. In all the simulations, three-phase faults are applied at time equal to 10 s. The used WTG model for the simulations is depicted in Figure 2 and the data used for the model can be found in Table I. These data are obtained from the nameplate of the transformer and generator. The SG model is a round rotor machine, and the used data can be found in Table II.

The DFIG and the SG are at full active power and zero reactive power injection, in the pre-fault time.

Three different fault cases have been simulated causing different remained voltages at WTG terminals.

The SCR of the used grid is five, and the X/R is kept constant and equal to 75°, for every case.

5.2. Simulation results

The following figures show the PSCAD simulation cases of the DFIG and the SG with the inductances and time constants tuned according to section IV.

The short circuit currents are measured at WTG terminals, see Figure 10.

In all three cases, it can be seen that the frequency of the short circuit current between the DFIG and the SG is different as a consequence of the slip presented in the DFIG. This difference in the frequency cannot be solved only by adjusting the parameters defining the SG circuitry, as this frequency is imposed by the rotational speed of the generator.

In Figure 11 (case B), higher AC component can be seen than in Figure 12 (case A). This is the effect of lower chopper action, since the severity of the fault is less compared with case A.

In Figure 13 (case C), the converter is blocked, but only during the first cycles of the fault period. After that, the rotor converter resumes action injecting rated reactive current.

Table I. Electrical data of wind turbine

Parameter	Value	Unit
S_{base}	2100	[kVA]
V_{base}	0.69	[kV]
Electrical Frequency	50	[Hz]
Stator Resistance	0.006	[pu]
Rotor Resistance	0.009	[pu]
Mutual Inductance	3.422	[pu]
Stator Inductance	0.072	[pu]
Rotor Inductance	0.101	[pu]
V_{DC}	0.910	[kV]
Rotor Converter Size	0.25	[pu]
S step-up Transformer 0.69 : 20 kV	2100	[kVA]
X/R step-up Transformer	6	
Z step-up Transformer	0.08	[pu]

Table II. Electrical data of SG.

Parameter	Value	Unit
S_{base}	2100	[kVA]
V_{base}	0.69	[kV]
Electrical Frequency	50	[Hz]
Stator Resistance	0.006	[pu]
Stator Leakage Reactance	0.08	[pu]
Direct, Quadrature Axis Synchronous Reactance	3.307	[pu]
Direct, Quadrature Axis Transient Reactance	0.186	[pu]
Direct, Quadrature Axis Sub-Transient Reactance	0.126	[pu]
Direct, Quadrature Axis Open Circuit Transient	0.1	[s]
Direct, Quadrature Axis Open Circuit Sub-Transient	0.001	[s]
X/R step-up Transformer	6	
Z step-up Transformer	0.08	[pu]

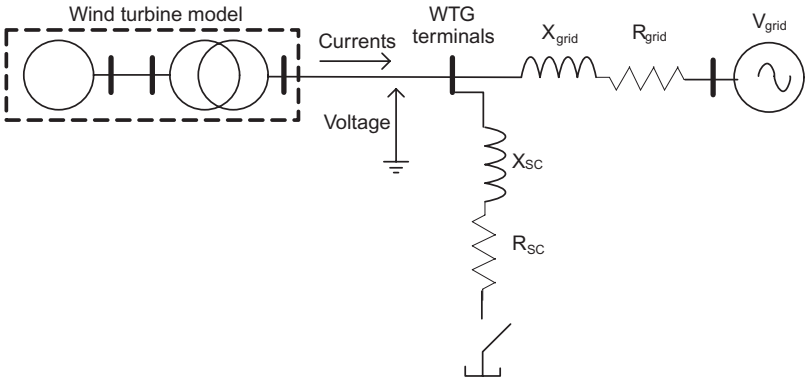

Figure 10. Simulation fault setup.

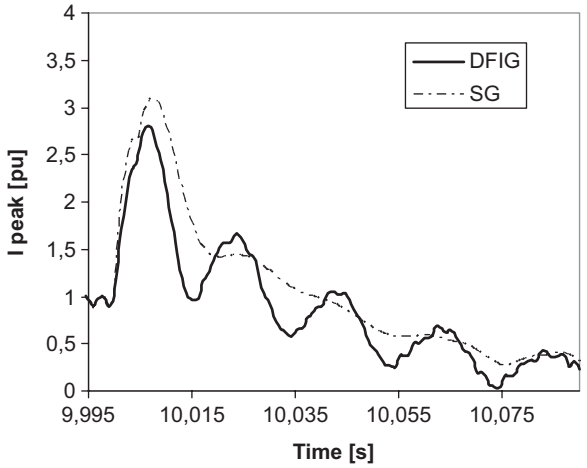

Figure 11. Case B: Short circuit current envelopes for 20% remaining voltage.

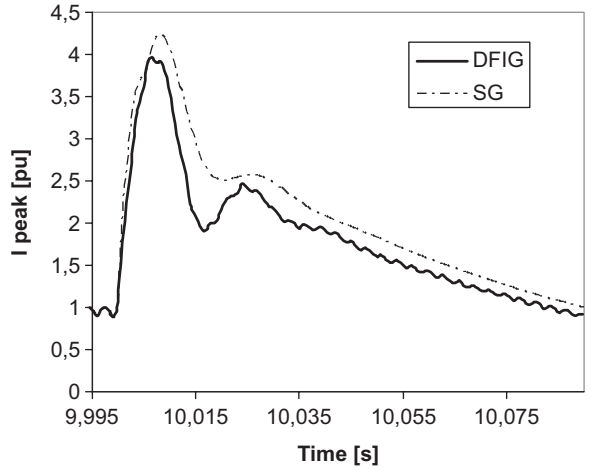

Figure 12. Case A: Short circuit current envelopes for 0% remaining voltage.

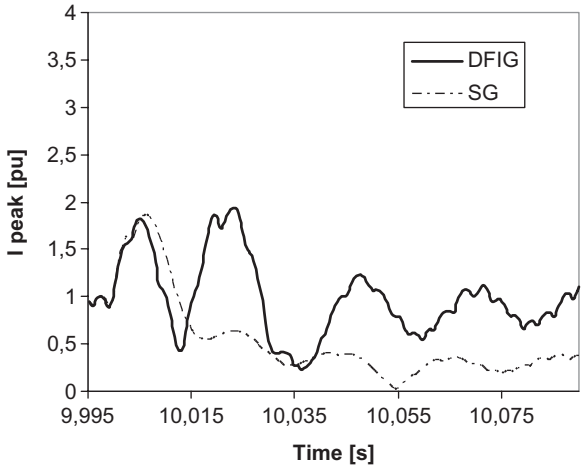

Figure 13. Case C: Short circuit current envelopes for 50% remaining voltage.

Table III. Peak values comparison.

Case	Remaining WTG terminals voltage [%]	Deviance in maximum peak [%]
A	0	7
B	20	9
C	50	1

Table III summarizes the deviance found in the peak current envelopes between the DFIG and the SG for the three different remaining stator voltages.

The short circuit generator peak current in the case of zero residual voltage is independent of the grid short circuit power. For distant faults, with non-zero residual voltage, the grid short circuit power and the grid ratio X/R will affect the short circuit current amplitudes and decay times.

6. CONCLUSIONS

This paper shows how adjusting the impedance data of an SG can provide a good approximation to the DFIG with chopper protection unit for short circuit current injection during grid faults.

The DIFG with chopper protection can be represented as an asynchronous generator with constant extra rotor resistance during severe faults, when the rotor converter is blocked and the chopper keeps the DC-link voltage constant, thus neglecting the rotor and grid converters.

The extra resistance attached to the rotor can be calculated as the equivalent of the maximum energy consumption during the first cycles of the fault by the converter; mainly for severe faults and at maximum slip, this resistance can be represented as the total chopper resistance. Using the generator data and this resistance value, the SG parameters can be calculated accordingly.

The slip of the machine has an indirect impact on the short circuit peak current values due to the chopper action of the DC-link. Since the modulation index of the chopper resistance value depends on the slip of the generator, different short circuit current values are expected for different slip values.

The accuracy of this representation depends on the capability of the converter to withstand the rotor current faults, meaning that this representation is valid for severe faults cases when the remaining voltage is low and the IGBT switching of the converters are stopped. When the rotor converter is under control, not in blocked state, the stator currents are under control at any moment, therefore, not being possible to use this equivalent representation. Note as well, that in most of the cases, asymmetrical faults will not block the converter, due to lower short circuit current peak values.

In conclusion, when doing this SG equivalence, attention should be drawn to the importance of the particular DFIG control of the rotor circuitry during short circuits. The DFIG short circuit fault currents will depend on the protective converter actions and when normal control is resumed during the fault again.

REFERENCES

1. Morren J, de Haan SWH. Ridethrough of wind turbines with doubly-fed induction generator during a voltage dip. *IEEE Transactions on Energy Conversion* 2005; **20**: 435–441.
2. Erlich I, Bachmann U. Grid code requirements concerning connection and operation of wind turbines in Germany. *IEEE Power Engineering Society General Meeting*, Vol. 2, 12–16 June 2005; 1253–1257.
3. Pena R, Clare JC, Asher GM. Doubly fed induction generator using back-to-back PWM converters and its application to variable speed wind-energy generation. Proceedings Institute of Electrical and Electronics Engineer Electrical Power Application, **143**(3), May 1996; 231–241.
4. Tleis ND. *Power Systems Modeling and Fault Analysis*. Elsevier Publishing Company: Burlington, MA, 2008,
5. Morren J, de Hann SWH. *Short-Circuit Current of Wind Turbines with Doubly Fed Induction Generator*. IEEE Transactions on Energy Conversion 2007; **22**(1): 174–180.
6. Boldea I, Nasar SA. *Electric Machine Dynamics*. MacMillan Publishing Company: Oxford, UK, 1986.
7. Krause *et al*. *Analysis of Electrical Machinery*. IEEE Press: Piscataway, NJ, 1994.
8. Adkins B, Harley RG. *The General Theory of Alternating Current Machines: Application to Practical Problems*. Chapman and Hall Publishing Company: London, UK, 1975.
9. Kundur P. *Power System Stability and Control*. Electric Power Research Institute, McGraw-Hill, Inc.: Palo Alto, CA, 1993.

DOI: 10.1002/we

A.6

"DFIG Turbine Representation for Small Signal Voltage Control Studies"
Jorge Martínez, Philip C. Kjær, Remus Teodorescu.

DFIG Turbine Representation for Small Signal Voltage Control Studies

Jorge Martínez, Philip C. Kjær, Remus Teodorescu, Senior Member, IEEE

***Abstract*— This paper addresses the representation of a wind power plant, based on wound rotor asynchronous generators, with a centralized voltage controller, by an equivalent transfer function, valid for small signal voltage control studies. This representation allows to investigate the influence of the centralized plant control gain and short circuit ratio on the system stability, for instance, by analyzing the zero-pole placement.**

Larger percentages of wind power penetration translate to more demanding requirements coming from the grid codes, for example voltage support at the point of connection has been introduced recently by several grid codes from around the world, making important to analyze this control when applied to wind power plants.

The performance of the equivalent transfer function has been evaluated and compared using an equivalent grid with different short circuit ratios and active power injection levels, the cases have been simulated with PSCAD/EMTDC program. Results show that this equivalence can be used for short circuit ratios between 5 and 25 for obtaining an accurate representation of the system voltage dynamics.

***Index Terms*—wind turbine generator, transfer functions, simulation, doubly fed induction generator, voltage control.**

I. Nomenclature

AC, DC	Alternate and Direct Current
COMM	Communication
Ctrl	Control
CT, VT	Current and Voltage Transformer
DFIG	Doubly Fed Induction Generator
EMT	Electromagnetic transient
f	Frequency
G	Generator
GC	Grid Converter
Meas	Measured device
P, Q	Active and Reactive power
PCC	Point of Common coupling
PI	Proportional and Integer control
PWM	Pulse Width Modulation
L, R, C	Inductance, Resistance, and Capacitance
RC	Rotor Converter
s	Laplace term
SCR	Short Circuit Ratio
V, I	Voltage, Current
WPPC	Wind Power Plant Control
WTG	Wind Turbine Generator
WTGT	Wind Turbine Generator Transformer
X	Reactance
Z	Impedance
ω	Angular Speed
λ	Flux

Subscripts

r, s, M	Rotor, Stator and Mutual
σ	Leakage
ref, f, m	Reference, filtered and measured
d, q	Direct and Quadrature

Jorge Martínez is with VESTAS Wind System, Power plant R&D, DK, (corresponding author e-mail: jomga@ vestas.com).

P. C. Kjaer is with VESTAS Wind System, Power plant R&D, DK, (e-mail: pck@ vestas.com).

R. Teodorescu is with Aalborg University, DK, (e-mail: ret@iet.aau.dk).

II. Introduction

DFIG technology is widely used in the wind industry. The variable speed and the reduced size of the power converters, normally 25% of the generator power, but high controllability offer a very competitive market solution. Since wind power is growing drastically, reaching high percentages of penetration into the power system becomes necessary to have a representation of the DFIG technology in standard simulation programs.

Wind power plants differ from other generation sources, and therefore are particular in certain aspects of their control. For a start, the energy source is fluctuating and unpredictable. Secondly, the generation plant is highly modular and composed by a large number of generation units, therefore having communication delays between the central control and the actuators. Thirdly, the wind power plants are often located far from the load locations. For these peculiarities, dedicated grid codes are done for the wind generation [1-5]. As voltage control is actuated by reactive power of the turbines, generally speaking it is possible to affirm that the voltage control design will cover an inner reactive power control loop and an outer voltage control loop [6,7].

The initial design and tuning of the plant voltage controller is done basis on some simplifications and linearization processes. The representation shown in this paper allows the use of classical control theory to get a first estimation of the stability and boundaries of the system.

III. SYSTEM DIAGRAM

The system to be studied is composed by a wind power plant of *n* DFIG turbines, which uses a centralized controller (WPPC) to control the voltage at the PCC. The following figure is used to represent the main elements of the system.

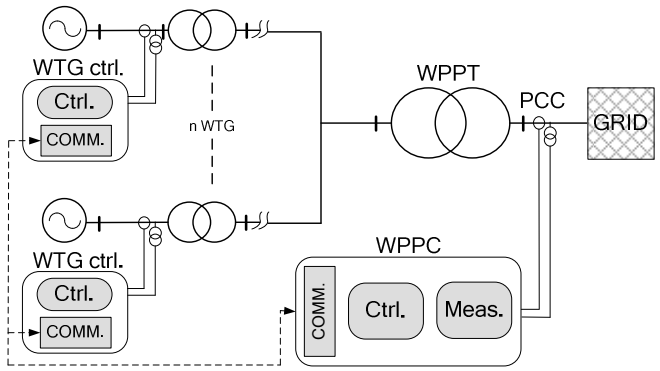

Fig. 1. WPP diagram.

Clearly, it is possible to classify the studied system in the following three groups:

WTGs: Which mainly include the converters, generator and its controllers, in the presented case, a DFIG is used.

Collector and grid system: These include the main electrical impedances of the system, e.g. the substation transformer (WPPT), and the equivalent grid impedance (GRID).

Plant control: It is the WPPC, which includes the measurement devices and the voltage controller, also called the outer voltage loop control.

The following sections describe in more details the listed elements.

IV. DFIG WTG

DFIG turbines have variable speed. The speed range of the generators will be different depending on the wind turbine manufacturer, but mainly it is in the range of ±15% of the synchronous speed.

The variable speed doubly-fed generator, see Fig. 2, allows full control of generator active and reactive power using the rotor-connected frequency converter. Its rating is in the order of 0.3 pu. Operating both with sub- and super-synchronous speed, the power can be fed both in and out of the rotor circuit. The grid converter (GC) is used only to regulate the voltage level of the DC-link. The simplified control of the rotor converter is depicted in Fig. 3, where the active and reactive power are controlled using the d and q axis respectively. The grid converter and its control are not represented, since they are not collaborating for the reactive current injection, and the DC-link voltage is considered fixed.

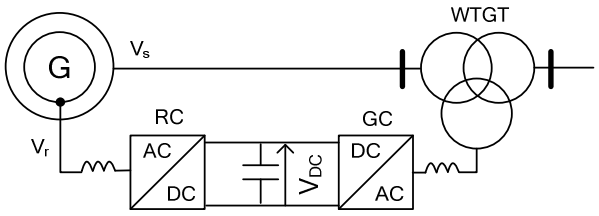

Fig. 2. DFIG simplified electrical single line diagram.

The DFIG controller will calculate or receive power references from an external controller, (P_{ref}, Q_{ref}). These references are processed using two PI-controllers in cascade; and they will generate the needed voltage references ($V_{ref\ d}$, $V_{ref\ q}$) which are translated by the PWM to pulse the rotor converter. Finally, the rotor is fed with a voltage that produces the desired P and Q at the stator terminals.

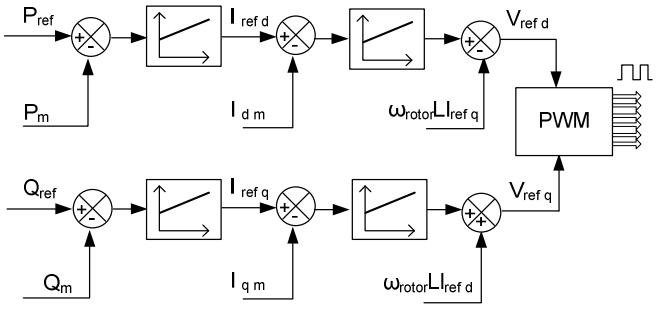

Fig. 3. DFIG simplified controller diagram

The WTG representation has to be simplified in order it can be represented using a simple transfer functions. Having a d-q control allows independent control of the reactive and active power injected at stator terminals as was mentioned, thus the mechanical part of the wind turbine, such as the drive train and the blades are not included, the decoupling is considered ideal. Only the q axes, the one related to the reactive current injection is represented. Therefore, when doing the control analysis the active power fluctuations can be considered as a disturbance. The GC is used only for regulating the voltage of the DC-link, thus not having a contribution to the voltage regulation. Basis on that, Fig. 4 is plotted, which included only the representative WTG components related to voltage control.

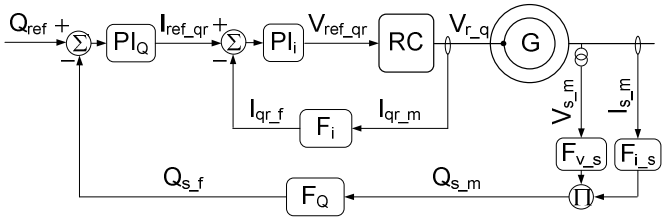

Fig. 4. WTG representation for voltage control studies.

In Fig. 4, the generator (G), the RC and its control for reactive power injection are represented. As can be seen in Fig. 3, the converter connected to the generator rotor is

controlled with two control loops; the inner one, which controls the rotor (I_q) current, and the outer one, which controls the reactive power (Q). Both controllers are based on PI control structures, and they are fed with the error between the references and the filtered measured signals.

A. Generator Model

Fig. 5 shows in a synchronous reference frame the steady state representation of DFIG with the excitation of the rotor circuit $\underline{V}_r$. The non saliency in the stator and rotor windings makes no difference between d-q axes.

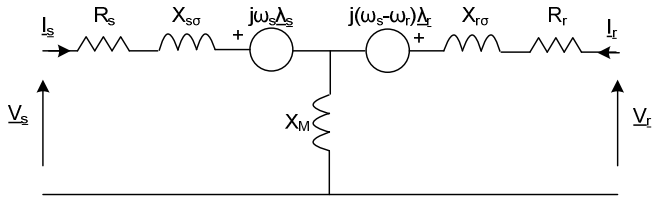

Fig. 5. DFIG representation.

The d-q equations of the generator, where the currents are pointed out from the T equivalent are the following:

$$\begin{aligned} L_s &= L_{\sigma s} + M \\ L_r &= L_{\sigma r} + M \end{aligned} \tag{1}$$

$$slip = \frac{\omega_s - \omega_r}{\omega_s} \tag{2}$$

$$\begin{aligned} v_{qs} &= -(R_s + sL_s)i_{qs} - sMi_{qr} - \omega_s(L_s i_{ds} + Mi_{dr}) \\ v_{ds} &= -(R_s + sL_s)i_{ds} - sMi_{dr} + \omega_s(L_s i_{qs} + Mi_{qr}) \\ v_{qr} &= -sMi_{qs} - (R_r + sL_r)i_{qr} - (\omega_s - \omega_r)(Mi_{ds} + L_r i_{dr}) \\ v_{dr} &= -sMi_{ds} - (R_r + sL_r)i_{dr} + (\omega_s - \omega_r)(Mi_{qs} + L_r i_{qr}) \end{aligned} \tag{3}$$

The same equations represented in pu system, are the following ones.

$$\begin{aligned} V_{qs} &= -\left(R_s + \frac{sL_s}{\omega_s}\right)I_{qs} - \frac{sMI_{qr}}{\omega_s} - (L_s I_{ds} + MI_{dr}) \\ V_{ds} &= -\left(R_s + \frac{sL_s}{\omega_s}\right)I_{ds} - \frac{sMI_{dr}}{\omega_s} + (L_s I_{qs} + MI_{qr}) \\ V_{qr} &= -\frac{sMI_{qs}}{\omega_s} - \left(R_r + \frac{sL_r}{\omega_s}\right)I_{qr} - slip(MI_{ds} + L_r I_{dr}) \\ V_{dr} &= -\frac{sMI_{ds}}{\omega_s} - \left(R_r + \frac{sL_r}{\omega_s}\right)I_{dr} + slip(MI_{qs} + L_r I_{qr}) \end{aligned} \tag{4}$$

Using the decoupling control terms in the current controller loops, (5) is obtained.

$$\begin{aligned} V_{qs} &= -\left(R_s + \frac{sL_s}{\omega_s}\right)I_{qs} - \frac{sMI_{qr}}{\omega_s} - (L_s I_{ds} + MI_{dr}) \\ V_{ds} &= -\left(R_s + \frac{sL_s}{\omega_s}\right)I_{ds} - \frac{sMI_{dr}}{\omega_s} + (L_s I_{qs} + MI_{qr}) \\ V_{qr} &= V_{ref\_qr} - slipL_r I_{dr} = -\left(R_r + \frac{sL_r}{\omega_s}\right)I_{qr} - \frac{sMI_{qs}}{\omega_s} - slip(MI_{ds} + L_r I_{dr}) \\ V_{dr} &= V_{ref\_dr} - slipL_r I_{qr} = -\left(R_r + \frac{sL_r}{\omega_s}\right)I_{dr} - \frac{sMI_{ds}}{\omega_s} + slip(MI_{qs} + L_r I_{qr}) \end{aligned} \tag{5}$$

Since the rotation orientation system PLL is synchronised with the d axis, V_{qs}=0 can be used.

Solving the above equations, the reactive current in the rotor circuit (I_{qr}) can be represented as an equation which depends on the terms; I_{dr}, V_{qr} and V_{ds}.

$$I_{qr} = G_1(s)V_{qr} + G_2(s)I_{dr} + G_3(s)V_{ds} \tag{6}$$

In the obtained transfer functions, the *s* terms with higher order than two are neglected, since they are inversely proportional to the same order in ω_s. e.g.; $(s^3/\omega_s^3) + (s^2/\omega_s^2) + (s/\omega_s)$ + constant.

Therefore, the transfer functions $G_i(s)$ can be represented in a generic way, as follows:

$$G(s)_{i=1,\ldots,5} = K_i \frac{1 + sT_{ai}}{1 + sT_{bi}} \tag{7}$$

The following terms for the transfer function G_1 are obtained.

The time constants T_{a1} and T_{b1} are equal to:

$$T_{a1} = \frac{2R_s L_s}{\omega_s(R^2{}_s - L^2{}_s)} \tag{8}$$

$$T_{b1} = \frac{2R_s R_r L_s + L_r R^2{}_s - M^2 L_s + L_r L^2{}_s}{\omega_s(R_r R^2{}_s + R_r L^2{}_s + slipM^2 R_s)} \tag{9}$$

And the gain K_1 is equal to:

$$K_1 = -\frac{R^2{}_s + L^2{}_s}{R_r R^2{}_s + R_r L^2{}_s + slipM^2 R_s} \tag{10}$$

The following terms for the transfer function G_2 are obtained.

The time constants T_{a2} and T_{b2} are equal to:

$$T_{a2} = \frac{R_s(1 + slip)}{slip\,\omega_s L_s} \tag{11}$$

$$T_{b2} = \frac{2R_s R_r L_s + L_r R^2{}_s - M^2 L_s + L_r L^2{}_s}{\omega_s(R_r R^2{}_s + R_r L^2{}_s + slipM^2 R_s)} \tag{12}$$

And the gain K_2 is equal to:

$$K_2 = \frac{slipM^2 L_s}{R_r R^2{}_s + R_r L^2{}_s + slipM^2 R_s} \quad (13)$$

The following terms for the transfer function G_3 are obtained.

The time constants T_{a3} and T_{b3} are equal to:

$$T_{a3} = \frac{L_s(slip-1)}{slip\,\omega_s R_s} \quad (14)$$

$$T_{b3} = \frac{2R_s R_r L_s + L_r R^2{}_s - M^2 L_s + L_r L^2{}_s}{\omega_s (R_r R^2{}_s + R_r L^2{}_s + slipM^2 R_s)} \quad (15)$$

And the gain K_3 is equal to:

$$K_3 = \frac{slipMR_s}{R_r R^2{}_s + R_r L^2{}_s + slipM^2 R_s} \quad (16)$$

Further, using (5) the transfer function from the reactive rotor current to the stator current can be represented as following:

$$I_{qs} = G_4(s) I_{qr} + G_5(s) V_{ds} \quad (17)$$

The following terms for the transfer function G_4 are obtained.

The time constants T_{a4} and T_{b4} are equal to:

$$T_{a4} = \frac{R_s}{\omega_s (R_s + L_s)} \quad (18)$$

$$T_{b4} = \frac{2L_s R_s}{\omega_s (R^2{}_s + L^2{}_s)} \quad (19)$$

And the gain K_4 is equal to:

$$K_4 = \frac{-M(L_s + R_s)}{(R^2{}_s + L^2{}_s)} \quad (20)$$

The following terms for the transfer function G_5 are obtained.

$$T_{a5} = 0 \quad (21)$$

Where the time constant T_{b5} is equal to:

$$T_{b5} = \frac{2L_s R_s}{\omega_s (R^2{}_s + L^2{}_s)} \quad (22)$$

And the gain K_5 is equal to:

$$K_5 = \frac{L_s}{(R^2{}_s + L^2{}_s)} \quad (23)$$

As can be seen in the previous equations, the slip affects the gains and time constants of the transfer functions. To analyse the slip impact in the transfer functions, specific generator data has been used, see Table II, to calculate the numerical values of the roots, for two different slips; -0.12 pu and 0.12 pu.

The results show that the difference between these two cases is the location of one pole; for -0.12 pu slip the pole is located at (902+0j), and for a slip equal to 0.12 pu the pole is located at (900+0j).

Considering that the next pole in the system is located at (34+0j) for both cases, it is possible to assume a constant value for the slip, since the dynamics of the system are dictated by the most closed poles to the origin.

Section IX compares the real model of the WTG with the obtained transfer function, when the transfer function uses a constant value in the slip of 0.12 pu.

B. Converter Model

The studied rotor converter of the DFIG uses PWM with third harmonic injection. This technique permits to extend the lineal modulation index range from $\left(\frac{\pi}{4}\right)$ to $\left(\frac{\pi}{2\sqrt{3}}\right)$, where the modulation index M_{od}, can be defined as; $\left(\frac{V_1 \pi}{2V_{DC}}\right)$, [8].

The converter itself can be represented as a first order system with a gain and a time constant, which includes; the processing timing, dead time, and sampling of the converter

The gain of the converter can be represented as the modulation index, and being the switching frequency f_{sw}, which is in the order of few KHz, the delay of the signal processing can be estimated as $0.5f_{sw}$ and the feedback delay will have an average value of $(0.5/2)f_{sw}$, therefore the sum of these terms will be in the range of $(1.5/2)f_{sw}$, [8], leading to the following converter transfer function (24).

$$G_c(s) = \frac{M_{od}}{1 + s0.75 f_{sw}} \quad (24)$$

The filters of the measured signals in the control are used to remove high frequency noise from the currents and voltages.

The transfer function of the filters can be represented as a first order function with the bandwidth of the real WTG filters. The generic transfer function for the filter is as (25).

$$F_i(s) = \frac{1}{1 + sT_{FI}} \quad (25)$$

The stator voltage and current filters have very high bandwidth compared with the power loop control; therefore the dynamic for these filters can be neglected. The equivalent transfer function used for these filters is shown in (26).

$$F_{V\_s, i\_s} = 1 \quad (26)$$

The filter used for the stator reactive power (F_Q) has as well the form indicated in (25).

The converter control, as was mentioned before, is based on a proportional and integer structure, having a typical PI transfer function, as (27) shows. Where K_p is the proportional gain, and T_i is the integer time.

$$PI(s) = K_p + \frac{1}{sT_i} \tag{27}$$

The communication delays in the WTG control for processing the external references and the different sampling and hold systems, can be modelled as a pure delay (e^{-sT}) with a time constant T.

V. DFIG Turbine Equivalent Representation

The following section groups and simplifies all the mentioned transfer functions.

A. Generator and Current Control

Grouping the generator and current control transfer functions (17) and (6), we achieve the structure depicted in Fig. 6, which shows the transfer function from the rotor currents reference and stator voltage, to the reactive stator current (I_{qs}).

From the rotor reactive current reference to the stator reactive current:

$$G_{Irefq}(s) = \frac{PI_i G_c G_1 G_4}{1 + PI_i G_c G_1 F_i} \tag{28}$$

From the rotor active current to the stator reactive current:

$$G_{Irefd}(s) = \frac{G_2 G_4}{1 + PI_i G_c G_1 F_i} \tag{29}$$

From the stator voltage to the stator reactive current:

$$G_{Vds}(s) = G_5 + \frac{G_4 G_3}{1 + PI_i G_c G_1 F_i} \tag{30}$$

The link of (28), (29) and (30) is show below.

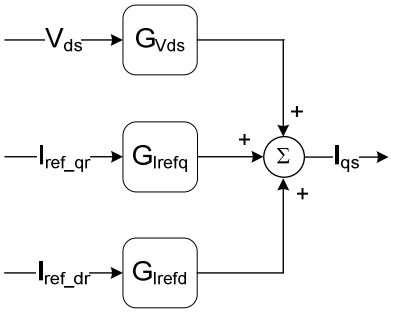

Fig. 6. Transfer function of the generator and current control

The transfer functions G_{Vds} and G_{Irefd} can be considered as a disturbance for the injected I_{qs}.

B. Generator, Current Control and Reactive power control

Grouping all the mentioned transfer functions, for the reactive power loop the following structure is obtained.

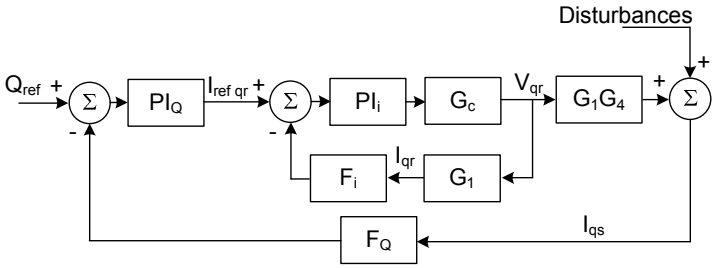

Fig. 7. Transfer function of the generator, current and Q control

Note that for representing the WTG reactive power control loop, the following assumption, valid for small signal analysis, has been made ($\Delta V \approx 0$).

$$\Delta Q = V_d \Delta I_q + \Delta V_d I_q \approx \Delta I_q \tag{31}$$

Therefore, the obtained structure for the reactive power WTG control loop is the following one.

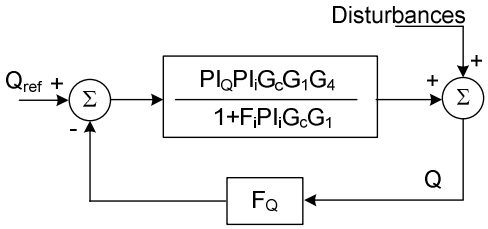

Fig. 8. Transfer function of the Q control loop

$$Q \approx I_{qs} = G_Q Q_{ref} \tag{32}$$

Where:

$$G_Q(s) = \frac{PI_Q PI_i G_c G_1 G_4}{1 + F_i PI_i G_c G_1 + F_Q PI_i PI_Q G_c G_1 G_4} \tag{33}$$

This transfer function can be simplified further, since the system response is dictated by the poles most closed to the origin. Therefore, the reactive power response of the WTG can be represented by a first order function (34) with the same bandwidth as (33).

$$G_Q(s) = \frac{1}{1 + sT_{WTG}} \tag{34}$$

VI. Grid Model

In this section the representation of the grid is studied. The impedances of the grid are considered as an L, R system, thus neglecting the small capacitances.

$$\underline{\Delta V} = R\underline{i} + \frac{d}{dt}\underline{\Psi} \tag{35}$$

ω_s is the fundamental frequency of the grid.

$$X = \omega_s L \tag{36}$$

Where the d axes is aligned with the direction of $\underline{V}$, and a positive I_q current is capacitive current.

$$\begin{aligned} \Delta V_d &= (R + s\frac{X}{\omega_s})i_d + Xi_q \\ \Delta V_q &= (R - s\frac{X}{\omega_s})i_q + Xi_d \end{aligned} \tag{37}$$

For small disturbances we can assume the following approximation:

$$\left|\underline{V} + \underline{\Delta V}\right| = \sqrt{(V + \Delta V_d)^2 + \Delta V_q^2} \approx V + \Delta V_d \tag{38}$$

Supposing that the active power is not changing (i_d=cte) the transfer function between the injected reactive current and the perturbed voltage system is written as:

$$\Delta V \approx \Delta V_d = Ri_d + Xi_q \tag{39}$$

Further, the Ri_d term can be considered as a perturbation to the control. Therefore assuming that the impedance of the grid is:

$$\underline{Z}_{GRID} = R_{GRID} + jX_{GRID} \tag{40}$$

Then, the final perturbed voltage, valid for small signal analysis is equal to:

$$\Delta V \approx -X_{GRID} i_q \tag{41}$$

VII. Plant Control

The proposed WPP used in the paper is controlled by a slope control, which is widely used in power system applications since it allows paralleling generators with individual voltage slope controllers without hunting phenomena or instability. This voltage controller will cause the injection of reactive power proportionally to variation of voltage levels [9].

The slope gain can be defined as follows:

$$Slope = \frac{\Delta V}{\Delta Q} \tag{42}$$

The control law that applied for the slope concept can be defined in a generic way as the following one:

$$Q_{ref} = Q_0 + \left(\frac{1}{Slope}\right)(V_{ref} - V_m) \tag{43}$$

The plant control receives the references and feedback (measurements) and outputs the turbine set-points. The control architecture is represented as a gain (K_{slope} = 1/Slope), following (43).

VIII. Wind Power Plant Model

This section presents the model of the WPP including the grid which is connected with. As can be seen in Fig. 9 all the previous models have been linked together coherently according to Fig. 1.

The measurement block or "grid meter" can be represented by a first order function with a time constant of T_m as (25), [10]. The "grid meter", which provides the feedback signals for control, samples at very high frequency values the output of the CTs and VTs, located at the PCC. This meter processes the signals by first calculating one cycle rms value of the signals, then filtering for anti-aliasing.

The communication delays and control sampling effect of the WTG and the WPPC can be represented together as an exponential delay function with a time constant T_{comm}. The exponential function should be linearized when doing the control analysis, e.g. by using Pade approximation.

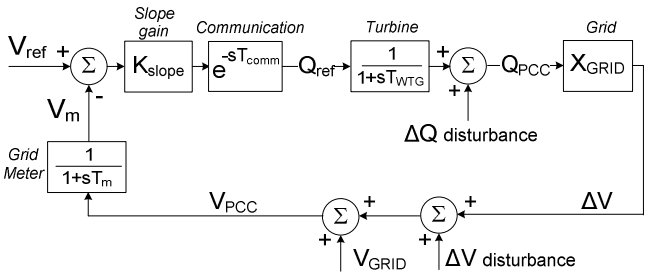

Fig. 9. Simplified representation of the WPP, grid and voltage control

IX. Model Validation

In order to validate the transfer functions listed in the above sections, some cases are simulated in PSCAD using a full representation wind turbine model, which includes the converters and the mechanical part [11].

The simulated cases show different slip operation points. For a maximum active power production, the slip is 0.12 pu, in this case the generator rotational speed is above synchronous speed. For low active power injection the rotational speed corresponds to a slip that is below synchronous speed.

The I_{ref_qr} has been stepped in every case, and the output I_{qs} of the detailed model and the transfer function, depicted in Fig. 6, are plotted. In the following figures; *TF* represents the model using the transfer functions with a fixed slip equal to 0.12 pu, and *PSCAD* represents the full model of the WTG simulated in PSCAD program.

A. *Generator and Current Control*

The simulation test setup can be seen in Fig. 6. In all the simulations the V_{ds}, I_{ref_qr} and I_{ref_dr}, obtained from the PSCAD WTG model, are used as an input to the transfer functions. The I_{ds} signals, obtained from the detailed WTG model and the transfer function, are plotted.

The tests show, for different levels of active power injection, the measured I_{qs} response when stepping the I_{qs} reference.

Fig. 10 shows the response to a step in I_{qs} reference when having maximum active power injection from the WTG.

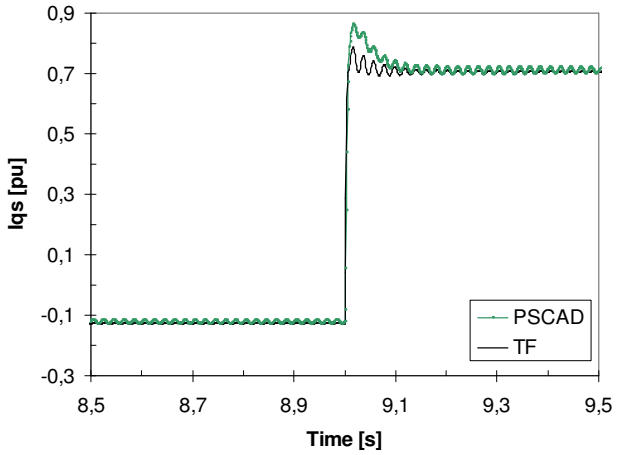

Fig. 10. I_{qs} response when having maximum active power injection.

Fig. 11 shows the response to a negative step in I_{qs} reference when having medium active power injection from the WTG.

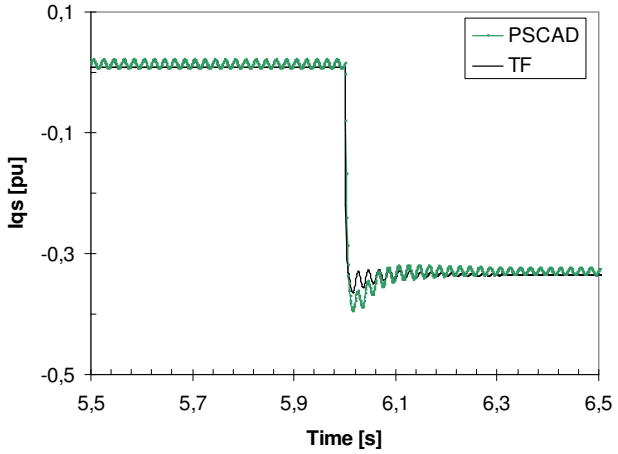

Fig. 11. I_{qs} response when having medium active power injection

Fig. 12 shows the response to a positive step in I_{qs} reference when having medium active power injection from the WTG.

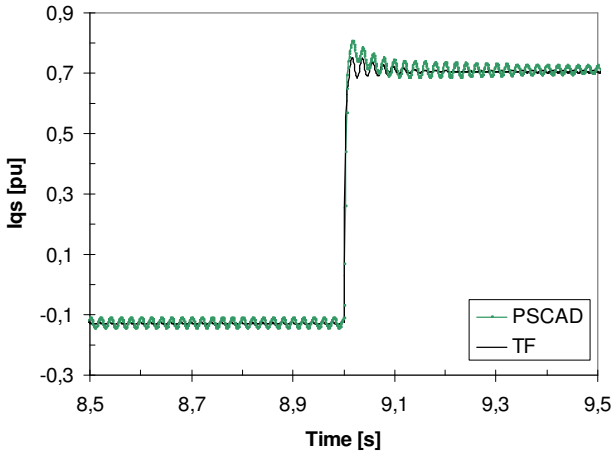

Fig. 12. I_{qs} response when having medium active power injection

Fig. 13 shows the response to a negative step in I_q reference when having low active power injection from the WTG.

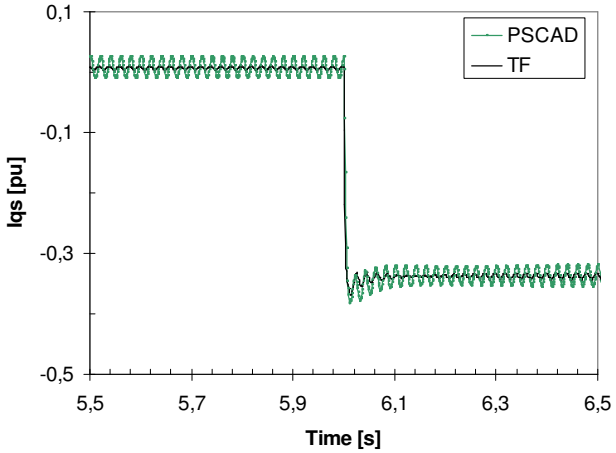

Fig. 13. I_{qs} response when having low active power injection

B. *WPP Control, Grid, Generator, Current Control and Reactive Power Control*

This section compares the dynamic behaviors between the transfer function representing the WPP with a centralized voltage controller (see fig. 9), with the detailed WPP model which includes the full WTG representation and the other electrical system components, such as the transformers and grid impedance (see fig. 14).

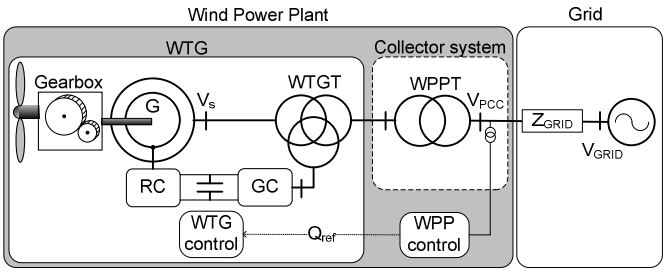

Fig. 14. Detailed model representation.

The schemes depicted in Fig. 9 and Fig. 14 are simulated in PSCAD program and compared.

The simulations have been made for different active power injection levels and SCR scenarios to check the validity of the applied simplifications and linearization to the transfer functions. In all the cases a disturbance in the grid voltage is applied. The voltage of the grid (V_{GRID}) is stepped down from 1 pu to 0.95 pu at 6 s, and after two second is stepped back to 1pu.

TABLE I
SIMULATED CASES

Case	*Active power [pu]*	*SCR*
A	0.15	10
B	1	10
C	0.15	25
D	1	25
E	0.15	5
F	1	5

The following figures show the results of the simulated cases. For every case, the measured voltage and reactive power at the PCC are plotted.

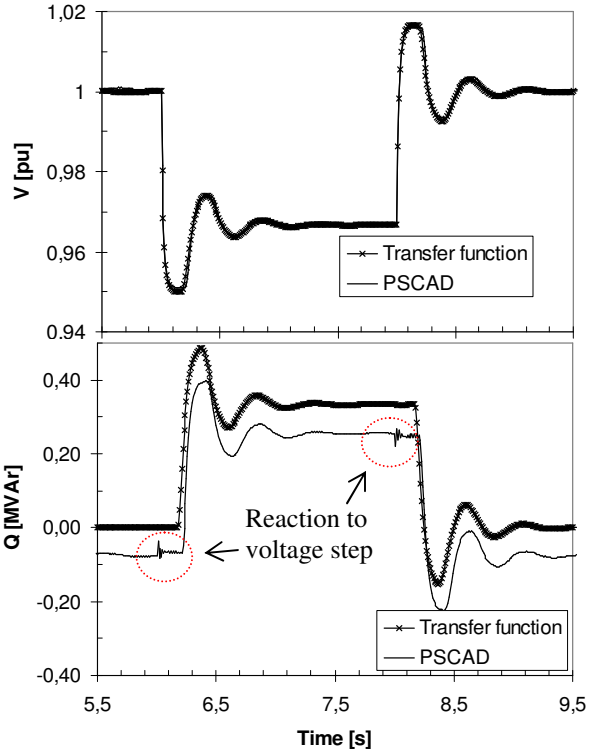

Fig. 15. Case A.

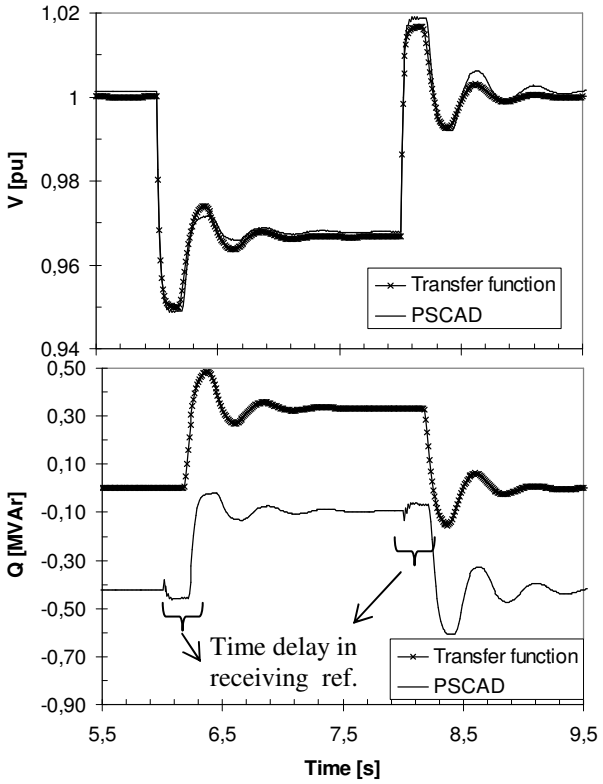

Fig. 16. Case B.

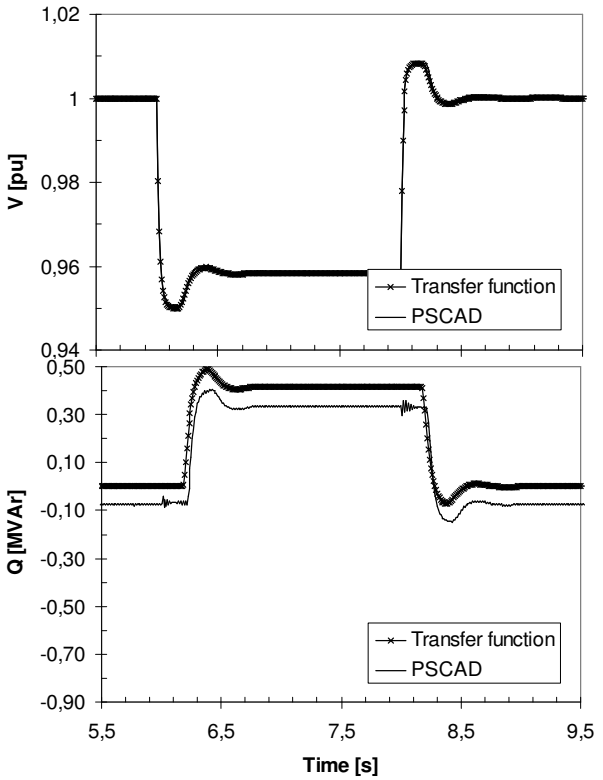

Fig. 17. Case C.

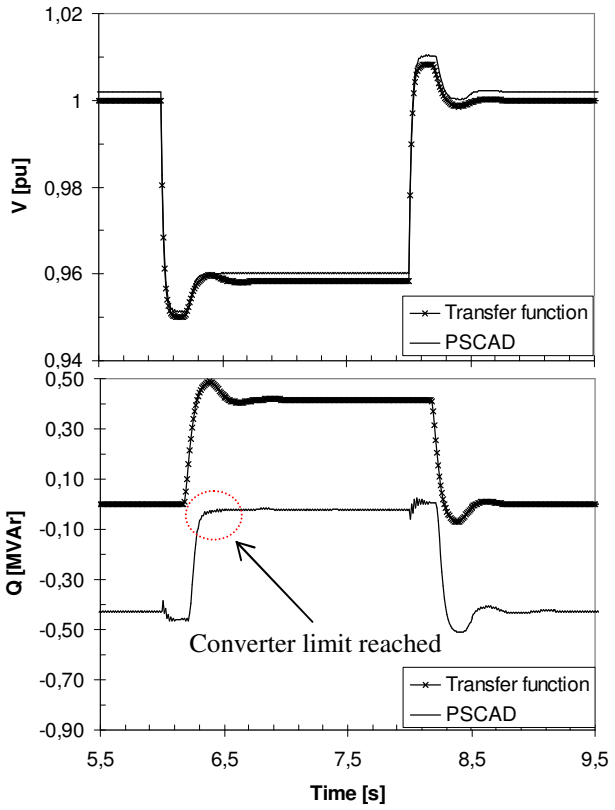

Fig. 18. Case D.

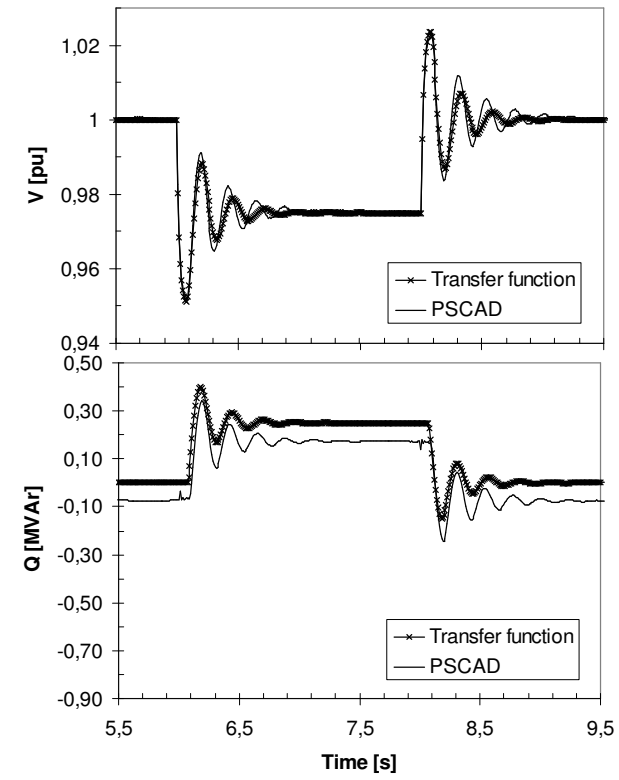

Fig. 19. Case E.

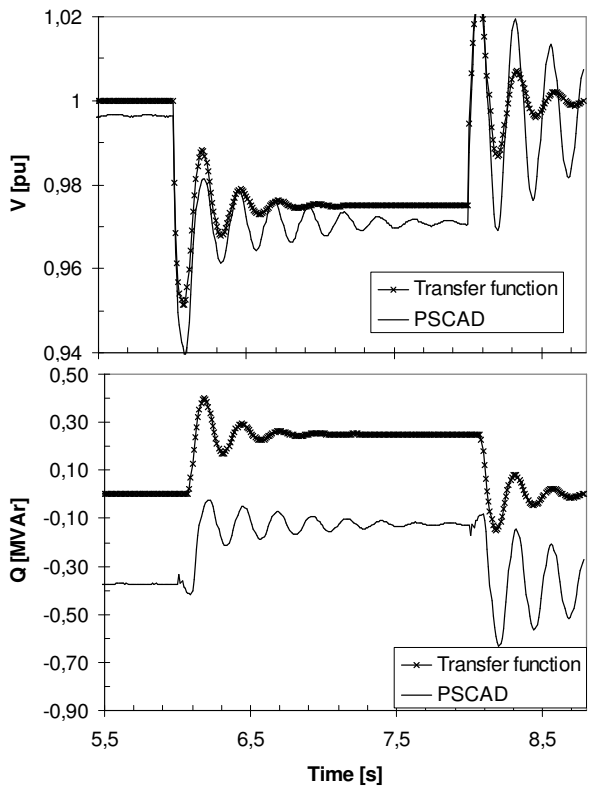

Fig. 20. Case F.

Basis on the previous figures, the following conclusions are extracted:

a) The simplified transfer functions of the system are representing the dynamics of the system in the bandwidth of interest.

b) At full active power, the Q measured at the PCC differs from the one calculated with the TF, since the internal reactive power losses that occurs inside the plant due to the current flowing (I) are not taken into account. To compensate for these losses a term can be added to the obtained reactive power, following (44). This term will offset the obtained value of Q, but will not change the dynamics of the system, therefore the same pole-zero map will be obtained. Fig. 21 shows Case A when using (44), for correcting the obtained Q.

$$Q\_corrected \approx Q - X_{WPP} I \tag{44}$$

c) At full active power injection and high SCR the voltage dynamics could differ at some points since the real WTG could enter into saturation limits when reaching the maximum reactive current injection

allowed by the rotor converter or generator. See Fig. 18.

d) For SCR ≤ 5 the dynamics of the simplified transfer functions are not valid since the coupling between the P-Q terms, see (37), starts influencing the dynamics of the voltage. See Fig. 19 and 20.

The boundaries for using this simplified system representation can be established. For high SCR the current injection limitation of the converters or generator could be presented, and for low SCR the assumption of a perfect decoupling between P-Q is not valid anymore, thus making not suitable the use of this simplified model.

To obtain more accuracy in the system voltage dynamics for low SCR, the WTG mechanical part and its control should be added into the system representation, thus making quite difficult to extract the zero-pole map of the system.

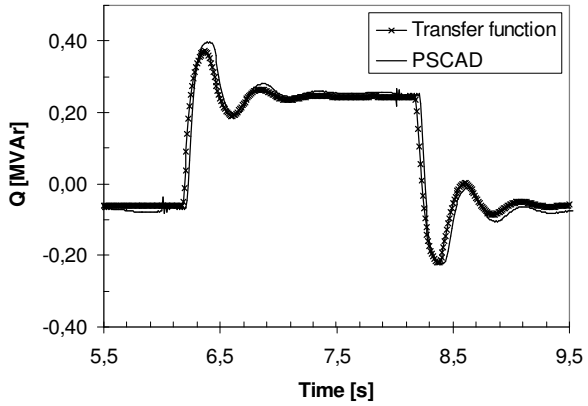

Fig. 21. Case A, with corrected Q.

X. Conclusions

This paper shows how a wind power plant of DFIG turbines with a centralized voltage controller can be represented as a simplified transfer function, in order the zero-pole map of the system can be used for WPP voltage control studies. This can be used as a preliminary adjustment of the WPP control. This first stage of tuning and understanding the system stability will help in the most complex process of re-tuning the plant control when using EMT models to represent the WPP components and grid.

The accuracy of this representation depends on two factors; the capability of the converter to inject current, meanly can be said that care should be taken for using the model inside the proper boundaries to avoid entering into saturation zones, and for low SCR the coupling between the active and reactive power in the voltage dynamics invalidates this representation.

In conclusion, it can be said that this simplified transfer function can represent with high accuracy the dynamics of the system when voltage control is of interest and when moving inside the above mentioned boundaries.

XI. References

[1] I. Erlich, U. Bachmann, "Grid Code requirements concerning Connection and Operation of Wind Turbines in Germany". IEEE Power Engineering Society General Meeting, 12-16 June 2005;1253-1257 Vol.2.

[2] P.O.12.2, "Connected installations to the transmission Spanish system: Minimum requirements for design and security", Red Electrica de Espana, Grid Code Requirements for installations connected to the transmission system in Spain.

[3] National Grid Electricity Transmission: "Guidance Notes for Power Park Developers ", 2008

[4] Alberta Electric System Operator (AESO): Wind Power Facility, Technical Requirements, Alberta, Kanda, November 2004.

[5] Hydro-Quebéc, Technical Requirements for the Connection of Generation Facilities to the Transmission Systems, Quebéc, Canada,

[6] G. Tapia, A. Tapia, and J. Ostolaza, "Proportional-Integral Regulator-Based Approach to Wind Farm Reactive Power Management for Secondary Voltage Control". IEEE Transactions on Energy Conversions, Vol.22, No.2, June 2007.

[7] El Moursi, M.; Joos, G.; Abbey, C., "A Secondary Voltage Control Strategy for Transmission Level Interconnection of Wind Generation", Power Electronics, IEEE Transactions on, Volume 23, Issue 3, May 2008 Page(s):1178 - 1190

[8] M. P. Kazmierkonski, R. Krishman. "Control in Power Electronic" Academic press 2002, Pages(s):92-130

[9] Stankovic, A.; Ilic, M.; Maratukulam, D. "Recent results in secondary voltage control of power systems", Power Systems, IEEE Transactions on ,Volume 6, Issue 1, Feb. 1991 Page(s):94 - 101.

[10] P. Kundur, "Power System Stability and Control", 1994 McGraw-Hill, Inc. ISBN 0-07-035958-X

[11] Morren J, de Haan SWH. "Ride through of Wind Turbines With Doubly-fed Induction Generator during a Voltage Dip". IEEE Transactions on Energy Conversion 2005; 20: 435–441.

XII. Appendix

TABLE II
Electrical Data of Wind Turbine

Parameter	Value	Unit
S_{base}	2100	[kVA]
V_{base}	0.69	[kV]
Electrical frequency	50	[Hz]
Stator Resistance	0.006	[pu]
Rotor Resistance	0.009	[pu]
Mutual Inductance	3.422	[pu]
Stator Inductance	0.072	[pu]
Rotor Inductance	0.101	[pu]
S step-up transformer 0.69:20kV	2100	[kVA]
Z step-up transformer	0.08	[pu]

TABLE III
Electrical Data of the System

Parameter	Value	Unit
X_{WTGT}	0.08	[pu]
R_{WTGT}	0.007	[pu]
X_{WPPT}	0.1191	[pu]
R_{WPPT}	0.0049	[pu]
X_{GRID} /R_{GRID}	3.75	
Medium voltage level	30	[kV]
High voltage level	115	[kV]

A.7

"Design and Coordination of a Capacitor and OLTC control for a Wind Power Plant of DFIG Wind Turbines"

Jorge Martínez, Philip C. Kjær, Pedro Rodriguez, Remus Teodorescu.

Design and Coordination of a Capacitor and OLTC control for a Wind Power Plant of DFIG Wind Turbines

Jorge Martínez, Philip C. Kjær, Pedro Rodriguez, Remus Teodorescu.

Abstract— **Larger percentages of wind power penetration into the grid translate to more demanding requirements coming from the grid operators, for example, voltage support at the point of connection has been introduced recently by several grid codes from around the world. For a wind power plant of DFIG turbines, reactive power capability can be a challenge.**

In this paper it is introduced a novel coordination and control strategy for capacitor banks and tap changer for a DFIG wind power plant. The capacitor banks are controlled by the wind power plant control in such way that the steady-state usage of the converters for reactive power injection is driven below to a maximum desired value of 0.1 pu. Also, the control transients due to the capacitor bank switching is minimized by using a suitable control structure. The tap changer control of the substation transformer is coordinated with the plant control to decrease the impact of the capacitors reactive power in the line drop calculation, thus reducing the amount of tap operations and improving the accuracy of the line drop voltage estimation.

The coordination of the central controller with the plant components is analyzed and tested through simulations with EMTP.

Index Terms—**Wind turbine generator, OLTC, capacitor bank, voltage control, doubly-fed generator, STATCOM.**

I. Nomenclature

COMM	Communication
CAP	Capacitor bank
DFIG	Doubly Fed Induction Generator
EMTP	Electromagnetic Transient Program
MSC, MSR	Mechanical Switched Capacitor and Reactor
MV, LV	Medium and Low Voltage
OLTC	On Load Tap Changer
P, Q	Active, Reactive power
PCC	Point of Common Coupling
PF	Power Factor
RTU	Remote Terminal Unit
SCR	Short Circuit Ratio
STATCOM	Static Compensator
TSO	Transmission System Operator
V, I	Voltage, Current
WPP, WTG	Wind Power Plant, Wind Turbine Generator
WPPC	Wind Power Plant Controller
WPPT	Wind Power Plant Transformer
ω	Angular frequency
X, R, L	Reactance, Resistance and Inductance
Z	Impedance

Subscripts

d, q	Direct and quadrate axes
ref	Reference

Manuscript June 28, 2010.

J. Martínez and P. C. Kjaer are with VESTAS Wind System, Power Plant R&D.
R. Teodorescu and P. Rodriguez are with Aalborg University.

II. Introduction

With increasing penetration of wind power generation, the requirements for the connection of WPPs to the electrical grid are defined by new and emerging grid connection codes. The grid connection requirements vary in different parts of the world, but they share common aims, such as permitting the development, maintenance and operation of a coordinated, reliable and economical transmission or distribution system. Wind power plants differ from other traditional generation sources; thus, they are particular in certain aspects of their control and layout [1]. Therefore, replacing traditional power plants, including their control characteristics, during periods of strong wind could be a concern. Grid operators are solving this challenge by means of creating specific sections in the grid codes for WPP performance.

The new requirements generally demand that wind power plants provide ancillary services to support the network in which they are connected [2]-[6]. In the present case, voltage regulation is of interest, and it has been introduced recently by some grid operators. Voltage regulation with wind power plants entails the integration of all the available control devices installed at the substation and plant. Mainly, these are the reactive power compensators and the OLTC control.

Normally, the requirements of the utilities can be solved by the turbines and the park controller. When the wind turbines are not enough to fulfill the grid code requirements, then reactive power compensation equipment should be installed. This equipment could be: static compensators (e.g. STATCOM) if the plant needs more voltage dynamic capability, mechanical switching capacitors/reactors if the requirement is related to steady state performance, or just it simply could be a combination of both. The adoption of each one of the possible solutions, and choosing the method and combination of components for voltage regulation is one of the design decisions. The prevalent position is minimizing the cost of investments while offering the fulfillment of the requirements.

In this paper, a wind power plant with a secondary voltage controller scheme is used in order a fast system reaction to voltage disturbances is achieved [7]-[12]. The implementation of this concept is done by including in the WTGs and the STATCOM a local voltage control, which will follow the voltage references calculated by the plant control.

The dynamic voltage regulation will be done based on the installed converter capacity, this is viewed primarily as a fast VAr source, whereas the OLTC and the capacitor banks are seen as steady-state compensators, used for keeping the voltage area of the WTGs inside limits and for reducing the use of the dynamic compensation during permanent disturbances.

It is clear that the coordination between the different controllers will improve the performance of the plant.

III. Studied Wind Power Plant

A diagram of the studied WPP is depicted in Figure 1. This WPP is comprised by DFIG wind turbines, which are represented as a single aggregated one, connected through an equivalent cable to the medium substation bus-bar, and a STATCOM unit which is connected to the same bus-bar and is located close to the main transformer, therefore the cables connecting it to the MV bus-bar can be neglected. Moreover, two mechanical switch capacitors are added, which are also located in the same substation. The main substation transformer includes an OLTC which is controlled locally. All these elements need to be coordinated by a central plant control (WPPC) since counter-action between them has to be avoided. The plant control used in this paper offers a coordinated voltage control at the PCC, where the energy has to be delivered following some grid code requirements.

The electrical single-line diagram of the WPP with all the main components is given in Figure 1. In this figure it can be seen how the main components are linked with a dotted line, representing the communication plant networks. This communication link is used by the plant control, among other things, to command the operation of the capacitor banks, WTGs and STATCOM. The WTGs and STATCOM inject the desired power dictated by the plant control. These WTGs and STATCOM use a conventional decoupled d-q control system which has been designed based on linear control system techniques and it consists of an outer loop voltage control which can be adjusted by the external reference sent by the plant control. This outer control loop sets the reference for the inner current control system. The active and reactive powers are controlled using the d and q axis respectively [13]-[14].

The variable speed doubly fed generator allows full control of generator active and reactive power, using the rotor-connected frequency converter. Its rating is in the order of 0.3 pu. Operating both with sub- and super-synchronous speed, the active power can be fed both in and out of the rotor circuit. The size of the rotor converter limits the reactive power injection capability, especially at full power.

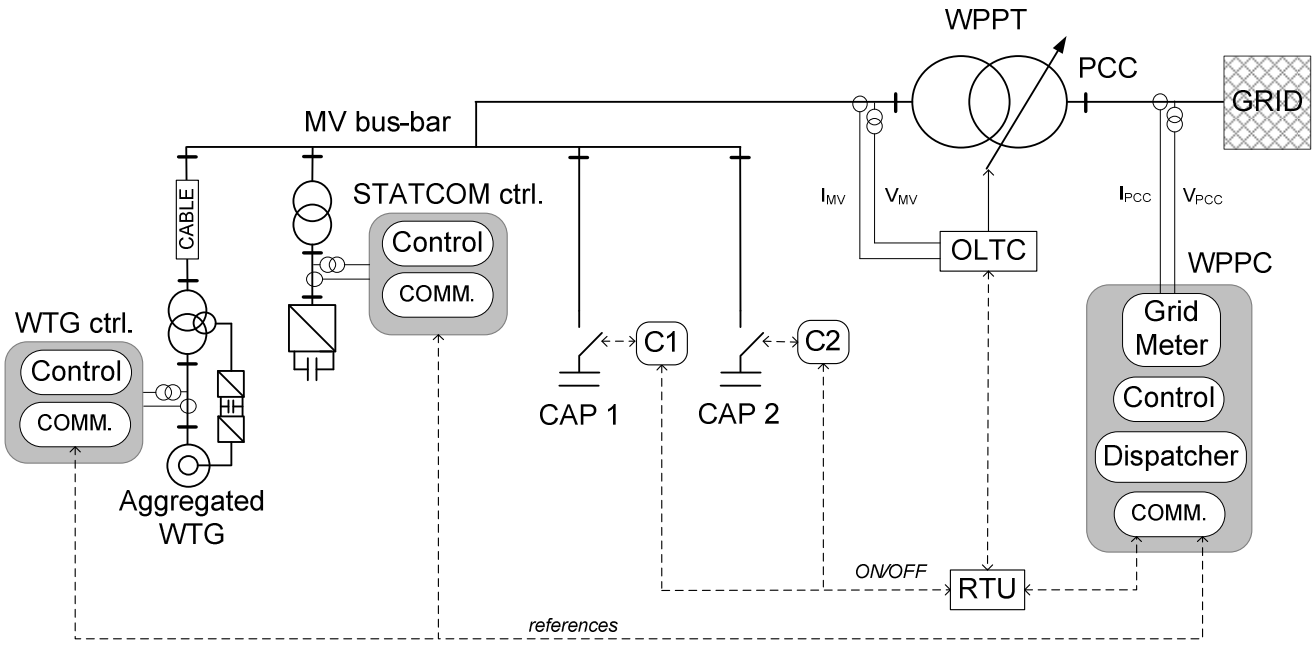

Figure 1. WPP single line diagram.

Since most of the grid codes ask for having a voltage capability regulation within a minimum power factor of 0.95 [4], the limited DFIG Q injection for high active power productions implies not fulfilling this requirement. To solve this situation, reactive power compensation equipment should be installed in the wind power plant.

Following figure shows the P-Q chart of the DFIG obtained at the generator stator terminals (dotted blue line) and at the PCC (black line). It can be seen how at the PCC level the reactive power losses inside the plant decrease the available capacitive reactive power, in the other hand the inductive power capability at the PCC is increased.

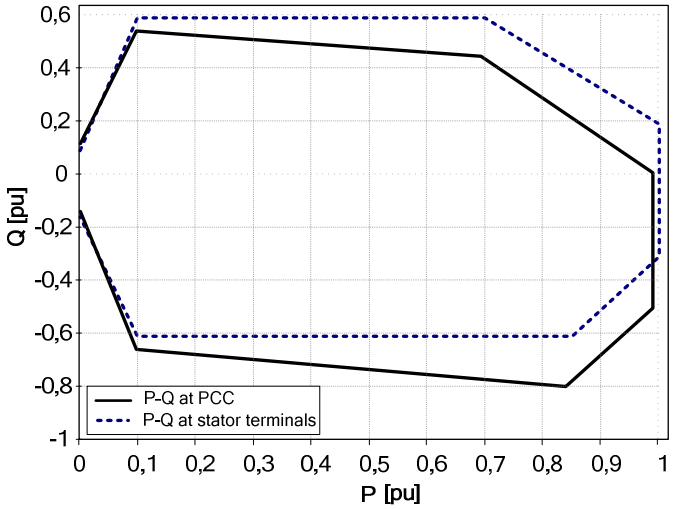

Figure 2. Load flow analysis at PCC and WTG level.

As it was expected, this reduced capacitive reactive power at PCC, almost PF = 1, makes necessary to install reactive power compensation equipments, such as a STATCOM and/or capacitor banks. The amount of extra VAr needed can be calculated by means of a load flow analysis for different wind level productions and grid voltages. The needed extra VAr can be supplied by a STATCOM (if fast response time to disturbances is required) or by capacitor banks (if no time or very slow response time is required). In the present case, the selection of the STATCOM is done based on grid code requirements related to fast time response to grid disturbances and it is sized basis on load flow calculations. The amount of extra dynamic VAR needed from the STATCOM is chosen to be 0.25 pu of the total plant power.

Voltage regulation including static converters, e.g. DFIG or STATCOM, is viewed primarily as a fast VAr source to

counteract rapid and unexpected voltage disturbances [15]-[18]. In order to fulfill this condition, it is necessary to ensure that the converters will have sufficient VAr capacity to handle unpredictable disturbances; for this reason the WPPs can include switchable capacitor (MSCs) for keeping the dynamic capability of the converters to the maximum and reducing the switching converter losses. It should be noted that the operation of these switchable components is considered as a way to offset the operation level and not as a voltage regulation itself.

The MSCs control strategy proposed in this paper is based on the idea that the steady state operation of the Q injected by the converters is inside the range ± 0.1 pu (which can be called steady-state converter operation band), in this way the step sizing of the capacitor banks and its control are designed accordingly. The maximum size of the capacitor steps has to be equal to the size of the chosen converter operation band. The change in system voltage upon capacitor bank switchings are also to be considered when deciding the maximum size of the banks in the design process. It is possible that the size of step-change in voltage from a switching event must be kept below a certain percent specified by the transmission owner.

One should realize that the bigger the steady state converter operation band, the lower the amount MSC switching operations, but the bigger the energy losses due to the transportation of Q inside the plant and converter switching.

For the inductive operation area, MSRs are not included for two reasons; firstly the DFIGs by themselves can reach more than needed the maximum inductive operation point at the PCC, and secondly with an operation band of 0.1 pu the required inductive reactive power (PF= 0.95 ind.) at the PCC is reached.

The following figure shows with a black line the combined operation of the DFIG and the MSCs for the capacitive area and for the inductive area only the DFIG operation is considered. The red line shows the P-Q grid code requirements at the PCC, and the dotted green lines are showing the P-Q profile obtained when the DFIG are operating at 0.1 pu capacitive and inductive. The flat green line shows the P-Q obtained when the DFIGs are operating at PF = 1 at generator terminals.

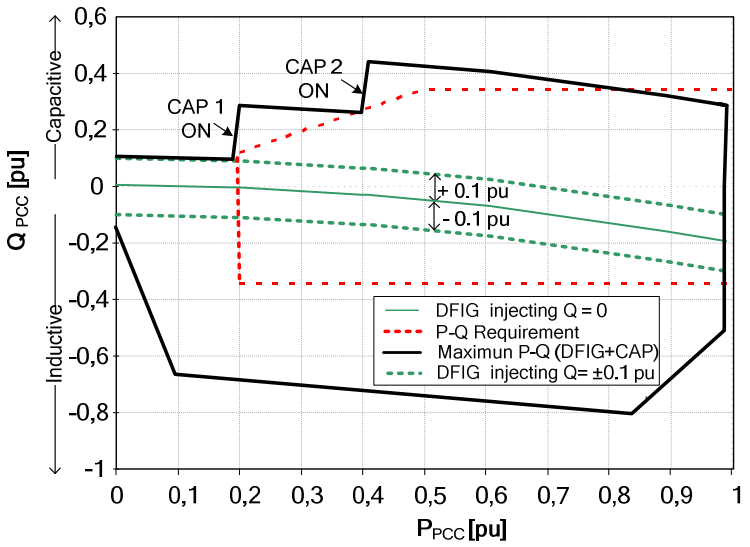

Figure 3. Wind power plant load flow analysis at the PCC and P-Q requirements.

It can be seen in the Figure 3, that at full power there is a lack of reactive power according to the requirement, but one should realize that the reactive power of the STATCOM is not included in this figure; therefore the requirement can be fulfilled without any concern.

IV. Wind Power Plant Controller (WPPC)

Whenever the WPPs are required to control the characteristics of the power injected at the PCC, a centralized control is needed, which supervises and commands the power injected at the PCC, following design requirements.

The plant control (WPPC) receives the references and feedback (measurements) and outputs the turbines and STATCOM set-points, and also the switching commands for the capacitor banks. This plant control includes a measurement device which senses the currents and voltages at the PCC, a dedicated computer which allocates the control and dispatcher algorithms, and a communication hub, which collects all the feedback, packs and sends all the necessary references for the correct operation of the WTGs, STATCOM and capacitor banks. This communication hub exchanges the control references and other signals with the WTGs, STATCOM and capacitor banks, using for that purpose the communication WPP Ethernet network and specific protocols. Figure 1 shows in details the connection between the plant components.

The voltage plant control used in this paper is based on a proportional controller, also called slope control. Normally, the gain of the voltage controller (K_{slope}) and the plant voltage reference (V_{ref_plant}) are defined by the TSO.

The plant control law can be defined as (1).

$$K_{slope} = \frac{1}{Slope} = \frac{\Delta Q_{PCC}}{\Delta V_{PCC}} \tag{1}$$

The slope controller is the outer loop, which is complemented with a plant reactive controller to compensate the Q losses that occur inside the plant. The output of this control is the total reference to be sent to the WPP components (V_{ref_total}). Before this reference is sent to them it is altered by the capacitor control, which may subtract/add a fraction (ΔV_{Cap}) to the reference, if one of the capacitor steps is going to be connected/disconnected, see Figure 4. This is done to minimize the transient effect of the capacitor switching in the plant control. After this, the reference (V_{ref}) is processed by the dispatcher block, which splits the calculated reference among the WTGs and STATCOM.

The dispatcher has the functionality of splitting the references calculated previously (V_{ref}) into the STATCOM and WTGs composing the WPP. The way of splitting the reference can be done following several strategies, e.g. minimization of lost of energy production. The strategy used in this paper is based on using the STATCOM as a reactive power back-up when the reactive power injected by the WTGs is not enough for grid code fulfillment.

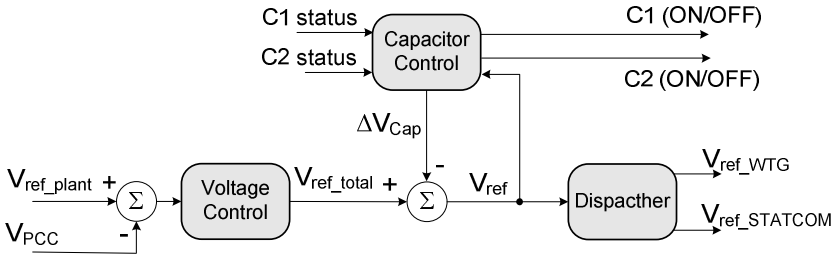

Figure 4. Plant voltage control, including the capacitor control.

The proposed Capacitor Control is depicted in Figure 5, and uses as an input the previous calculated V_{ref} to calculate the needed reactive power (Q_{ref_cap}) by using (2), where K_{WTG} is the slope gain of the local voltage control of the WTGs and STATCOM. This Q_{ref_cap} reference is compared with a threshold value (Converter operation steady-state); if the reference is greater than this level, then the output is set to Q_{ref_cap} otherwise it remains 0. The Switching Logic block processes this signal and decides which step to connect/disconnect based on some timer functions and the current status of the capacitors. Finally, the outputs of the block are the switching commands to the capacitor steps and the ΔV_{Cap}, which will offset the V_{ref_total}.

The effect of this ΔV_{Cap} is to center the disturbance of the capacitor connection, thus decreasing the peak value of the transient. The action of the ΔV_{Cap} offset is disabled when disconnecting the capacitors and the measured voltage is greater than 1.08 pu, as well as when connecting capacitors and the voltage is below 0.93 pu. In these situations, it is better not to center the transient, to avoid increasing/decreasing the voltage even more.

Attention should be drawn to the input reference connected to the capacitor control (V_{ref} instead V_{ref_total}), doing in the way that is shown in Figure 4, it is ensured that the processed V_{ref} is the one related to the operation of the WTGs and STATCOM.

$$(1-V_{ref})K_{WTG} \approx Q_{ref\_cap} \tag{2}$$

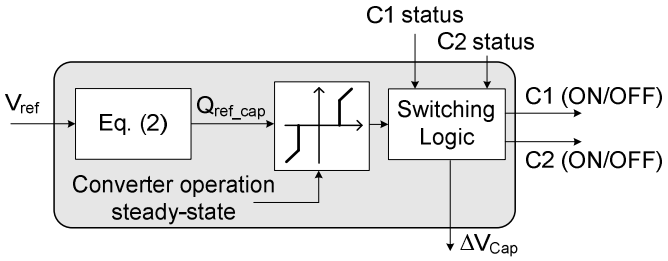

Figure 5. Proposed capacitor control.

V. RTU

Usually a substation RTU monitors the field digital and analog parameters received from the different elements composing the substation, and transmits relevant data to communicate to other RTUs and control centers, as well as it is able to execute

simple supervisory tasks related to protection. The RTU can be interfaced with different communication media, usually Ethernet and can support standard protocols to interface any third party software. The gathering of direct-wired process information and its transfer to a higher level control system is one of the major tasks of the remote control application. The concentration of several functions on a central communication gateway reduces the number of required communication lines to higher control level. This approach results in higher availability for the electrical system [19]. As it can be seen in Figure 1, the RTU monitors the transformer tap position and status of capacitor breakers and contactors, and receives the switching commands to the capacitors sent by the WPPC. The RTU will transfer these commands to the capacitor switches when the security and integrity checking have been done.

VI. OLTC

The wind power plant transformer includes an OLTC and its voltage control. The tap changer voltage control commands the transformer on load tap changer, so that the controlled voltage, in this case the medium voltage side (the OLTC measurement sensors are located at medium voltage side of the transformer) is practically constant independently from the wind speed level and voltage grid conditions. To achieve this, the tap control will select the right position of the OLTC in the power transformer. An important requirement for tap control is, however, not only to keep the voltage profile but also to suppress the frequency of operations to the lowest possible. These requirements basically contradict each other since frequent operations are usually needed to perform a higher quality of voltages.

On-load tap changers are applied within several types of voltage control strategy used by transmission and distribution grid operators and some methods have been compared, discussed and proposed [20]-[21]. In this paper, a tap control strategy for a wind power plant is proposed, where the line drop used in the tap control is dependant on the capacitor bank status.

The line drop compensation function is to regulate the voltage at a remote point along the feeder. This voltage is estimated by computing the voltage across a fictitious impedance (gain K_L in Figure 6). By removing the capacitor current from the total MV current, the line drop function estimates the voltage with more accuracy. As a consequence of that, better voltage regulation and less tap movement actions are expected.

The main impedance between the WTGs and the medium voltage side of the substation transformer terminals is the WTG transformer. Choosing a half compensation of this impedance has been found to be a good compromise, since the higher the value of this impedance the bigger the deviation of the nominal medium voltage at MV bus-bar where other elements are connected, such as the capacitor banks.

The voltage plant and voltage tap controllers can be considered decoupled, for two main reasons: different control time response and different location of the voltage to control. The tap controller is controlling the medium voltage side, by changing the transformer winding ratio, whereas the WPPC is controlling the voltage at the high side of the substation transformer, by injecting Q. Looking at the time response of these two controllers it can be said that the WTGs and STATCOM are used for dynamic voltage control while the OLTC is used for steady-state voltage control.

A simplified diagram of a typical OLTC and its control is shown in Figure 6 [22]. The block called LOGIC includes the conditions to increase or decrease the tap position and is based on the input V_{error}, and typically allocates a timer which determines the duration of the voltage error exceeding the dead band value (D). The timer is increased if the error is outside the dead band and, it is reset if the error is within the dead band, either if there is a tap change or if the error oscillates above and below the dead band. Its operation is blocked in case that the voltage falls below some defined limits, (undervoltage blocking), and also when voltage or current exceeds another user defined limit (overvoltage or overcurrent blocking) [23].

Typical line drop compensations are calculated based on the measured reactive current at medium voltage side (I_{q_MV}) and a gain K_L. The DELAY block is used to prevent unnecessary tap changes in response to transient voltage variations or self-correcting voltage variations and to introduce the desired time delay before a tap movement is commanded. The tap motor action is modeled as a pure delay with a time constant T_m.

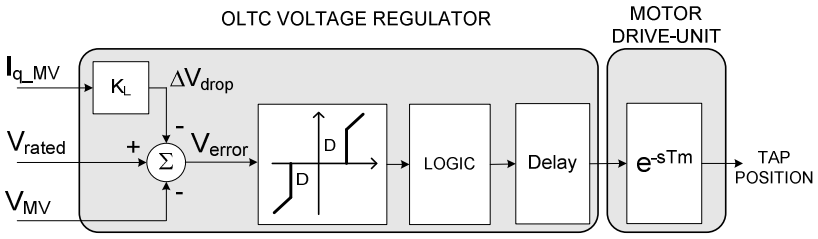

Figure 6. Typical OLTC scheme.

A. Proposed OLTC line drop compensation

In order the line drop calculation of the tap control works with more accuracy, the reactive current injection from the

capacitor banks should be removed. The reactive current injected by the MSCs is generated just at the MV bus-bar, thus is distorting the voltage drop related to the real distance to the converters, which the line drop should estimate. The following equations are used to explain this concept in more details, and they are extracted using the diagram depicted in the Figure 7. The resistances of the impedances are neglected.

$$V_{LV} = V_{MV} + X_w I_{q\_LV} \tag{3}$$

If no decoupling of the reactive current injected by the MSCs is done, (4) is obtained. In this case a deviance of $I_{q\_c}K_L$ in the line drop (ΔV_{drop}) is expected.

$$V_{ref} = V_{rated} - \overbrace{K_L I_{q\_MV}}^{\Delta Vdrop} = V_{rated} - K_L(I_{q\_c} + I_{q\_LV}) \tag{4}$$

If the decoupling of the MSCs current is done in the OLTC control, (5) is obtained and as it can be seen the K_L line drop gain can remove more clearly the impedance effect from the MV bus-bar to the WTGs. See (3) and (5).

$$V_{ref} = V_{rated} - \overbrace{K_L I_{q\_LV}}^{\Delta Vdrop\_improved} \tag{5}$$

This last $\Delta V_{drop\_improved}$ offers a close solution to what really is intended to do.

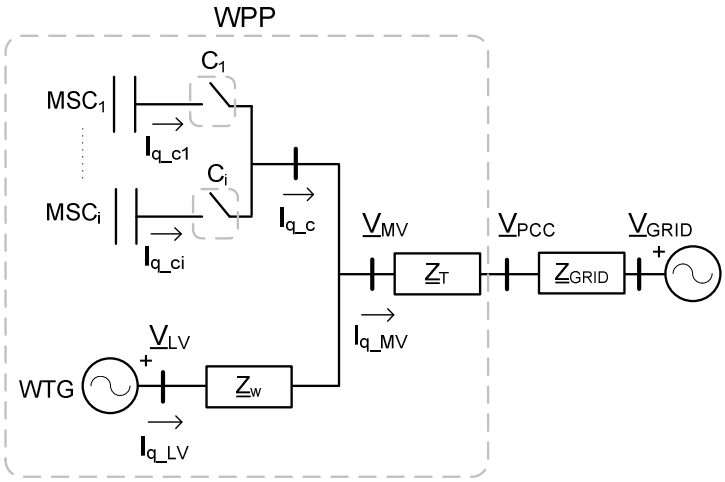

Figure 7. Single line diagram of a generic WPP with capacitor banks.

The desired current for the line drop control can be achieved by several ways. As an example, either the subtraction of the measured capacitor current (I_{q_c}) to the total measured current at MV (I_{q_MV}) is done, or the total reactive current injected by the WTGs and STATCOM is used directly. In both cases to implement these solutions it is needed to add new hardware.

One simple solution, without additional hardware requirements, is to send to the OLTC control the switch status ($C_1 \ldots C_i$) of the capacitor banks. This solution implies that the RTU exchanges the needed data with the tap control about the capacitor switch status in the existing communication link. Also, it is needed to add a simple algorithm inside the OLTC control, which will translate the received signals into the current injected by the connected capacitors. This current is calculated based on the rated capacitance of the capacitors and the measured voltage at medium side. As an example for 2 capacitor steps, the control function (6) can be used.

$$\begin{aligned}
&IF_(C1_ON.AND.C2_ON) \Rightarrow I_{q_c} = I_{q_c1} + I_{q_c2} \\
&IF_(C1_ON.AND.C2_OFF) \Rightarrow I_{q_c} = I_{q_c1} \\
&IF_(C1_OFF.AND.C2_ON) \Rightarrow I_{q_c} = I_{q_c2} \\
&IF_(C1_OFF.AND.C2_OFF) \Rightarrow I_{q_c} = 0
\end{aligned} \tag{6}$$

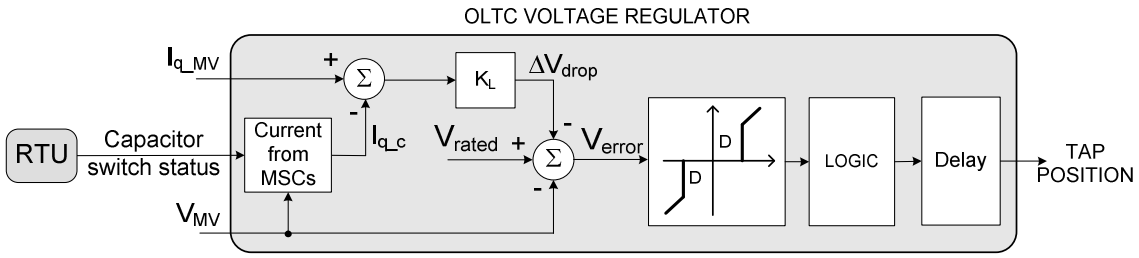

Figure 8. Proposed OLTC voltage control.

B. Interaction between the Plant and Tap Controls

The OLTC and plant controls work independently, thus they can not be considered perfectly decoupled, small interactions among the control actions are a natural consequence. This section studies the interactions of the OLTC voltage regulator in the voltage plant control, and the voltage plant control in the OLTC voltage regulator.

1) Affection of the OLTC Voltage Control into the Voltage Plant Control

The tap operation affects the medium bus voltage causing a consequent variation in the injected current at high voltage side of the transformer, which will cause at the end a variation in the voltage at the PCC. This is a clear counteraction between controllers, since an increment in the tap position to increase the MV will cause a decrement in the voltage at the PCC.

To study the magnitude of this counteraction the Figure 9 is used, which shows a simplified diagram of a transformer connected to a grid characterized by its impedance Z_{GRID}. I_{q_MV} is the reactive current injected at medium voltage side of the transformer. All the system is reduced to a pu system, and r reflects the tap position, for the neutral position r is equal to 1.

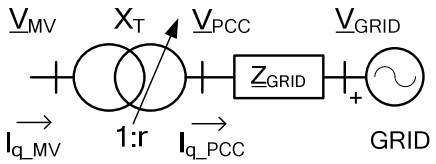

Figure 9. Simplified diagram to study the tap changer effect in the V_{PCC}.

Thus, using the above scheme the interactions of the tap control with the plant voltage control can be analyzed.
Neglecting the resistances of the impedances, the following equations can be extracted.

$$V_{PCC} = X_{GRID} I_{q\_PCC} + V_{GRID} \tag{7}$$

$$V_{MV} = X_T I_{q\_MV} + V_T \tag{8}$$

Where V_T is representing the measured voltage before the transformer positive sequence leakage reactance X_T.

$$V_T = rV_{PCC} \tag{9}$$

$$I_{q\_MV} = I_{q\_PCC} / r \tag{10}$$

Applying small increments, the following equations are obtained:

$$\Delta V_{PCC} = X_{GRID} \Delta I_{qPCC} + \Delta V_{GRID} \tag{11}$$

$$\Delta V_{MV} = X_T \Delta I_{q\_MV} + \Delta V_T \tag{12}$$

$$\Delta V_T = \Delta r V_{PCC0} + r_0 \Delta V_{PCC} \tag{13}$$

$$\Delta I_{q\_MV} = (\Delta I_{q\_PCC} / r_0) + (I_{q\_PCC0} / \Delta r) \tag{14}$$

For the sake of simplicity, I_{q_PPC0}=0 is considered before the perturbation.

$$\Delta V_{MV} = X_T \Delta I_{q\_MV} + \Delta r V_{PCC0} + r_0 \Delta V_{PCC} \tag{15}$$

$$\Delta r = (\Delta V_{MV} / V_{PCC0}) - (X_T \Delta I_{q\_MV} / V_{PCC0}) + (r_0 \Delta V_{PCC} / V_{PCC0}) \tag{16}$$

$$\Delta r = \left(\frac{1}{V_{PCC0}}\right)\Delta V_{MV} + \left(\frac{X_T}{r_0 X_{GRID} V_{PCC0}}\right)\Delta V_{GRID} - \left(\frac{X_T + r_0^2 X_{GRID}}{r_0 X_{GRID} V_{PCC0}}\right)\Delta V_{PCC} \tag{17}$$

Thus, the coefficient which correlates the variation of the tap position with the voltage at the PCC is as follows:

$$\Delta V_{PCC} = -\left(\frac{r_0 X_{GRID} V_{PCC0}}{X_T + r_0^2 X_{GRID}}\right)\Delta r \tag{18}$$

Following figure shows the variation of the voltage at PCC for different short circuit ratios and transformer reactances, when a change in the tap position of Δr = -0.01 pu is done. And as it was expected, tap operations with low SCRs and high transformer reactances are translated in higher voltage changes at PCC.

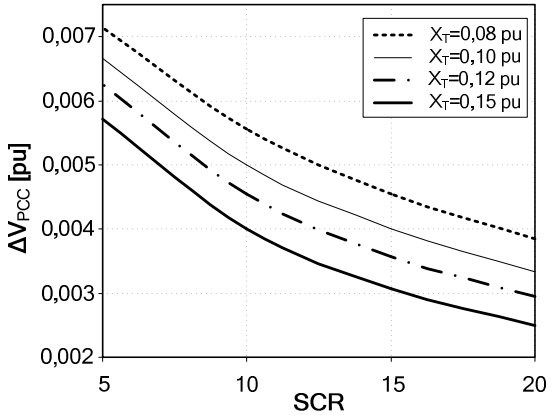

Figure 10. SCR vs. Changes in voltage at PCC for different transformer impedances.

2) Affection of the Voltage Plant Control in the OLTC Voltage Regulator

Also it is important to analyze the effect of the plant voltage controller in the voltage at medium side, where the OLTC control is located. For this purpose (19) can be used to obtain (20).

$$\Delta I_{q\_PCC} = K_{slope} \Delta V_{PCC} \tag{19}$$

$$\Delta V_{MV} = \frac{r - X_T K_{slope}}{1 + X_{GRID} K_{slope}} \Delta V_{PCC} \tag{20}$$

It can be said that lower slope gains make the system more independent from the SCR, and higher slope gains make the system more dependant on the grid impedance.

The impact of the line drop gain in the amount of tap changes can be extracted by looking to Figure 11 and Figure 12. The bigger the line drop gain the closer the OLTC voltage reference variations to ΔV_{LV}, and the smaller the gain the more closer to ΔV_{MV}.

Using the above equations and a disturbance in the grid voltage of 0.1 and 0.02 pu, the Figure 11 and Figure 12 are depicted. In these figures, it is represented the deviation values from the rated MV and LV for different slope gains and SCR values.

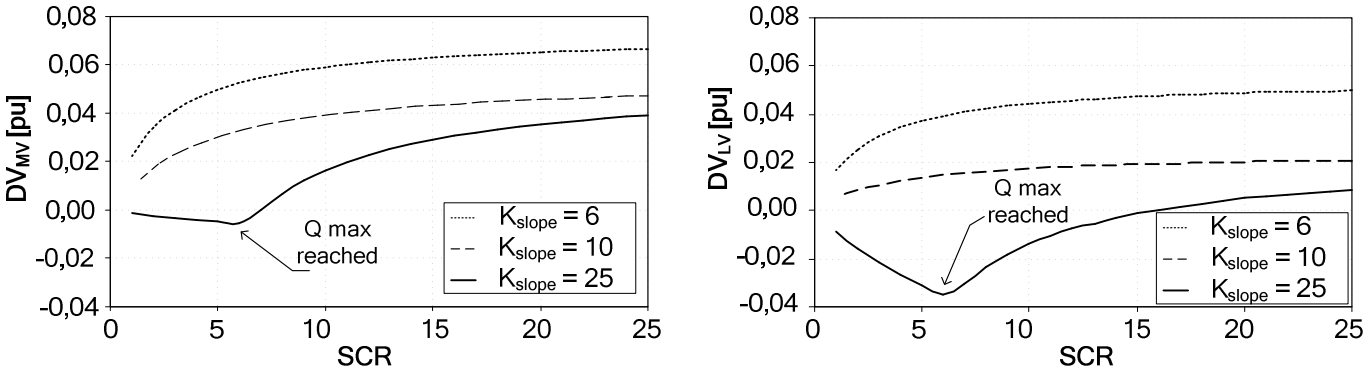

Figure 11. -0,1 pu grid voltage change, r= 1, X_T= 0,12 pu X_w= 0,08 pu.

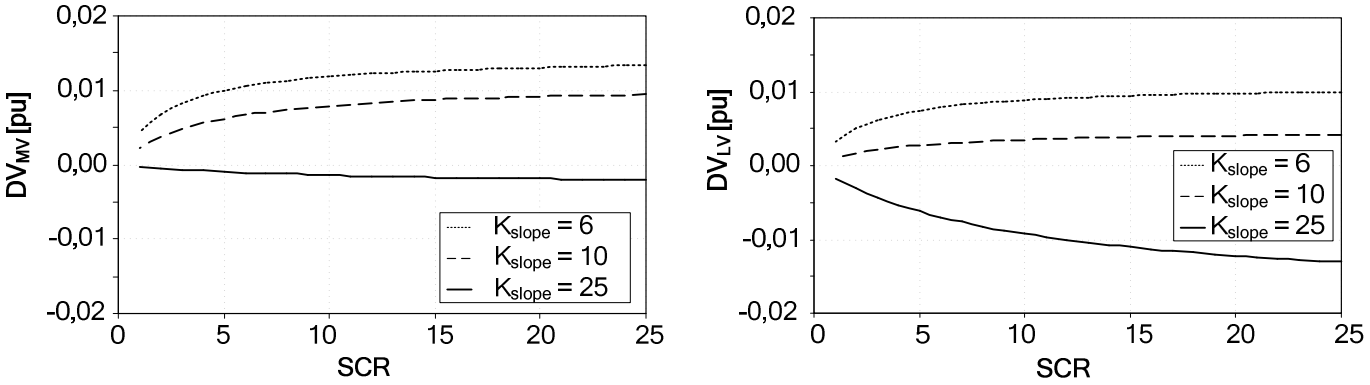

Figure 12. -0,02 pu grid voltage change, r=1, X_T= 0,12 pu X_w= 0,08 pu.

It can be seen that for high slope gains and lower SCR values the amount of tapping operation are lower when the OLTC has a small drop line gain. For lower slope gains the amount of tap operations will be lower when using higher gains in the line drop compensator. The maximum reactive power injection is limited to 0.346 pu (which correspond to a PF=0.95). It can be seen that the maximum Q is reached for high slope gains and big grid disturbances.

VII. Simulation Setup and Result Analysis

The WPP diagram shown in Figure 1 which includes the aforementioned controllers has been tested through EMT simulations. The WPP is tested under different SCRs and active power injection scenarios, analyzing the transient response of the capacitor bank switching, the performance of the tap control and the overall design concept.

The WPPC slope gain of the plant voltage control is chosen to be 4 % in all the simulated cases, and the modeled plant layout and data are based on an existing installation.

An aggregated WTG has been used, as it is shown in Figure 1, due to computational reasons. This WTG is connected through a step-up transformer to the collector bus by means of a subterranean cable. This collector bus is stepped up to the high voltage level, by means of the substation transformer, WPPT in Figure 1. The high voltage side of this transformer is connected to the next substation through an overhead line. Upstream of this point, the whole electrical system is reduced to an equivalent impedance, defined by its SCR and X/R, and an ideal voltage source (GRID).

The subterranean feeder cable is modeled as a Π equivalent with its corresponding project data. The substation and WTG transformers are modeled with 12 % and 8 % impedance and an X/R ratio of 24 and 10, respectively. The grid is represented by an equivalent Thevenin circuit with different SCRs, according to the simulated cases. See more simulation data in the appendix tables.

A. OLTC Analysis Performance

1) Comparison Performance of the OLTC controller

Some simulations have been done to check the performance of the proposed OLTC control. In these simulations the OLTC control shown in Figure 6 (called “normal”) and Figure 8 (called “improved”) are used for comparing the performance.

In the simulated cases the SCR is equal to 5, the K_L is 8 %, and the active power injection of the plant is kept constant to a level of 0.7 pu. The voltage of the grid (V_{GRID}) is stepped up and down 0.1 pu. The following figures show the grid voltage (V_{GRID}), the tap position (Tap position), the voltage at medium side (V_{MV}) and the voltage at WTG level (V_{LV}) for both cases

(normal and improved). See Figure 13.

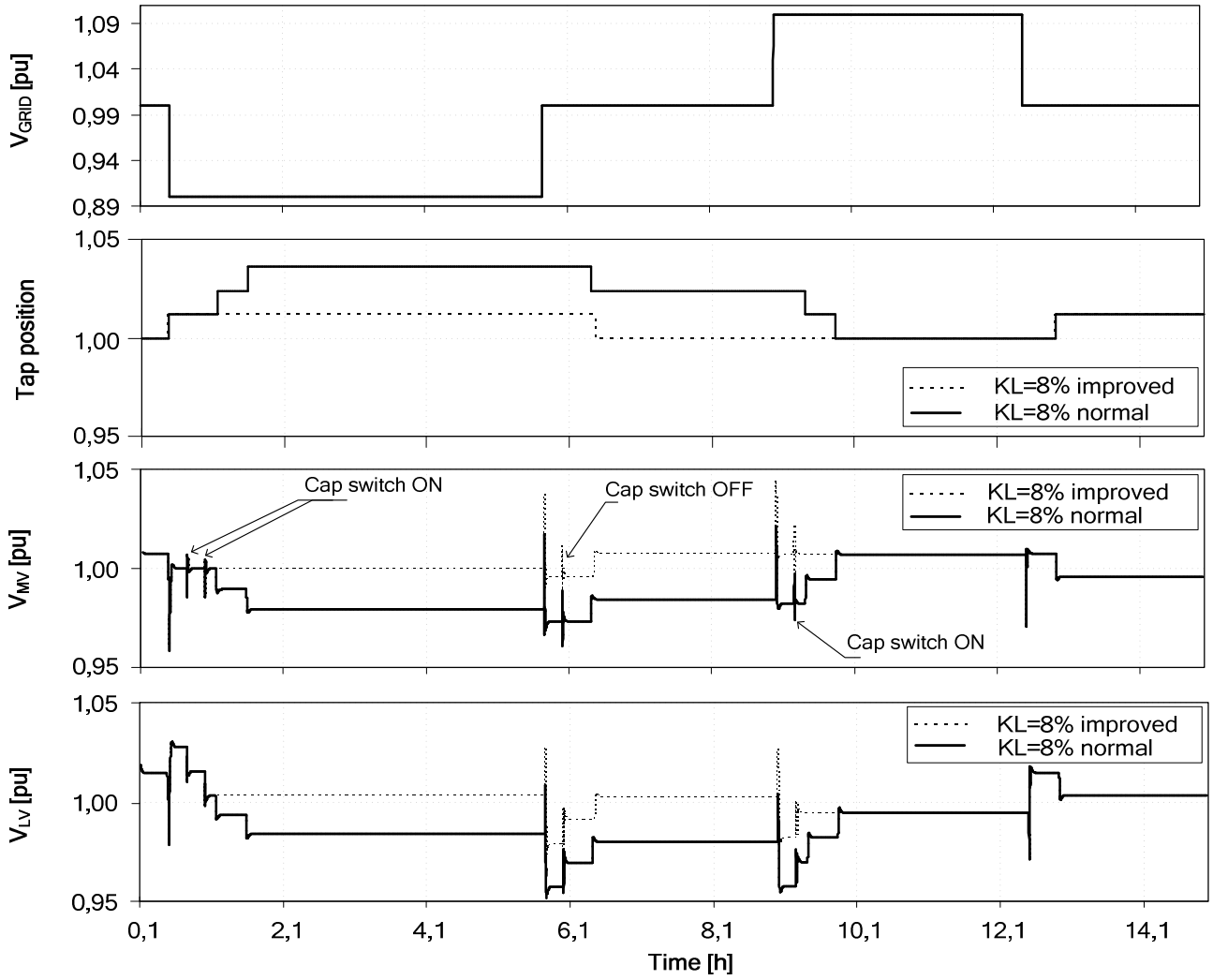

Figure 13. Comparison of two tap control configurations

Using the scheme shown in the Figure 8, the calculated ΔV_{drop} allows a better estimation of the voltage at another location in the plant.

It can be seen how the number of tap operation is reduced drastically and the voltage at WTG terminals is closer to the nominal value when the proposed OLTC control is used.

2) Performance of the Proposed OLTC Control under Different Conditions

Several EMTP simulations are done to show the amount of tap operations for different SCRs, slope gains and line drop values. The summary of these simulations are shown in Table I. The grid voltage used in the simulations is the same as the one shown in Figure 13.

The amount of tap operations is directly related to the magnitude ΔV_{LV} when the line drop gain is high (K_L= 8 %), or ΔV_{MV} when the line drop gain is low (K_L= 0 %). Higher ΔV values are translated into more tap change operations.

It can be checked that the graphs shown in Figure 11 are in accordance with the simulation results.

By looking at Table I some conclusions can be extracted. When high K_{slope} gains are used in the voltage plant control, low SCR values make lower tap operations compared to high SCR values. For low K_{slope} gains the amount of tap operations is almost independent of the SCR value.

TABLE I
SIMULATED CASES

CASE	Slope [%]	K_L [%]	SCR	Tap operations
1	4	0	5	*0*
2	4	8	5	*3*
3	4	0	25	*9*
4	4	8	25	*6*
5	15	8	5	*11*
6	15	8	25	*12*

B. Capacitor Control Analysis Performance

In the Figure 14, it is shown the transient effects of the capacitor switching in the voltage and reactive power at the PCC. Two different cases are simulated, and in both cases it is shown the performance when the function which calculates the ΔV_{Cap} is activated (ΔV_{Cap} ON) and when is not (ΔV_{Cap} OFF). When it is activated, it can be seen how the transients are centered on the previous Q and V values.

Two cases are simulated. Case A: one capacitor is connected with a SCR of 5, a grid voltage of 0.95 pu and the WPP active power level injection is 1 pu. Case B: one capacitor is disconnected with a SCR of 10, a grid voltage of 1 pu and the WPP active power level injection is 1 pu. The voltages at the PCC bus (V_{PCC}), and the Q injected at the PCC (Q_{PCC}) are plotted for every simulated case.

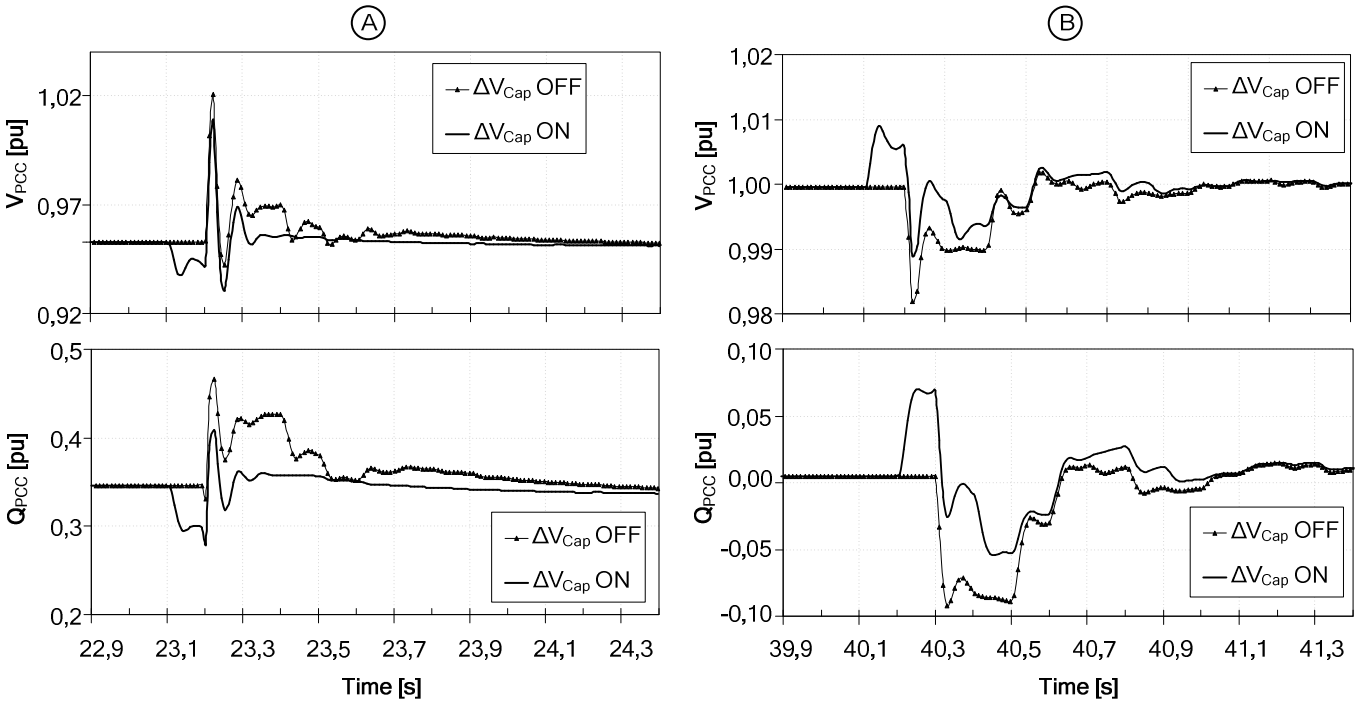

Figure 14. Capacitor switching transients: Case A: switching in 1 capacitor. Case B: switching Out 1 capacitor.

C. Full system Analysis Performance

The performance of the plant under different conditions is shown in the following figures. The used line drop gain is 4 %.

In Figure 15, the aggregated WTG is programmed to inject the active power measured at the PCC of a real WPP and the voltage of the grid is kept constant and equal to 1 pu. It can be seen how the capacitors are switched in and out to keep the steady state reactive power converter action of the plant within 0.1 pu.

In the following figure: the injected active power at PCC, the injected reactive power by the WTGs, STATCOM and capacitors, and the voltage at WTG, STATCOM, and capacitor terminals (MV side of the transformer) are depicted.

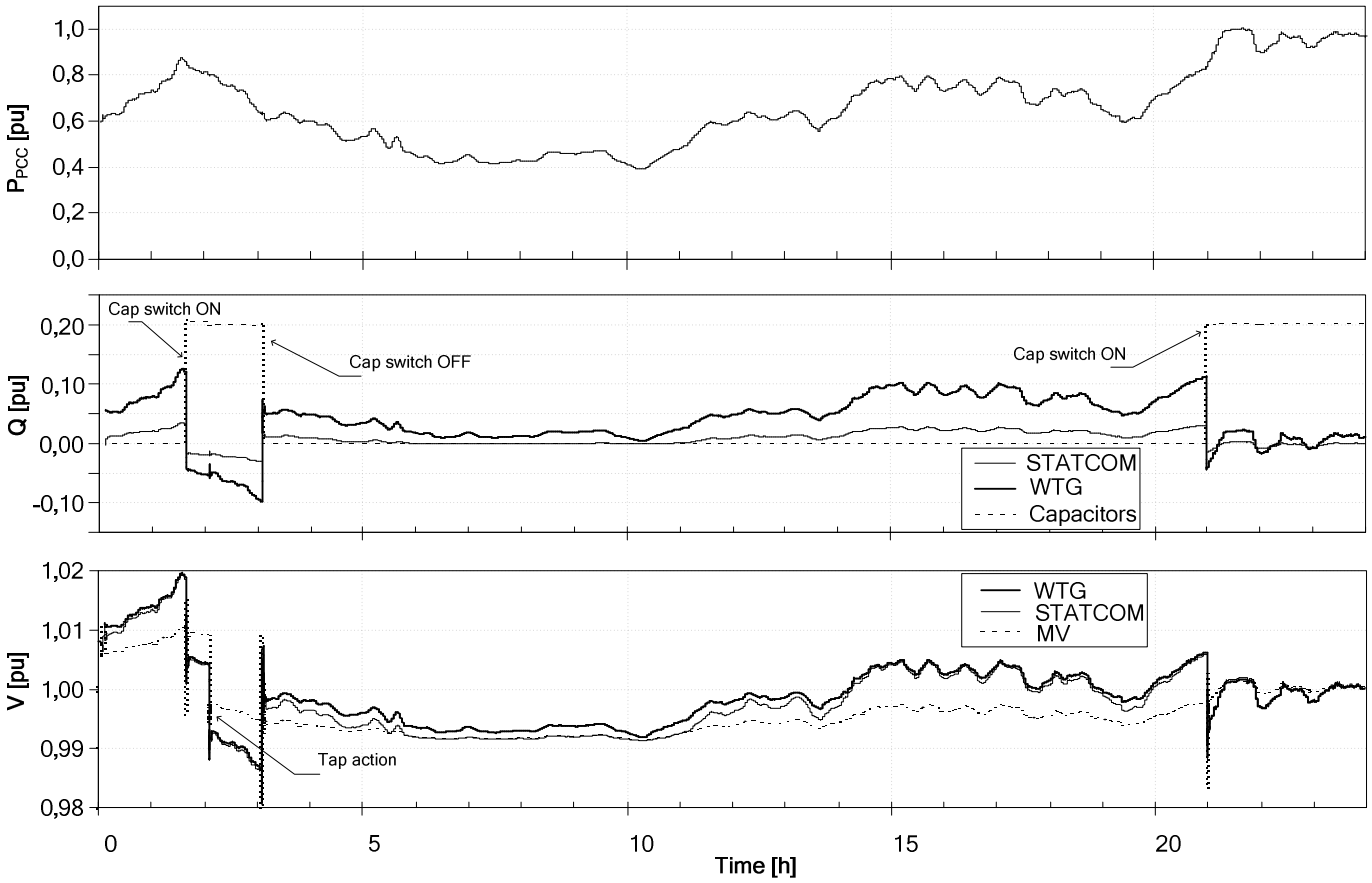

Figure 15. Real time series injection of active power. Vgrid = 1 pu = cte, SCR = 5

In the Figure 16, the aggregated WTG is programmed to inject a constant active power equal to 0.7 pu, but in this case the voltage of the grid is stepped up and down 5 %. It can be observed that only one tap operation is done in this period, even that the voltage of the grid is steeped up and down 5 %, which corresponds to the conclusion of the previous results shown in Figure 11. In the following figure, the injected reactive power from the WTG, STATCOM, capacitors, and the measured voltages at the grid, PCC and MV buses, are depicted.

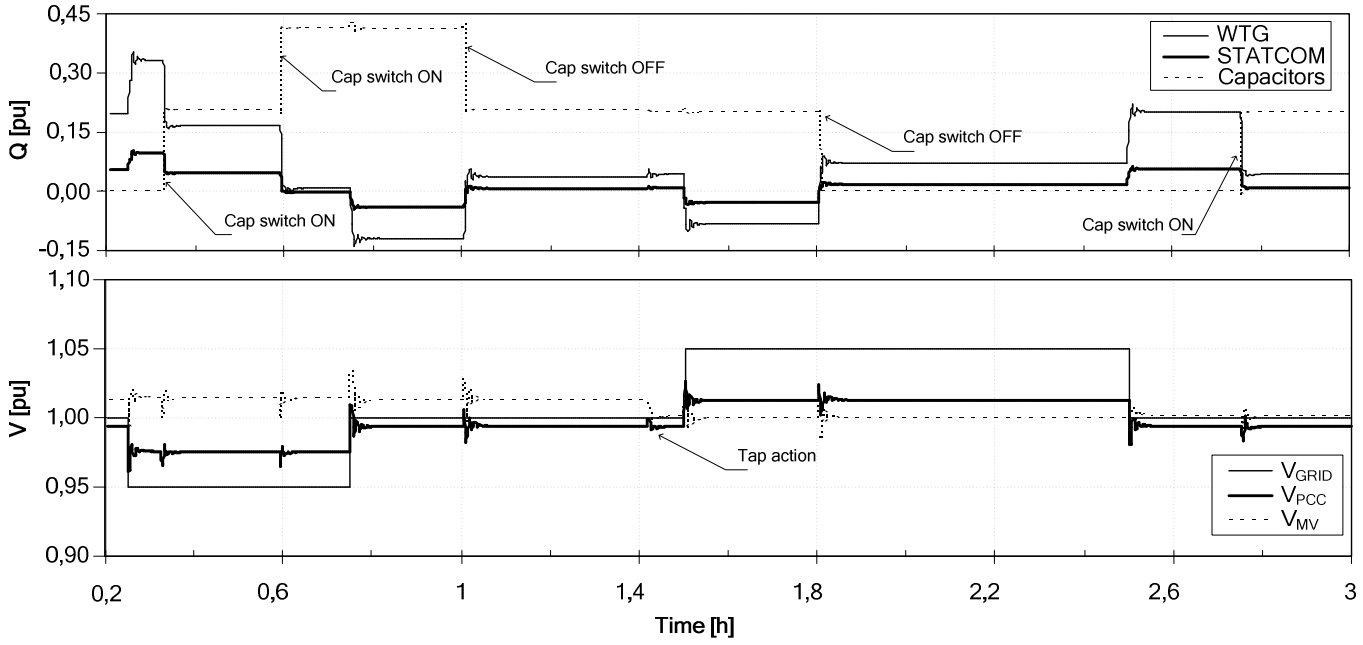

Figure 16. Voltage of the grid steeped up and down 5 %, P = 0.7 pu = cte. SCR = 5

It can be seen as well, how the plant control connects and disconnects the capacitor banks in order the amount of used reactive power from the converters is kept below a desired operation band of 0.1 pu, it should be mentioned that this operation band has been found as a compromise to avoid excessive switching operations of the capacitors and reduce losses due to the converter usage. The simulations show that the transformer voltage tap control can run independently of the plant voltage control without any conflict.

VIII. Conclusions

The operation analysis of a wind power plant with a central voltage controller, including DFIG WTGs, STATCOM, capacitor banks and OLTC is shown and tested through simulations. The STATCOM unit is introduced in the plant due to the lack of reactive power capability from the WTGs and fast time reaction requirements to voltage disturbances in the grid. Capacitor banks are included in the plant to ensure that the converters will have sufficient VAr capacity to handle unpredictable grid disturbances and to reduce the losses due to the reactive power transportation inside the plant. The STATCOM and MSCs are sized according to the load flow analysis at the PCC and the capacitor control characteristics.

These MSCs are controlled by a novel capacitor control, which is integrated successfully in the plant controller, allowing the reduction of the capacitor switching transients and limiting the converter operation for reactive power injection during steady-state. Moreover, the coordination of the STATCOM, WTGs and capacitor banks can be done in such way that the “steady-state” reactive power usage of the converters is less than a desired band of 0.1 pu, which is a compromise between switching converter losses and capacitor switching operations.

It is shown that for a wind power plant, if the current injection from the capacitor banks is removed from the OLTC voltage control, the performance is improved. Therefore, the proposed OLTC voltage control is coordinated with the plant control, in order the current provided by the capacitors can be removed from the total medium voltage current, thus reducing the amount of tap operations and obtaining a better estimation of the line drop voltage.

IX. Appendix

Table II
Electrical Data of Wind Turbine

Parameter	Value	Unit
S_{base}	2100	[kVA]
V_{base}	0.69	[kV]
Electrical frequency	50	[Hz]
Stator Resistance	0.006	[pu]
Rotor Resistance	0.009	[pu]
Mutual Inductance	3.422	[pu]
Stator Inductance	0.072	[pu]
Rotor Inductance	0.101	[pu]
S step-up transformer 0.69:20kV	2100	[kVA]
Z step-up transformer	0.08	[pu]

Table III
Electrical Data of the Wind Power Plant & Grid

Parameter	Value	Unit
Number of WTGs	23	[-]
X_{OVL}	1.81	[%]
R_{OVL}	0.89	[%]
C_{OVL}	0.51	[%]
L_{OVL}	10.2	[km]
X_{WPPT}	11.91	[%]
R_{WPPT}	0.49	[%]
S_{WPPT}	55000	[kVA]
Angle of grid	75	[deg]
Medium voltage level	20	[kV]
High voltage level	115	[kV]

TABLE IV
ELECTRICAL DATA OF STATCOM

Parameter	Value	Unit
S_{base}	14000	[kVA]
V_{base}	0.69	[kV]
Electrical frequency	50	[Hz]
S step-up transformer 0.69:20kV	15000	[kVA]
Z step-up transformer	0.09	[pu]

X. REFERENCES

[1] V. Akhmatov "Experience with Voltage Control from Large Offshore Windfarms: the Danish Case", WIND ENERGY, p- 692-711, 11 Feb 2009,

[2] I. Erlich, U. Bachmann, "Grid Code Requirements Concerning Connection and Operation of Wind Turbines in Germany". IEEE Power Engineering Society General Meeting, 12-16 June 2005; 1253-1257 Vol.2.

[3] P.O.12.2, "Connected Installations to the Transmission Spanish System: Minimum Requirements for Design and Security", Red Electrica de Espana, Grid Code Requirements for installations connected to the transmission system in Spain.

[4] National Grid Electricity Transmission: "Guidance Notes for Power Park Developers ", 2008

[5] Alberta Electric System Operator (AESO), "Wind Power Facility, Technical Requirements", Alberta, November 2004.

[6] Hydro-Quebéc: Technical Requirements for the Connection of Generation Facilities to the Transmission Systems, Quebéc, Canada.

[7] G. Tapia, A. Tapia, and J. Ostolaza, "Proportional-Integral Regulator-Based Approach to Wind Farm Reactive Power Management for Secondary Voltage Control". IEEE Transactions on Energy Conversions, Vol.22, No.2, June 2007.

[8] El Moursi, M.; Joos, G.; Abbey, C., "A Secondary Voltage Control Strategy for Transmission Level Interconnection of Wind Generation", Power Electronics, IEEE Transactions on, Volume 23, Issue 3, May 2008 Page(s):1178 - 1190

[9] M. S. El-Moursi, "A novel line drop secondary voltage control algorithm for variable speed wind turbines", WIND ENERGY, published online 2010.

[10] Stankovic, A.; Ilic, M.; Maratukulam, D., "Recent Results in Secondary Voltage Control of Power Systems", Power Systems, IEEE Transactions on , Volume 6, Issue 1, Feb. 1991 Page(s):94 - 101.

[11] Gehao Sheng; Yadong Liu; Dapeng Duan; Yi Zeng; Xiuchen Jiang, "Secondary Voltage Regulation Based on Wide Area Network", Power & Energy Society General Meeting, 2009. PES '09. IEEE 26-30 July 2009 Page(s):1 - 7

[12] Al-Majed, S.I., "Secondary Voltage Control: Enhancing Power System Voltage Profile", Power and Energy Conference, 2008. PECon 2008. IEEE 2nd International, 1-3 Dec. 2008 Page(s):1218 – 1221

[13] May 2003.Liwei Wang, Sina Chiniforoosh, and Juri Jatskevich, "Simulation and Analysis of Starting Transients in Rotor-Chopper-Controlled Doubly-Fed Induction Motors" 2008 IEEE Electrical Power & Energy Conference.

[14] Morren J, de Haan SWH., "Ridethrough of Wind Turbines with Doubly-fed Induction Generator during a Voltage Dip". IEEE Transactions on Energy Conversion 2005; 20: 435–441.

[15] Hammad and A.E, "Analysis of Power System Stability Enhancement by Static Var Compensators", IEEE Trans. Power Syst., vol. E-1, no. 4,1986, pp. 222–227

[16] Wei Qiao; Harley, R.G., "Power Quality and Dynamic Performance Improvement of Wind Farms Using a STATCOM". Power Electronics Specialists Conference, 2007. PESC 2007. IEEE 2007, Page(s): 1832 – 1838.

[17] Hingorani NG, Gyugyi L., "Understanding Facts". IEEE Press Series on Power Engineering. IEEE Press: Piscataway, New Jersey, 2000; 432. p 194-197

[18] G. Romegialli, H. Beeler "Problems and concepts of static compensator control", IEEPROC, Vol. 128, Pt. C, No. 6, NOVEMBER 1981, p- 382-388

[19] GE Energy, http://www.gepower.com/prod_serv/products/substation_automation/en/index.htm

[20] G. Celli, E. Ghiani, M. Loddo, F. Pilo, "Voltage Profile Optimization with Distributed Generation" Power Tech, 2005 IEEE Russia: 2005 , Page(s): 1 – 7

[21] Bonhomme, A.; Cortinas, D.; Boulanger, F.; Fraisse, J.-L. "A new voltage control system to facilitate the connection of dispersed generation to distribution networks", 2001. Part 1, CIRED. 16th International Conference and Exhibition on Electricity Distribution (IEE Conf. Publ No. 482)Volume: 4, 2001.

[22] Kundur P. Power System Stability and Control. Electric Power Research Institute, McGraw-Hill, Inc.: Palo Alto, CA,

[23] 1993. GE Energy, www.GEindustrial.com/Multilin, "Transformer Tap Change Controller: DTR"

A.8

"Centralized Slope Voltage Control for a DFIG Wind Power Plant with STATCOM"
Jorge Martínez, Philip C. Kjær, Pedro Rodriguez, Remus Teodorescu.

Centralized Slope Voltage Control for a DFIG Wind Power Plant with STATCOM

Jorge Martínez, Philip C. Kjær, Pedro Rodriguez, Member, IEEE, Remus Teodorescu, Senior Member, IEEE.

***Abstract*— Wind power plants are growing in percentage of penetration into the electrical grid compared with traditional generation. Larger percentages of wind power penetration translate to more demanding requirements coming from the grid codes, for example, voltage support at the point of connection has been introduced recently by several grid codes from around the world. For a wind power plant of DFIG turbines, fast voltage response and reactive power capability can be a challenge.**

In this paper, a novel strategy and control architecture for a wind power plant, DFIG turbine and a STATCOM unit is introduced. The implemented voltage control scheme is based upon the secondary voltage control concept. The proposed local voltage control is only activated during grid voltage transients allowing equal loading of the VAR sources.

Results of simulations in EMTP show that the combination of the proper plant, WTGs, and STATCOM control can offer fast response to grid voltage changes, and the fulfillment of the design requirements can be extended for a wide range of short circuit ratios.

***Index Terms*—Wind turbine generator, slope control, power system, voltage control, doubly-fed generator, STATCOM.**

I. Nomenclature

Ctrl	Control
COMM	Communication
CT, VT	Current and Voltage Transformer
DC, AC	Direct Current, Alternate Current
DFIG	Doubly Fed Induction Generator
DB	Dead Band
EMTP	Electromagnetic Transient Program
G	Generator
LPF	Low Pass Filter
P, Q	Active, Reactive power
PCC	Point of Common Coupling
PF	Power Factor
PI	Proportional and Integer control
PWM	Pulse Width Modulation
s	Laplace term
SCR	Short Circuit Ratio
STATCOM	Static Compensator
TSO	Transmission System Operator
V, I	Voltage, Current
OVL	Overhead Line
WPP, WTG	Wind Power Plant, Wind Turbine Generator
WPPC	Wind Power Plant Controller
WPPT	Wind Power Plant Transformer
ω	Angular frequency
X, R, L	Reactance, Resistance and Inductance
Z	Impedance

Subscripts

a, b, c	Three phase quantities
d, q	Direct and quadrature axes
ref	Reference
m	Measured

Manuscript June 10, 2010.

J. Martínez and P. C. Kjaer are with VESTAS Wind System, Power Plant R&D. Denmark.

R. Teodorescu and P. Rodriguez are with Aalborg University. Denmark.

II. Introduction

With increasing penetration of wind power generation, the requirements for the connection of wind power plants (WPPs) to the electrical grid are defined by new and emerging grid connection codes. The grid connection requirements vary in different parts of the world, but they share common aims, such as permitting the development, maintenance and operation of a coordinated, reliable and economical transmission or distribution system. The new requirements generally demand that wind power plants provide ancillary services to support the network in which they are connected [1].

Depending on the used wind turbine technology, different reactive power capabilities can be obtained at the point of common coupling (PCC). If the available reactive power from the wind turbines is not enough to fulfill the requirements, extra reactive compensation equipment should be installed in the plant. If this is the case, coordination between the WTGs and the reactive power compensation device is needed.

Since WPPs are modular (composed by a large number of generation units), the communication delays of the operational set points sent by the plant controller could be in the range of hundreds of milliseconds. Therefore, when fast reaction time to voltage disturbances is required, some local voltage control scheme can be implemented at turbine level [2]-[3]. In the other hand, the local voltage control has the undesired effect of loading unequally the converters, since the reactive power injected by every unit is dictated not only by the reference of the central control, but also by the individual local voltage.

In this paper, it is presented a new voltage plant control, including the dispatching functions to coordinate the

STATCOM with the WTGs, and a local voltage control strategy, where the local voltage control collaborate in the reactive power injection only during voltage transients.

III. Voltage Control Requirements

Small-signal performance measures provide a means of evaluating the response of the closed-loop excitation control systems to incremental changes in system conditions. In addition, small-signal performance characteristics provide a convenient means for determining or verifying excitation system model parameters for system studies. Small-signal performance may be expressed in terms of performance indices used in feedback control system theory. For a time response output, the associated indices of interest are the following: rise time, overshoot, and settling time [4].

When tuning the voltage regulator, an improvement to one index will most likely be to the detriment of other indices.

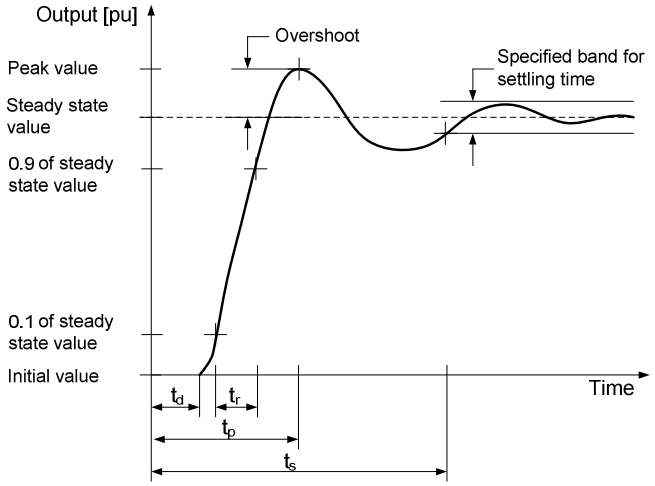

Fig. 1. IEEE std. for a typical transient response of a feedback control system to a step change in input [4].

The most demanding indices, related to Fig. 1, are extracted from different grid codes [5]-[8] and compiled in Table I. The indices listed in Table I will be used in the following sections as control design criteria. The referred indices are used to evaluate the measured voltage at PCC.

TABLE I
DESIGN REQUIREMENST ACCORDING TO FIG. 1

Parameter	Value	Unit
Overshoot	5	[%]
Band for settling time	2.5	[%]
t_d	0.2	[s]
t_r	1	[s]
t_p	Not defined	[s]
t_s	2	[s]

IV. Wind Power Plant

The wind power plant of interest is composed by 23 DFIG turbines, which are distributed in 4 feeders, having 6, 7, 6 and 4 WTGs respectively. These WTGs are connected through a set-up transformer to the collector bus by means of a subterranean cable. This collector bus is stepped up to the high voltage level, by means of the substation transformer, WPPT in Fig. 2. The high voltage terminal of this transformer is connected to the next substation through an overhead line (Z_{OVL}). Upstream of this point, the whole electrical system is reduced to an equivalent impedance, defined by its SCR and X/R (Z_G), and an ideal voltage source (GRID). See following figure.

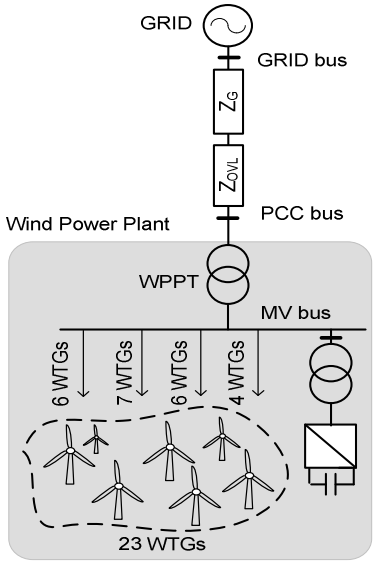

Fig. 2. Simplified diagram of the WPP, composed with 23 DFIG and 1 STATCOM.

It can be seen that the main active components of the plant are DFIG turbines and a STATCOM. The following sections describe in more detail these two components.

A. DFIG Turbine

The variable speed doubly-fed generator, see Fig. 3, allows full control of generator active and reactive power, using the rotor-connected frequency converter. Its rating is in the order of 0.3 pu. Operating both with sub- and super-synchronous speed, the power can be fed both in and out of the rotor circuit.

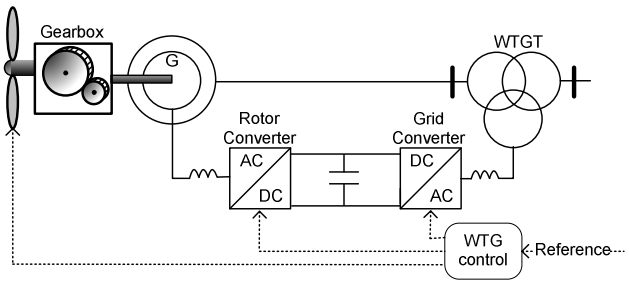

Fig. 3. DFIG turbine simplified diagram.

Typical DFIG controls can be seen in [9]-[10], where the active and reactive power are controlled using the d and q axis respectively.

The following figure shows the P-Q chart of a DFIG

turbine. The asymmetry in the figure with respect to the Q capability is due to the excitation of the generator and the limited size of the converters. All P-Q combinations, inside the plotted area, can be injected. Clearly, the maximum Q injection is dependent on the instantaneous P value.

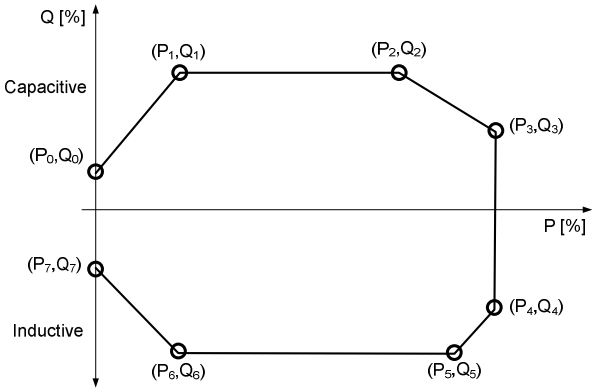

Fig. 4. P-Q DFIG chart measured at stator terminals.

B. STATCOM

Most of the grid codes require voltage capability regulation within a minimum power factor of 0.95 [6], for the whole active power range. As it can be seen in Fig. 4, the limited DFIG Q injection for high active power productions can be a problem. To solve this situation, a STATCOM can be installed in the wind power plant.

Flexible AC transmission systems based on voltage-source converters, such as STATCOMs, have found increasing utilization in power systems because of their ability to provide improved performance [11]. The primary purpose of a STATCOM is to support bus-bar voltage by providing appropriate capacitive and inductive reactive power into the system.

The single line diagram of the STATCOM for reactive power supply to the system is shown in Fig. 5, where V_{LV} is the voltage of the bus-bar which is connected to, and V_{ST} is the controllable output voltage bus.

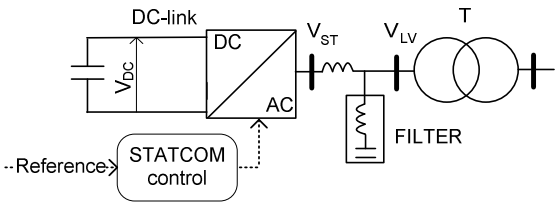

Fig. 5. STATCOM simplified diagram.

The STATCOM can be operated over its full output current range even at very low system voltage levels. In other words, the output current can be maintained almost independently from the AC system voltage. The Q generation or absorption changes linearly with the AC system voltage.

Fig. 6 represents the typical I-V chart for a STATCOM.

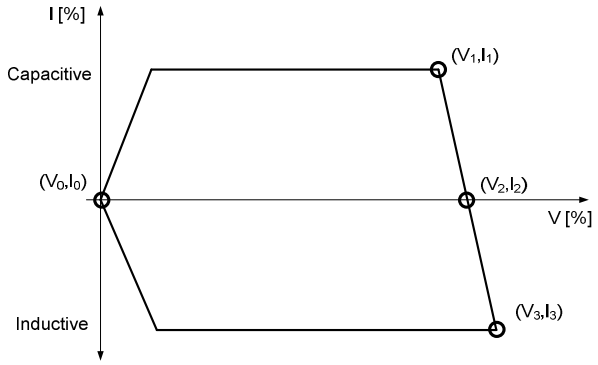

Fig. 6. V-I STATCOM chart measured at V_{LV} bus.

1) Sizing the STATCOM for the Wind Power Plant

The amount of VAr needed from the STATCOM can be calculated by means of a load flow analysis for different wind level productions and grid voltages.

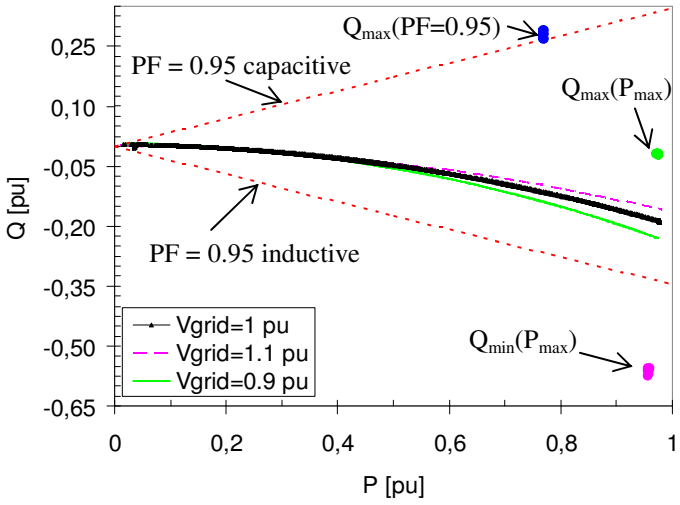

Fig. 7. Load flow analysis of the wind power plant at PCC bus.

Fig. 7 shows the load flow analysis of the WPP depicted in Fig. 2, when the WTGs are operating at PF equal to 1 at stator terminals. Thus, the reactive power consumption of the WPP components for different levels of active power injection and grid voltage levels can be evaluated.

The dotted lines show the maximum reactive power capacity (inductive and capacitive) needed for every active power injection (PF = 0.95).

The blue dot shows the intersection between the Q produced at the PCC and the PF = 0.95 capacitive requirement, when the turbines are operating at maximum capacitive reactive power. Beyond this active power level, the DFIGs are not able to fulfill the PF requirement by themselves. Therefore, this point determines when the STATCOM is starting to be needed to fulfill the PF = 0.95 requirement.

The green dot shows the maximum capacitive reactive power capability at PCC when the WTGs are injecting their maximum capacitive reactive power at maximum active power injection, and it can be used to determine the amount of VAr

needed from the STATCOM.

The pink dot shows the maximum inductive reactive power capability at PCC when the WTGs are injecting their maximum inductive reactive power at maximum active power injection.

V. Secondary Slope Voltage Control

The secondary voltage control concept is well known in the literature. The main thrust of the secondary voltage control scheme is to counteract, in real time, reactive power flow changes in the system, by adjusting terminal voltages of generators system-wide. The amount of voltage adjustment is proportional to the voltage derivations at monitored buses [12]-[14]. This concept can be applied to a wind power plant [3], where the pilot bus is located at the PCC bus, and the wind turbines include their own voltage controller.

Slope voltage control is widely used in power system applications since it allows paralleling generators with individual voltage slope controllers without hunting phenomena or instability. When there is high SCR, as in most of the cases in the transmission system, a slope controller will offer the best solution. Slope control provides a coordinated reactive power system, since it is known which the equilibrium point will be for every voltage disturbance, independently of the time reaction of the controller and the Q compensators. In this way, it is easy to manage how the generators will share the reactive power injection for a certain voltage disturbance.

The control law that is applied for the slope concept can be defined in a generic way as follows:

$$Q_{ref} = Q_0 + \left(\frac{1}{Slope}\right)(V_{ref} - V_m) \tag{1}$$

Considering a wind power plant composed by a large amount of generators, and everyone having its own slope voltage control, it is important to investigate the interaction between these controllers and the central plant control. For studding this interaction, a generic system formed by two units and a central control is used.

The single line diagram of this system is depicted in Fig. 9, which shows two generation units. On top of that, a central control unit (Central Ctrl.) is placed to control the voltage at PCC by commanding these two units.

The following equation shows the control law applied to unit #1.

$$(V_{ref} - V_1)K_1 = I_{q1} \tag{2}$$

The following equation shows the control law applied to unit #2.

$$(V_{ref} - V_2)K_2 = I_{q2} \tag{3}$$

The following equation shows the control law applied to the PCC.

$$(V_{rated} - V_{pcc})K_{pcc} = I_{qpcc} \tag{4}$$

Note that in the above equations, the voltage reference (V_{ref}) will be equal to its nominal bus-bar voltage value, when the central control unit is disabled, otherwise V_{ref} will be dictated by the central control.

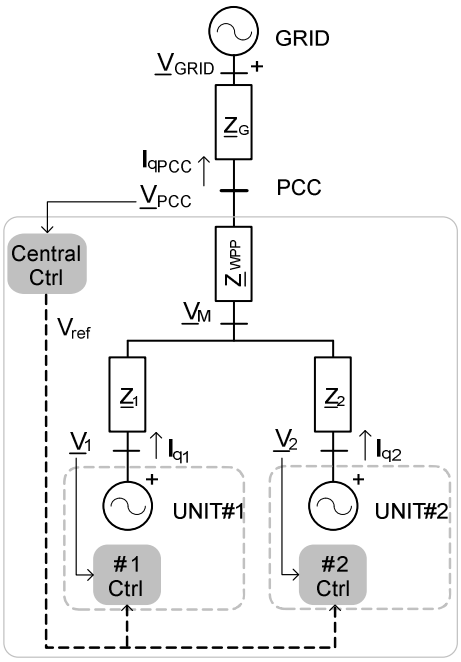

Fig. 8. Simplified diagram of a system with two generator units and a central control.

As it can be seen, these three controllers use different slope gains (K_1, K_2 and K_{pcc}) when controlling their local bus-bar voltage.

A. System Performance: Two Slope Voltage Control Units without Central Control.

This section shows the system analysis when the central controller located at PCC, see Fig. 8, is disabled and only the local controllers of the units are activated.

In the following figures, it is shown the characteristics of the reactive current for the units (UNIT 1 and UNIT 2), the system characteristics for different voltages of the grid (Sys PCC), and the characteristics of the combination between these two slope controls (UNIT 1+2). The amount of reactive current injected from every unit can be calculated as the intersection with their respective characteristic curves.

Fig. 9 shows the equilibrium points, and the characteristics of the controls and system, when the voltage of the grid is stepped from 1 pu to 0.9 pu.

Point 1 shows the equilibrium point when the voltage of the grid is 1 pu, and point 2 shows the equilibrium point when the voltage of the grid is 0.9 pu.

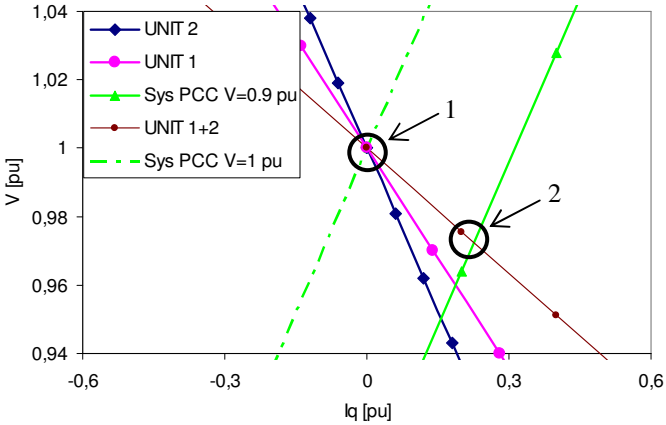

Fig. 9. Characteristics of two generator units with slope voltage control and without a Central control.

Fig. 10 shows the same as Fig. 9, but in this case a simulation with EMTP is done and plotted to show the trajectory of the equilibrium point of the system when stepping the grid from 1 pu to 0.9 pu, and back. This trajectory is shown by the red line called (Simulation_without_PCC_ctrl), which shows how the equilibrium points are located at the intersection between the system (Sys PCC) and the control characteristics (UNIT 1+2).

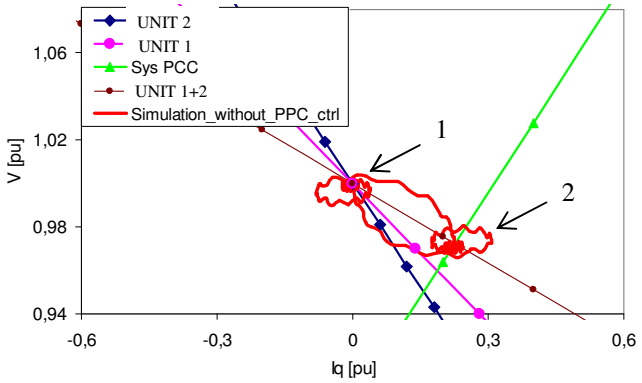

Fig. 10. Characteristics of two generator units with slope voltage control and without a Central control, including EMTP simulation.

Fig. 11 shows how the resistances and active power injection can affect the previous equilibrium points. In this case, the units #1 and #2 are injecting the same active power level, but the resistance value connecting them to the PCC is different, $R_1 = 2R_2$. As it can be seen, the effect of this active power injection is to displace the previous equilibrium point 1 to a new position 1', making Iq1r inductive and Iq2r capacitive for a grid voltage equal to 1 pu. This offset could lead to undesired behavior when having a centralized controller, since all the units should collaborate in the same reactive power direction.

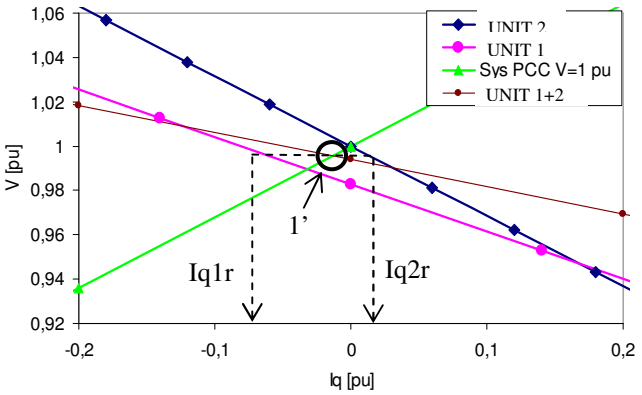

Fig. 11. Active power effect in the slope control equilibrium points.

B. System Performance: Two Slope Voltage Control Units with Central Control (secondary voltage control concept)

This section includes the system analysis when the central slope voltage controller is activated (Central ctrl), and sends the voltage references to the generator controls, see Fig. 8. This configuration is called secondary voltage control scheme [15]. This configuration offers a first and fast reaction to grid disturbances from the individual unit controls and later it is compensated by the slower central control unit. This central control unit sends voltage references to the units according to the central slope characteristics.

For this case, another curve is plotted (Ctrl PCC) which shows the characteristics of this centralized controller.

The equilibrium point is located in the intersection between this characteristic and the system one (Sys PCC). As in the previous cases, the voltage of the grid is stepped from 1 pu (point 1) to 0.9 pu (point 3), see Fig. 12.

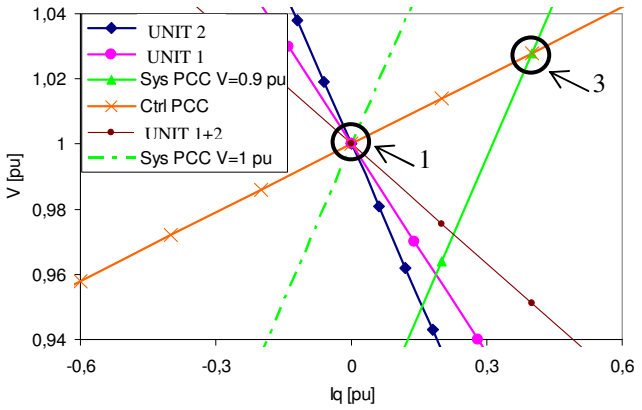

Fig. 12. Characteristics of two generator units with slope voltage control and with a Central control.

Fig. 13 includes the EMTP simulation response when stepping the grid from 1 pu to 0.9 pu and back. This is shown by the red line (Simulation_ with_PPC_ctrl).

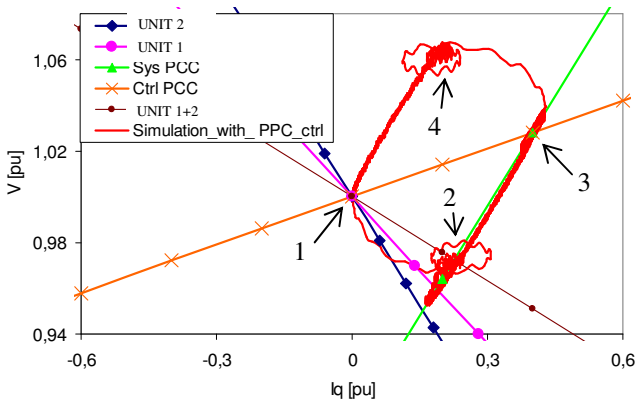

Fig. 13. Characteristics of two generator units with slope voltage control and with a Central control, including EMTP simulation.

The followed I_q-V trajectory shows several interesting points. Since there is some delay in the communication of the central PCC control when sending the references to the local units, it can be seen how the first system reaction is to reach their local controller equilibrium point (point 2), being this point the same as in Fig. 10, then the reference from the central control arrives moving the equilibrium to point 3. After that, when the grid voltage is stepped back to 1 pu, it is possible to see a similar reaction. The first reaction from point 3 to point 4 is done by the local controls and then point 4 is moved to 1 through the central control action.

VI. Wind Power Plant, WTG and STATCOM Controls

Wind power plants are required to control the characteristics of the power injected at the PCC [16]-[17]. Therefore, a centralized control is needed to supervise and command the power injected at the PCC. And as it was mentioned before, the control concept used in this paper is based on the secondary slope voltage control.

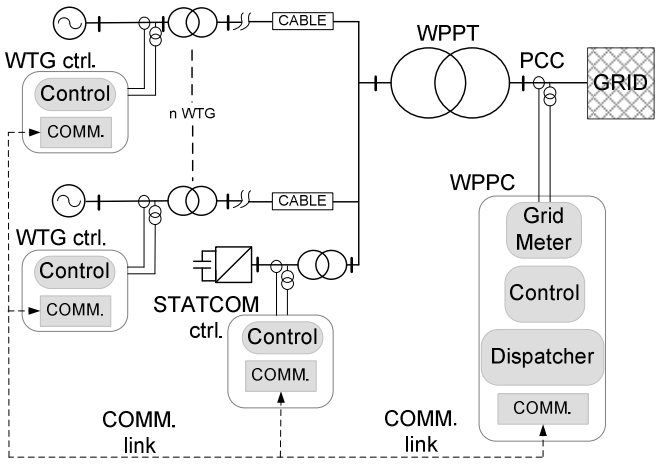

Fig. 14. WPP control and communication link diagram.

As voltage control is actuated by reactive power, it is possible to affirm that the voltage control design will cover an inner and fast reactive power/voltage control loop, located at turbine level, and an outer voltage control loop, located at the PCC where it is intended to control the voltage. In general, this control structure allows fast response and improves the overall performance, since the same tuning that was limited by the gain and delays in the system can be extended now to cover a greater range of SCRs.

The implementation of the secondary slope voltage control is done by including additional structures in the WTG and STATCOM q-axis controller. The WPPC is adapted to provide new references according to the new WTG and STATCOM control.

A. Wind Power Plant Control

The plant control (WPPC) receives the references and feedback (measurements) and outputs the turbines and STATCOM set-points. This controller is formed by a measurement device, which senses the currents and voltages at the PCC, a dedicated computer which allocates the control algorithms, and a communication hub. This communication hub will exchange control references and other signals with a large amount of WTGs, using for that purpose the communication WPP Ethernet network and particular protocols.

As it is shown in Fig. 14, the power plant controller is formed mainly by the following blocks:

1) Grid Meter

The measurement device or "Grid Meter", samples at very high frequency values the output of the CTs and VTs located at the PCC. This meter processes the signals by first calculating one cycle rms value of the signals, and then filtering for anti-aliasing. These rms signals are used by the control as the feedback.

2) Proposed Plant Control

The plant control included in this paper is based on a proportional controller, also called slope control. Normally, the gain of the voltage controller and the reference to the plant are fixed by the TSO.

The slope can be defined as follows:

$$Slope = \frac{\Delta V}{\Delta Q} \tag{5}$$

The control gain is defined in (6).

$$K_{slope} = \frac{1}{Slope} \tag{6}$$

It is clear that for high system gains, small slope and SCR values (SCR can be defined in pu as the inverse of the grid impedance, and it is a ratio between the installed power and the grid short circuit capacity) the system becomes more difficult to be controlled, moreover, the delays in the communication processes reduce the control stability margin

when the gain of the system increases. In order to expand the stable area of the system, normally a lag compensator is added to the control.

A phase-lag compensator tends to shift the root loci towards the right-half plane. For this reason, the pole and zero of a lag compensator must be placed close, usually near the origin, so they do not appreciably change the transient response or stability characteristics of the system.

The tuning objective of the control is to achieve a settling time of less than 1 s and an overshoot below 5 %. See Table I.

The plant slope controller is extended with a plant reactive controller which calculates the voltage references to be sent.

Since the slope controller is meant to inject Q at the PCC, proportionally to PCC voltage variations, it is important to compensate the Q losses which occur inside the WPP, to reach the dictated Q_{ref} by the plant slope control. For this reason, a closed loop using the feedback Q_m is added to the control structure, which ensures that the Q at PCC is matching with the Q_{ref} calculated by the slope gain. The output of the plant control (V_{ref}) will be processed by the dispatcher block.

The resulting diagram of the WPPC structure is shown in the following figure.

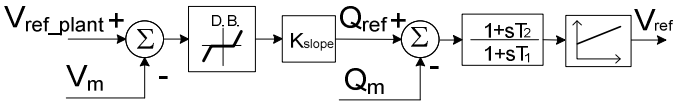

Fig. 15. Proposed plant control.

3) Dispatcher

The dispatcher has the functionality of splitting the references calculated by the plant control into the different elements composing the WPP. The way of splitting the reference can be done following several strategies, e.g. minimization of lost of energy production.

The strategy proposed in this document is based on using the STATCOM as the Q back-up for the system when the reactive power injected by the WTGs is not enough for grid code fulfillment.

Following figure shows the dispatcher block in a schematic way, where the active power measured at the PCC "P_m" is filtered with a low pass filter (LPF) and used for calculating a "K" factor with a look-up table.

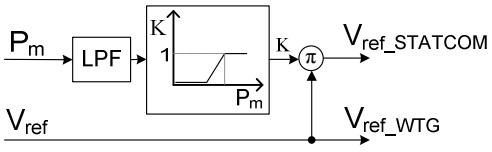

Fig. 16. Dispatcher block.

The settings of the look-up table are obtained from the load flow analysis. This "K" factor varies between 0 and 1, and multiplies the "V_{ref}", calculated by the control, thus obtaining the reference for the STATCOM; "$V_{ref\_STATCOM}$". It can be seen that the reference for the WTGs "V_{ref_WTG}" is "V_{ref}".

4) Communication

This block (COMM. in Fig. 14) represents the communication hub which collects all the feedback, packs and sends all the necessary references for the correct operation of the WTGs and STATCOM. This process adds delays in the control loop.

B. Proposed WTG Control

In the proposed WTG rotor converter control, shown in Fig. 17, the reactive current reference (I_{qref}) is generated according to the difference between the stator turbine terminal voltage, represented by V_m, and the V_{ref} sent by the WPPC. Therefore, the WTG outer control loop is a local voltage control, which can be adjusted by an external set-point.

The references (P_{ref}, V_{ref_WTG}) are processed by the WTG control loops, which generate the needed voltage references ($V_{d\ ref}$, $V_{q\ ref}$) which are translated by the PWM to pulse the rotor converter, see Fig. 17. Finally, the rotor is fed with a voltage that produces the desired P and Q at the stator terminals.

The WTG grid converter is only used to regulate the voltage level of the DC-link, and its control is not shown in this paper.

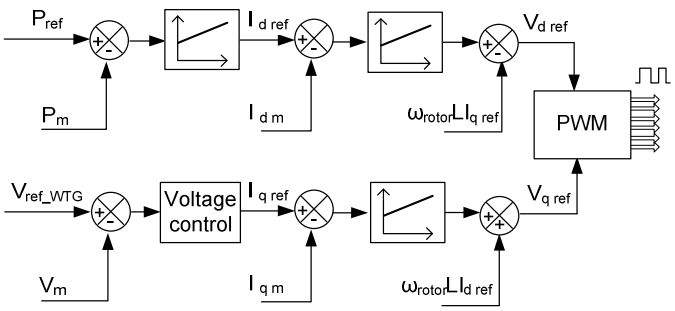

Fig. 17. Proposed DFIG rotor converter control diagram.

Following figure shows in more details the local voltage control of the WTG. The main difference with other secondary controls shown in the literature [3] is that this local voltage control will be active only during voltage transients.

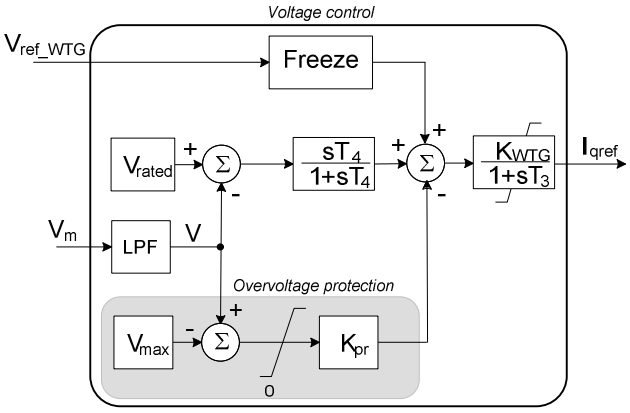

Fig. 18. Proposed WTG voltage control.

In this voltage control, the WTG slope gain and time constant, K_{WTG} and T_3 respectively, are calculated to provide fast reactions to voltage changes at generator terminals. The stator voltage variations are filtered with a differential pole filter with a time constant T_4, therefore, only reacting to changes on the stator voltage but not to steady state voltage errors. Thus, removing the voltage offset effect, caused for instance by the active power injection and the resistance of the cables.

By using a differential filter, it is possible to say that this voltage control is only active during voltage transients, during steady-state the I_{qref} is proportional to the one dictated by the plant control and does not depend on the stator voltage, having all the units of the plant the same I_{qref}.

The voltage control includes, as well, a protection against DFIG stator overvoltage, performed by a secondary loop, see Fig. 18, and an over-under voltage protection, which is installed in the reference signal sent by the central control (V_{ref}). If the value V_m is greater or lower than some threshold levels, normally 1.1 and 0.9 pu, and the V_{ref} increases or decreases respectively, then the block "Freeze", which is allocating this supervisory conditions, will freeze this external reference until these conditions are not fulfilled anymore.

C. Proposed STATCOM Control

The conventional de-coupled control system based on an outer loop control system that sets the reference for the inner control system is depicted in Fig. 19, where V_{DCm} is the measured DC-link voltage and V_m is the measured voltage at STATCOM terminals.

The proposed scheme for the local voltage control is the same as the one depicted in Fig. 18.

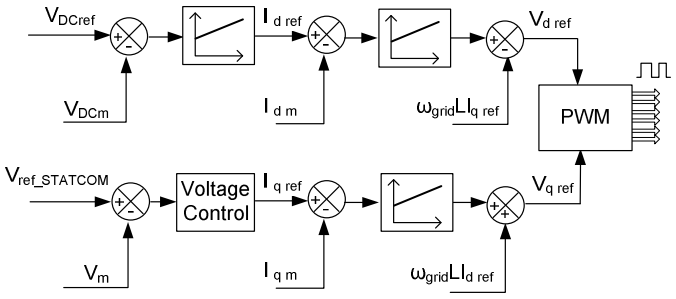

Fig. 19. STATCOM proposed control diagram.

The outer control loops independently regulate the reactive power injection and the DC-link voltage of the STATCOM. The inner current control loop generates the d-q voltage components, V_d and V_q, at the AC-side of the converter, and they are used by the PWM module to generate the gate control signals to the converter [18].

VII. Simulation Setup

The proposed cases of table II have been simulated in PSCAD. The modeled plant layout and data are based on an existing installation. The WPP is tested under different SCRs and active power injection scenarios. The WPPC slope controller is chosen to be 4 % in all the simulated cases. The grid bus voltage is stepped from 1 pu to 0.9 pu in all the cases. A step of 0.1 pu has been chosen as a representative case, since most of the grid operators define the normal range of operation in between ± 0.1 pu of the rated value.

The WPPC has been tuned for an optimal output at SCR equal to 5, even though a wide range of different SCRs are tested to prove the concept of the proposed controllers.

The following table shows an overview of the simulated cases.

TABLE II
Simulated Cases

CASE	SCR	Active Power	GRID bus disturbance [pu]
1	5	Medium	1.0→0.9
2		Full	1.0→0.9
3	10	Medium	1.0→0.9
4		Full	1.0→0.9
5	25	Medium	1.0→0.9
6		Full	1.0→0.9

A. WPP Layout

Fig. 2 is used to represent the layout of the studied system. The subterranean feeder cables are modeled as a Π equivalent with its corresponding project data. The OVL (Z_{OVL}) is also modeled as a Π equivalent. The substation and WTG transformers are modeled with 12 % and 8 % impedance and an X/R ratio of 24 and 10, respectively. The grid is represented by an equivalent Thevenin circuit (Z_G) with different SCRs, according to the simulated cases. See more simulation data in the appendix tables.

B. Wind Turbine Generator Model

The used WTG model is a detailed model, which includes the back to back converters with their respective controls. The mechanical part is modeled as a two mass system, coupled by a shaft [19]-[20].

A schematic representation of the WTG model is depicted in Fig. 3.

C. STATCOM Model

The used STATCOM model is essentially a current source behind a coupling reactance with the corresponding V-I characteristic shown in Fig. 6 [21]- [22].

The STATCOM current control is based on d-q vector control as described in previous sections, where the q-axis is defined such affects the reactive power and d-axis affects the active power component.

VIII. Simulation Results

In the following, each of the simulated cases is plotted. In all of the following simulations, the grid voltage is stepped at time equal to 10 s, from 1 pu to 0.9 pu.

The voltage at the grid and PCC buses, the Q reference and the Q injected at PCC are plotted for every case.

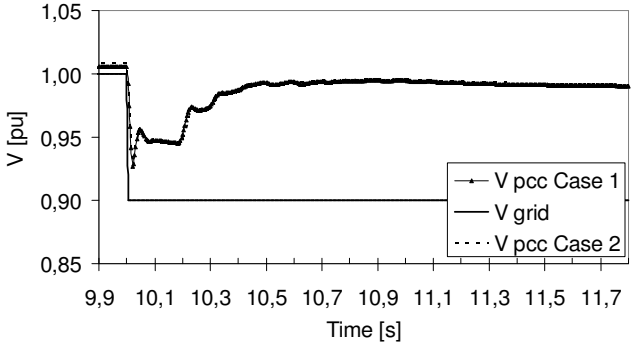

Fig. 20. Case 1 and Case 2: voltages at PCC and GRID bus.

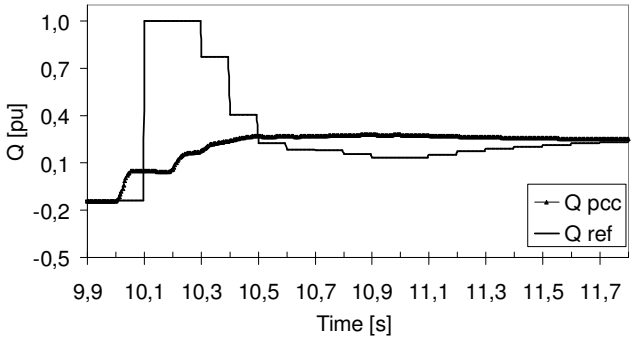

Fig. 21. Case 1: Q reference and injected at PCC

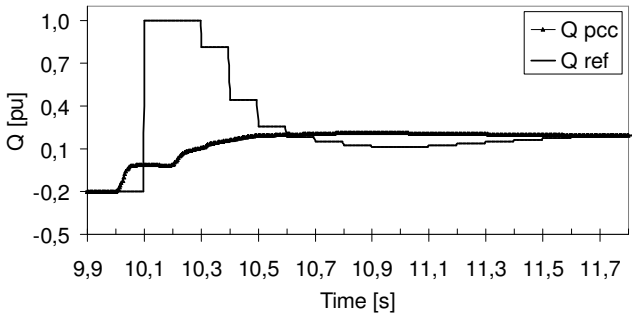

Fig. 22. Case 2: Q reference and injected at PCC

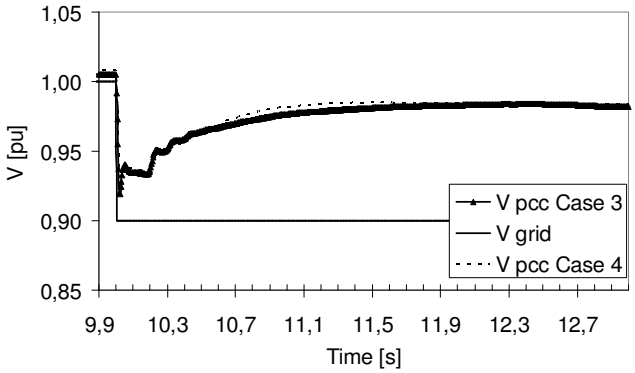

Fig. 23. Case 3 and Case 4: Voltages at PCC and GRID bus.

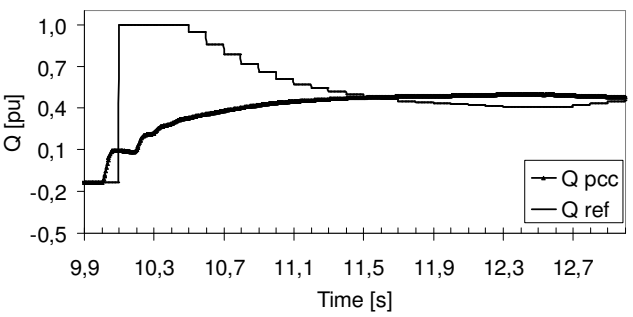

Fig. 24. Case 3: Q reference and injected at PCC

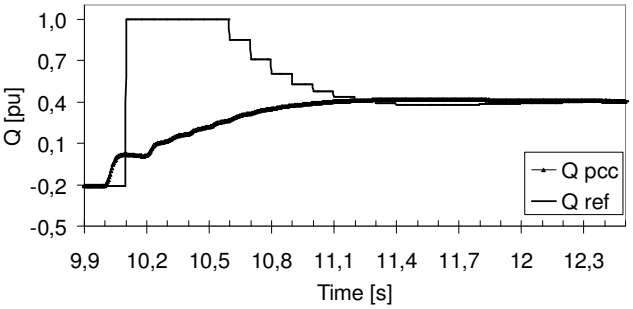

Fig. 25. Case 4: Q reference and injected at PCC

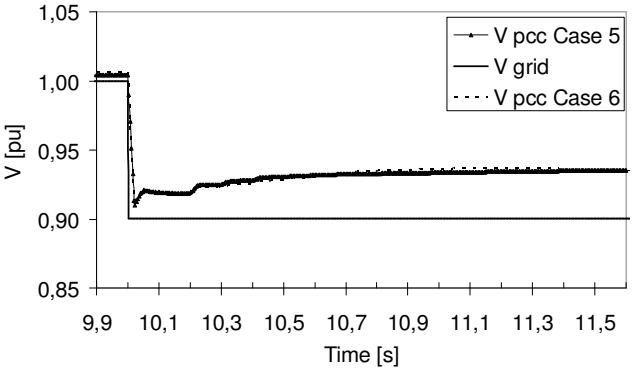

Fig. 26. Case 5 and Case 6: Voltages at PCC and GRID bus.

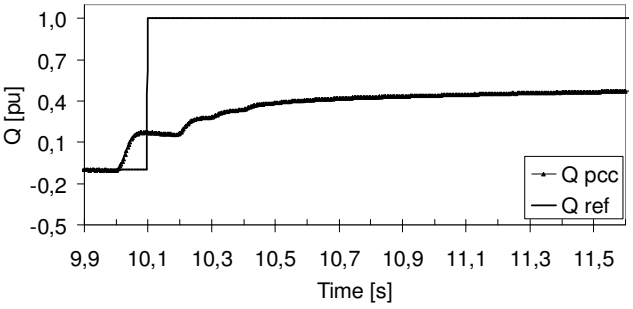

Fig. 27. Case 5: Q reference and injected at PCC

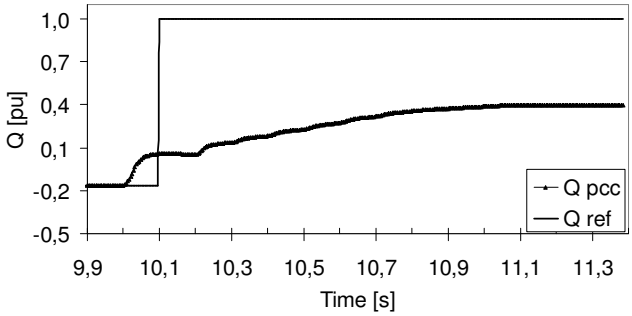

Fig. 28. Case 6: Q reference and injected at PCC

IX. Analysis of the Results

The following table summarizes the results obtained for every simulated case, according to the indices shown in Fig. 1. All cases fulfill with the design criteria.

TABLE III
PERFORMANCE EVALUATION OF THE SIMULATED CASES

CASE	Overshoot [%]	t_d [s]	t_r [s]	t_s [s]
1	1	0.02	0.32	0.69
2	1	0.02	0.32	0.69
3	0	0.02	0.72	0.92
4	0	0.02	0.72	0.92
5	0	0.02	0.61	0.70
6	0	0.02	0.80	0.93

As the waveforms in the previous graphs demonstrate, the SCR influences the results. With high SCR values, the WPP is nearly unable to move the voltage level at PCC, see Fig. 26. In the cases in which the turbines are at full production, the generators reach the ceiling reactive power, needing the STATCOM action to reach the desired Q at the PCC. The action of the STATCOM makes almost no difference between the cases at full and medium active power injection; see Fig 20, 23 and 26.

It can be seen that the possible maximum reactive power delivered at full active power production at the PCC is close to the one corresponding to the requirement of PF = 0.95, see Fig. 27 and Fig. 28.

For the sake of illustration, Fig. 29 is included to show the references sent by the WPPC to the STATCOM (Ref STATCOM) and to the WTGs (Ref WTG) for the case 1. For full production cases the references for the WTG and STATCOM are the same according to the dispatcher action.

Clearly, having this secondary voltage control implemented in the WTGs and STATCOM in conjunction with the appropriate plant control, the delay in the response (t_d) is reduced to very low levels for all the simulated cases, and the fulfillment of the design requirements is extended to a wide range of SCR values, even though the design was done to have an optimal response for a SCR of 5.

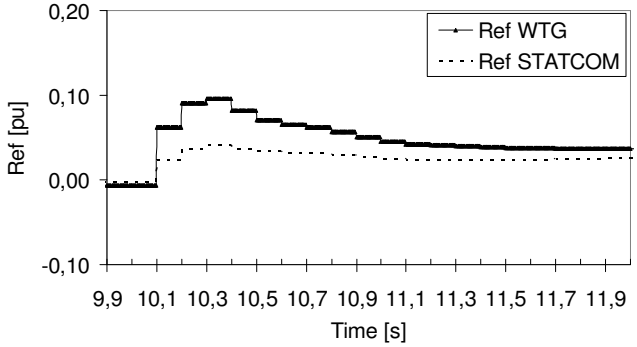

Fig. 29. Case 1: References sent to the WTGs and STATCOM

X. Conclusions

The design and analysis of a novel slope voltage controller for a wind power plant, DFIG turbine and a STATCOM, based in the secondary voltage control concept, are shown. The STATCOM unit is integrated in the plant control by a novel dispatching function. The STATCOM compensates the lack of reactive power of the turbines during periods of high wind speed.

The voltage control performance of the WPP is improved by placing some voltage controllers inside every unit. These local voltage controllers are designed in such way, that they are only active during voltage transients.

In so doing, the following is achieved:

-The wind power plant still offers fast response to voltage transients, since the local voltage controllers are activated during the transients. Therefore, the tuning of the controllers can be used for a wide range of SCRs since communication delays have less impact into system stability.

-This fast local voltage control reaction is removed slowly by a differential pole filter; meanwhile, the references sent by the central plant control command the WTGs and STATCOM to the desired operational point. As a consequence, the reactive power loading of every unit is the same, and is the one dictated by the central plant control. Having all the units loaded equally, avoids counter-action and stressing more some units than others.

XI. Appendix

TABLE IV
DISPATCHING LOOK-UP TABLE

P_m [%]	K
0	0
45	0
65	1
100	1

TABLE V
V-Q STATCOM CHART COORDINATES

Point	V	I	Unit in STATCOM base
0	0	0	[%]
1	92	100	[%]
2	100	100	[%]
3	108	100	[%]

TABLE VI
P-Q DFIG CHART COORDINATES

Point	P	Q	Unit in WTG base
0	0	10	[%]
1	10	60	[%]
2	70	60	[%]
3	100	20	[%]
4	100	30	[%]
5	85	60	[%]
6	10	60	[%]
7	0	15	[%]

TABLE VII
ELECTRICAL DATA OF WIND TURBINE

Parameter	Value	Unit
S_{base}	2100	[kVA]
V_{base}	0.69	[kV]
Electrical frequency	50	[Hz]
Stator Resistance	0.006	[pu]
Rotor Resistance	0.009	[pu]
Mutual Inductance	3.422	[pu]
Stator Inductance	0.072	[pu]
Rotor Inductance	0.101	[pu]
S step-up transformer 0.69:20kV	2100	[kVA]
Z step-up transformer	0.08	[pu]

TABLE VIII
ELECTRICAL DATA OF THE WIND POWER PLANT & GRID

Parameter	Value	Unit
Number of WTGs	23	[-]
X_{OVL}	1.81	[%]
R_{OVL}	0.89	[%]
C_{OVL}	0.51	[%]
L_{OVL}	10.2	[km]
X_{WPPT}	11.91	[%]
R_{WPPT}	0.49	[%]
S_{WPPT}	55000	[kVA]
Angle of grid	75	[deg]
Medium voltage level	20	[kV]
High voltage level	115	[kV]

TABLE IX
ELECTRICAL DATA OF STATCOM

Parameter	Value	Unit
S_{base}	14000	[kVA]
V_{base}	0.69	[kV]
Electrical frequency	50	[Hz]
S step-up transformer 0.69:20kV	15000	[kVA]
Z step-up transformer	0.09	[pu]

XII. REFERENCES

[1] I. Erlich, U. Bachmann, "Grid Code Requirements Concerning Connection and Operation of Wind Turbines in Germany". IEEE Power Engineering Society General Meeting, 12-16 June 2005, Vol. 2, pp: 1253-1257.

[2] G. Tapia, A. Tapia, and J. Ostolaza, "Proportional-Integral Regulator-Based Approach to Wind Farm Reactive Power Management for Secondary Voltage Control". IEEE Transactions on Energy Conversions, Vol. 22, No. 2, June 2007.

[3] El Moursi M., Joos G., Abbey C., "A Secondary Voltage Control Strategy for Transmission Level Interconnection of Wind Generation", IEEE Transactions on Power Electronics, Volume 23, Issue 3, May 2008, pp: 1178 – 1190.

[4] IEEE Std. 421.2-1990, "IEEE Guide for Identification, Testing, and Evaluation of the Dynamic Performance of Excitation Control Systems".

[5] P.O.12.2, "Connected Installations to the Transmission Spanish System: Minimum Requirements for Design and Security", Red Electrica de Espana, Grid Code Requirements for installations connected to the transmission system in Spain.

[6] National Grid Electricity Transmission: "Guidance Notes for Power Park Developers", 2008.

[7] Alberta Electric System Operator (AESO), "Wind Power Facility, Technical Requirements", Alberta, November 2004.

[8] Hydro-Quebéc: Technical Requirements for the Connection of Generation Facilities to the Transmission Systems, Quebéc, Canada, May 2003.

[9] Liwei Wang, Sina Chiniforoosh, and Juri Jatskevich, "Simulation and Analysis of Starting Transients in Rotor-Chopper-Controlled Doubly-Fed Induction Motors" 2008 IEEE Electrical Power & Energy Conference.

[10] Morren J, de Haan SWH, "Ridethrough of Wind Turbines with Doubly-fed Induction Generator during a Voltage Dip". IEEE Transactions on Energy Conversion, 2005; 20, pp: 435–441.

[11] Hammad and A.E, "Analysis of Power System Stability Enhancement by Static Var Compensators", IEEE Transactions on Power Systems, vol. E-1, no. 4, 1986, pp: 222–227.

[12] Stankovic A., Ilic M., Maratukulam D., "Recent Results in Secondary Voltage Control of Power Systems", IEEE Transactions on Power Systems, Volume 6, Issue 1, Feb. 1991 pp: 94 - 101.

[13] Gehao Sheng, Yadong Liu, Dapeng Duan, Yi Zeng, Xiuchen Jiang, "Secondary Voltage Regulation Based on Wide Area Network", Power & Energy Society General Meeting, 2009. PES '09. IEEE 26-30 July 2009, pp: 1 – 7.

[14] Al-Majed, S.I., "Secondary Voltage Control: Enhancing Power System Voltage Profile", Power and Energy Conference, 2008. PECon 2008. IEEE 2nd International, 1-3 Dec. 2008, pp: 1218 – 1221.

[15] S. Narita and M. Hamman, "Multi-computer Control of System Voltage and Reactive Power on Real-time Basis", IEEE Transactions on Power system. Vol. PAS-92, no. 1, 1973.

[16] J. Rodriguez-Amenedo, S. Arnalte, and J. Burgos, "Automatic generation control of a wind farm with variable speed wind turbines," IEEE Transactions on Energy Conversion, vol. 17, 2002, pp: 279-284.

[17] R. de Almeida, E. Castronuovo, and J. Pecas Lopes, "Optimum Generation Control in Wind Parks When Carrying out System Operator Requests," IEEE Transactions on Power Systems, vol. 21, 2006, pp: 718-725.

[18] Wei Qiao, Harley, R.G., "Power Quality and Dynamic Performance Improvement of Wind Farms Using a STATCOM". Power Electronics Specialists Conference, 2007. PESC 2007. IEEE 2007, pp: 1832 – 1838.

[19] R. Pena, J. Clare, and G. Asher, "Doubly Fed Induction Generator Using Back-to-back PWM Converters and its application to Variable-speed Wind Energy Generation," Proc. Inst. Elect. Eng., Electric Power Applications, vol. 143, no. 3, May 1996, pp. 231–241.

[20] Ren-jie Ye, Hui Li, Zhe Chen, Qiang Gao, "Comparison of Transient Behaviors of Wind Turbines with DFIG considering the Shaft Flexible Models", 2008. ICEMS 2008. International Conference on Electrical Machines and Systems, Publication Year: 2008, pp: 2585 – 2590.

[21] Gerardo Escobar, Aleksandar M. S and Paolo Mattavelli, "An Adaptive Controller in Stationary Reference Frame for D-Statcom in Unbalanced Operation", IEEE Transactions on Industrial Electronics, vol. E-51, no. 2, Apr. 2004, pp: 401-409.

[22] J. Martinez, J. Navarro, "Behavior Improvement during Faults of Fixed Speed Stall Control Induction Generator Wind Turbines" WIND ENERGY 2009; 12, pp: 527–541.

A.9

"Design and Analysis of a Slope Voltage Control for a DFIG Wind Power Plant"
Jorge Martínez, Philip C. Kjær, Pedro Rodriguez, Remus Teodorescu.

Design and Analysis of a Slope Voltage Control for a DFIG Wind Power Plant

Jorge Martínez, Philip C. Kjær, Pedro Rodriguez, Member, IEEE, Remus Teodorescu, Senior Member, IEEE.

***Abstract*—This paper addresses a detailed design of a wind power plant and turbine slope voltage control in the presence of communication delays for a wide short circuit ratio range operation.**

The implemented voltage control scheme is based upon the secondary voltage control concept; which offers fast response to grid disturbances, despite the communication delays, i.e., this concept is based on a primary voltage control, located in the wind turbine, which follows an external voltage reference sent by a central controller, called secondary voltage control, which is controlling the voltage at the point of connection with the grid.

The performance has been tested using PSCAD/EMTDC program. The plant layout used in the simulations is based on an installed wind power plant, composed of 23 doubly-fed generator wind turbines. The resulting performance is evaluated using a compilation of grid code voltage control requirements. The results show that fast response to grid disturbances can be achieved using the secondary voltage control scheme, and the fulfillment of the design requirements can be extended for a wide range of short circuit ratios.

***Index Terms*—Wind turbine generator, slope control, power system, voltage control, doubly-fed generator, grid codes.**

I. Nomenclature

COM	Communication
CT	Current Transformer
DC, AC	Direct Current, Alternate Current
DFIG	Doubly Fed Induction Generator
DB	Dead Band
G	Generator
L	Inductance
LPF	Low Pass Filter
P, Q	Active, Reactive power
PCC	Point of Common Coupling
PI	Proportional-Integral controller
s	Laplace term
SG	Synchronous Generator
SCR	Short Circuit Ratio
PWM	Pulse Width Modulation
V, I	Voltage, Current
VT	Voltage Transformer
OVL	Overhead Line
WPP, WTG	Wind Power Plant, Wind Turbine Generator
WPPC	Wind Power Plant Controller
WPPT	Wind Power Plant Transformer
WTGT	Wind Turbine Generator Transformer
ω	Angular frequency
X, R	Reactance, Resistance
Z	Impedance

Subscripts

a, b, c	Three phase quantities
d, q	Direct and quadrature axes
ref	Reference
m	Measured

Manuscript December 17, 2009.

J. Martínez and P. C. Kjaer are with VESTAS Wind System, Power Plant R&D.

R. Teodorescu and P. Rodriguez are with Aalborg University, DK

II. Introduction

Wind power plants (WPPs) are growing in percentage of penetration into the electrical grid. Larger percentages of wind power penetration translate to more demanding requirements coming from the grid codes, for example, voltage support at the point of connection has been introduced recently by several grid codes from around the world [1]-[4]. The grid connection requirements vary in different parts of the world, but they share common aims, like to permit the development, maintenance and operation of a coordinated, reliable and economical transmission or distribution system. The new requirements generally demand that WPPs provide ancillary services to support the network in which they are connected [5].

WPPs differ from other generation sources; therefore, they are particular in certain aspects of their control. The main differences with traditional power plants with synchronous generators (SGs) are that the energy source fluctuates, it is unpredictable, and the WPPs are highly modular by being composed of a large number of generation units. This introduces communication delays when sending the operational set points, these delays can be in the range of hundredths of milliseconds. Additionally, the SGs inject the reactive power directly to the transmission system through their unit transformer, this provides a more efficient voltage regulation, since the reactive power is not transported over a long distance and through several transformers, as the wind turbine generators (WTGs) do. Finally, WTGs have bigger limitations in their reactive power and current capability due to the size of their electronic power converters. Therefore, replacing traditional power plants, including their control

characteristics during periods of strong wind, could be a concern. Grid operators are solving this challenge by means of redacting specific sections in the grid codes for WPP performance.

Usually, the requirements of the utilities can be solved by the turbines and the park controller. The wind power plant control (WPPC) can take place at park level, and/or turbine park level combination.

When designing a voltage control for a WPP, in addition to the communication delays, the variable grid configuration, especially during contingencies, has to be taken into account. In the present case the short circuit range (SCR) moves from 5 (contingency operation) to 25 (normal operation). The aim of this paper is to overcome these challenges by using traditional control structures distributed between the WTGs and the plant controllers. These distributed voltage controls can be seen as a typical secondary voltage control scheme [6].

As voltage control is actuated by the reactive power from the WTGs, it is possible to affirm that the voltage control design covers an inner reactive power/voltage control loop, located at WTG level, and an outer voltage control loop, located at the point of common coupling (PCC) where it is intended to control the voltage [7]-[8].

III. Voltage Control Requirements

Small-signal performance measures provide a means of evaluating the response of the closed-loop excitation control systems to incremental changes in system conditions. In addition, small-signal performance characteristics provide a convenient means for determining or verifying excitation system model parameters for system studies.

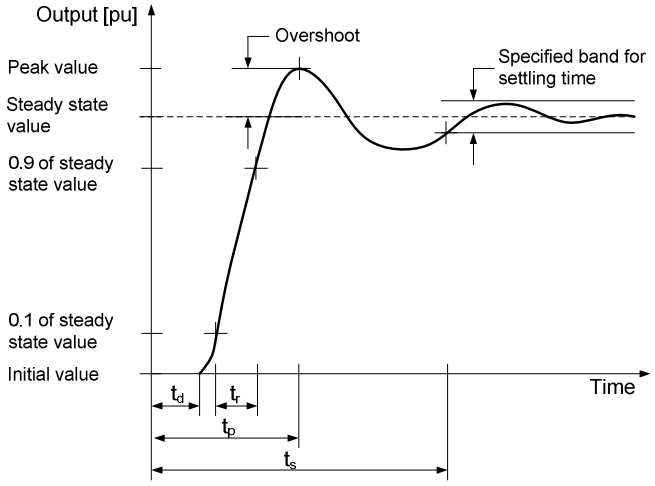

Fig. 1. IEEE std. for a typical transient response of a feedback control system to a step change in the input [9].

Small-signal performance may be expressed in terms of performance indices used in feedback control system theory. For a time response output the associated indices of interest are; rise time, overshoot, and settling time [9].

When tuning the voltage regulator, an improvement to one index will most likely be to the detriment of other indices.

The more demanding indices, related to

Fig. 1, were extracted from different grid codes [1]-[4] and compiled in Table I.

TABLE I
DESIGN REQUIREMENST ACCORDING TO FIG. 1

Parameter	Value	Unit
Overshoot	5.0	[%]
Band for settling time	2.5	[%]
t_d	0.2	[s]
t_r	1.0	[s]
t_p	Not defined	[s]
t_s	2.0	[s]

The indices listed in Table I will be used in the following sections as control design criteria. The referred indices will be applied to the measured voltage at PCC.

IV. Doubly Fed Induction Generator Wind Turbine

The variable speed DFIG wind turbine, see Fig. 2, allows for full control of the generator's active and reactive power using the rotor-connected frequency converter. Its rating is in the order of 0.3 pu. Operating both with sub- and super-synchronous speed, the power can be fed both in and out of the rotor circuit. The rotor-connected converter can employ various power dissipation solutions during severe transients, sometimes referred to as active crowbar, which is located at the rotor terminals, or as a chopper, located in the DC-link, Rch in Fig. 2. The grid converter is used to regulate the voltage level of the DC-link. The simplified control of the rotor converter is depicted in Fig. 3, in which the active and reactive powers are controlled using the d and q axis respectively [10]-[11].

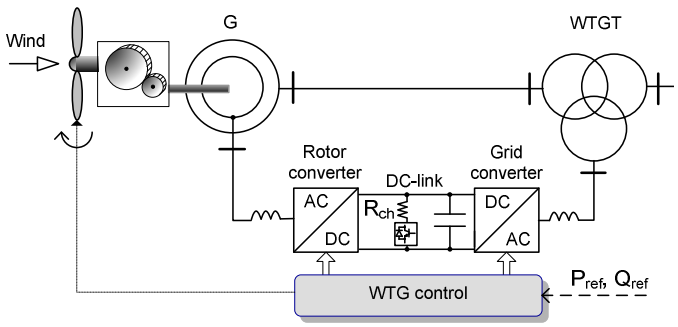

Fig. 2. DFIG wind turbine simplified single line electrical diagram.

The DFIG controller calculates or receives power references from an external controller (P_{ref}, Q_{ref}). These references are processed using two PI-controllers in cascade, which generate the needed voltage references ($V_{d\ ref}$, $V_{q\ ref}$) which are then translated by the PWM to pulse the rotor converter. Thus, the rotor is fed with a voltage that produces the desired P and Q at the stator terminals.

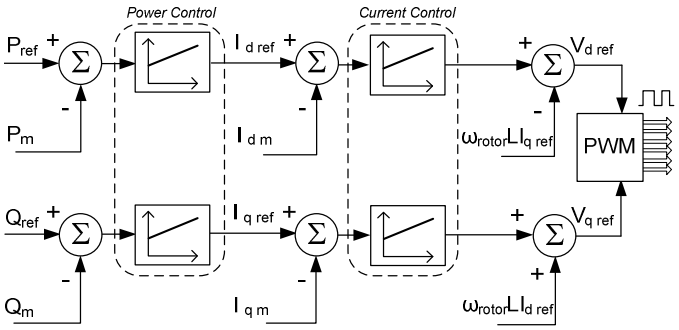

Fig. 3. DFIG simplified controller diagram

Fig. 4 shows the P-Q chart obtained from the stator terminals of a DFIG machine. The asymmetry in the figure with respect to the Q injection is due to the excitation of the generator. All P-Q combinations, inside the plotted area, can be injected. Clearly, the maximum Q injection is dependent on the current P value, $Q_{max}= f(P)$. The ratio Q/P gets its maximum value at 10 % active power injection.

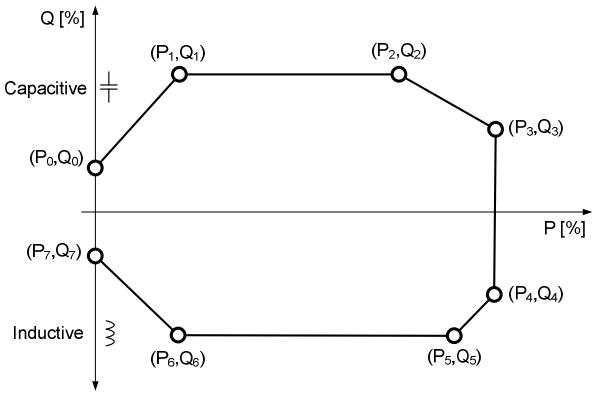

Fig. 4. DFIG P-Q chart.

TABLE II
DFIG P-Q CHART COORDINATES

Point	P	Q	Unit in WTG base
0	0	10	[%]
1	10	60	[%]
2	70	60	[%]
3	100	20	[%]
4	100	30	[%]
5	85	60	[%]
6	10	60	[%]
7	0	15	[%]

V. Power Plant Controller

Usually, WPPs are required to control the characteristics of the power injected at the PCC. Therefore, a centralized control is needed to supervise the power injected at PCC level. This controller is formed by a measurement device, which senses the currents and voltages at the PCC, a dedicated computer which allocates the control algorithms, and a communication hub. This communication hub will exchange control references and other signals (using the communication WPP Ethernet network) with a large amount of WTGs.

In Fig. 5 the dotted lines represent the communication network of the WPP.

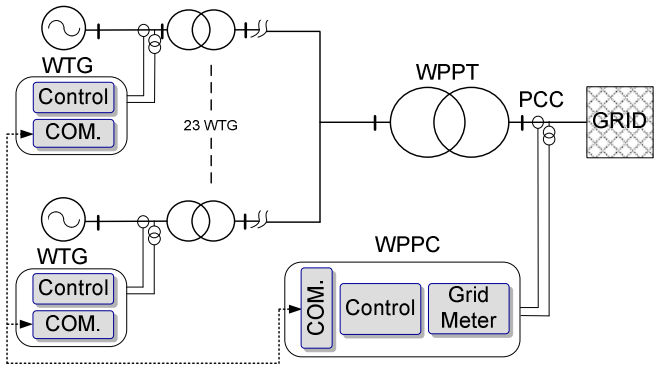

Fig. 5. WPP diagram.

VI. Slope Voltage Control

Slope control is widely used in power system applications since it allows paralleling generators with individual voltage slope controllers without hunting phenomena or instability. When there is high SCR (the SCR of a system is defined as the ratio between the installed power and the grid short circuit capacity) as in most of the cases in the transmission system, a slope controller will offer the best solution. Slope voltage control provides a coordinated reactive power system, since it is known which will be the equilibrium point for every voltage disturbance, independently of the time reaction of the controller and the Q compensator dynamics.

This voltage controller will cause the injection of reactive power proportionally to variation of voltage levels; thus, it supports the grid voltage recovering process after disturbances.

The slope of the voltage control can be defined as follows:

$$Slope = \frac{\Delta V}{\Delta Q} \tag{1}$$

The control law that applied for the slope concept can be defined in a generic way as the following one:

$$Q_{ref} = Q_0 + \left(\frac{1}{\text{Slope}}\right)(V_{ref} - V_m) \tag{2}$$

Fig. 6 can be used as an illustrative example of slope control performance. In this case the grid voltage is stepped from 1 pu to 0.9 pu and back to 1pu, the total impedance from the WTG to the grid is 0.31 pu, and the control slope is 5 %.

Fig. 6 shows the equilibrium point (point 2) after stepping down the grid voltage, and the equilibrium point (point 1) when setting the voltage of the grid to 1 pu again. It can be seen that the equilibrium points are located at the intersection of the system and control characteristics.

The horizontal axis shows the magnitude of the reactive power, and the vertical axis displays the voltage at WTG

terminals. The trajectory during the transient event from point 1 to 2, and from 2 to 1, is depicted with a green line.

By adding a certain offset to the slope controller (Q_0) or to the voltage reference (V_{ref}) the control characteristic (grey line in Fig. 6) can be shifted upwards or downwards, thus regulating the generator Q injection. In this way, it is easy to manage how the generators will share the reactive power injection for a certain voltage disturbance.

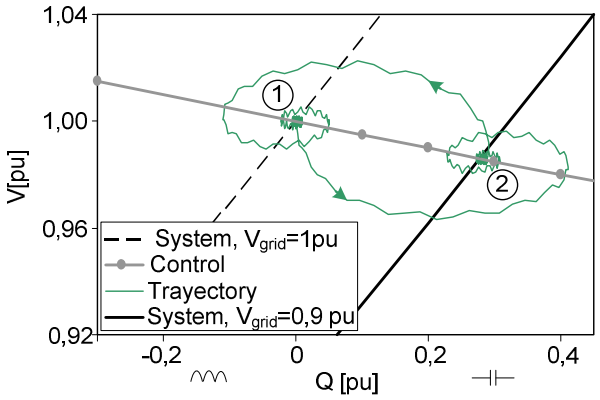

Fig. 6. Slope control and system characteristics.

VII. System Analysis

In order to study the system control behavior, both the WPP and the grid will be subjected to simplifications and linearization processes, as explained in the following sections.

A. Wind Turbine Generator Representation

For the sake of simplicity, the WTG reactive power dynamics can be characterized by a low-pass filter with the bandwidth of the outer PI power controller [12], see Fig. 3.

As mentioned, the WTG controller is formed by two PI cascade controllers. The inner one (current controller) is designed with a bandwidth approximately 10 times faster than the outer power control loop. Therefore, the above approximation is possible since the dynamics of the system are dictated by the closest poles to the origin [13].

$$F_{WTG}(s) = \frac{1}{1+sT_{WTG}} \tag{3}$$

The communication delay (T_{COM}) can be represented by the first order Pade function [13].

$$F_{comm}(s) = e^{-sTCOM} \approx \frac{1-s\frac{T_{COM}}{2}}{1+s\frac{T_{COM}}{2}} \tag{4}$$

B. Grid and Collector System Representation

For the sake of simplicity, in the representation of the transformers and the cables, all shunt elements are neglected, i.e. only the resistances and inductive series impedances are considered. Therefore, the voltage drop across these impedances can be defined as (5) and (6).

$$\underline{\Delta V} = R\underline{i} + \frac{d}{dt}\underline{\Psi} \tag{5}$$

$$\underline{\Psi} = L\underline{i} \tag{6}$$

ω_s is the angular frequency of the grid.

$$X = \omega_s L \tag{7}$$

The d axis is considered to be aligned with the direction of $\underline{V}$. By replacing (6) and (7) in (5), (8) and (9) are obtained.

$$\Delta V_d = (R + s\frac{X}{\omega_s})i_d - Xi_q \tag{8}$$

$$\Delta V_q = (R + s\frac{X}{\omega_s})i_q + Xi_d \tag{9}$$

Additionally, for small disturbances we can assume the following approximation:

$$\left|\underline{V} + \underline{\Delta V}\right| = \sqrt{(V + \Delta V_d)^2 + \Delta V_q^2} \approx V + \Delta V_d \tag{10}$$

Hence, the transfer function between the injected reactive current and the voltage drop becomes:

$$\Delta V = Ri_d - Xi_q \tag{11}$$

C. Wind Power Plant Control Representation

As it is shown in Fig. 5, the power plant controller is formed mainly by the grid meter and the control.

C.1 Grid Meter

A measurement device or "grid meter"; which samples at very high frequency the output of the CTs and VTs, located at the PCC. This meter processes the signals by calculating one cycle rms value and anti-aliasing filtering.

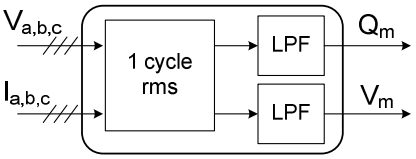

Fig. 7. Grid meter representation.

The calculated rms signals (Q_m and V_m) are used by the control as the feedback. The rms calculations and filtering actions can be represented by a first order function with a time constant T_m [14].

$$F_m(s) = \frac{1}{1+sT_m} \tag{12}$$

C.2 Control

The plant control receives the external references and feedback (measurements), and then issues the turbine set-points. The sample time (T_s) of the control is represented as a pure delay using half of the sampling time. Additionally, this can be linearized by the Pade function [13]. The control architecture is represented as a gain (K_{slope}) following (2).

D. System Gain Analysis

The simplified system is represented in Fig. 8. The communication and sampling delays are represented, as mentioned previously, with T_{COM} and T_s respectively.

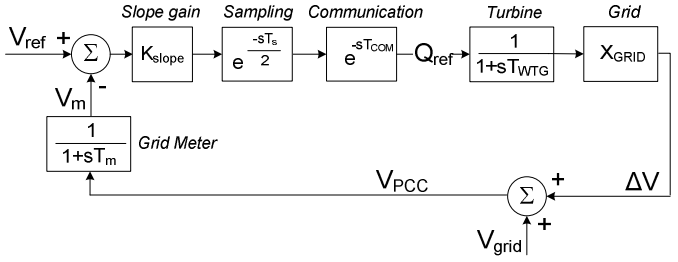

Fig. 8. Simplified system diagram.

Using this representation it is possible to investigate the influence of the slope gain and SCR on the system stability. The SCR can be defined in pu as the inverse of the X_{GRID}. Hence, with high SCR, the grid becomes less sensitive to the plant operation, but also less dependent.

The open loop gain (K_T) is defined in (13).

$$K_T = X_{GRID} K_{slope} = \frac{X_{GRID}}{Slope} \tag{13}$$

By grouping together the communication and sampling times, the total time delay (T) is defined.

$$T = 0.5T_s + T_{COM} \tag{14}$$

The closed loop transfer function (V_{PCC}/V_{ref}) can be calculated as follows.

$$\frac{V_{PCC}}{V_{ref}} = F(s) = \frac{K_T(1+sT_m)}{(1+sT_{WTG})(1+sT_m)+K_T e^{-sT}} e^{-sT} \tag{15}$$

By using the assumption and simplification of $T_m << T_{WTG}$ (T_m is in the order of one grid cycle, and the T_{WTG} is in the order of several hundredths of milliseconds) the close loop transfer function can be represented as follow.

$$F(s) \approx \frac{K_T(1+sT_m)}{(1+sT_{WTG})+K_T e^{-sT}} e^{-sT} \tag{16}$$

F(s) can be linearized by replacing e^{-sT} with the Pade function, obtaining (17). Therefore, the poles of the system can be calculated. See (21).

$$F(s) \approx \frac{K_T(1+sT_m)(1-s0.5T)}{(1+sT_{WTG})(1+s0.5T)+K_T(1-s0.5T)} \tag{17}$$

By calculating the poles of the system a clear picture can be seen about the stability for different slope gains and SCRs. See Fig. 9.

E. Practical Application

The following data has been replaced in (17): T_m = 15 ms, T_{WTG} = 160 ms, and T = 150 ms (T is obtained by using T_{COM}= 100 ms and T_s= 100 ms). Hence, Fig. 9 is obtained.

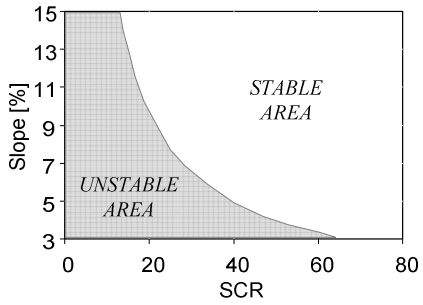

Fig. 9. Stability operation area.

It is clear that for high system gains (small slope and SCR values) the system becomes more difficult to control.

For example, a WPP operating with a 4 % slope and a SCR equal to 5 would create instability, as shown in Fig. 9.

In order to expand the stable area of the system, a lag compensator is added to the control slope gain.

A phase-lag compensator tends to shift the root loci towards the right-half plane. For this reason, the pole and zero of a lag compensator must be placed close, usually near the origin, so they do not appreciably change the transient response or stability characteristics of the system.

The transfer function of this controller is:

$$F_{ctrl}(s) = K_{slope}\left(\frac{1+sT_2}{1+sT_1}\right) \tag{18}$$

Fig. 10, shows the resulting diagram of the WPPC structure. A dead band module (D.B.) is included for the sake of illustration, since it is quite often used when doing voltage control. Additionally, some grid codes may ask for this.

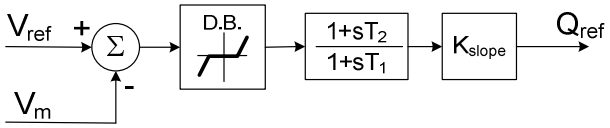

Fig. 10. WPPC slope control. Centralized voltage control concept.

The tuning objective of the lag compensator is to achieve a settling time of less than 1 s, and an overshoot below 5 %. See Table I.

The time constant T_2 can be roughly estimated by using the time communication delay of the system, and T_1 has to be tuned to provide a stable system operation under low SCR values, in which the grid gain reaches high values. However, the selected value for T_1 may be unsuitable (slow time response) for high SCRs, where the X_{GRID} is lower.

For low SCR values the following lag compensator tuning is obtained: T_2= 0.17 s and T_1= 1.7 s.

With these values the total gain of the system (K_T) can be placed between 3.17 and 5.5 for fulfilling the design requirements. The maximum calculated gain to reach instability is 8.3.

$$3.17 < K_{slope} X_{GRID} < 5.5 \tag{19}$$

It can be checked that with this setting the WPP will fulfill the design criteria only under some specific SCRs. If the gain of the grid decreases, meaning that the SCR increases, one of the poles will move toward the right half plane, slowing the system. For this reason and to fulfill the settling time of 1, another set of parameters is needed, i.e., one set of values for low SCRs and another for medium and high SCRs.

For medium and high SCRs the following values are obtained: T_2= 0.17 s and T_1= 0.53 s. With this setting the maximum system gain ($K_{slope}X_{GRID}$) is equal to 1.6, and the minimum gain is equal to 0.61 in order for the design requirements to be fulfilled. The maximum system gain value for reaching instability is 3.1.

$$0.6 < K_{slope} X_{GRID} < 1.6 \tag{20}$$

Usually, the slope of the controller is fixed by the system operator. In some cases the system operator could decide to change the predefined slope to another value, but since it is a known data, the controller can be adapted with new constants for the phase-lag compensator according to the new slope. However, changes in the SCR of the system are happening constantly and cannot be foreseen, which could require the addition of gain-scheduling based controllers [15].

TABLE III
LAG CONTROLLER PARAMETERS FOR THE PRACTICAL APPLICATION

CASE	SCR	Parameter	Value	Unit
A	Low	T_1	0.17	[s]
		T_2	1.70	[s]
B	Medium-High	T_1	0.17	[s]
		T_2	0.53	[s]

Table IV shows under which conditions the previous settings (CASE A and B) meet the design criteria. Blank spaces in the table indicate that none of them fulfill the requirements.

TABLE IV
FULFILLMENT OF DESIGN CRITERIA FOR DIFFERENT SCR & SLOPES

Slope [%] / SCR	4	6	8	10	12
4	A	A	A		
6	A				B
8	A		B	B	B
10			B	B	B
12		B	B	B	B
14		B	B	B	B
16	B	B	B	B	
18	B	B	B	B	
20	B	B	B		
22	B	B	B		
24	B	B			
26	B	B			

It is clear that communication delays in the system reduce the control stability margin when the gain of the system increases. See table IV.

It can be said that using a centralized WPP controller in the presence of large communication delays will require the WPP to have a different set of control parameters for different SCR scenarios. Moreover, the fulfillment of the required t_d could be physically impossible to achieve, if the total sampling and communication control delays are bigger than the required t_d.

VIII. SECONDARY SLOPE VOLTAGE CONTROL

A secondary voltage control strategy is implemented in order to overcome the limitations previously listed, thus achieving fast system reaction and extension of the fulfillment of the design requirements to a wide range of SCRs.

The secondary voltage control concept is well known in the literature. The main thrust of the secondary voltage control scheme is to counteract, in real time, reactive power flow changes in the system, by adjusting terminal voltages of generators system-wide. The amount of voltage adjustment is proportional to the voltage derivations at monitored buses [16].

The implementation of this concept can be done by replacing the WTG reactive power controller by a voltage controller, allowing the WTG to react faster to generator terminal voltage changes. Moreover, the WPPC is changed to provide voltage references to the WTG voltage control. In general, this new control structure allows the improvement of the overall performance, since the same tuning that was limited by the system gain and control delays can be extended to cover a greater range of SCR values.

Additionally, the previous plant controller (see Fig. 10) is complemented with an inner Q control loop. It is important to compensate the Q losses that occur inside the WPP (i.e. due to the power transformers) to reach the dictated Q_{ref} by the WPPC. A closed Q loop using Q_m as the feedback is added, which will ensure that the injected Q at the PCC is matching with the Q_{ref} calculated by the slope gain.

Fig. 11 and Fig. 12 show the proposed controllers for the WPP and the WTG, respectively.

A. WPPC

The WPP controller is extended with a plant reactive controller which calculates the V reference (V_{ref}^{WTG}) to be sent to the WTGs. This ensures that the needed Q_{ref} at PCC is injected.

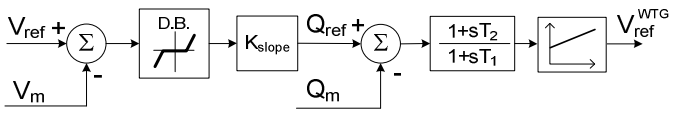

Fig. 11. WPPC, secondary slope voltage control concept.

B. Wind Turbine Voltage Control

The WTG reactive power control, shown in Fig. 3, is replaced by the one depicted in Fig. 12. In this way, the reactive current reference (I_{qref}) is generated according to the difference between the stator turbine terminal voltage (V in Fig. 12) and the voltage reference sent by the WPPC (V_{ref}^{WTG}). Therefore, the WTG outer control loop is changed from being a reactive power control, following Q references, to a local voltage control, which can be adjusted by an external set-point [8].

The gain and time constant of the WTG voltage control, K_{WTG} and T_3 respectively, are calculated to provide fast reactions to voltage changes at generator terminals.

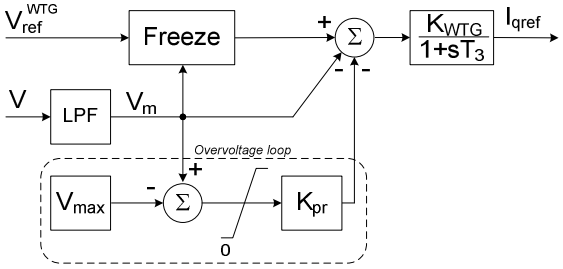

Fig. 12. WTG voltage control, secondary slope voltage control concept.

The control includes a protection against stator overvoltages, overvoltage loop in Fig. 12. After filtering the stator voltage (V), V_m is obtained, which is compared with a maximum voltage level (V_{max}). In the case that the V_m is greater than V_{max}, the gain K_{pr} will multiply the difference between V_m and V_{max} and this value will be subtracted from the V_{ref}^{WTG}.

Another voltage protection is installed in the reference sent by the WPP. If the value V_m is greater or lower than some threshold levels, normally 1.1 and 0.9 pu, and the V_{ref}^{WTG} increases or decreases respectively, then the block "Freeze", which allocates this supervisory logics, will freeze the external reference (V_{ref}^{WTG}) until these conditions are not fulfilled anymore.

IX. Simulation Setup

The proposed cases of table V have been simulated in PSCAD/EMTDC. An installed WPP has been used to model the plant layout and the main electrical components. The WPP is tested under different SCRs and active power injection scenarios. The slope is chosen to be 4 % in all the simulated cases. The grid bus voltage is stepped from 1 pu to 0.9 pu.

The WPPC has been tuned for an optimal output at SCR equal to 5, even though a wide range of different SCRs are tested to prove the robustness of the proposed concept.

Table V shows the overview of the simulated cases.

TABLE V
SIMULATED CASES

CASE	SCR	Active Power	GRID bus [pu]
1	5	Medium	1.0→0.9
2		Full	1.0→0.9
3	10	Medium	1.0→0.9
4		Full	1.0→0.9
5	25	Medium	1.0→0.9
6		Full	1.0→0.9

A. Wind Power Plant layout

The WPP is composed by 23 DFIG WTGs, which are distributed in 4 radials, having every one of them: 6, 7, 6 and 4 units, respectively. See Fig. 13. These WTGs are connected through a set-up transformer to the collector bus by means of a subterranean cable.

This collector bus is stepped up to the high voltage level by means of the substation transformer (WPPT). The high voltage terminal of this transformer is connected to the next substation through an overhead line (Z_{OVL}). Upstream of this point, the whole electrical system is reduced to an equivalent (Z_G), defined by its SCR and X/R.

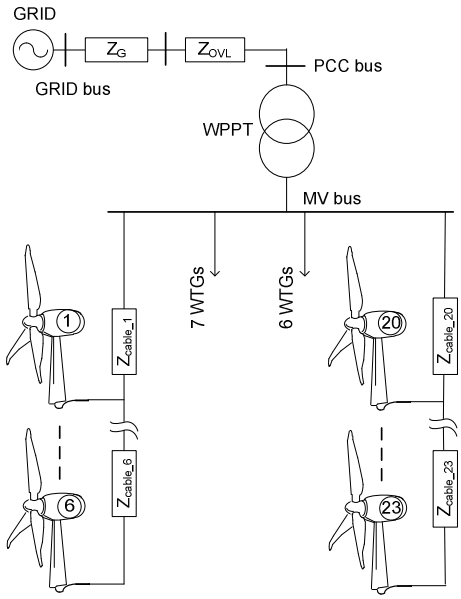

Fig. 13. Simplified diagram of the simulated WPP, composed by 23 WTGs.

The subterranean feeder cables are modeled as a Π

equivalent with its project data (Z_{cable_i}). The OVL (Z_{OVL}) is also modeled as a Π equivalent. The substation and WTG transformers are modeled with 12 % and 8 % impedance and an X/R ratio of 24 and 10, respectively. The grid is represented by an equivalent Thevenin circuit with different SCRs, according to the simulated cases (Z_G). See more data simulation details in the appendix tables.

The grid voltage is stepped in all the simulated cases, following table V, to check the response of the system.

B. Wind Turbine Generator Model

The wind input to the WTG model is based on a real wind speed time series data, measured at the top of the WTG nacelle. Since this data has been measured after the blades, it needs to be filtered to obtain similar power spectrum between the WTG model and the real WTG. Hence, the 1P and 3P harmonics have been filtered out in the measured wind data.

The aim of using real wind data as an input to the WTG model is to introduce similar fluctuations in the injected active power than obtained in reality; this will cause voltage fluctuations according to the grid impedance, thus testing the robustness of the controller.

Fig. 14 shows the time series for the DC, 1P and 3P active power components, obtained by the simulated WTG model (Sim) and the real WTG (Real).

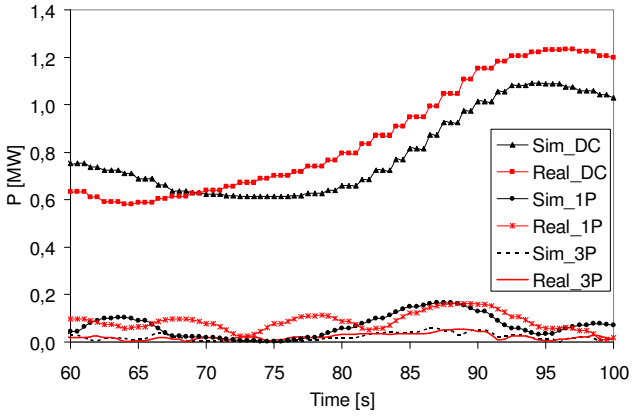

Fig. 14. Active Power Time series comparison, between the model and the real WTG.

The filtered wind speed time series is used as the input to the mechanical module of the WTG model, which includes the pitch control, the Cp-λ curves, and the drive train, which is modeled as a two mass system [17].

X. Simulation Results

In this section, each of the simulated cases is plotted. The test circuit used in the simulations is shown in Fig .13.

Additionally, and for the sake of illustration Fig. 24 is included, which shows the performance of the different controllers mentioned in this paper.

In all of the following simulations the grid voltage is stepped at time equal to 10 s from 1 pu to 0.9 pu, the voltages at the grid and PCC buses, and the reference and the injected Q at PCC are plotted.

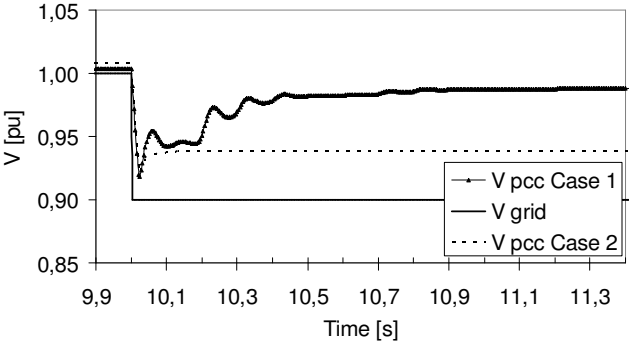

Fig. 15. Case 1 and Case 2: voltages at PCC and grid bus.

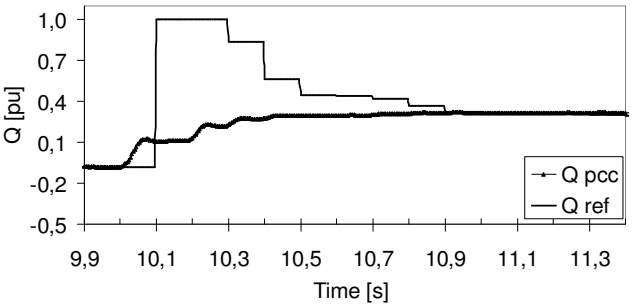

Fig. 16. Case 1: Q reference and injected at PCC

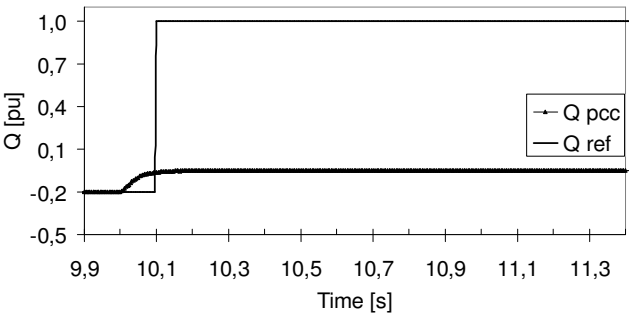

Fig. 17. Case 2: Q reference and injected at PCC

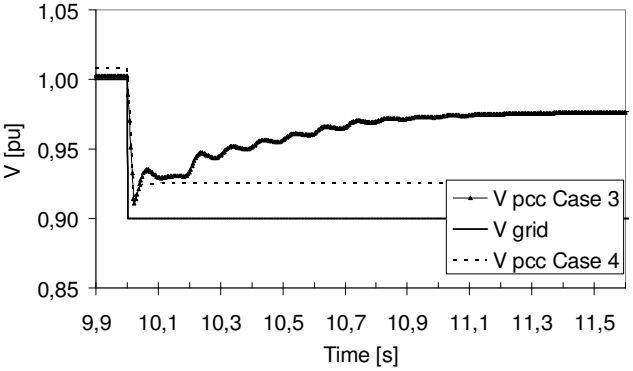

Fig. 18. Case 3 and Case 4: Voltages at PCC and grid bus.

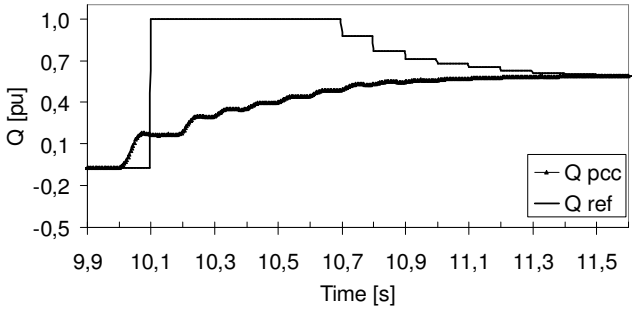

Fig. 19. Case 3: Q reference and injected at PCC

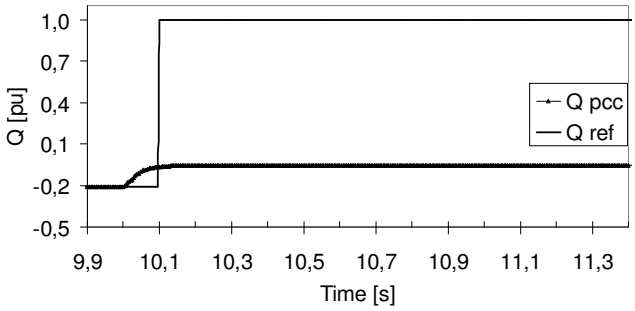

Fig. 20. Case 4: Q reference and injected at PCC

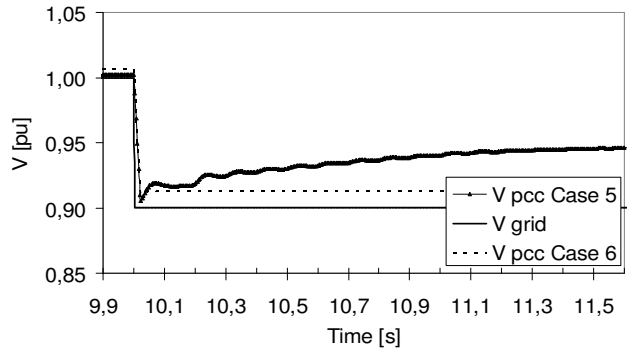

Fig. 21. Case 5 and Case 6: Voltages at PCC and grid bus.

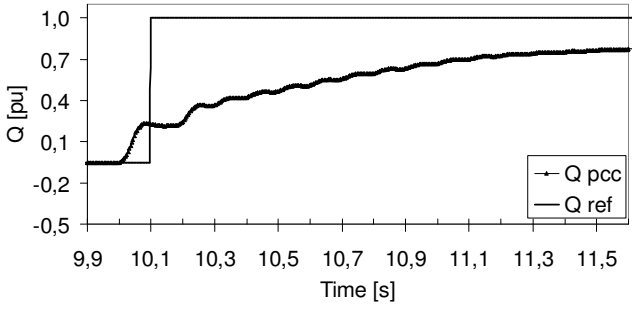

Fig. 22. Case 5: Q reference and injected at PCC

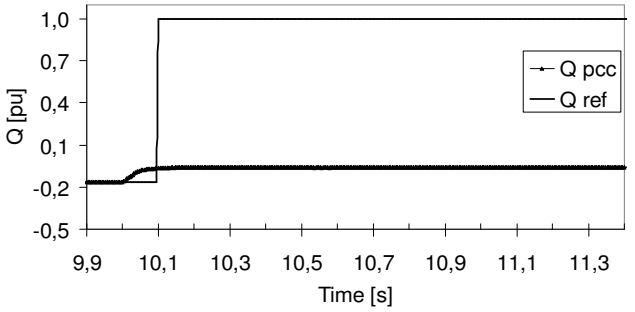

Fig. 23. Case 6: Q reference and injected at PCC

XI. Analysis of the Results

It can be observed that the SCR influences the results; with higher SCR values the WPP is nearly unable to move the voltage level at PCC (see Fig. 21), whereas for low SCR values the WPP can change the voltage at PCC without any limitation (see Fig. 15).

Moreover, the amount of Q injected is higher the higher the SCR is, see Fig. 16 and Fig. 22. This is due to the stiff characteristic of the grid for high SCRs. In the cases in which the WTG is at full production or the SCR is 25, the generators reach the ceiling reactive power. See Fig. 17, Fig. 20 and Fig. 23. This is a combination effect of the P-Q chart of the WTG (see Fig. 4) and the reactive power losses inside the WPP.

In any case, it can be seen that the time delay is very low (≈ 20 ms) since the WTGs react first with its own voltage controller, e.g. see Fig. 22 where it can be seen how the reactive power (Q_{pcc}) starts increasing before the first WPPC reference is issued (Q_{ref}).

Although, the time response is increased for high SCRs since the system tuning is done based on the contingency case (SCR 5), i.e. the lower the grid impedance is the slower time response is, the selected parameters and control configuration shown that the design requirements can be fulfilled for a wide range of SCRs.

Table VI summarizes the results obtained for every simulated case, according to the indices shown in Fig. 1.

TABLE VI
Performance Evaluation of the Simulated Cases

CASE	Overshoot [%]	t_d [s]	t_r [s]	t_s [s]
1	0	0.02	0.32	0.69
2	0	0.02	0.05	0.06
3	0	0.02	0.71	0.91
4	0	0.02	0.05	0.06
5	0	0.02	1.06	1.31
6	0	0.02	0.05	0.06

Clearly, the delay in the response (t_d) is reduced to very low levels for all the simulated cases, and the fulfillment of the design requirements is extended to a wide range of SCR values. Note that the requirement for t_r cannot be fulfilled for SCR values equal or greater than 25.

XII. Conclusions

The use of a centralized voltage control scheme in a WPP with communication delays, in which the WTGs are following Q references, shows some limitations in terms of time response to grid disturbances and SCR sensitivity. This SCR sensitivity may lead to the use of different control set parameters according to the SCR range of interest

However, by installing in the WTGs a local voltage controller (secondary voltage control concept) the following can be achieved; higher time reaction to system disturbances, without comprising the stability, and extension of the control tuning for a wide range of SCR values, while still fulfilling the design requirements.

By making the WTGs participate actively in the voltage regulation, faster reaction response can be achieved, since the WTG will contribute with a fast reaction, proportional to the voltage variations at its generator terminals, meanwhile the slower references coming from the WPPC arrive to the WTG control.

XIII. Appendix

TABLE VII
ELECTRICAL DATA OF WIND TURBINE

Parameter	Value	Unit
S_{base}	2100	[kVA]
V_{base}	0.690	[kV]
Electrical frequency	50	[Hz]
Stator Resistance	0.006	[pu]
Rotor Resistance	0.009	[pu]
Mutual Inductance	3.422	[pu]
Stator Inductance	0.072	[pu]
Rotor Inductance	0.101	[pu]
S step-up transformer 0.69:20kV	2100	[kVA]
Z step-up transformer	0.080	[pu]

TABLE VII
ELECTRICAL DATA OF THE SYSTEM

Parameter	Value	Unit
Number of WTGs	23	[-]
X_{OVL}	1.81	[%]
R_{OVL}	0.89	[%]
C_{OVL}	0.51	[%]
L_{OVL}	10.200	[km]
X_{WPPT}	11.91	[%]
R_{WPPT}	0.49	[%]
S_{WPPT}	55000	[kVA]
Angle of grid	75	[deg]
Medium voltage level	20	[kV]
High voltage level	115	[kV]

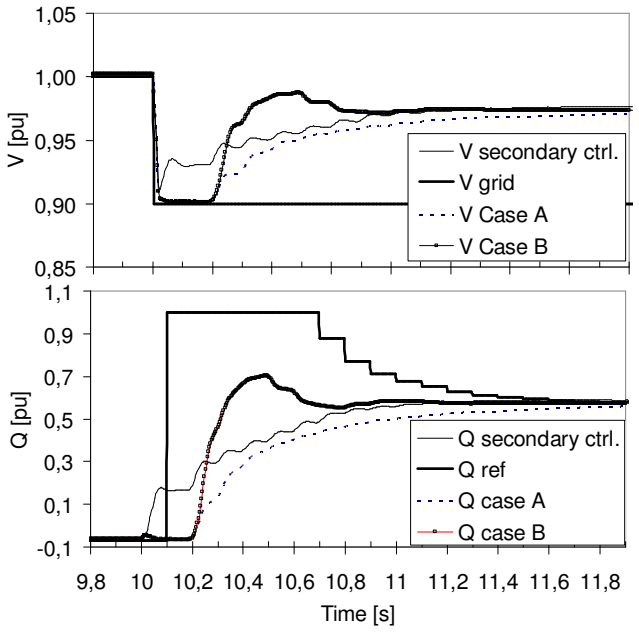

Fig. 24. Comparison between controllers. Case with SCR 10 and medium power active power production.

$$s_{1,2} = -\frac{0.5}{TT_{WTG}}\left(T + 2T_{WTG} - K_T T \pm \sqrt{T^2 - 4T_{WTG}T - 2KT^2 + 4T_{WTG}^2 - 12T_{WTG}TK_T + K_T^2 T^2}\right) \quad (21)$$

XIV. References

[1] P.O.12.2, "Connected installations to the transmission Spanish system: Minimum requirements for design and security", Red Electrica de España, Grid Code Requirements for installations connected to the transmission system in Spain.

[2] National Grid Electricity Transmission, "Guidance Notes for Power Park Developers", 2008.

[3] Alberta Electric System Operator (AESO), "Wind Power Facility, Technical Requirements", Alberta, November 2004.

[4] Hydro-Quebéc, Technical Requirements for the Connection of Generation Facilities to the Transmission Systems, Quebéc, Canada.

[5] I. Erlich, and U. Bachmann, "Grid Code Requirements Concerning Connection and Operation of Wind Turbines in Germany", *IEEE Power Engineering Society General Meeting*, vol.2, pp: 1253-1257, June 2005.

[6] A. Stankovic, M. Ilic, and D. Maratukulam, "Recent Results in Secondary Voltage Control of Power Systems", *IEEE Transactions on Power Systems*, Volume 6, Issue 1, pp: 94 – 101, February 1991.

[7] G. Tapia, A. Tapia, and J. Ostolaza, "Proportional-Integral Regulator-Based Approach to Wind Farm Reactive Power Management for Secondary Voltage Control", *IEEE Transactions on Energy Conversions*, vol. 22, No. 2, pp: 488 – 498, June 2007.

[8] M. El Moursi, G. Joos, and C. Abbey, "A Secondary Voltage Control Strategy for Transmission Level Interconnection of Wind Generation", *IEEE Transactions on Power Electronics*, vol. 23, issue 3, pp: 1178 – 1190, May 2008.

[9] *IEEE Std. 421.2-1990*, "IEEE Guide for Identification, Testing, and Evaluation of the Dynamic Performance of Excitation Control Systems"

[10] L. Wang, S. Chiniforoosh, and J. Jatskevich, "Simulation and Analysis of Starting Transients in Rotor-Chopper-Controlled Doubly-Fed Induction Motors", *IEEE Electrical Power & Energy Conference (EPEC)*, pp: 1 – 6, 2008.

[11] J. Morren, and S. W. H. de Haan, "Ridethrough of Wind Turbines With Doubly-fed Induction Generator during a Voltage Dip", *IEEE Transactions on Energy Conversion*, vol. 20, issue 2, pp: 435 – 441, 2005.

[12] J. Martinez, P. C. Kjær, and R. Teodorescu, "DFIG Turbine Representation for Small Signal Voltage Control Studies". *Conference on Optimization of Electrical and Electronic Equipment (OPTIM)*, 20-22, pp: 31 – 40, May 2010.

[13] G. Ellis, *Control System Design Guide*, 2004 Elsevier academics press, ISBN 0-12-237461-4.

[14] P. Kundur, *Power System Stability and Control*, 1994 McGraw-Hill, Inc. ISBN 0-07-035958-X.

[15] T. Lee; J. Jeng; and C. Shih, "Using neural networks to improve gain scheduling techniques for linear parameter-varying systems", *International Workshop on Advanced Motion Control*, 18-21, vol. 1, pp: 299 – 304, March 1996.

[16] A. Stankovic, M. Ilic, and D. Maratukulam, "Recent results in secondary voltage control of power systems", *IEEE Transactions on Power Systems*, vol. 6, pp: 94 – 101, February 1991.

[17] S. K. Salman, and A. L. J. Teo, "Windmill modeling consideration and factors influencing the stability of a grid-connected wind power-based embedded generator", *IEEE Transactions on Power Systems*, vol. 18, no. 2, pp: 793-802, May 20.

[18] G. Sheng, Y. Liu, D. Duan, Y. Zeng, and X. Jiang, "Secondary voltage regulation based on wide area network", *IEEE Power and Energy Society General Meeting*, 2009, 26-30, pp: 1 – 7, July 2009.

[19] S. I. Al-Majed, "Secondary Voltage Control: Enhancing power system voltage profile", *IEEE Power and Energy Conference (PECon)*, 1-3, pp: 1218 – 1221, December 2008.

[20] S. Narita and M. Hamman, "Multi-computer control of system voltage and reactive power on real-time basis", *IEEE transactions on Power systems,* vol. PAS-92, issue: 1, pp: 278 – 286, 1973.